Rapid photo-curing and property evolution in resin-composites

A thesis submitted to The University of Manchester for the degree of Doctor of Philosophy in the Faculty of Biology, Medicine and Health

2022

Hamad Algamaiah

Biomaterial Science and Dental Technology

Division of Dentistry, School of Medical Sciences,

The University of Manchester

Table of contents

List of Figures

List of Tables

List of Abbreviations

BisGMA	Bisphenol A Glycidyl Methacrylate
TEGDMA	Triethylenglycol dimethacrylate
UDMA	Urethane dimethacrylate
BisEMA	Ethoxylated bisphenol-A dimethacrylate
ORMOCERS	Organically-modified ceramics
C=C	Carbon double bonds
CQ	Camphorquinone
DMAEMA	Dimethylamino ethylmethacrylate
MPTS	3-methacryloxypropyltrimethoxysilane
BHT	Butylated hydroxytoluene
MEHQ	monomethyl ether of hydroquinone
LCU	Light cure unit
QTH	Quartz Tungsten Halogen
PAC	Plasma Arc Curing
AL	Argon-ion Lasers
LED	Light Emitting Diodes
URPBF	ultra-rapid photo-polymerized bulkfills
RAP	Rapid Amplified Photo-polymerization
AFCT	addition-fragmentation chain transfer
DC%	Degree of conversion
DoC	Depth of cure
FTIR	Fourier-Transform Infrared Spectroscopy
SEM	Scanning electron microscopy
VHN	Vickers hardness
RI	Refractive index

List of Units

h	Hour
s	Second
N	Newton
MPa	Megapascal

mW/cm^2	Milliwatts per centimeter squared (Irradiance)
J	Jules
J/cm^2	Jules per centimeter squared (Radiant exposure)
nm	Nanometer
μm	Micrometre (10^{-6} m)

Word count: ≈ 40600 word

Abstract

Since resin composites were first introduced to dentistry, their formulations have been developed significantly. Recently, a new class of ultra-rapid photo-polymerized bulk-fill 'URPBF' resin-composites has been introduced. Due to the incorporation of Addition-fragmentation chain transfer (AFCT) agent, these materials are claimed to photopolymerize within only 3 s under high irradiance from a PowerCure™ light-curing unit (LCU). Therefore, the focus of this thesis was to study early-stage properties of this new composite system, during and following photopolymerization, including methods-development to measure mechanical-property evolution.

Using FTIR spectroscopy, the degrees of conversion, conversion kinetics and their development post-irradiation for these URPBF materials were measured at both 1 mm and 4 mm depths, sub-surface. Following 3 s high-irradiance, PFill and PFlow materials were found to be broadly comparable to their predecessors: ECeram and EFlow (both irradiated for 20 s), over 24 h post-irradiation, at both depths.

Polymerization shrinkage and shrinkage-stress development were studied via bonded disk and Bioman II methods to determine effects of high irradiance photopolymerization, using 2 LCUs. URPBF material, PFill, had reduced polymerization shrinkage under high-irradiance (1.6 % and 1.7 % for PowerCure™ and VALO™ LCUs, respectively) compared to 10 s (1.8 %). These results were also lower than for its predecessors, ECeram (2.7 %).

PFill exhibited slightly higher shrinkage-stress (2.2 MPa and 2.3 MPa) under high-irradiance from PowerCure™ -3s and VALO™, respectively) compared to 10 s curing (1.8 MPa), but the stress was still lower than the comparator, ECeram (2.6 MPa). Similar behavior was seen with PFlow, except for the 3s VALO™ group which produced significantly higher shrinkage stress (3.6 MPa).

The exothermic reaction during intra-dental photo-irradiation and the effect of high irradiance on temperature fields in situ were also investigated by thermography. This produced 2D temperature maps and temperature/time plots. The maximal temperature rise (ΔT) was seen within the material bulk, at 2 mm depth. This was significantly higher in PFill and PFlow polymerized via PowerCure™ -3s (21.8 and 27.1 °C),

compared to the same LCU in standard 10 s mode (17.8 and 22.9 ºC). However, PowerCure™ -3s generally produced comparable temperature rise to Elipar S10™- 10 s. Nonetheless, only 1 mm of remaining dental thickness was sufficient to ensure a minimal temperature rise at 1 mm within dentine. This suggests freedom from significant thermal damage from rapid photopolymerization and thus the clinical safety of this treatment.

A method to study early surface viscoelastic integrity was proposed, using a flat-ended macroscopic indentor axially aligned over each specimen immediately (< 2min) post-irradiation. This applied 14 MPa compressive stress for a period of 2 h. Then, indentation-recovery measurements were made on unloaded specimens. This indentation-creep method characterizing URPBF surface integrity immediately post-irradiation. Flowable materials showed deeper indentation compared to non-flowable bulkfills. PFill and PFlow polymerized in 3 s resulted in immediate indentations comparable to their counterparts: ECeram and EFlow. With delayed indentation at 24 h, no differences were detected between materials in maximum indentations regardless of the material type or curing protocol. This is attributed to further network development.

The ability of this indentation-creep method to characterize several representative resin-composites, including RBCs with varied clinical applications, was then assessed. The method was successfully applied to eight representative RBCs, including three bulkfills, three conventional non-flowables, and conventional flowables. Network developments by 24 h significantly improved the indentation resistance of all materials. Viscoelastic properties evaluated by this method confirmed that highly filled RBCs were more indentation resistant.

Declaration

No portion of the work referred to in the thesis has been submitted in support of an application for another degree or qualification of this or any other university or other institute of learning.

Conflicts of interest

The authors do not have any financial interest in the company whose materials are studied.

Copyright Statement

The author

I graduated from King Saud University (Riyadh, Saudi Arabia), in 2011, gaining a BDS degree. Then I was appointed as a faculty member in the Restorative Dental Science department at King Saud University.

In 2014, I was awarded a scholarship by the university to continue my postgraduate studies. So, in 2014, I was enrolled in a *Teaching in Dental Education* fellowship program at NYU and I received the certificate in 2015. During the program, I was fortunate to work with great mentors and was able to expand my knowledge in dental education, clinical and esthetic dentistry and work in the dental materials laboratory. Then I was accepted at the University of Iowa for the Master's degree and clinical residency in Operative Dentistry. During my 3-year program, I expanded my knowledge in restorative dentistry and dental materials. At the same time, I applied my knowledge in teaching as I was a clinical supervisor for undergraduate dental students. In 2018, I received my Master's degree and clinical certificate and, in September 2018, I began a full-time four-year PhD in Biomaterials and clinical dentistry (Restorative Dentistry) at the University of Manchester.

During my residency I have been enrolled as an honorary clinical lecturer for undergraduate dental students at the University of Manchester. I am also a reviewer for *Dental Materials* and the *European Journal of Oral Sciences*.

Throughout my residency I was fortunate to participate in the following dental meetings:

- Workshop leader and guest speaker at the *British Undergraduate Dental Research Conference* for the workshop titled "Smile Design", Manchester, March 2019.
- Poster presentation at the Division of Dentistry PGT & PGR Presentation Event, June 2019.
- Poster and Oral presentation at the *European Dental Materials Conference*, Brussels, August 2019.
- ADM 2020 virtual meeting "Polymers and Ceramics on the Dental Material Horizon"
- SDMS-CSA & ADM joined hybrid meeting (*Forum on Advanced Dental Biomaterials*), May 2021
- *British Society for Oral and Dental Research* meeting, September 2021

- ADM 2021 virtual meeting "*Progress in Adhesion, Ceramic Materials and Dental Engineering*", October 2021
- Oral presentation at the *American Association for Dental, Oral, and Craniofacial Research* (AADOCR) in Atlanta, GA, March 2022

I was also privileged to publish the following papers during my PhD program:

- ***Algamaiah H***, Danso R, Banas J, Armstrong SR, Whang K, Rawls HR, Teixeira EC. The effect of aging methods on the fracture toughness and physical stability of an oxirane/acrylate, ormocer, and bis-GMA-based resin composites. *Clin Oral Investig,* 2019.
- ***Algamaiah H***, Silikas N, Watts DC. Conversion kinetics of rapid photo-polymerized resin composites. *Dent Mater,* 2020; 36: 1266-1274.
- ***Algamaiah H***, Silikas N, Watts DC. Polymerization shrinkage and shrinkage stress development in ultra-rapid photo-polymerized bulk fill resin composites. *Dent Mater*, 2021; 37: 559-567.
- Watts DC, ***Algamaiah H***. Characterizing surface viscoelastic integrity of ultra-fast photo-polymerized composites: Methods development. *Dent Mater,* 2020; 36: 1255-1265.
- Yang J, ***Algamaiah H***, Watts DC. Spatio-temporal temperature fields generated coronally with bulk-fill resin composites: A thermography study. *Dent Mater,* 2021: 1237-1247.
- ***Algamaiah H*****,** Watts DC. Post-irradiation surface viscoelastic integrity of photo-polymerized resin-based composites. *Dent Mater,* 2021; 37: 1828-1833.
- Alshabib A, ***Algamaiah H***, Silikas N, Watts DC. Material behavior of resin composites with and without fibers after extended water storage. *Dental Materials Journal,* 2021: 2020-2028.
- Bin-Shuwaish M, AlFawaz YF, ***Algamaiah H***, AlSani AS, Abobakr IB, Alzahrani KM, Almutairi B, Attar EA, Vohra F, Abduljabbar T. Technical accuracy of dental laboratories in the quality and shade matching of porcelain fused to metal crowns: An in vitro study. *International Journal of Environmental Research and Public Health,* 2021; 18: 2722.

Dedication

In the name of God, the all-knowing, the most wise,

I would like to dedicate this work to my family, specifically my mother **Nadia Almohanna** and my father **Ali Algomaiah**, for their endless love, support, and dedication. To them, I am forever indebted. I also wish to dedicate this work to my lovely wife **Bashayer** and my kids, Ali and Alya. Thank you for getting me through this journey through times of stress and frustration. You have kept me going and I couldn't have done this without your unfailing support. This thesis is also dedicated to my beloved siblings: **Nada**, **Muath**, **Roqayah**, **Mohammed**, and **Maan** for their great encouragement throughout my study.

Acknowledgement

First and foremost, praise to ALLAH, the almighty and the greatest for guiding me throughout my life and for giving me the strength and determination to pursue my study. It is impossible to recognize everyone who has helped me during my eight years postgraduate training period at New York University, University of Iowa, and the University of Manchester. I'm thankful for everyone who helped me to be where I am now, and lucky to have or known some people during that time. Firstly, I will forever be indebted to my father **Ali** and my mother **Nadiah** for their endless love and support throughout my life. Special appreciation goes to my lovely wife **Bashayer** for her endless support and patience during our time away from home. For this, I am forever grateful.

Now, I would like to express my sincere gratitude to my supervisors Professors **David Watts** and **Nick Silikas**. Thank you for your continuous guidance and support during my time in Manchester. To Professor **David Watts,** I am thankful for all the time and energy you have given to make my work the best that it can be. Equal gratitude goes to my clinical supervisor Professor **Reza Roudsari** for his help and encouragement during my clinical training which made my clinical experience enjoyable. I would also like to thank Professor **Nick Grey** for his support as my academic advisor.

My highest gratitude and appreciation go to the Kingdom of Saudi Arabia, specially to King Saud University and the Saudi Cultural Bureau in London for sponsoring me throughout my studies.

CHAPTER ONE

Introduction and literature review

1.1 Overview

Resin composites are currently the mostly-used direct restorative material. They were introduced in the early 1960s by *Rafael Bowen* and have been modified subsequently by creation of many different formulations. These modifications and advancements have led to a significant improvements in their clinical performance [1, 2]. Other advantages of resin composites include enhanced working times, good handling properties, high esthetic outcomes and, most importantly, conservation of tooth structure. The shift from mercury-free restorations has also resulted from legal restraint treaties against mercury based products, published by the United Nations Environment program [3] and the World Health Organization [4].

One of the main reasons for resin composite use is to conserve tooth structure. The cavity-design requirements - for resin composite placement - are more conservative compared to those for amalgam placement [5, 6]. Micro-mechanical retention together with universal adhesive formulations provided for resin composites help in achieving minimally invasive preparation. Also, these materials can be maintained and repaired (as can amalgam), hence increasing the life span of restorations. Therefore, resin-based composite materials became the most commonly used restoratives in dentistry, ranging from pit and fissure sealants (PFS), direct and indirect restorative materials, core build-up materials, crowns, inlays, onlays, resin cements to root canal filling materials.

In 2015, it was estimated that 800 million resin composite restorations were placed worldwide [7]. Heintze *et al* 2017*,* anticipated that in 10 years, 96 million out of 800 million restorations will show significant wear and 32 million will be repaired or replaced due to failure limited to fracture [7]. Clinicians plays a significant part in in the success of resin composite restorations [8]. Careful attention to the material's light-

curing requirements can enhance the quality of restoration. Therefore, it is important to understand the cause of possible failures and at the same time focus on identifying factors that can enhance the material's physical and mechanical performance.

One of the main aspects of recent modifications on resin composites is in shortening clinical steps and time needed for restoration placements. This was - for long time - one of clinicians 'wish-list' as clinicians spend around 57% of their clinical time placing restorations [9]. Recent advances in polymer chemistry, specifically in photoinitiators, have increased the potential for ultra-rapid photopolymerization. Also, developments in Light-Curing technologies have enabled the delivery of higher energy as well as wider spectrum to cover/match different photoinitiators.

However, there is still concern over the adequacy of basic understanding and practice of light-curing by many dentists [9, 10]. According to Kopperud *et al*. (2017), more than half of participants did not know the irradiance of their Light Curing Unit (LCU) and they do not perform regular maintenance on their LCUs. Another recent study have found out that more than two thirds of the LCUs are either damaged or contaminated [10]. Therefore, this shows a general concern of the overall light curing practice of dentists.

However, clinicians still request bulk-filling materials and shorter LC protocols to save their clinical time. So the question is: Is it possible to achieve such rapid photopolymerization while maintaining resin composite key properties?

According to the *hierarchy of evidence,* more clinically relevant conclusion can be drawn from clinical evaluation. However, during any period of 5 or more years, over which a structured clinical methodology was designed to evaluate a new restorative material, either a significant modification or an entirely new material is typically introduced to replace the current material, which can limits the significance that may

be drawn from such clinical trials [11]. Other factors complicating clinical trials include the patient's compliance and operator reproducibility and reliability [8, 12].

Nevertheless, the durability of resin composite materials still needs to be further investigated. Optimum restoration performance requires attention to the material's handling and light-curing requirements. These start from *in-vitro* studies to understand the material's physical and mechanical behavior and anticipating their clinical performance prior to *in-vivo* studies [13]. Therefore, the main goal of this thesis was to study the photo-polymerization and polymerization-related properties of a new generation of resin composite system and their early-stage properties. Below is a general outline of our literature review (**Figure 1.1**).

.

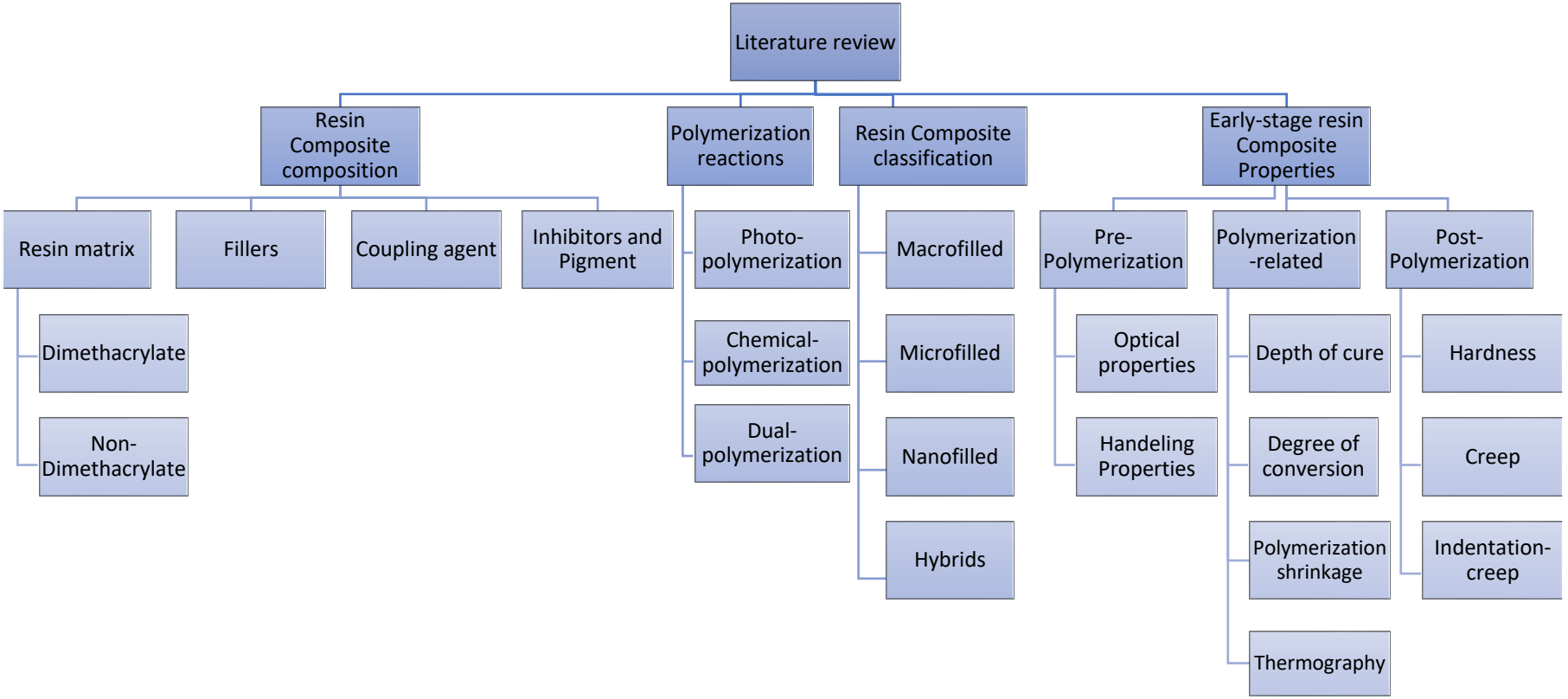

Figure 1.1: General outline of the literature review

1.2 Resin composite composition

Composites -in general- are defined as the mixing of two or more different materials with different properties, resulting in a third one with characteristics transcending the individual materials. In dentistry, resin composites consist of three main components: the resin matrix, inorganic fillers, and the coupling agent. As formulated by the manufacturer, the first component, the resin monomer, will function (upon polymerization in situ) as the organic matrix of the material, which establishes many of the chemical and physical properties of the composite. Inorganic fillers are incorporated into the matrix and enhance mechanical and optical properties. Finally, the coupling agent (coating the filler particles) is crucial in bonding fillers to the resin matrix.

Resin matrix

The resin matrix is the three-dimensional continuous phase of a resin composite. This holds the entire composite together. Without this, the filler particles alone would be a pile of powder. Therefore, the resin matrix is responsible for the overall composite physical stability and mechanical properties, particularly viscoelasticity [14]. The performance of the resin composite material is influenced by each specific monomer's properties and how they can be utilized in the overall final structure. The viscosity, degree of hydrophobicity, refractive index, reactivity, crosslinking ability all are parameters to consider when choosing a monomer system [15].

One of the main requirements for monomer selection in dental resin composites is having a functional group that permits free-radical polymerization [14]. But alternative polymerization mechanisms do exist, notably step-growth polymerization. Ideally, the monomer should exhibit a sufficient degree of conversion with minimum shrinkage, good long-term physical and mechanical properties and biocompatibility [16]. Some monomers provide rigidity and relatively low shrinkage; however, they exhibit high viscosity to a point where filler incorporation and handling becomes very challenging. Therefore, other (diluent) monomers with low viscosity are used to reduce the overall viscosity of the monomer mixture to improve handling properties and subsequently allow for higher filler load. Most dental monomers incorporate methacrylate-group functionality, which has sufficient reactivity for fast polymerization [14, 17].

Dimethacrylate-based monomers

The evolution or resin composite materials started in the early 1960s with *Bowen's* resin formulation of Bis-GMA 2,2-bis [4-(2-hydroxy-3-methacryloxypropyl) phenyl] monomer (**Figure 1.2**) [18]. This monomer is still widely used in dental restorative materials, due to the relatively low polymerization shrinkage and good mechanical properties, when it is optimally polymerized [19, 20]. However, it has some drawbacks such as the high viscosity, polymerization shrinkage stress, high water sorption and tendency for degradation [14, 20].

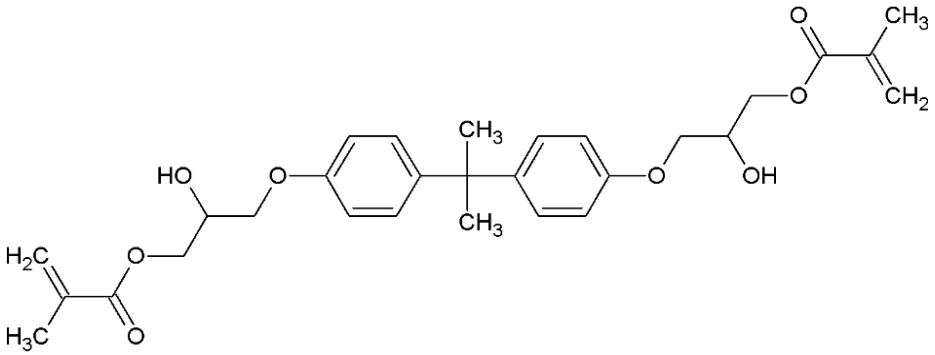

Figure 1.2: Chemical structure of Bis-GMA monomer

Bis-GMA monomer has high molecular mass (510.6 g/mol) and hydroxyl groups leading to inter-molecular hydrogen bonds and a high viscosity (η = 1200 Pa.s). Therefore manufacturers dilute it with other co-monomers with lower viscosity [14]. Triethylene glycol dimethacrylate (TEGDMA) (**Figure 1.3**) is a common co-monomer with low viscosity (η = 0.006 Pa.s) used to modify the viscosity with Bis-GMA to facilitate filler incorporation and improve handling properties [14]. Traditionally, a 1:1 (w/w) ratio was used. However, due to the low molecular mass of TEGDMA (286.3 g/mol), it is prone to high polymerization shrinkage and also water sorption [21, 22]. Thus, the use of TEGDMA is often limited, being replaced by other co-monomers (e.g., bis-EMA and UDMA).

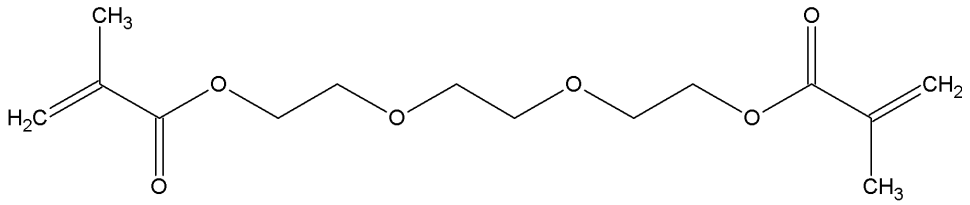

Figure 1.3 Chemical structure of TEGDMA monomer

Another dimethacrylate monomer available commercially is urethane dimethacrylate monomer (UDMA) (**Figure 1.4**) developed by Foster and Walker in 1970s [23]. These monomers are less viscous than Bis-GMA due to reduced molecular mass and flexible urethane links, requiring less diluent monomer [14]. UDMA monomers have higher degree of conversion compared to some Bis-GMA: TEGDMA combinations, which improves biocompatibility [24, 25]. Also, there are some differences in physical and mechanical properties, arising from the flexible urethane linkages. Nevertheless, UDMA-based composites may develop higher polymerization shrinkage and water uptake [24-27].

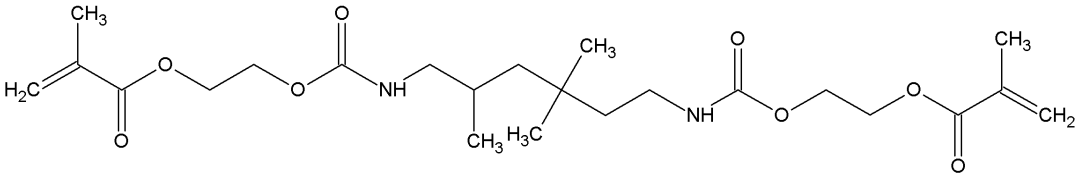

Figure 1.4: Chemical structure of UDMA monomer

Ethoxylated bisphenol-A-dimethacrylate (Bis-EMA) (**Figure 1.5**) is commonly employed dental monomer (Bis-EMA is a generic term for a large homologous series of molecules). It is an analogue of Bis-GMA monomer but lacks the hydroxyl groups and thus the associated H-bonding. The degree of conversion (DC) is enhanced due to the flexible ethylene glycol spacers [14, 24, 28]. Bis-EMA is produced as a mixture of multiple molar masses, (or lengths of ethylene oxide chains). Some Bis-EMA based resin composites have surpassed Bis-GMA based resin composites in degree of conversion [28].

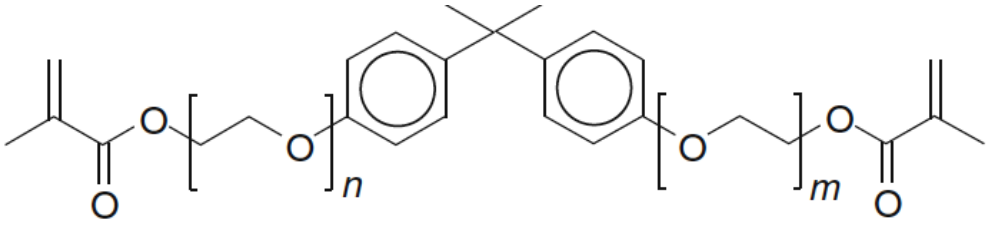

Figure 1.5 Chemical structure of Bis-EMA monomer – n and m are variable.

Possible alternatives to dimethacrylate- monomers

Recent improvements in resin composite materials were generally focused on altering the structure or chemistry to produce either a formulation with superior performance, or to achieve similar results with less working time and clinical steps. The motive to look for alternative formulations was partly due to the lack of biochemical stability of dimethacrylate-based restorations in the oral environment [29, 30]. The ester links, present in dimethacrylate monomers, are susceptible to degradation by hydration and enzymes [13].

It was hypothesized that the higher the hydrophobicity, the greater would be resin composite stability in an aqueous environment. Therefore, an alternative (Silorane) formulation was introduced based on an Oxirane ring-opening monomer (**Figure 1.6**). This composite system was much less soluble in an aqueous environment and exhibited low polymerization shrinkage [31-34]. However, the cationic ring-opening crosslinking of oxirane was rather slow, compromising early mechanical properties [35]. Also, silorane-based resin composites exhibited significantly lower degree of conversion compared to its competitors [36]. This, added to the material's low bond strength, lead to the discontinuation of the silorane-based resin composite.

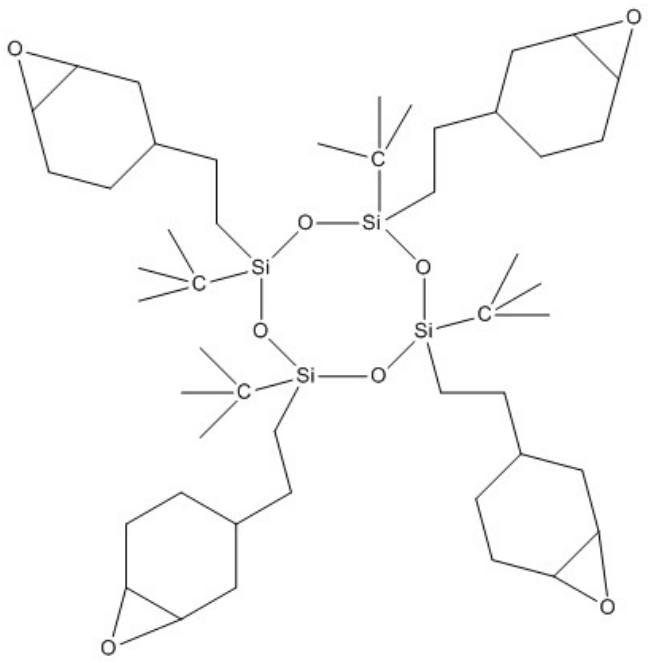

Figure 1.6: Chemical structure of Silorane monomer

Another alternative non-dimethacrylate monomer is Ormocer monomer (organic modified ceramics) (**Figure 1.7**), based of inorganic-organic co-polymers with silanated fillers. The resin matrix contains oligomers with condensed silane. Both the long inorganic backbone and the ceramic polysiloxane monomer contributed to the low polymerization shrinkage. Ormocer based composites have been available since 1998 and went through several structural modifications to overcome inconsistent performance [37]. While some research evaluated pure ormocer-based composite showed maintained surface integrity and hardness values over 7 days aging [38], others show inferior long-term performance [37].

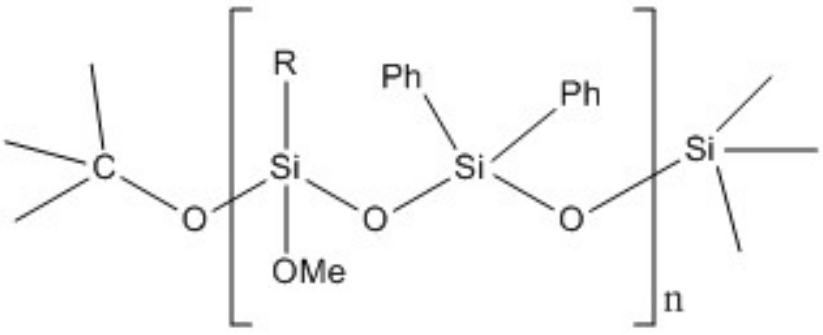

Figure 1.7: Chemical structure of Ormocer monomer

Fillers

Inorganic (and sometimes organic or mixed) fillers are added (as a *dispersed* phase) to resins to enhance the overall properties and performance of the composite materials. The addition of reinforcing fillers to a resin matrix enhances the handling properties of the unset paste and increases the modulus of elasticity and stiffness of the set material, along with other mechanical properties e.g., strength, fracture toughness and wear resistance [39, 40]. Reinforcing fillers also enhances physical properties: reducing polymerization shrinkage, water sorption and coefficient of thermal expansion [39, 41, 42]. Positive correlations have been established between mechanical properties and filler fraction [40, 43]. However, beyond a certain amount (*ca.*57-65 vol %) some properties may start to plateaus and then decrease [44-46]. Filler type, size, density, refractive index and morphology all collectively influence the physical and mechanical properties and performance [39, 47-49].

The fillers used in resin composites are mostly selected from silica and silica-based glasses due to their good optical properties and their polishability. Quartz fillers were originally used but are now replaced with barium and strontium borosilicate glasses, zirconium oxide or combinations [50, 51].

Most resin composite products are reinforced with hybrid-sized fillers in micro- and nano-size scales. These may be in the form of microfillers, micro-clusters, agglomerated nano-clusters, discrete nano particles, pre-polymerized fillers or various combinations (**Figure 1.8**) [14]. These fillers can be manufactured traditionally through crushing a large glass or stone particles. However, to achieve standardized nano-particles, other manufacturing methods are utilized: such as pyrolysis or sol-gel reactions [50-52].

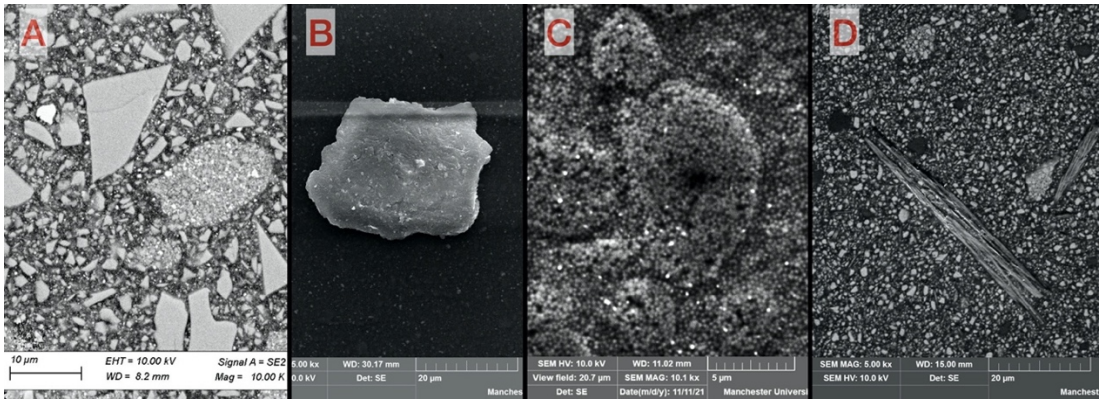

Figure 1.8: Reinforcing fillers in resin composite. (A): microhybrid; (B): pre-polymerized cluster; (C): Combination of discrete nano fillers and nano-clusters; (D): Fiber-reinforced.

Coupling agent

The structural integrity of a resin-composite greatly affected by the integrity of the interface between the organic resin matrix and the dispersed (mainly inorganic) particles. If the matrix/filler bonding is compromised, the differences in *elastic modulus* between resin matrix (1–3 GPa) and filler particles (≫10 GPa) can compromise particle-resin cohesion, which can result in voids and accelerated matrix degradation during function [14, 53]. Strong bonding between filler particles and the matrix can transmit and distribute forces throughout the structure, leading to good physical and mechanical performances. A molecular coupling agent is bi-functional and creates primary bonds between the inorganic particles and the organic matrix. The most common coupling agent used in dental resin composite materials is 3-methacryloxypropyltrimethoxysilane (MPTS) [50] (**Figure 1.9**). Chemical adhesion is promoted through covalent bonding to hydroxyl group in the silica particles at one end and co-polymerization of the methacrylate group to the resin matrix at the other end (**Figure 1.9**). This significantly improves the overall material strength and its resistance to hydrolytic degradation [53-56].

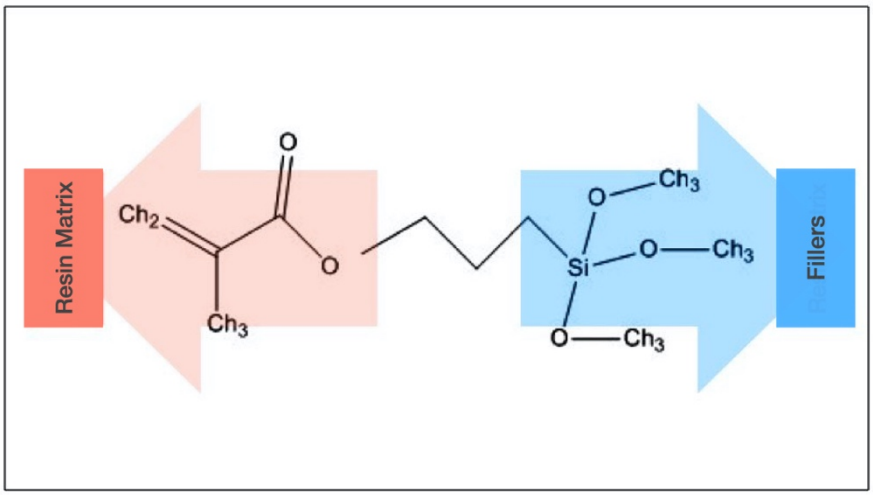

Figure 1.9: The chemical structure of the silane coupling agent, 3 Methacryloxypropyltrimethoxysilane (MPTS)

Inhibitors and pigments

Inhibitors are reactive compounds used to prevent premature polymerization thereby ensuring chemical stability and increasing the shelf-life of the material. Butylated hydroxytoluene (BHT) and monomethyl ether of hydroquinone (MEHQ) are common phenolic compounds used as inhibitors [57]. Pigments in resin composites are metallic oxides incorporated into the resin composite to simulate the color of natural teeth. With different types and concentrations of metallic oxides, multiple distinct shades can be achieved to duplicate different dental shades [58].

1.3 Resin composite classification

Resin composite materials can be classified in different ways, based on their clinical application, monomer system, consistency or by filler size. One classic grouping, by Lutz and Philips [59], is by the size of the reinforcing fillers: macrofill, microfill, nanofill or hybrids (**Figure 1.10**).

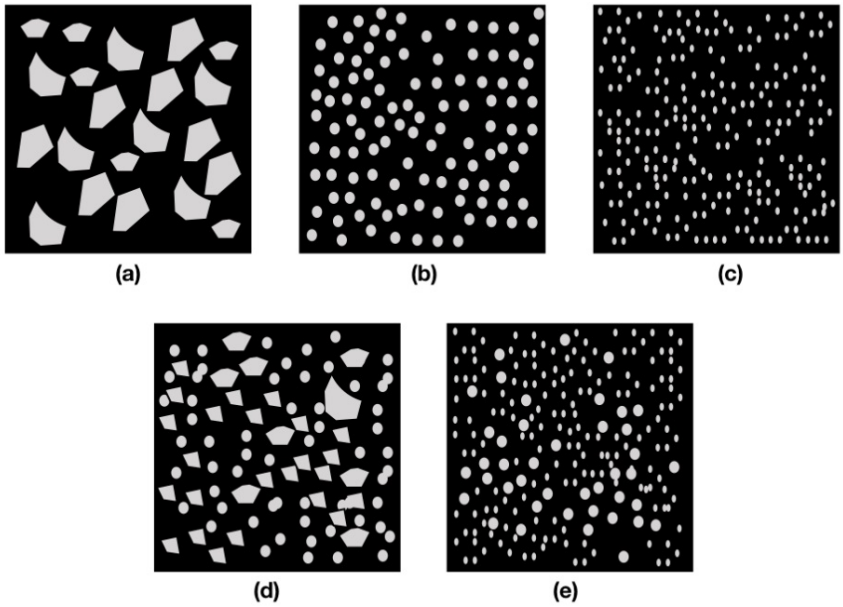

Figure 1.10: Resin composites classification based on filler particles: (a) Macrofilled; (b) Microfilled; (c) Nanofilled; (d) Microhybrid; (e) Nanohybrid.

Macrofilled resin composite

Macrofilled resin composites were the first form of filler-reinforced resin composite restoration, which was introduced in 1950s [60]. Using glass, ceramic or quartz particles crushed into 10-50 μm average size fillers (**Figure 1.10**). Their mechanical properties were generally good however, serious issues with wear, polishability and long-term esthetic outcome severely limited their use.

Microfilled resin composite

These types of materials were developed to overcome the esthetic shortcomings of macrofills (**Figure 1.10**). They displayed an excellent polishability and long term gloss

retention due to low filler content (30-60 wt%) and the small 40-50 nm average size fillers [61]. However, their mechanical properties are inferior to the other resin composites with almost 50% higher failure rate than hybrid composites [62]. Therefore, microfill resin composites are considered contraindicated in stress-bearing areas and their application should be restricted to certain esthetic and non-functional areas [60].

Nanofilled resin composite

The incorporation of nano-sized particles to resin formulations has led to new materials with some enhanced properties. With advanced production methods, average particle sizes of 5-100 nm can be controlled using pyrolysis or sol-gel processes (**Figure 1.10**) [50, 61]. Particles this small can aid in increasing the filler load up to 90% by weight- if needed - as well as enhancing the optical properties of the resin composite materials [52]. The challenge is in silanating these nano-sized fillers, as the cumulative surface area of the dispersed fillers is very large. Therefore, the proportions of matrix-dispersed nano-fillers are severely limited.

Hybrid resin composite

The incorporation of various sizes of fillers in resin composite material can result in good esthetic properties as well as superior mechanical performance. The fillers in hybrid resin composite are generally between 40 nm to 10-50 μm (**Figure 1.11**) [61]. Therefore, hybrid resin composites are sub-grouped based on the range of size difference into:

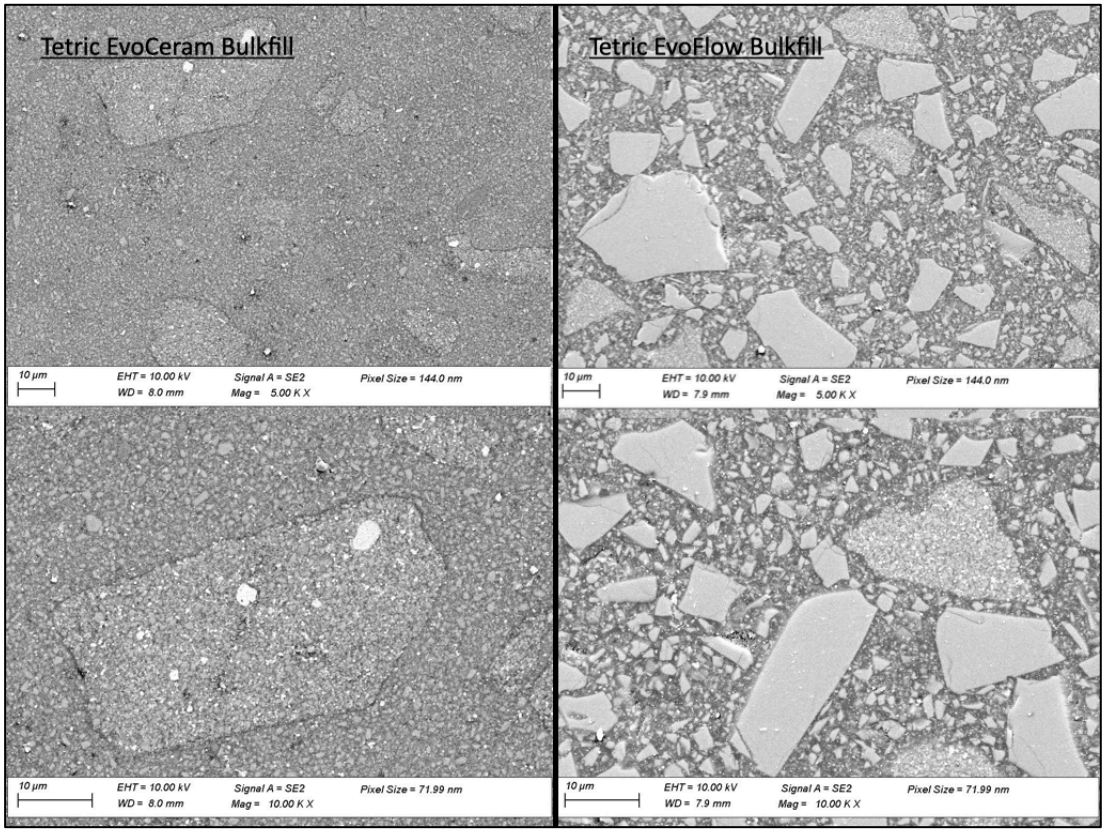

Figure 1.11: Scanning electron microscopy (SEM) images obtained in back scattered electron mode (x5 k,10 k) of hybrid composites

Microhybrid resin composites

This subgroup became one preferred for anterior restorations. The combination of good esthetic results with good mechanical properties were facilitated by the utilization of 40 nm- 20 µm filler size range (**Figure 1.11**).

Nanohybrid resin composites

The higher filler load was achieved using controlled-size nano particles which promoted an improvement in physical and mechanical properties. Smaller particles of 5 nm - 1 µm size are used in the form of either non-agglomerated, agglomerated or nano-clustered fillers (**Figure 1.11**) [50, 61].

A recent proposal for resin-composite classification

Many classifications of resin composites have been based on particle sizes and their distributions. But these type of classifications can be ambiguous. Some manufacturers

used the label ‘nanofilled composite’ with the trend of nano technology. Fillers used were even the same, but the scale used changed from um to nm.

There is no strong correlation between ‘particle size’ classifications and the material’s mechanical properties. Randolph *et al* 2018, proposed to focus on filler content, which is better suited for classification, being correlated with the flexural modulus and solvent sorption of the material. The motive was to have an informative classification that is predictive of such properties, that can help practitioners in choosing suitable materials [14, 39, 63].

This classification approach considered two intrinsic factors:

- The (reinforcing) filler volume;
- Handling behavior: thixotropy and the tendency to shear thinning or thickening.

The suggested classifications were as follow[14]:

(i) Ultra-low fill resin composite (< 50 vol%)

(ii) Low-fill resin composite (50 -74 vol%)

(iii) Compact resin composite (> 74 vol%)

1.4 Polymerization reaction

The polymerization reaction in dental resin-composites is a complex phenomenon. It consists of a series of chemical reactions resulting in a cross-liked polymer network incorporating dispersed filler particles. Two main types of polymerization may be utilized in dental resin composites or in other materials used in dentistry. These are Addition *versus* Step-Growth (or Condensation) polymerization.

The first and most common reaction mechanism is *addition* polymerization: normally via free radical **(FR** or **R***) addition polymerization of carbon/carbon (**C=C**) double bonds, within the monomer - which become linked (to form polymer chains) by single **C-C** covalent bonds. (Ring-opening polymerization is another– rare – possibility).

Reaction begins by ***activation*** (production) of free radicals (chemical species with unpaired electrons: **R***). This can occur by either (i) mixing and reaction of two components ('chemical' activation); (ii) photo-initiation (using visible light irradiation of a photo-initiator system); or (iii) by heating a formulation containing (e.g.) benzoyl peroxide, which splits into two free radicals at 60 ^{o}C.

This leads to the ***Initiation*** phase, where free-radicals react, by addition, to C=C groups in monomer molecules forming strong covalent bonds *and* residual unpaired electrons (R*) within the resultant molecular structure: M+R*.

Propagation, is the continuation of this process through reaction of M+R* species with further **C=C** groups in other monomer molecules, forming M+M+R*, etc. Ideally, this process could continue to produce complete 100% 'conversion' of **C=C** bonds into **C-C** linked polymeric chains.

However, normally the process is halted by ***Termination*** reactions, which can be of different varieties. These include a *combination reaction* (where two free radicals react with each other – and thereby self-annihilate *as free-radicals*, becoming incapable of further reaction). (**Figure 1.12**) [17, 64].

More generally, with dimethacrylate monomers – containing two C=C groups – one at each 'end' of the molecule, polymerization leads to *crosslinking* between polymer chains and formation of a 3-D polymer matrix **network**. When the *degree of conversion* (**DC**) of **C=C** groups exceeds 50 % the physical state of the system has passed from an initial *fluid* state, via a *gelation* state (rubbery state) to *vitrification*

(formation of a solid *glassy* state). Throughout this polymerization (or 'cure') process, it becomes progressively self-limiting, so the internal viscosity of the system increases exponentially. Polymeric chains become mutually trapped, preventing translational movement. Only slow segmental movement is possible. Thus, beyond 50-60 % the **DC** can only increase very slightly and increasingly slowly.

The second polymerization reaction is the *condensation* polymerization reaction. This type of polymerization involves replacing some molecules upon reaction and usually results in by-products. The polymerization reaction goes through three important steps: *initiation, propagation* and *termination*. [65, 66].

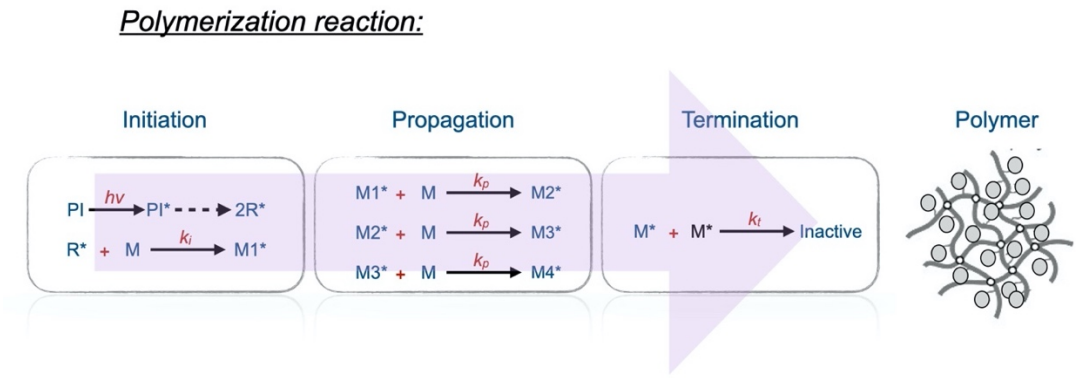

Figure 1.12: Free-radical polymerization: successive steps.

'Chemical'-polymerized

Early resin composite products used a two paste system. One contains the *initiator* (Benzoyl peroxide) and the other contains the *accelerator,* tertiary aromatic amine (mostly N, N-bis (2- hydroxyethyl)-p-toluidine). The two pastes would be dispensed equally and mixed before application [67]. Currently, chemically-polymerized resins are mainly used as a core build-up material, root canal filling materials or resin cements.

Photo-polymerized

The development of current light-activated resin composites was to overcome challenges associated with the chemically-polymerized ones. They required mixing,

had short working times and a limited shelf-life. These deficiencies were removed following the introduction of photo-polymerized single paste resin composites. These incorporated a photoinitiator system to initiate the polymerization reaction. The original and still the most common photoinitiator system is ***camphoroquinone*** (CQ) and its co-initiator, a ***tertiary*** **amine** - such as dimethylaminoethylmethacrylate (DMAEMA). This system requires a light source delivering wavelengths ranging from **450-475** nm (**Figure 1.13**) [68]. The CQ initiator absorbs photons of this blue wavelength range and, in the resultant excited state, reacts with the co-initiator to produce free radicals. The optimal concentration of CQ/amine ranges between 0.4 and 1.6 wt%, where higher concentrations have been shown to produce sub-optimal degree of conversion and hardness [69, 70].

CQ photoinitiator reacts when exposed to visible light due to the α-diketone group in CQ. This has a peak absorption in the visible blue range. A consequence of absorbing blue light is that the compound is yellow, which affects the possible shades that can be produced of resin composites. Moreover, residual amine co-initiator can affect color stability. Several alternative photoinitiators (**PI**s), have been explored to try to overcome some of these drawbacks. These PIs include Lucirin (TPO), 1-phenyl-1, 2-propanedione (PPD), Irgacure 819, p-octyloxyphenyl-phenyl iodonium hexafluoroantimonate (OPPI) and 9-anthracene (BAPO) [71, 72].

Lucirin (TPO) photoinitiator has been used in white or bleached shade resin composite. TPO may produce a higher degree of conversion compared to the CQ system [73]. Its absorption spectrum ranges between **380-425** nm (FIGURE **1.13**). Another photoinitiator, PPD, has a wide spectral absorption range from **350-490** (**Figure 1.13**) [71].

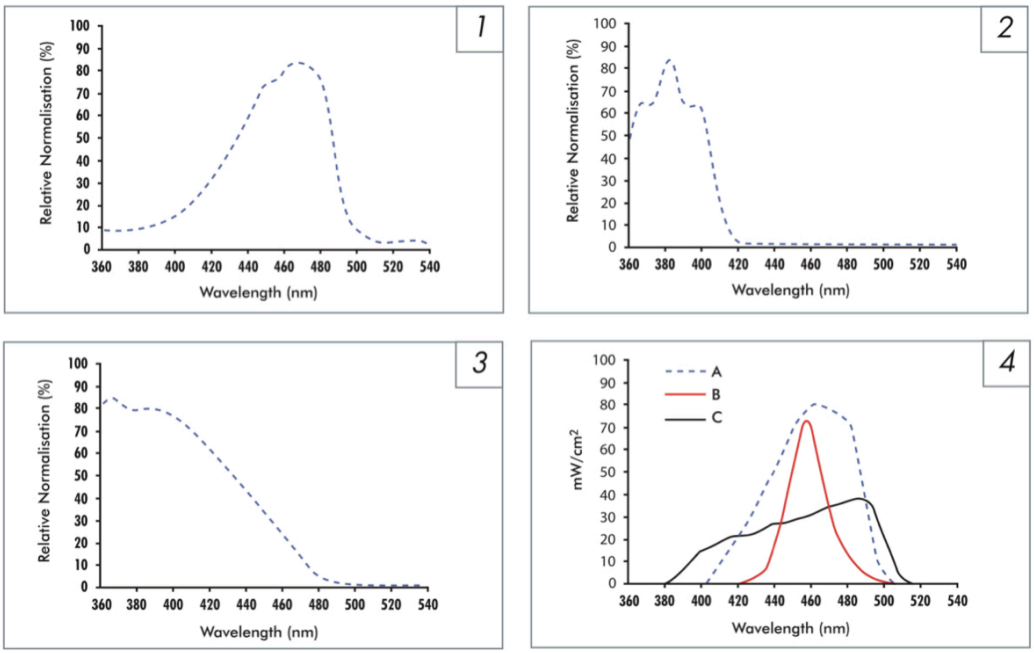

Figure 1.13: Illustration of absorption spectrum of: CQ (1); Lucirin TPO (2); PPD (3); [CQ (A) superimposed by light output of LED (B) and QHT(C) light curing unites] (4). [71]

The efficacy of the photopolymerization is controlled by many aspects. Operator-controlled factors are paramount. For instance, the shade selected, increment thickness, irradiance, polymerization time, curing tip distance/angulation and/or the curing protocols all must be considered to achieve a successful restoration [71, 74, 75]. Therefore, special care must be taken by dentists to understand the composition and requirements of their materials. Failure to consider these factors can possibly lead to placement of compromised restorations [71, 74, 75].

Light Curing units

LCUs for dentistry normally deliver light from the blue region of the visible spectrum that corresponds to the wavelength range over which incorporated photoinitiator(s) can absorb energy. Light curing units were initially developed in the 1970s. Since then, different types and designs have been produced.

Quartz Tungsten Halogen (QTH) was the light-bulb technology used in the first dental LCUs. They were considered to be the standard curing device for several years. Inherently, they produce broad-spectrum white and infra-red light, but filtration delivers an output range between 370-550 nm. However, a long polymerization time (40 – 60 s) was required to achieve sufficient polymerization. Also, a significant reduction in curing efficiency occurred after only 100 hours of use (due to light bulb degradation by heat generation) [76].

Plasma Arc Curing (PAC) devices were developed to reduce the polymerization time. They emit light through glowing plasma gas generated in a mixture of ionized molecules (e.g., xenon, argon). Their high irradiance, but narrow range (470 nm), enabled their manufacturers to claim the sufficiency of a 3 s curing time. However, this has been disputed and the current recommendation is to cure for (3 x 3) seconds [76].

Argon-ion Lasers (AL) emit a very high output of blue-green light with 450-500 nm. However diverse results were reported of their efficiency in rapid curing [76].

Light Emitting Diodes (LED) are the most recent type of light curing unit. These use junctions of doped Gallium nitride semiconductors to generate light with a specific band width. The development of efficient blue LEDs required three decades of advancements. But now, current LEDs can serve for several thousand hours before significant reduction in light output.

The dental application of blue-LEDs was shown to be possible by Mills, Jandt and Ashworth in 1999, however the radiant emittance of the early LEDs were relatively low [77]. Since a blue light source of sufficient radiant emittance was the pre-requisite for LCUs to excite CQ photoinitiator, further development of high irradiance single LED chips enabled high-irradiance.

A third generation (polywave-emission) LED-LCU outputs a wide range of blue and violet light. This was introduced to cover the peak absorption range of alternative

photoinitiators (e.g., TPO and Ivocerin) in the violet range. They produce two or more distinct emission bands via two LED chips - of either 470 nm (blue) or 410 nm (violet) peak-spectral output. This multiple spectrum covers both CQ absorption spectrum as well as the main alternative photoinitiators [78, 79].

Early LED LCUs -like most QTH- were initially limited by the irradiance they can produce. An average QTH LCU produce 400 to 500 mW/cm2 irradiance, therefore an extended curing time up to 40s to 60 s were justified[80]. However, early LEDs were unable to produce high radiant flux, but the radiant flux in the blue spectrum (450–470 nm) provides much more output within this area compared to QTH LCUs [81, 82]. This enabled similar resin composite curing in shorter time [83]. Therefore, further developments in LED technology have enabled great increase in output power to achieve high irradiance to facilitate shorter curing time [83].

Dual-polymerized

In some clinical situations, where the location or depth of the cavity might prevent light from transmitting throughout the depth of the material, a hybrid mix of the two polymerization systems was suggested. These composites consist of a two paste system: base and catalyst. One paste contains CQ photoinitiator and the other contains benzoyl peroxide/ BPO chemical initiator, with co-initiator tertiary aromatic amine N, N-bis (2- hydroxyethyl)-p-toluidine. A slow rate of chemical polymerization occurs initially then the reaction is supplemented with light energy to start photo-polymerization to boost the polymerization rate. [57, 60].

1.5 Recent advances in resin composites

Developments in resin matrices

Polymeric materials are involved in every aspect of dentistry. The constant demands from practitioners for materials that are easy to use, have few clinical steps and are durable have kept the R&D departments of dental material manufacturers very busy. Specifically, and more realistically, resin composite materials have been significantly improved since their introduction, but still have some way to go to satisfy all those demands. This is due to their complex composition and the many factors that are involved in their durability. Also, the clinical evaluation period required to challenge such new materials is too long to evaluate their failure - if they fail. For example, following the development of an alternative (non-dimethacrylate) Silorane composite (Filtek LS, 3M ESPE St Paul, USA) it was withdrawn from the market some years after its introduction.

Bulk-fill resin composites

Bulk-fill resin composites have gained popularity in the past decade by requiring fewer working steps and showing good clinical results [84, 85]. These materials have shown an adequate depth of cure enabling bulk filling of cavities up to 4 mm [86]. This was achieved through different approaches severally or in combination, including: (i) modification of the photoinitiator systems by either increasing the concentration or by using novel systems as an alternative or booster; (ii) decreasing the filler load; (iii) using larger fillers; (iv) modifying the resin matrix composition and/or refractive indices of the material; (v) reducing the viscosity of the resin paste by sonification or thermal activation [87-89].

Rapid photo-polymerization

The first photo-cured dental resin-composites required an irradiation time of t = 60 s. Subsequent developments have enabled irradiation times to be reduced to10 s for most current products. This was facilitated by the advancements in polymer chemistry and photoinitiation systems. Manufacturers have produced resin composite products that allow for efficient and fast photopolymerization, without compromising their physical and mechanical properties. For example, Tokuyama resin composites (Tokuyama Dental Corporation, Japan) adapted *Rapid Amplified Photo-polymerization* technology

(***RAP***) to reduce the amount of photoinitiators and polymerization time (1/3 compared to conventional). The CQ photoinitiator found in their resin composites gets recycled within the reaction, leading to a single CQ molecule producing multiple radicals. The excited CQ initiator produces the radicals, then goes back to ground state which can be excited again as a cycle (according to the manufacturer's report).

Another recent advance in photo-polymerization is the utilization of Germanium-based photoinitiator chemistry. These photoinitiators, specifically ***Ivocerin*** (Ivoclar Vivadent AG, Liechtenstein), have shown strong light absorption. This patented photoinitiator is one of the constituents in any photo-polymerized resin composite products of Ivoclar. Furthermore, a newly developed resin composite system by Ivoclar enabled the concept of ultra-rapid-cure. This was facilitated by (i) refinements of the photoinitiator system and (ii) boosting the irradiance of the LCUs. This Ivoclar system, PowerCure system, comprises an advanced Bluephase PowerCure LED-LCU able to deliver 3050 mW/cm^2 for 3 s irradiation and two specially formulated composites: PowerFill and PowerFlow. PowerFill contains addition-fragmentation chain transfer (AFCT) reagent incorporation with the aim of inducing a more homogenous network, thus improved conversion with controlled shrinkage stress [90, 91].

Ultra-rapid polymerization-TPO photoinitiator

A major challenge in recent years to obtain a restorative system that can produce an improved conversion in shorter curing time. Yet if the resultant DC is not sufficient, the mechanical properties and physical stability of the restoration might be compromised. One previous approach to explore the possibility of ultra-fast photopolymerization were by the replacement of Norrish Type II photoinitiators with Type I [92]. Photoinitiations like monoacylphosphine oxide photoinitiator (Lucirin-TPO) and phenylbis (2,4,6-trimethylbenzoyl) phosphine oxide (MAPO) were investigated for possible future replacement of the CQ/amine photoinitiator system. Monoacylphosphine oxides have higher molar absorptivity compared with CQ, as well as high reactivity. TPO molecules can cleave into two active radicals due to their greater quantum yield efficiency, compared to the CQ molecule which only yields one active radical [92, 93]. High DC results were seen even with 1 s irradiation of 1 W/cm^2 Irradiance [94].

As a result, significantly higher DC was achieved using TPO-based resin composites compared to CQ-based ones, even in a shorter curing time, due to the increased rates of polymerization enabled by TPO [94]. The rapid autoacceleration seen in TPO-based resin composite was accompanied by an early onset of gelation and somewhat delayed vitrification, however this resulted in higher stress rates compared to the CQ-controls [94, 95]. TPO-based resin composite – irradiated for a short time - produced an improved conversion and mechanical properties, with lower monomer elution when compared to CQ-based resin composite.

Addition–fragmentation chain transfer

During photopolymerization a rapid increase in the elastic modulus occurs at the stage of vitrification, where the resin-composite becomes a glassy-solid, and main-chain segmental movement is greatly restricted. A recent approach toward reducing shrinkage stress employs *covalent adaptable networks* (CANs), which are networks constructed by dynamic covalent bonds that allow the network structure to be adaptable when subjected to appropriate stimuli [96, 97]. Covalent bonds in the network dynamically break, relax, and rearrange to form new bonds once a stimulus is applied. One example of these networks is the addition–fragmentation chain transfer mechanism, which can achieve this adaptable behavior.

Reversible addition–fragmentation chain transfer (RAFT or AFCT) is a process of controlling free radical polymerization. It was invented in 1998 by a team of several researchers in Australia, and currently implemented in several areas including diagnostic applications, drug and gene delivery, tissue engineering and regenerative medicine [96].

When addition–fragmentation chain transfer (AFT) monomers are incorporated into a dimethacrylate monomers, AFT agents participate in network formation by copolymerizing with multifunctional methacrylates. This process occurs simultaneously with the photopolymerization of the AFT monomer (AFM) as well as the other methacrylate monomers leading to polymer stress relaxation through network reconfiguration [96, 97]. Moreover, AFCT addition has shown to reduce shrinkage and shrinkage stress development due to polymerization-induced phase separation- as a part of step growth photo- polymerization reactions.

When AFCT agents are incorporated in dimethacrylate monomers, the excited free radicals can potentially attack either (i) C=C bonds in methacrylate monomer, which results in methacrylate addition; or (ii) C=C bonds of AFCT monomer (e.g. a β-allyl sulfone), resulting in chain transfer. The growing radical chain (in the case of chain transfer) is terminated by the formation of an intermediate radical which undergoes fragmentation to form a sulfonyl radical as well as a new double bond. The resultant multiple shorter chains can lead -in principle- to a more homogenous network and delayed gel point compared to conventional radical long-chain network [90, 98].

AFCT monomers incorporated into the Bis-GMA/ TEGDMA system in different concentration have shown a progressive reduction in DC and DC rates. This is due to the production of radical species with higher stability in acrylate and methacrylate networks. However, reductions in DC corresponded to reductions in shrinkage stress [97].

Self-adhesive resin composites

Self-adhesive resin composites were recently introduced to reduce clinical steps. They contains self-etching monomers such as glycol phosphate dimethacrylate [88]. Some promising results were obtained in bonding to both mineralized and demineralized tooth structure [88]. A study by Sampaio *et al* (2017), showed comparable polymerization shrinkage to both conventional and some bulk-fill resin composites [99]. However, the high susceptibility to hydrolytic degradation remains a major concern to be addressed [88].

Antimicrobial resin composites

The use of antibacterial agents in restorative materials was rationalized because the most common failure mode is recurrent caries [8, 100, 101]. This supported the development of resin composite restoration that has both bactericidal and antifouling (inhibit bacterial adhesion) effects [88]. Materials such as Quaternary ammonium methacrylates (QAMs), methacryloxylethylcetyl ammonium chloride (DMAE-CB), Dimethylaminododecyl methacrylate (DMAHDM) and bis (2-methacryloyloxyethyl) dimethylammonium bromide (QADM) were added to resin composites, and have shown promising antibacterial effects, with comparable mechanical properties to conventional resin composites [88, 102]. While these materials are showing positive antibacterial effects on the surface of the restoration, unreacted monomers leaching

out in the oral environment could lead to cytotoxicity and further research is needed [88].

Stress-reduction

The stability of resin composite starts with surviving initial polymerization stresses. The challenge is to achieve high degree of conversion with minimum shrinkage stresses. Cramer *et al,* assessed thiol-ene–methacrylate systems as the resin phase [103]. Thiol-ene-based monomers undergo an altered polymerization process, utilizing radical-mediated step-growth (condensation) reaction as an alternative to a chain-growth (addition) process [88, 103]. However, when combined with methacrylate monomer, an additional carbon radical propagation step is seen to lead to a combined system (both step-growth and chain-growth) [103].

Thiol-ene systems offers several advantages when used in dental restorative materials. They display fast polymerization with a high conversion rate prior to any vitrification. This decreases the polymerization shrinkage, shrinkage stress and the quantity of unreacted monomers [103, 104]. Thiol-ene monomers are not affected by oxygen and therefore do not show a surface inhibited layer. Two main drawbacks associated with this system: the strong sulphur odor and short shelf live [103]. Bacchi *et al,* studied the use of high molecular mass pre-polymerized thio-urithane oligomer added to Bis-GMA: TEGDMA methacrylate monomer (70:30 wt%) up to 20 wt%. A significant increase of degree of conversion with 20 wt% added oligomers was reported. There was almost twofold increase in fracture toughness (K_{IC}) when 20 wt% of oligomers were added in comparison to control groups. With the addition of 20 wt% oligomers, the polymerization shrinkage stress also showed a significant reduction being 44% lower than control group [104].

Self-healing composites

Continuous masticatory forces exerted on resin composite restorations can lead to microcracks within the restorations, which could result in bulk fracture. This self-healing concept was introduced to increase the service live of dental restorations. The idea was based on a healing monomer and catalyst both being encapsulated within the material. Once the crack propagated cleaving internal capsules, fast self-healing monomers is then activated and initiates chemical polymerization to seal the microcrack and prevent further propagation [88, 105, 106].

Developments in filler particle systems

The main purpose of filler particle addition was to reinforce resin composites, but researchers are now exploring ways to expand their functions. With nano technology, a new era of potential advancements arose [107]. Some nanoparticles were found to have an antimicrobial effect such as zirconia (ZrO_2), titanium (TiO_2) and silver (Ag) [108]. Besinis *et al,* have shown that a formulation containing Ag nanoparticles was superior to other dental disinfectants against *streptococcus mutans* [109]. Furthermore, an experimental resin composite containing Ag nanoparticles showed similar mechanical properties compared to a commercial resin composite, with additional antibacterial effects [110]. Other nanoparticles were proposed to be effective in reinforcement and remineralization of tooth structure such as nano sized hydroxyapatite, amorphous calcium phosphate, tetracalcium phosphate, carbon, zirconia and silica [107, 108]. Fiber reinforcement is another development in toughening resin composites. Different fibers, with varied sizes, were introduced to dental restorative materials such as carbon, polyethylene, glass and hydroxyapatite [14]. Fiber reinforced resin composites showed some improved physical and mechanical properties compared to particle-based composites, but with rough surfaces and poor wear resistance and usually poor esthetics [14, 111].

1.6 Resin composite properties

The predicted performance of resin composite restorations depends on several vital and complicated factors. Clinical studies are favored in terms of evidence, however their complex study designs require standardization, the time required to obtain long-term evidence is extensive and there is variability in operator skills, procedures and evaluation criteria.

As a result, standardized properties were identified to be evaluated via laboratory studies to predict at least some aspects of material performance. The *Academy of Dental Materials* has published two papers critically appraising in-*vitro* evaluation methods for resin composites. These serve as guidelines by experts on the most important properties and their measurement methods, as supported by the literature [112, 113]. Several positive correlations were found between laboratory properties and clinical performance [7, 13]. For instance, both fracture toughness and flexural strength have shown to be correlated with bulk fracture and wear, respectively [7, 13].

Early-stage resin composite properties are classified in this section (**Figure 1.14**).

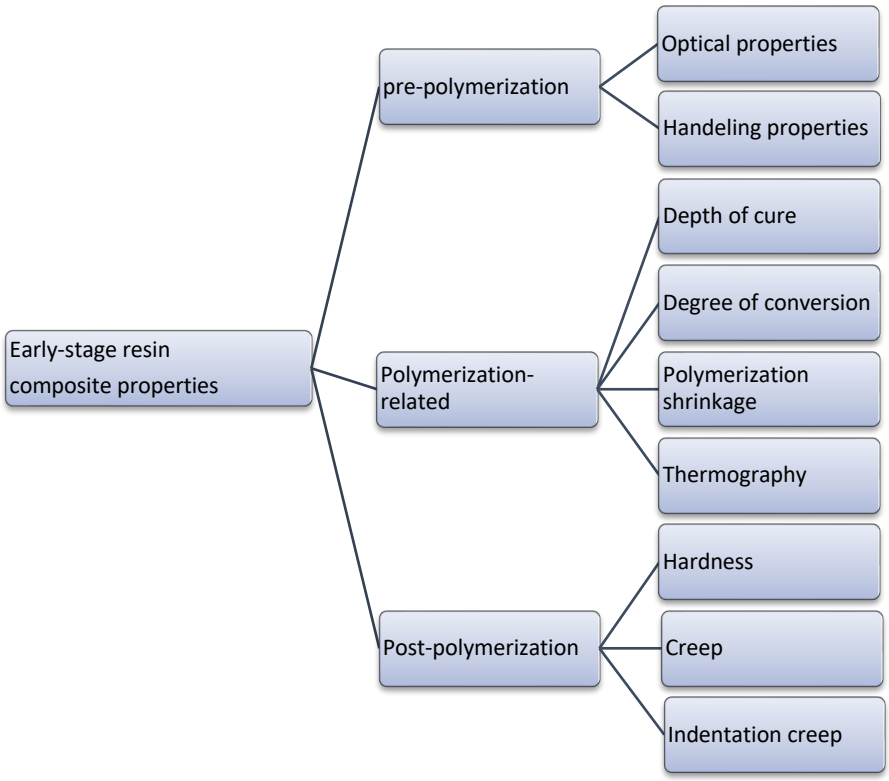

Figure 1.14: Outline of some key early-stage resin composite properties

Pre-Polymerization properties

Optical properties

Resin composite optical properties directly influence their photo-polymerization as well as their esthetic results. They affect the amount of light transmission and the ability to match the natural tooth structure, based on shade, opacity and lightness. Human eyes perceive colors when a white light is either reflected or transmitted through the object [114]. To evaluate the shade, all three elements of color (value, chroma, hue) must be considered.

As the light passes through resin composites, the light waves will undergo transmission, absorption or scattering processes. This will directly affect the depth-of-cure (DoC) as light irradiance drops upon propagation through liquid or solid media. Attenuation of light irradiance *by absorption* - and equivalent parameters such as translucency - are heavily influenced by the light wavelength, material-increment, composition and shade [115]. The behavior is expressed by the Beer-Lambert law. Light *scattering* depends upon two main factors: (i) the difference in refractive index between filler particles and matrix; and (ii) the particle size of the fillers, but this relationship is complex. However, particles with diameters much less than the wavelength of light do not change the light path.

The refractive index (RI) is the ratio of the velocity of light in air (vacuum) to the velocity in the material. Once the light hits the surface, the speed reduces and the direction changes. The RI of vacuum space is 0, for water 1.333 and for enamel 1.655. To translate this (other things being equal), “matched refractive indices result in a transparent solid, whereas large differences result in opaque materials” [114]. For example, the closer the RI between monomers and fillers the more light is transmitted across the increment thus higher depth of cure. Factors affecting the refractive index of resin composites includes the structure of resin matrix used, the molecular mass and the polarizability [112]. There are several ways to determine the refractive indices. However, the RI needs to be measured to an accuracy of at least 3 decimal places. One method, based of ISO 489:1999 standard, uses an Abbe refractometer [116, 117]. However, this is unsuitable for measuring the refractive index of a material in powder form.

Handling properties

The stickiness and difficulty in packing of resin composite materials are two main clinical-handling challenges [118]. One method to evaluate the stickiness is by measuring the "Composite flag" resulted from a flag-shaped metal instrument tip applied on uncured specimen with 350 g force then pulled out slowly and cured upon separation [112].

Another important property to consider is the viscosity, defined as the measure of a liquid's resistance to forces that cause it to flow [119, 120]. It is affected by intrinsic (properties of the fillers and resin matrix used) and extrinsic factors (e.g. surrounding temperature) [121]. One widely used method to evaluate the viscosity is by parallel-plate rheometer under rotational shear [112].

Polymerization-related properties

Depth of cure

As light transmits through a resin composite, it attenuates through the thickness with reduced amount of energy delivered to the bottom of the cavity, following the Beer-Lambert Law. The depth of cure (DoC) is a major characteristic of resin composite materials, defined as "the maximum thickness of a composite that can be adequately cured in a single layer". More accurately defined as "maximum thickness that should be used for each successive RBC increment – as the depth at which the resin matrix switches from a glassy to a rubbery state" [122]. Thus, it determines how much thickness of an increment should be applied in a single layer [122]. Therefore, a long irradiation time was often considered crucial in delivering sufficient photons to lower thicknesses (irradiation time ≈ 40 s). Improvements in radiant exitance of LCUs reduced irradiation times to 20 s. However, DoC was not improved significantly as light attenuation is influenced by several factors such the type of monomers used, refractive indexes of both monomers and fillers, type and concentration of the photoinitiator system used, shade and opacity of the resin composites and the size and load of fillers. These all affect the way light is absorbed and/or scatters within the resin composite [93, 114].

Bulkfill resin composites was introduced during the past 15 years, and this is one of the main advances in resin composites in the 21st century. Achieving 4 mm DoC was possible by implementing different approaches to modify chemical structure of the resin composites: (i) by modifying filler, either by reducing filler load or by using larger filler size [123]; (ii) using monomers and fillers with matching refractive indexes, thus more light transmission; (iii) using more reactive and efficient photoinitiator systems [86, 124].

Depth of cure can be evaluated by several methods, such as the very crude scraping test (based on ISO standard 4049). Microhardness can also be used to evaluate DoC by comparing top to bottom hardness values or - better - by hardness profile measurements [112, 125]. Different spectroscopy measurements can also evaluate depth of cure, by measuring DC at different thicknesses [93, 112]. Another method that takes into account the glassy to rubbery transition depth using electron

paramagnetic imaging (EPR), differential scanning calorimetry (DSC) and atomic force microscopy (AFM) [122].

Degree of conversion

The durability of resin composite restorations is highly dependent on specific polymerization-related parameters such as the degree of conversion (DC). DC expresses the efficiency of polymerization as the quantity of crosslinked (reacted) methacrylate groups. For direct resin composites, DC generally ranges between 40-75% following photopolymerization, which continues significantly for 24 h [126, 127], and can go for 7 days post-irradiation or longer [128].

As explained above, in section 1.1.4, the photopolymerization of direct resin composites does not produce a DC anywhere approaching 100%. This is due to the chemistry of dimethacrylates [129, 130]. At the end of the propagation phase of polymerization, the maximum rate of polymerization (RP_{max}) is reached in around 5-20% DC, which coincides with increased viscosity [17, 131]. Beyond this point, restriction to molecular mobility, as a result of the network vitrification, prevent further network development and significantly decreases reaction speed. Hence, a number of C=C groups remains unreacted [131, 132]. Other factors also preventing 100% DC include the concentration and distribution of photoinitiators in the material and oxygen presence at the surface [131, 133]. The unreacted monomers of commercial resin composites range between 23-48% which can cause physical and mechanical instability as well as cytotoxicity upon elution [129, 134].

A material with high DC essentially means more resistance to monomer elution, which could improve its mechanical properties, dimensional stability and biocompatibility [29, 129]. For a given formulation, increased DC leads generally to higher surface and bulk properties [134, 135]. However, excessively high DC is also associated with increased polymerization shrinkage and shrinkage stress [136].

The DC is affected by monomer composition, type and concentration of photo-initiators, type and load of fillers, light exposure time, irradiance and finally surrounding temperature [93, 137, 138]. DC can be evaluated by direct or indirect methods. Indirect evaluation of DC can be through dilatometry or via optical properties associated with polymerization, elastic modulus development or surface hardness [112, 139]. However, indirect evaluation should only be considered as an estimation

of DC. Direct evaluation enables real-time measurement of the polymerization reaction. Several methods are available: Mid-IR, Near-IR and Raman spectroscopies as well as differential scanning calorimetry (DSC) [112].

The most commonly used method for DC is Fourier transform infrared (FTIR) spectroscopy. This uses electromagnetic radiation in the mid-IR spectrum (~4000–400 cm^{-1}) that interacts with vibrations of molecular groups. With most resin composites, FTIR compares the distinctive absorbance bands associated with both aliphatic carbon/carbon double bond (C=C) at 1,638 cm^{-1} and the C=C associated with the aromatic ring 1,608 cm^{-1} in dimethacrylate monomers, before and after polymerization [93, 112, 130]. The aromatic C=C peak (1,608 cm^{-1}) in dimethacrylate monomers such as Bis-GMA is used as an internal reference to calculate DC. The aliphatic C=C stretching peak (at 1,638 cm^{-1}), is proportional to the changing C=C concentration. Thus, the relative change in peak height (or area) permits calculation of DC.

Polymerization shrinkage and shrinkage stress

Polymerization reaction of dimethacrylates produces randomly cross-linked polymer, with a high density of cross-links. During reaction, the intermolecular spaces significantly reduce from 0.4 nm to 0.15 nm producing stronger and shorter intramolecular covalent bonds. As a result, this densely packed polymer undergoes progressive molecular densification which is manifest at the bulk level as polymerization shrinkage (PS) [20, 140-142]. The reported volumetric shrinkage was 5.2% for Bis-GMA monomer and 12.5% for TEGDMA. However, the shrinkage magnitudes of filled composites are lower (2-3 %) because a major part of the volume consist of non-shrinking fillers [143].

The clinical importance of such shrinkage is that volumetric shrinkage is associated with shrinkage stresses (SS). While volumetric shrinkage is a material property, shrinkage stress is not since it depends on the quantity (mass or volume) of the material *and its local constraint* (proportion of bonded walls and their compliance) within a cavity [144-146]. During radical cross-linking, the increase in stiffness from sol to gel stage and finally to a glassy rigid structure causes build-up of internal stresses. These stresses, when transmitted to cavity walls via adhesive bonding, can exert stresses up to 23 MPa which can lead to cuspal deflection, enamel micro-fractures, microleakage and possibly secondary caries [147-150].

In general, polymerization shrinkage is affected by the material's composition, cavity and surrounding environmental conditions as well as by operator-related factors. The extent of this polymerization shrinkage is influenced by the monomer molecular mass and functionality; hence shrinkage is proportionally linked with degree of conversion [20, 141, 151]. It is also strongly affected by the non-shrinking filler load, initial viscosity, modulus of elasticity, cavity geometry and bonding condition [140-142, 144, 145, 152].

Resin-based-composites (RBCs) with low initial viscosity may develop higher double-bond conversion, thus higher post-gel shrinkage [136, 140]. Higher filler fractions proportionately reduce the volume of resin phase and thus reduces the shrinkage, for a given DC. Large spherical particles tend to reduce PS and SS [41, 42].

Cavity related factors, such as the cavity size and configuration factor (C-factor), which is the ratio of bonded to unbonded cavity surfaces, significantly affect PS [152]. A complex relationship is also reported between SS per unit mass and C- factor [153, 154]. Clinicians' understanding of composite composition and polymerization requirements is key aspect in delivering successful restorations. For instance, controlling the irradiance, distance, angulation and time of irradiation can significantly change the radiant exposure received by the material, which possibly affect their long-term performance [74, 155, 156]. Similarly, the quality of the adhesive layer, the resin composite placement technique and light irradiation protocols – all controlled by operators - can significantly affect the shrinkage and shrinkage stress [143, 152, 153].

Several strategies have been adopted to reduce polymerization shrinkage. These include altering RBC formulations, modifying application techniques or changing irradiation protocols. Some Bis-GMA-alternative monomer systems have been investigated either to replace Bis-GMA completely or added to the composition to reduce polymerization shrinkage and shrinkage stress [33, 104, 143, 157]. A ring-opening system or a long polysiloxane have also been investigated [32, 158].

Incremental and "elastic cavity wall" application techniques were suggested to reduce the cavity configuration factor (C-factor), as a cavity with high C-factor is associated with higher polymerization shrinkage stress [159]. The basis is that adding smaller increment with lower elastic modulus would increase the bonding compliance, thus a lower stress development with uniform distribution [143]. Other approaches to reduce

PS and SS were by modifying the light irradiation protocols. Pulse curing, soft start, ramped curing and pulse delay were curing methods investigated to reduce shrinkage magnitudes [160]. In theory, prolonging the pre-gel phase can promote more mobility for viscous flow and non-rigid shrinkage thus reducing the overall SS [161-163].

Volumetric shrinkage has been measured via several methods, including: the bonded disk system, optical instruments, mercury dilatometer, video imaging device, resin replicas, Archimedes method or pycnometer methods [112, 164]. A non-destructive method uses micro-computed tomography (μCT) to scan the material before and after the polymerization. The constructed 3D images can be then used to quantify and visually analyze polymerization shrinkage. The constructed 3D images in the μCT evaluation method can assess in tracing the amount and location of any volumetric changes in any timeframe, which can even be a valuable tool in analyzing pattern of degradation [152].

Polymerization shrinkage stress can be evaluated by several methods such as using a universal testing machine in a tensile load [112]. A more widely used method, the *Bioman* instrument was designed at the University of Manchester to evaluate shrinkage stresses in real time [165]. The instrument measure the stress created during the polymerization [112, 165].

Post-Polymerization properties

Hardness

Hardness is a surface property defined as "the ability of the material to resist permanent surface indentation, penetration and abrasion" [166]. The information from such measurements are considered highly relevant to a material's ability to withstand future deformation [113]. Hardness is generally measured by applying a load to a material for a specific time using an indentor with a specific geometry and then calculated by dividing the applied maximum load by the plastically deformed area. Hardness was classified as macro, micro or nano scaled - based on the indentor used and the magnitude of the applied force. Macro scale forces range between 2 N-30 KN; Micro scale below 2 N with a minimum limit of 0.2 μm indentation depth; nano scale depends on the shape of the indenter [113]. Resin composite hardness has been roughly correlated with clinical wear and abrasion, meaning that a material with lower hardness is likely to wear faster [13]. Low hardness may suggest an inferior filler-matrix

interface, [167]. Vickers and Knoop hardness are two widely used geometries for resin composite materials (ISO 6507). Vickers hardness is expressed as:

$$H = 1.854\, x \frac{F_{max}}{A}$$

Where H=hardness, F_{max}=maximum load and A=area of contact.

To measure the hardness of the material, an indentation is performed with a significantly harder material (Diamond indentor). Diamond tips with a specific geometry are used to indent the material causing an elastic and plastic deformation. The load used depends on the material with a range between a few grams to 1 kg for a few seconds of dwell time. Upon removal, the residual impression resulting from plastic deformation is measured.

The need for more sensitive evaluation of thin coated materials and localized surface surfaces in a submicron scale led to nanoindentation methods, introduced in late 1980s to overcome some limitations of microhardness. Nanoindentation has enabled the application of small controlled loads in millinewtons (mN) to probe thin surfaces at a nanometer scale (nm) with high sensitivity [168]. With resin composites, nanoindentation can generate anomalies due to possible nano-indentation of particle phases, rather than the organic matrix, due to the nano-scaled-size indentor.

Creep

Resin composites change in form from paste to solids in quite a short time, which is the reason for their complex viscoelastic behavior during and following photopolymerization. [169, 170]. Following setting (cure), upon loading below the elastic limit, resin composites deform elastically, meaning that they fully recover upon unloading. However, when a fixed stress level is applied for a long period, a viscoelastic (creep) component to deformation can be seen. Subsequently, upon stress removal (unloading), the material exhibits partial elastic recovery followed by slower viscoelastic partial recovery (**Figure 1.15**).

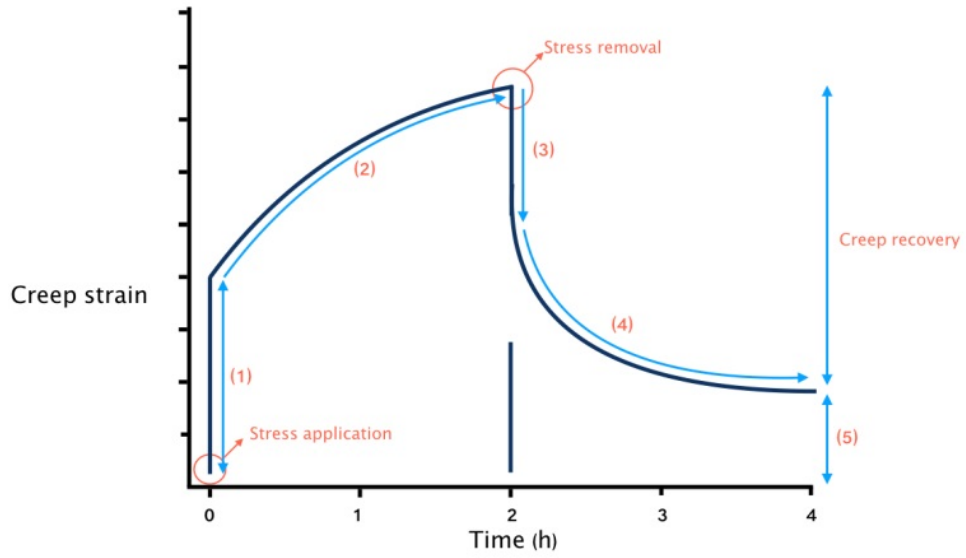

Figure 1.15: Schematic illustration of resin composite creep behavior:

(1) rapid elastic deformation; (2) viscoelastic deformation; (3) Rapid elastic recovery

(4) viscoelastic recovery; (5) permanent set.

Viscoelastic characteristics of resin composites are important for understanding and predicting their behavior under clinical loading. Creep is a time-dependent plastic strain of solid materials subjected to static or cyclic load, which reflects their viscoelastic nature [60].

In resin composites, viscoelastic recovery affords some resistance to permanent deformation upon cyclic loading during mastication. Mathematically, the dimensional changes resulted from creep is expressed as:

$$\textit{Creep strain \%} = (L_o - L_f)/ L_o \, x100$$

where L_o is the original specimen's length before loading and L_f is the specimen length after loading.

Several *modes of loading* have been used to measure creep deformation in dental materials including: indentation [171], compression [172, 173], torsion [174], bending

[175] and cantilever methods [176]. During creep measurements, specimens are subjected to a controlled load, which cause stress below their elastic limits, for a period of time (such as 2 hours), followed by unloading and monitoring the recovery for another 2 hours. The maximum creep deformation of resin composites range between 1- 6 %, and is affected by several factors including material composition, degree of conversion and environmental conditions such as temperature [172, 173].

The magnitude of deformation is highly dependent on the filler load, size and distribution [44, 173, 177, 178]. Monomer compositions and their DC influence the viscoelastic recovery of resin composites [179, 180]. The stress environment including the magnitude, stress application time, surrounding environment and temperature are all factors that also influence creep behavior [179].

Flat-punch indentation (Indentation creep)

Flat-punch, Indentation creep, is a method proposed in material science and engineering to evaluate local surface viscoelastic behavior of polymeric materials utilizing an axisymmetric indentor to load specimens [171, 181]. The name “Flat-Punch” refers to a flat-ended rod which contacts the specimens surface [181]. Indentation creep methodology has both similarities and differences from bulk compressive creep measurements.

CHAPTER TWO

General Aims and Objectives

2.1 Statement of the problem

Resin composites have improved significantly since their introduction in 1960s. Since then, resin composite became the first choice as a direct restorative materials. Their micromechanical retention to tooth enamel and the availability of dentine-bonding systems has allowed for the conservation of tooth structure, both in cavity preparation and in restoration repair. Furthermore, the enhanced working time, good handling properties and high esthetic outcomes have led to their use for both posterior and anterior restorations. Nonetheless, dentists are always looking for an efficient way to manage their practice including fast set materials, shortened clinical steps and overall economies of time and materials. This continues to motivate dental material manufacturers to produce innovative products.

With the large worldwide usage of resin composite materials [7], Kopperud *et al*. have estimated that average general dentist spends almost 57.5% of their clinical time placing restorations [9]. A cross sectional study investigating the knowledge of general dentists on the practical aspects of light-curing showed that almost 78.3% of the respondents were unaware of the irradiance of their curing lights and do not perform any sort of regular maintenance on their light-curing units [9]. Altaie *et al*, studied 233 LCUs from general dental practices and 2 dental hospitals in the UK. They reported concerning findings as more than half of the LCU-tips investigated were compromised, either damaged or contaminated, resulting in significantly low irradiance outputs [10]. This raises a concern over the quality of placed restorations as the survival of resin composites depends critically on following the polymerization requirements as well as controlling both dentist and patient related factors [8]. Under-polymerized resin composite materials are prone to fail physically and mechanically [182].

With manufacturers goal to produce materials with efficient photopolymerization and good stability in the oral environments, a new *ultra-rapid photopolymerization concept* was adopted in a bulkfill resin composite system (Ivoclar). Such composites can be cured within 3 seconds via high-irradiance photopolymerization. The argument was that 3 seconds curing can generate sufficient conversion to produce good physical and mechanical properties and at the same time - because of the short irradiation time - eliminate some operator-related errors. This was supported by the *polyvision* feature

in their LCU, where any movement of the LCU during curing will trigger an automatic turn off (within a response speed of 100 ms = 0.1 s). However, the effects of high-irradiance photo-curing is not fully understood, especially early-stage properties. This highlights the importance of developing a deeper understanding of rapid photopolymerization of resin composites and their polymerization-related properties. This will help in building future knowledge and requirements for creating durable restorative materials.

Ferracane (2013), discussed the challenges of predicting clinical performance of resin composite materials [13]. He concluded that it is still difficult to identify a level of required properties or characteristics that ensure clinical success of a new restorative material [13]. Thus, based on current knowledge on the longevity of resin composites, there are still areas of improvements to enhance clinical stability.

General aim

The aim of this research is to study photopolymerization and early-stage properties of resin composites and particularly materials with a potential for ultra-rapid photo-polymerization.

Objectives

Objectives were stated to answer clinically-based research questions (**Figure 2.1**):

Objective 1	**Can URFPBF composite achieve satisfactory DC?**
Objective 2	**What shrinkage phenomenon are exhibited by URFPBF composites?**
Objective 3	**What spatio-temporal temperature fields are generated coronally with URFPBF composites? A thermography study**
Objective 4	**Can URFPBF composites produce immediate surface viscoelastic integrity?**
Objective 5	**What are the immediate post irradiation surface viscoelastic characteristics of RBCs?**

Figure 2.1: Research questions

Therefore, the objectives were stated as follow:

(1). To evaluate the degree of conversion (DC), conversion kinetics, and the effect of a 24 h post-irradiation period on *Ultra-Rapid Photo-Polymerized BulkFill* (URPBF) composites at depths-within-specimens of 1 and 4 mm, relative to the irradiated surface.

(2). To evaluate the polymerization shrinkage (%) and shrinkage stress (MPa) characteristics of *Ultra-Rapid Photo-Polymerized BulkFill* (URPBF) composites.

(3). To investigate the effects of high-irradiance light-curing protocols on 2D temperature-rise maps during intra-dental photo-irradiation within a molar cavity restored with resin-based composites (RBCs): particularly *Ultra-Rapid Photo-Polymerized BulkFill* (URPBF) composites.

(4). To propose a novel method to evaluate *Ultra-Rapid Photo-Polymerized BulkFill* (URPBF) composite's early surface viscoelastic integrity, which involve immediate time-dependent Indentation-recovery creep measurements, with a *rigid loaded axisymmetric cylindrical flat-ended* punch, into a plane photo-polymerized composite surface.

(5). To assess the ability of indentation-creep/recovery methodology to characterize representative resin-composites from a range of manufacturers, including RBCs with varied clinical applications, immediately and after 24 h delay.

Summary outline of research project chapters can be seen below (**Figure 2.2**):

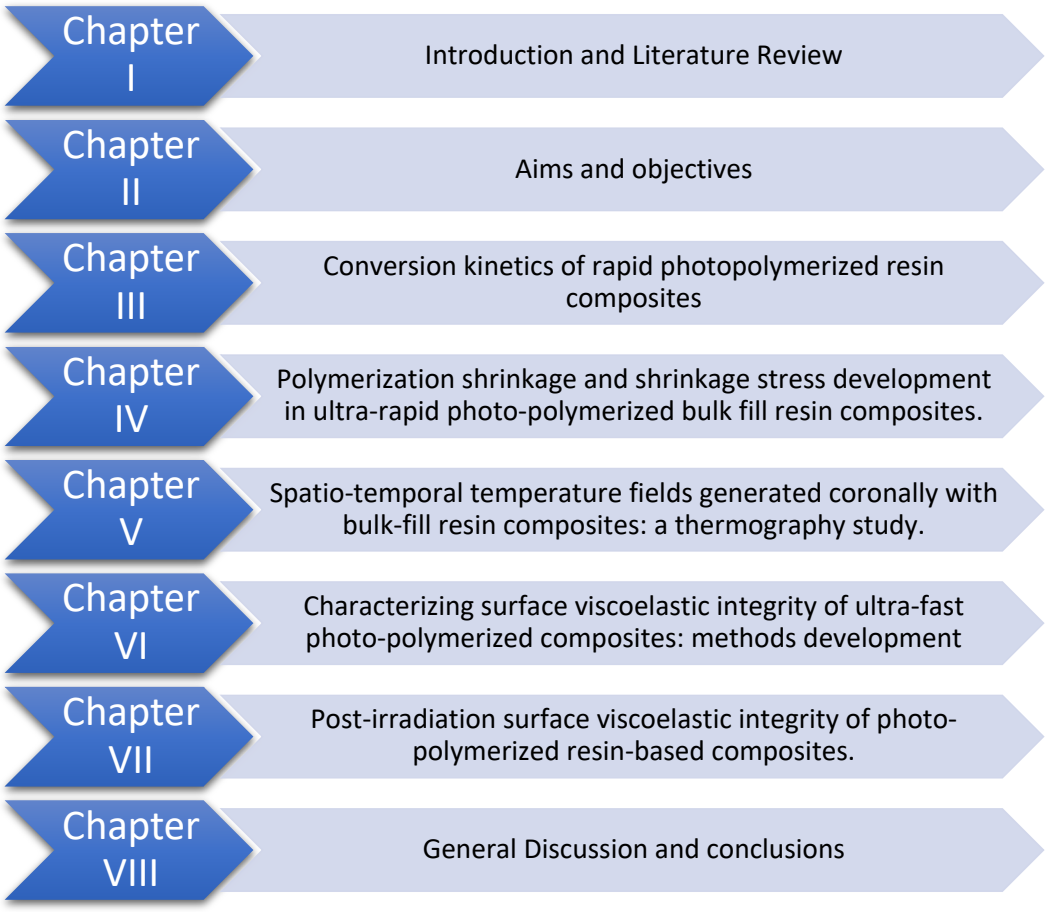

Figure 2.2: Summary outline of research project chapters.

CHAPTER THREE

Conversion kinetics of rapid photo-polymerized resin composites

Hamad Algamaiah[a,c,*], Nikolaos Silikas[a], David C Watts[a,b,**]

[a] Biomaterials Science, Division of Dentistry, School of Medical Sciences, University of Manchester, UK

[b] Photon Science Institute, University of Manchester, UK

[c] Department of Restorative Dental Science, College of Dentistry, King Saud University, Saudi Arabia

Published *in Dental Materials 36 (2020)1266–1274 (Appendix A)*

3.1 Abstract

Objective: To measure the degrees of conversion (DC), conversion kinetics, and the effect of post-irradiation time on rapid photo-polymerized bulk-fill resin composites under conditions equivalent to clinical depths of 1 and 4 mm.

Methods: 36 specimens (n=3), based on two resin composites incorporating PowerCure rapid-polymerization technology in two consistencies (PFill; PFlow) and two comparators with matching consistencies (Eceram; EFlow), were investigated from the same manufacturer (Ivoclar AG, Liechtenstein). Specimens were prepared within 4 mm diameter cylindrical molds of either 1 mm or 4 mm depths respectively, to simulate near-surface and deep locations in a bulk-fill restoration. The independent variables in this study were: materials, thickness and time. Two high irradiance polymerization protocols were utilized for PowerCure materials: 2000 and 3050 mW/cm^2 for 5 and 3 s, respectively. A standard (1200 mW/cm^2) polymerization protocol was used with control materials. FTIR was utilized to measure DC in real-time for 24 h post-irradiation. The data were analyzed using multiple *Welch's*-ANOVA, *Games-Howell post-hoc test*, kinetic dual-exponential sum function and multiple independent sample *t*-tests (p=0.05).

Results: The DC of the materials ranged between 44.7-59.0 % after 5 min, which increased after 24 h reaching 55.7 -71.0 % ($p<0.05$). Specimen thickness did not influence the overall DC. At 5 min, the highest DC was shown in EFlow. But PFlow, irradiated for 3 s and 5 s exhibited comparable results ($p>0.05$). PFill composite irradiated with the 3 s and 5 s protocols did not differ from ECeram ($p>0.05$). Specimen thickness and material viscosity affected polymerization kinetics and rate of polymerization (RP_{max}). Faster polymerization occurred in 1 mm specimens (except PFill-5s and ECeram). PFill and PFlow exhibited faster conversion than the controls. RP_{max} varied across the specimen groups between 4.3-8.8 %/s with corresponding DC $_{RPmax}$ between 22.2-45.3 %.

Significance: Polymerization kinetics and RP_{max} were influenced by specimen thickness and material viscosity. PFill and PFlow materials produced an overall comparable conversion at 5 min and 24 h post-irradiation, despite the ultra-short irradiation times, throughout the 4 mm specimen thickness.

Keywords: Resin composite; Photopolymerization; FTIR; Degree of Conversion; AFCT; Polymerization kinetics.

3.2 Introduction

A representative general dentist spends more than half of their clinical time placing direct restorations, most of which are resin composites [9]. These have become the preferred type of direct restorative materials owing to the recent advancements in their properties. Furthermore, dentists are always looking for an efficient way to manage their practice including fast set materials and shortened clinical steps to reduce overall expenses.

This was endorsed by composite manufacturers via recent facilitation in resin composite application, with less clinical steps and shorter photo-polymerization time. However, this requires operators to develop increased understanding of their materials and their applications [8, 9, 183]. Even though the polymerization reaction is essentially chemical, operators still control some key aspects of the reaction. The radiant energy and exposure time determine the amount of energy delivered to excite the photoinitiators and thus the rate and quality of polymerization [126, 184]. Also, the selected filler load, shade, increment thickness, distance and angulation of light-curing tip are all operator-related factors that affect material behavior upon polymerization and future properties [71, 74, 75]. Sub-optimal delivery of energy can cause low degree of conversion and physical instability leading to further complications such as marginal deterioration, recurrent caries, and bulk fracture [62, 138, 185-188].

Photo-polymerization of resin composite begins as light propagates through the material depth. Photon energy activates the free radical generators (photoinitiators). Depending on the photoinitiator type (Norrish type I, II), these photoinitiators will generate free radicals seeking another electron to bond with. Methacrylate groups, in most dental monomers, will instantly bond to the free radical, at one end of the (C=C) double bond. The other end will become a radical and the reaction will continue to propagate. This chain reaction will auto-accelerate rapidly, until the concentration of the available monomers diminishes and/or the densification process limits the monomer movements and hinders further reaction [17]. Random rapid crosslinking can ultimately reduce molecular movements, resulting in a nonhomogeneous network and potentially a less-than-optimal DC. This can lead to future elution of unreacted monomers, causing compromised physical stability and mechanical properties [29].

One approach to improve the physical stability of the resin composites is by controlling the polymer network architecture through the radical polymerization. The idea is that by modifying the radical chain growth to a step-like polymerization, a more homogenous polymer network with improved physical and mechanical properties will be achieved. The reversible addition-fragmentation chain transfer (RAFT) polymerization mechanism, by the addition of β-allyl sulfone (AFCT) reagent, was proposed previously to be incorporated in dental polymers [90]. Incorporating (AFCT) reagent to a dimethacrylate network has been shown to improve the network architecture during polymerization leading to enhanced network homogeneity, thermal glass transition temperature, and mechanical properties [90, 91]. This promising modification was utilized in a bulkfill resin composite materials as part of a restorative system, PowerCure, (PowerFill and PowerFlow; Ivoclar Vivadent AG, Liechtenstein). These restorative materials were designed to work with high irradiance (3050±10% mW/cm^2) received from a polywave light-curing unit (LCU: Bluephase PowerCure).

The efficacy of polymerization may decrease in deep layers due to light attenuation in 2-3 mm depth. A reduced number of photons reaching the bottom layer means fewer activated photoinitiator molecules [127, 189]. Therefore, the bottom layer DC is important to understand polymerization-related properties. Fourier transform infrared (FTIR) spectroscopy is routinely used to measure DC [112]. The mid-IR spectrum ranges between 4000-400 cm^{-1} which interacts with molecular vibration modes [112, 130]. Following irradiation, polymerization may continue for more than 7 days post-irradiation [128]. However, 24 h post irradiation measurements are sufficient to determine polymer matrix formation [126, 127].

The effect of using such high irradiance light-curing units is still not fully explored. Therefore, the aim of this study was to evaluate the degree of conversion (DC), conversion kinetics, and the effect of 24 h post-irradiation time on rapid photo-polymerized resin composites at depths-within-specimens of 1 and 4 mm, relative to the irradiated surface. The null hypotheses were that: there are no differences in the DC between rapid photo-polymerized resin composites and conventional photo-polymerized comparator composites: (a) at 1 and 4 mm depths; and (b) for 5 min and 24 h post-irradiation times.

3.3 Materials and methods

Study design

The independent variables in this study were: materials, thickness, and time. Two resin composite materials incorporating rapid-polymerization technology and two comparators were investigated. Data on the resin composite compositions were obtained from the manufacturer (**Table 3.1**;**Figure 3.1**). PowerCure materials are available in flowable (lower viscosity) and non-flowable (regular viscosity) consistencies. Two comparator materials were studied with matching consistencies. The purpose of this study was to investigate the PowerCure materials within their system. Therefore, two high irradiance light protocols were utilized for the PowerCure materials: 2000 mW/cm^2 for 5 s and 3050 mW/cm^2 for 3 s, respectively. A standard (1200 mW/cm^2) light curing unit (LCU) was used with the control materials (**Table 3.2**). The radiant emittances were all verified with a calibrated MARC^{TM}-LC instrument (BlueLight Analytics, Halifax, Ca).

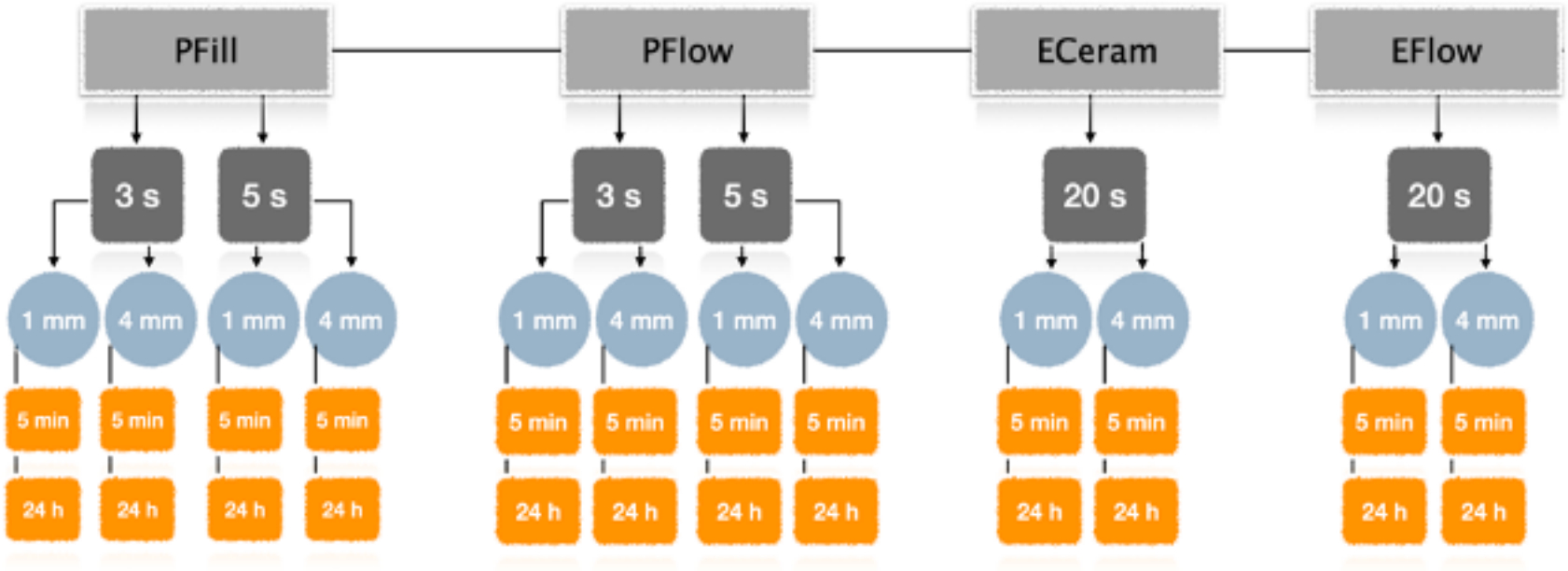

Figure 3.1: Representation of the study design (n=3)

Specimen preparation

Specimens were prepared within 4 mm cylindrical molds of either 1 or 4 mm depth (thickness) to simulate, respectively, near-surface and deep locations in bulk-fill restorations. All specimens were fabricated and measured at 23 ±1 ºC. Twelve specimen groups (n=3) were created for each permutation of material /irradiation protocol and the two measurement depths (**Table 3.1**;**Table 3.2**). The sample size was confirmed using G*power software (V. 3.1.3; Heinrich Heine University, Germany) based on a pilot study. A sample size: n = 3 was sufficient to give a power over 80%.

Table 3.1 Materials used in this study. All manufactured by Ivoclar-Vivadent AG, Liechtenstein

Material code	**Product name**	**Lot number**	**Resin matrix***	**Filler load % (wt);(vol)**
PFill	Tetric PowerFill	W92823	Bis-GMA, Bis-EMA, UDMA, Aromatic Dimethacrylate, DCP	79%; NA
PFlow	Tetric PowerFlow	WM1175		71%; NA
ECeram	Tetric EvoCeram Bulk Fill	U53769	Bis-GMA, Bis-EMA and UDMA	80; 61%
EFlow	Tetric EvoFlow Bulk Fill	U42390	Bis-GMA, Bis-EMA, TCDD	68.2; 46.4%

*Matrix monomer: Bis-GMA: bisphenol-A-diglycidyl dimethacrylate; Bis-EMA: bisphenol-A-polyethylene-glycol-diether dimethacrylate; UDMA: urethane dimethacrylate.

Filler percentages and contents reported by the manufacturers. Typical content: Ba/Al- silicate glass, Isofiller, YbF_3, spherical mixed oxide.

Table 3.2: Light-curing units.

Light-curing unit	Emission spectral type	Protocol	Time	Irradiance mW/cm^2	Radiant exposure J/cm^2	Manufacturer
Bluephase PowerCure (P-Cure)	wide spectrum	3 s	3 s	3000	9	Ivoclar Vivadent AG, Liechtenstein
		Turbo	5 s	2000	10	
Elipar S10 (S10)	narrow spectrum	Standard	20 s	1200	24	3M ESPE, MN, USA

Degree of Conversion

The DC of the materials was measured by a Fourier-transform infrared (FTIR) spectrometer (ALPHA II, Bruker, Massachusetts, USA), with a single reflection ATR accessory. Uncured composite materials, within 1 or 4 mm deep molds, were placed over the ATR crystal (**Figure 3.2**). The spectrum of each uncured material was recorded for the duration of two scans (10 s). The specimens were then irradiated using the designated LCU, for specified periods (**Table 3.2**). Using OPUS software (BRUKER OPTIK GmbH, Ettlingen, Germany), FTIR spectra were recorded in real-time for 24 h post-irradiation. That is, each specimen remained in position at 23^{o}C on the ATR crystal for 24 h, while spectra were recorded continuously. Subsequently, from the resultant datasets, DC (%) values at selected relevant time intervals (5 s, 60 s, 5 min, 24 h) were plotted as a function of Log_{10} time (s), (**Figure 3.3**). The parameters were as follows: 4000-400 cm^{-1} wavelength; 4 cm^{-1} resolution. The instrument was calibrated daily by generating a background spectrum to be implemented in the specimen's spectrum.

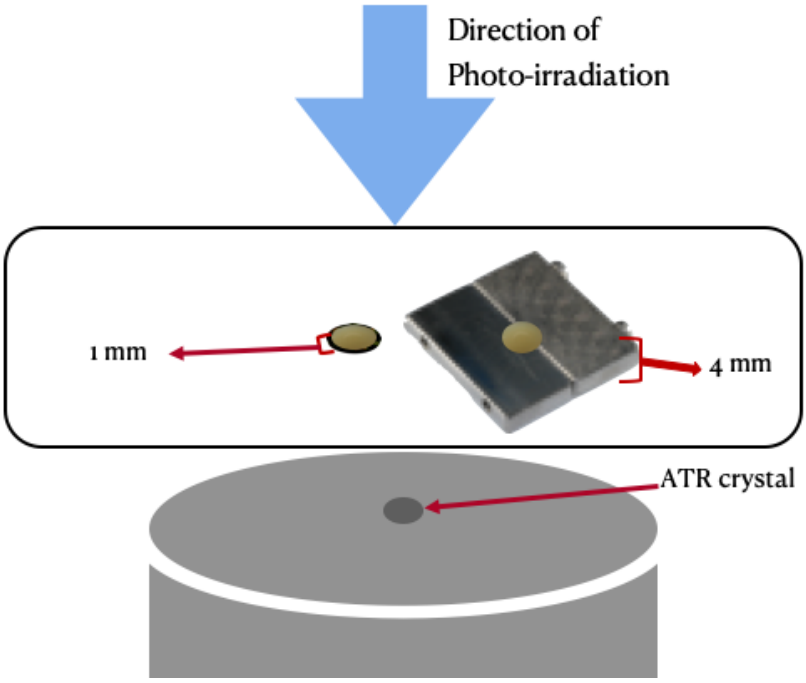

Figure 3.2: Schematic representation of the DC measurement using FTIR. Two different mold types were used to fabricate 1mm and 4 mm thick specimens each of 4 mm diameter (to cover ATR crystal). The distance from the LCU optic tip to specimen surface was 0 mm. The FTIR spectra were obtained from the lower specimen surfaces.

To calculate DC, the variation in peak height ratio using the two-frequency technique (C=C stretch at 1637 cm^{-1} against an internal reference frequency at 1608 cm^{-1}) was utilized. The per-cent degree of conversion, from equation (1), was calculated and plotted over time.

$$DC\% = \left[1 - \left(\frac{\left(\frac{1637\,cm^{-1}}{1608\,cm^{-1}}\right)\text{peak heights after polymerization}}{\left(\frac{1637\,cm^{-1}}{1608\,cm^{-1}}\right)\text{peak heights before polymerization}}\right)\right] X\ 100 \quad \textbf{(1)}$$

An average of 20 scans were used to obtain spectral data at 5 min and 24 h post-irradiation. Closer analysis of the C=C double bond conversion over the first 300 s was conducted via a dual-exponential sum function, defined by the parameters a, b, c, and d (equation 2).

$$DC = a.(1 - e^{-b.t}) + c.(1 - e^{-d.t}) \quad \textbf{(2)}$$

Here: a, b, c, d are modulation factors to optimally fit the model function to the experimental curves of DC *versus* time (t). These parameters represent propagation of polymerization in which "a" and "b" parameters correspond to the gel phase. The second pair of parameters, "c" and "d", correspond to the onset of vitrification, when the material enters the glassy state. The rate of C=C double bond conversion over time (RP_{max}) was calculated and plotted. The DC_{RPmax}, correspondent to (RP_{max}), was also calculated and tabulated.

Statistical analysis

The *Shapiro-Wilk* test confirmed normality of the data distribution. However, the equality of variance assumption failed *Levene's test*. Therefore, the data were analyzed using multiple *Welch's* ANOVA, followed by the *Games-Howell post-hoc test* at 5% level of significance. Additionally, multiple independent sample t-tests were utilized to evaluate the effect of specimen depth and post-irradiation time (p=0.05).

3.4 Results

Degree of Conversion

The effect of the materials and time on the DC were statistically significant ($p<0.05$) (**Figure 3.3**;**Table 3.3**). The DC of the materials ranged between 44.7-59.0 % after 5 min, which increased after 24 h reaching 55.7 -71.0 %. Subsequent analysis – comparing materials based on their viscosity (Flowables/non-flowables) – showed higher conversion of flowable materials *versus* non-flowables. EFlow had generally the highest DC at 5 min and 24 h, regardless of the thickness. DC for PFlow specimens, irradiated for 3 s and 5 s, were comparable to EFlow for all times and both depths ($p>0.05$). similarly, PFill composite irradiated for 3 s and 5 s, did not differ from ECeram comparator material ($p>0.05$). All materials increased in DC after 24 h post-irradiation. More specifically, all flowable materials, along with 1 mm thick PFill -3s, significantly increased in DC after 24 h ($p<0.05$).

Table 3.3: Degrees of Conversion (DC %), of specimens at 1 and 4 mm depths, at 5 min and 24 h post-irradiation. Different lower-case letters compare materials and depths, within each time point. Different capital letters across rows represent statistically significant differences between times.

Materials	DC %			
	5 min		24 h	
	1 mm	4 mm	1 mm	4 mm
Pfill-3s	50.1 (0.7) ^{cdA}	46.1 (4.7) ^{abcA}	61.1 (1.5) ^{cB}	60.9 (6.6) ^{abcA}
Pfill-5s	46.2 (4.4) ^{abcA}	44.7 (2.1) ^{bcA}	57.9 (8.2) ^{abcA}	55.7 (3.1) ^{bcA}
Pflow-3s	54.1 (0.2) ^{abcA}	53.5 (1.2) ^{abcA}	66.6 (0.3) ^{abcB}	66.0 (1.6) ^{abcB}
Pflow-5s	55.4 (0.9) ^{aA}	55.6 (1.8) ^{adA}	66.4 (0.4) ^{abcB}	68.0 (1.8) ^{abcB}
ECeram	53.6 (1.7) ^{abcA}	52.7 (3.4) ^{abcA}	62.2 (1.1) $_{cA}$	63.3 (2.4) ^{abcA}
EFlow	59.0 (1.6) ^{aA}	57.1 (0.7) ^{aA}	71.0 (1.4) ^{aB}	68.9 (0.7) ^{abB}

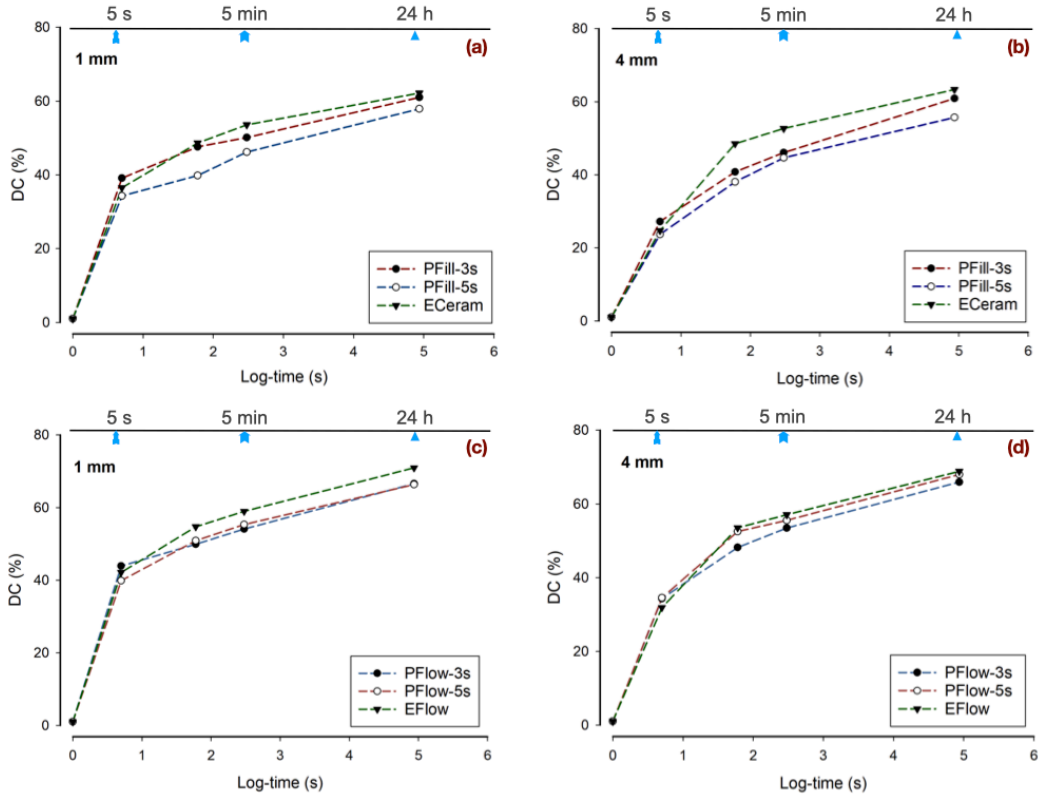

Figure 3.3: DC (%) as a function of log-time up to 24 h for: PFill-3s, PFill-5s, and ECeram at (a) 1 mm and (b) 4 mm depths; PFlow-3s, PFlow-5s, and EFlow at (c) 1 mm and (d) 4 mm depths.

Polymerization kinetics

The change in DC in real time for the first 300 s were analyzed and described by an exponential sum function, defined by the parameters a, b, c, and d (Equation 2;**Figure 3.4**; **Table 3.4**).

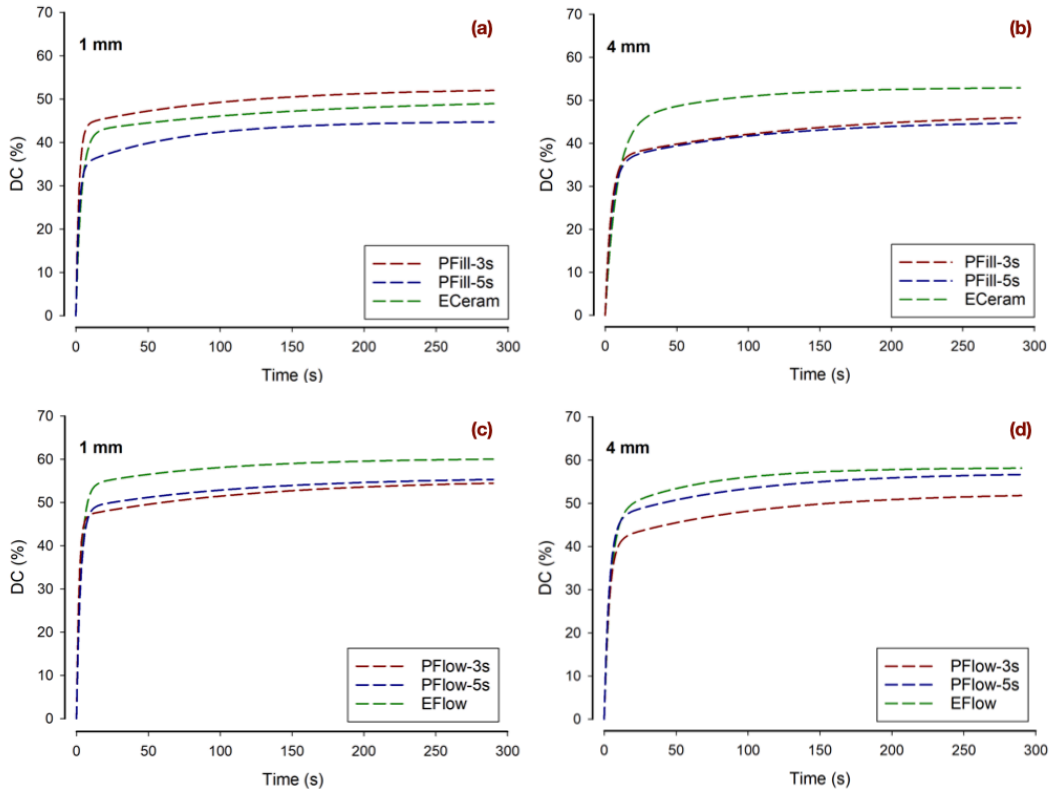

Figure 3.4: Real-time degree of conversion (DC %) during the first 300 s post-irradiation for: PFill-3s, PFill-5s, and ECeram at (a) 1 mm and (b) 4 mm depths; PFlow-3s, PFlow-5s and EFlow at (c) 1 mm and (d) 1 mm depths.

Table 3.4: Mean (SD) of conversion kinetic parameters for the dual-exponential function (equation 2) and the correlation factors (R2).

Materials	Thickness	Parameters				R^2
		a	b	c	d	
PFill-3s	1 mm	43.9 (3.1)	0.5 (0.3)	8.5 (0.5)	0.01 (0.003)	0.97
	4 mm	36.7 (2.1)	0.2 (0.3)	11.0 (1.6)	0.01 (0.01)	0.96
PFill-5s	1 mm	35.2 (4.1)	0.5 (0.03)	10.2 (1.9)	0.01 (0.01)	0.97
	4 mm	36.0 (0.7)	0.2 (0.02)	9.7 (2.6)	0.01 (0.003)	0.97
PFlow-3s	1 mm	46.9 (1.5)	0.6 (0.1)	8.7 (0.4)	0.01 (0.002)	0.99
	4 mm	41.2 (1.2)	0.3 (0.01)	11.3 (0.4)	0.01 (0.001)	0.99
PFlow-5s	1 mm	48.7 (1.0)	0.4 (0.1)	7.4 (0.3)	0.01 (0.001)	0.99
	4 mm	46.3 (3.4)	0.3 (0.02)	10.9 (1.1)	0.01 (0.003)	0.99
ECeram	1 mm	42.2 (2.2)	0.3 (0.01)	7.5 (2.9)	0.01 (0.01)	0.98
	4 mm	43.8 (2.7)	0.1 (0.08)	9.0 (4.4)	0.02 (0.01)	0.98
EFlow	1 mm	54.0 (0.8)	0.3 (0.01)	6.6 (0.6)	0.01 (0.003)	0.99
	4 mm	47.5 (4.2)	0.2 (0.02)	10.8 (1.7)	0.02 (0.01)	0.99

The curve-fitted conversion parameters varied with the depth, materials evaluated and their viscosity. All materials, except PFill-5s and ECeram had higher “a” and “b” parameters, indicating faster conversion, at 1 mm - closer to the irradiated surface, compared to 4 mm. By contrast, parameter “c” was lower at 1 mm depth compared to 4 mm (except for PFill-5s). Parameter “d” was invariant for all materials.

Considering the rate of polymerization (conversion; DC%/s), the maximum rate, RP_{max} occurred at about 5 s, in all cases. It varied with material and specimen depth (**Figure 3.5**;**Table 3.5**), ranging across the specimen groups between 4.3-8.8 %/s with correspondent DC $_{RPmax}$ ranging between 22.2-45.3 %. Material viscosity and specimen depth significantly influenced the RP_{max} ($p<0.05$). The highest RP_{max} was apparent for PFlow, irradiated for 3 s and ECeram showing the lowest RP_{max}. DC_{RPmax}

was generally high for all materials, which strongly correlated with RP_{max} (r=0.96). That is, with higher rate of polymerization, high corresponding DC occurred.

As seen in (**Figure 3.5** (a)), a further small peak in RP was apparent between 15-20 s for the PowerCure materials: PFill and PFlow at 1 mm depth; but much less apparent at 4 mm.

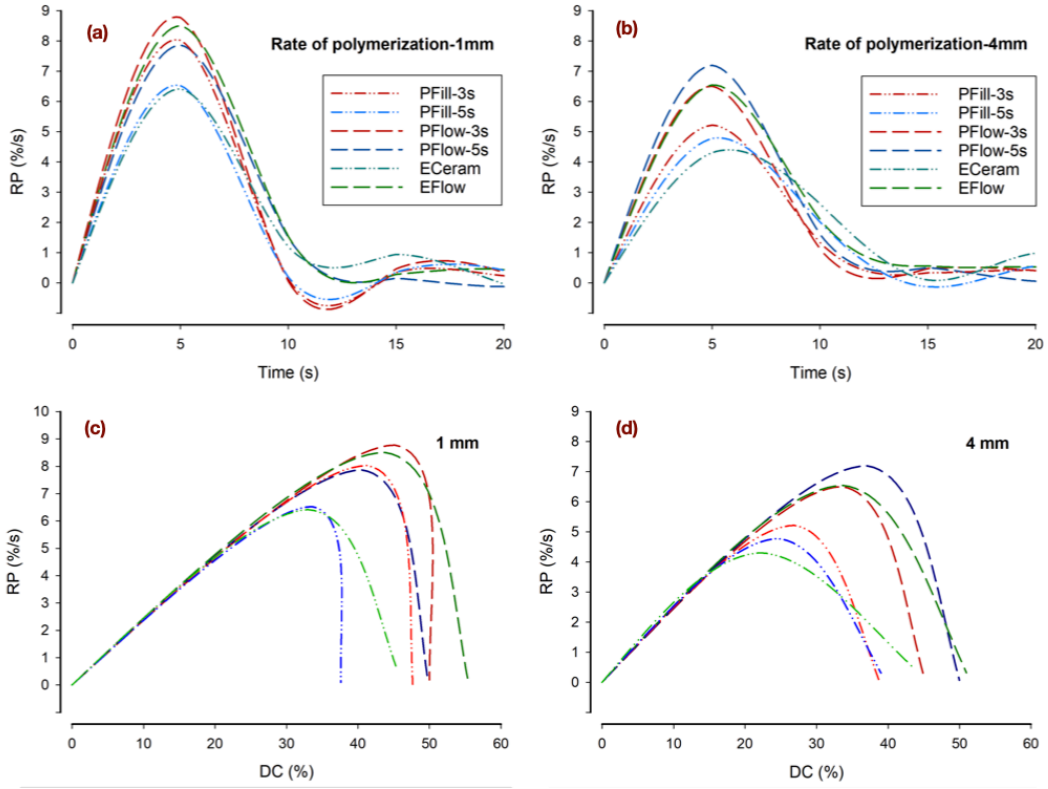

Figure 3.5: (a, b): Rate of polymerization RP (%/s) *versus* time (s) for the first 20 s of polymerization for: (a) 1 mm and (b) 4 mm depths as a function of material; (c,d): rate of polymerization *versus* degree of conversion (DC %) for: (c) 1 mm and (d) 4 mm depth.

Table 3.5: Mean (SD) of maximum rate of polymerization RP_{max} and the degree of conversion DC_{RPmax} at that time-point

Materials	Thickness	$RP_{(max)}$	$DC_{(RPmax)}$ (%)
PFill-3s	1 mm	8.0 (0.5) $_{ab}$	41.3 (2.8)
	4 mm	5.2 (1.2) $_{cde}$	26.8 (5.9)
PFill-5s	1 mm	6.7 (1.1) $_{abcd}$	34.4 (5.6)
	4 mm	4.8 (0.5) $_{de}$	24.6 (2.6)
PFlow-3s	1 mm	8.8 (0.5) $_{a}$	45.3 (2.7)
	4 mm	6.5 (0.2) $_{bcde}$	33.4 (1.1)
PFlow-5s	1 mm	7.8 (1.0) $_{a}$	40.2 (4.9)
	4 mm	7.2 (0.9) $_{abc}$	36.9 (4.5)
ECeram	1 mm	6.4 (0.4) $_{bcde}$	33.0 (1.9)
	4 mm	4.3 (1.6) $_{e}$	22.2 (8.4)
EFlow	1 mm	8.5 (0.2) $_{ab}$	43.8 (1.0)
	4 mm	6.6 (0.2) $_{abcde}$	33.7 (0.8)

3.5 Discussion

This study was designed to evaluate the degree of conversion and polymerization kinetics of rapid-cure resin composites, as well as the effect of 24 h post-irradiation time and specimen thickness on their behavior. FTIR is widely accepted for measuring degree of conversion and polymerization kinetics [112, 190]. OPUS software (BRUKER OPTIK GmbH, Ettlingen, Germany) enabled integration and analysis of the FTIR spectral variations.

There are conflicting reports on the influence of delivering the same radiant exposure by different irradiance intensities on resin composite polymerization [191, 192]. For PFill and PFlow materials cured in 3 and 5 s, the polywave LCU was used to deliver 9 and 10 J/cm^2 radiant exposure respectively. That was less than half of the radiant exposure delivered to ECeram and EFlow control materials (24 J/cm^2). The high radiant exposure delivered to control groups were beyond the manufacturer recommended dose to ensure optimum polymerization and to compensate for the single (narrow) blue spectrum delivered by the LCU [126]. The high energy delivered in a short time via the wide-spectrum LCU was sufficient to produce an adequate DC, due to the materials' ability to absorb energy from both types of wavelengths (violet and blue spectra) and its high reactivity to the lower wavelength [73, 187]. Having a type I photoinitiator in the evaluated materials, our findings were generally in line with the Bunsen–Roscoe exposure reciprocity law, which assume that the photo-response depends on the radiant exposure rather than irradiance power and time [95, 193, 194]. Furthermore, the high irradiance used in PFill and PFlow produced sufficient DC after 24 h and mainly affected the polymerization kinetics, evidently seen at 1 mm depth.

DC measured at 4 mm thickness was at the clinically representative depth for bulk fill materials. 1 mm thick specimens were added to represent proximity to the surface layer. In our study, the thickness did not have a significant effect on the overall DC, which was reported previously [189, 195]. Therefore, the first null hypothesis was retained. Moreover, the material viscosity did have a significant effect on conversion, with superior DC results and a significant increase for up to 24 h seen in flowable materials compared to non-flowable materials. At 5 min, EFlow presented the highest conversion regardless of the thickness, with both PFlow-3s and PFlow-5s being

comparable. However, ECeram was higher in its category (non-flowable) although PFill-3s and PFill-5s gave similar results. Monomer conversion continued significantly for over 24 h, for most materials, with a minimum of 16.8 % increase from 5 min, thus the second null hypothesis was rejected.

After 24 h post-irradiation, all materials were generally comparable, reaching a clinically acceptable conversion degree for bulkfill resin composites (50-79%), which also has been shown to continue for over 7 days post-irradiation [127, 128, 196-198]. The real time DC % evaluation for 24 h in this study was at 23±1°C tempereture, which might be considered a limitation. The ambient intra oral temperature might have promoted higher DC [199].

The termination phase of polymerization mostly occurs as a result of rapid increase in internal molecular stiffness, restricting molecular movement and diffusion, rather than termination by total conversion (or coupling or disproportionation). This explains the prolonged conversion over time [200].

The polymerization kinetics in our study were investigated by the use of an exponential sum function, based on superposition of two exponential functions representing the gel (parameters a and b) and glassy vitrification (parameters c, d) phases [190]. All materials, except PFill-5s and ECeram had higher “a” and “b” parameters, indicating faster conversion, at 1 mm compared to 4 mm. More specifically, parameter “a” was apparently material-dependent as ECeram and EFlow were slightly higher than PFill and PFlow materials for both thickness (except ECeram, 1 mm), this could also be related to the higher radiant exposure (over longer time) delivered to these materials. Parameter “b” reflects the gel phase in relation to gradient steepness. A 1 mm depth exhibited a higher “b” parameter indicating higher C=C double bond conversion compared to 4 mm thick specimens. That is, a lower parameter b indicated a somewhat delayed gel-point in deeper zones, suggesting possibly fewer network crosslinks [189, 190]. Moreover, the higher “b” parameter seen in PFill and PFlow compared to ECeram and EFlow indicating faster gelation of these highly irradiated composites, which could be further investigated [91].

The main structural monomer composition of the evaluated materials was mostly similar, with only a few important modifications to PFill and PFlow. These were: (1) the elimination of Lucerin TPO, (2) addition-fragmentation chain transfer (AFCT)

reagent, (3) addition of tricyclodocane dimethanol dimethacrylate (DCP) monomer and (4) addition of propoxylated Bisphenol A dimethacrylate monomer. AFCT reagent (β-allyl sulfone) is the main modification, present to modify the polymerization mechanism by controlling the polymer architecture and end group functionality. This methacrylate reagent has shown to enhance the overall properties of the polymer by improving the homogeneity, glass transition temperature and mechanical properties, thus possibly to overcome the polymerization shrinkage and shrinkage stress associated with higher irradiance [90].

The RP_{max} occurred at 5 s, mainly affected by specimen thickness and material viscosity. PFlow and PFill materials cured for 3 s had the highest RP_{max} in 1 mm thickness, explained by high irradiance received in low depth. As light transmission reduced in deeper layers, following the Beer-Lambert law, RP_{max} reduced [189]. Following the main propagation phase of polymerization in AFCT-methacrylate-containing materials, a second, minor peak was apparent after 15 s in the R_p plot measured at 1 mm depth (Figure 5a). This suggests further network conversion and may be due to rapid thermal diffusion from 0 to 1 mm, under semi-adiabatic conditions, through the heating effect of the PowerCure LCU [18, 36]. Furthermore, high irradiance received by the resin composite materials can cause a slight delay in auto-acceleration to occur at higher DC leading to generally higher DC_{RPmax}, as seen in our study [132, 194]. Furthermore, a strong positive correlation (r=0.96) seen between higher RP_{max} and DC_{RPmax}, indicating sufficient conversion even with high conversion rate.

PFlow and EFlow generally outperformed the non-flowable materials PFill and ECeram in their overall DC and kinetics. High concentration of highly-viscous monomers with high molecular weight, such as Bis-GMA and UDMA, can hinder the radicals and monomer movements significantly, which affects their reactivity compared to materials with lower viscosity [189, 201, 202]. High filler content, independent of the filler type, was also associated with limiting conversion, seen in highly-filled materials, causing molecular mobility restriction [203, 204].

The AFCT reagent added to methacrylate-based resin composites produced an equivalent overall conversion to their comparators in our study as well as others [91]. While polymerization related properties can be evaluated during polymerization via

DC, further investigation is needed to explore the effect of AFCT reagent on polymerization shrinkage as well as early viscoelastic properties, specifically in the early glass stage. The crosslink density and the long-term stability against chemical degradation of the matrix network should also be investigated.

3.6 Conclusion

PFill and PFlow materials produced an overall comparable conversion at clinically relevant times, 5 min and 24 h post-irradiation, despite the ultra-short irradiation times, regardless of the specimen depth. Polymerization kinetics and the rate of polymerization were significantly influenced by specimen thickness and material viscosity.

Acknowledgements

The authors thank Ivoclar-Vivadent AG for provision of composite materials. The authors declare no conflict of interest.

Discussion of Points raised by the External Examiner

1. What is the polymerization mechanism of AFCT (addition-fragmentation chain-transfer)?

   Addition–fragmentation chain transfer (AFCT) agents, some of which may be monomers, can be incorporated into a dimethacrylate monomers. They participate in network formation by modifying the reaction of multifunctional methacrylates. This process occurred simultaneously with the photopolymerization of the AFCT monomer as well as the other methacrylate monomers leading to polymer stress relaxation through network reconfiguration [96, 97]. Moreover, AFCT addition has shown to reduce shrinkage and shrinkage stress development due to polymerization-induced phase separation- as a part of step growth photopolymerization reactions.

   In AFCT/ methacrylate reaction, the excited free radicals can potentially attack either (i) C=C bonds in methacrylate monomer, which results in methacrylate addition; or (ii) C=C bonds of AFCT monomer (e.g., a β-allyl sulfone), resulting in chain transfer. The growing radical chain (in the case of chain transfer) is terminated by the formation of an intermediate radical which undergoes fragmentation to form a sulfonyl radical as well as a new double bond. The resultant multiple shorter chains can lead -in principle- to a more homogenous network and delayed gel point compared to conventional radical long-chain network [90, 98].

2. Why would these systems benefit from high irradiance when standard systems would not?

   The rapid increase in reaction rate resulting from high irradiance can produce early onset of vitrification, which may cause higher post-gel stresses. However, the incorporated AFCT monomer can lead to polymer stress relaxation through constant network reconfiguration during the reaction. This generally causes

reduction in reaction rate. This can be compensated by a high-irradiance light curing protocol.

3. What is the rationale for using DC for a comparison between different materials, since this does not provide an absolute value but is relative to the initial monomer content, which is dissimilar between RBCs? Why not compare hardness or modulus instead?

   Measuring DC is not just for a comparison between materials but to compare the same material with different irradiation protocols. It was, however, essential to evaluate the conversion of URPBF resin composites cured in 3 s, compared to the established comparator irradiated with a standard light curing protocol. The resin-phase proportions in both RBCs is understood to be very similar. However, hardness could have been measured for supplementary information.

4. What is a "clinically acceptable" degree of conversion?

   The minimum DC for a clinically satisfactory restoration has not yet been established precisely however, an in-*vivo* study has established a negative correlation between wear depth and DC in the range of 55–65% (Ferracane *et al*. 1997). This suggests that, at least for occlusally restorative layers, DC above 55% is needed.

5. There is some evidence (Palin *et al*. *Shining light*…) that a 'non-BF' RBC can be light cured in the same way at 1 mm and 4 mm. Would you consider such materials as 'Bulk Fill'.

   To consider a material a "bulk-fill", the material should be cured in 4 mm, but at the same time produce low polymerization shrinkage and shrinkage stress as well as acceptable mechanical properties.

6. On p.81, you say: “The termination phase of polymerization mostly occurs as a result of rapid increase in internal molecular stiffness, restricting molecular movement and diffusion, rather than termination by total conversion (or coupling or disproportionation). This explains the prolonged conversion over time [181]. Please explain more fully. Are you referring to monomolecular termination?

   In early stages of polymerization, the autoacceleration phase results in a rapid increase in radical reaction with monomer until reaching the *peak* curing rate. Up to this point, there may also be significant biomolecular termination. However, beyond the vitrification point, the increase in internal molecular stiffness (or reduction in segmental mobility) drastically slows down further molecular movement, so that only a small proportionate increase in polymerization continues over time.

CHAPTER FOUR

Polymerization shrinkage and shrinkage stress development in ultra-rapid photo-polymerized bulk fill resin composites

Hamad Algamaiah[a,c,*], Nikolaos Silikas[a], David C Watts[a,b,**]

[a] Biomaterials Science, Division of Dentistry, School of Medical Sciences, University of Manchester, UK

[b] Photon Science Institute, University of Manchester, UK

[c] Department of Restorative Dental Science, College of Dentistry, King Saud University, Saudi Arabia

Published *in Dental Materials 37 (2021)559–567 (Appendix B)*

4.1 Abstract

Objective: To determine the polymerization shrinkage (%) and shrinkage stress (MPa) characteristics of ultra-rapid photo-polymerized bulk fill resin composites.

Methods: Two ultra-rapid photo-polymerized bulk fill (URPBF) materials: PFill and PFlow were studied, along with their comparators ECeram and EFlow. PFill contains an *addition fragmentation chain transfer* (AFCT) agent. The URPBR materials were irradiated using two different 3 s high irradiance protocols (3000 and 3200 mW/cm^2 based on Bluephase *PowerCure* and VALO LCUs, respectively) and one 10 s standard protocol (1200 mW/cm^2 based on a Bluephase *PowerCure* LCU). Bonded disk and Bioman II instruments were used to measure Polymerization shrinkage % and shrinkage stress MPa, respectively, for 60 min at 23 ±1 ºC (n=5). Maximum shrinkage-rate and maximum shrinkage stress-rate were also calculated for 15 s via numerical differentiation. The data were analyzed via multiple One-way ANOVA and Tukey post-*hoc* tests (α=0.05).

Results: PFill groups, regardless of their irradiance protocol, showed significantly lower PS than the comparator, ECeram ($p<0.05$). However, PFlow irradiated via different protocols, was comparable to EFlow and ECeram ($p>0.05$). PFill produced comparable stress results regardless of the curing protocol ($p>0.05$), except when polymerized via a 10s protocol, which was significantly lower than ECeram ($p<0.05$). PFlow materials only exhibited significantly higher shrinkage stress when polymerized with the 3sVALO protocol ($p<0.05$).

The maximum shrinkage strain-*rate* (%/s) was significantly lower in PFill-10s and PFill-3s groups (using *PowerCure* LCU) compared to ECeram. However, no differences were seen between PFlow and EFlow ($p>0.05$). The maximum shrinkage stress-*rate* of PFill and PFlow was comparable between different irradiation protocols, as well as to their comparators ECeram and EFlow ($p>0.05$).

Significance: High irradiation protocols over ultra-short periods led to slightly lower shrinkage strain but slightly higher stress, possibly due to reduced network mobility. The AFCT agent incorporated in PFill composite seemed to reduce shrinkage stress development, even with high irradiance protocols.

Keywords: Polymerization; Photopolymerization; Resin composite; Bulk Fill; URPBF; Shrinkage; Stress; AFCT; Bioman II.

4.2 Introduction

Numerous advantages of photo-polymerized *resin-based composites* (**RBC**s) have led to their status as one of the most commonly used materials in dentistry. In particular, bulk fill types of RBC are widely used because they simplify clinical placement [205]. Nevertheless, several concerns remain about the long-term performance of RBCs [8]. One of these is the inherent bulk volumetric shrinkage caused by molecular densification when intermolecular van der Waals separations are replaced by more compact covalent C-C bonds [206, 207]. Polymerization shrinkage simultaneously occurs with the elastic modulus development and the consequent stress can immediately affect the bonding area between the restorative material and the cavity walls. Several effects can result: (i) *If the interfacial adhesive bonds remain largely intact*, interfacial stresses may cause cuspal deflection, particularly in certain cavity geometries. This could lead to micro-crack formation and fracture in either the hard-tissue substrate or the RBC that could potentially reduce the longevity of the restoration [145, 208]. Alternatively, (ii) *the stresses may be relieved by adhesive failure* resulting in interfacial gap formation, microleakage and (possibly) sensitivity [145, 208].

Several factors can influence the magnitude of polymerization shrinkage (PS) and shrinkage stress (SS). However, it should be recalled that while shrinkage is a material property, shrinkage stress is not since it depends on the quantity (mass or volume) of the material and its local constraint (proportion of bonded walls *and* their compliance) whether that be within a tooth cavity or in a particular measurement assembly. Material composition is a major factor influencing shrinkage magnitudes. The type, reactivity, functionality, molecular mass, size, viscosity and degree of conversion (DC) of the monomer systems used largely determine the shrinkage and shrinkage stress magnitudes [27, 144]. In general, RBCs with low viscosity develop higher double-bond conversion, with higher post-gel shrinkage [143, 162]. High filler content (% w/w or % v/v) proportionately reduces the volume of resin phase and thus reduces the shrinkage, for a given DC. However, the elastic modulus increases with filler content and affects shrinkage-*stress*. Large spherical particles tend to reduce shrinkage and shrinkage stress [41, 42].

Clinically related factors, such as the cavity configuration factor (C-factor), quality of adhesive layer, placement technique and light irradiation protocols can all significantly affect the shrinkage and shrinkage stress [143, 152, 153]. Bonded cavity walls and bulkfill materials have shown to produce lower PS [152]. Previous studies have also shown a complex relationship between SS *per unit mass* and C-factor, which is the ratio of bonded to unbonded cavity surfaces [153, 154].

Positive correlations between DC *versus* PS and SS [184, 209] have led to multiple attempts to control the polymerization shrinkage. Modifications to the monomer composition, altering the photoinitiators, or introducing alternative or additional monomer systems have been investigated to reduce polymerization shrinkage and shrinkage stress [33, 104, 143, 157]. Other approaches were by modifying the light irradiation protocols. Pulse curing, soft start, ramped curing and pulse delay were investigated to reduce shrinkage magnitudes [160]. The hypothesis was to prolong the pre-gel phase to promote more mobility and thus reduce shrinkage stress. However, results were inconsistent and clinically inefficient [162, 163, 210]. Calheiros *et al*. found a significant reduction in SS through the reduction of radiant exposure to 13.5 J/cm^2 without significantly affecting the DC % [209]. This was followed by another study suggesting that 12 J/cm^2 radiant exposure might be adequate to obtain good conversion with sufficient mechanical properties without increasing shrinkage stress [161].

Recently, some *ultra-rapid photopolymerized bulk fill* (URPBF) resin composites were introduced (*PowerCure* system, Ivoclar Vivadent AG, Liechtenstein). They are available in two consistencies, designed to be photopolymerized in 3 s by a high-irradiance light curing unit (LCU). This was achieved by incorporation, in the higher viscosity formulation, of an *addition-fragmentation chain transfer* (AFCT) agent (β-allyl sulfone), to modify the random radical polymerization reaction to produce more homogeneous networks [90]. Some studies have already evaluated the efficacy of this system, which showed comparable conversion results to their sufficiently polymerized comparators [91, 211]. Moreover, their initial viscoelastic stability was also similar to other bulkfill materials polymerized via standard 20 s photo-polymerization [212]. But the question remains: *How do high irradiance protocols affect polymerization shrinkage behaviour* of URPBF RBCs? Therefore, in this investigation, the polymerization shrinkage (%), shrinkage stress (MPa) and their rates were evaluated

for ultra-rapid photo-polymerized bulk fill resin composites as well as their comparators.

The research hypotheses are as follows:

1) The use of recently developed URPBF resin composites is able to reduce the polymerization shrinkage when compared to traditional materials, regardless of the viscosity considered.
2) The use of recently developed URPBF resin composites is able to reduce the polymerization stress when compared to traditional materials, regardless of the viscosity considered.

4.3 Materials and Methods

Study design

The shrinkage strain and shrinkage stress of two URPBF composites with different consistencies, along with their comparators, as control groups, were determined (**Table 4.1**;**Table 4.2**). The URPBF materials were evaluated using two different high irradiance light-curing protocols (3000 and 3200 mW/cm^2 based on Bluephase *PowerCure* and VALO LCUs, respectively) and one standard irradiation protocol for the control materials (1200 mW/cm^2 based on a Bluephase *PowerCure* LCU) (**Table 4.2**).

The radiant emittance of each LCU was verified for each set of specimens using a radiometer (MARC^{TM}-Light Collector, Blue-light Analytics Inc., Halifax, NS, Canada). This device has superseded the previous MARC^{TM}-RC device by enabling measurement over the entire light-optic exit area, whereas the MARC^{TM}-RC only measured over the central (4 mm diameter) optic area.

Five specimens per group were measured (n=5) (**Table 4.3**). All specimens were fabricated and evaluated at 23 ±1 ºC.

Table 4.1 Materials studied: Manufacturer: Ivoclar Vivadent AG, Liechtenstein

Material code	**Product name**	**Lot number**	**Resin matrix***	**Filler load % (wt);(vol)**
PFill	Tetric PowerFill	W92823	Bis-GMA, Bis-EMA, UDMA, Aromatic Dimethacrylate, DCP	79%; NA
PFlow	Tetric PowerFlow	WM1175		71%; NA
ECeram	Tetric EvoCeram Bulk Fill	U53769	Bis-GMA, Bis-EMA and UDMA	80; 61%
EFlow	Tetric EvoFlow Bulk Fill	U42390	Bis-GMA, Bis-EMA, TCDD	68.2; 46.4%

*Matrix monomer: Bis-GMA: bisphenol-A-diglycidyl dimethacrylate; Bis-EMA: bisphenol-A-polyethylene-glycol-diether dimethacrylate; UDMA: urethane dimethacrylate.

Filler percentages and contents reported by the manufacturers. Typical content: Ba/Al- silicate glass, Isofiller, YbF_3, spherical mixed oxide.

Table 4.2: Light-curing units (LCUs)

LCU	Emission spectra	Mode	Time	* Radiant Emittance mW/cm²	Radiant exposure J/cm²	Manufacturer
Bluephase *PowerCure* (PC)	Polywave	3 s	3 s	3000	9	Ivoclar Vivadent AG, Liechtenstein
		Standard	10 s	1200	12	
VALO	Polywave	Xtra power	3 s	3200	9.6	Ultradent Inc, UT, USA

* When the LCU tip is placed in virtual contact with the RBC material, the Irradiance received is numerically equivalent to the Radiant Emittance.

Shrinkage strain % and strain rate (%/s)

To evaluate the shrinkage strain and shrinkage strain rate, the bonded disk technique was utilized in a 23±1 ºC environment (**Figure 4.1**) [213, 214]. A 15 mm internal diameter brass ring of 1 mm thickness and square cross-section was bonded to a 3 mm rigid glass plate. Within the brass ring an 8 mm diameter x 1 mm wax ring was placed centrally to hold the uncured RBC materials. A 0.1 mm thick coverslip (22 x 22 mm) was placed over both the RBC and the brass ring. It was pressed by another thick glass plate to ensure parallelism and to create a standardized uncured RBC disk of 1 mm thickness, without voids.

The ring/plate assembly was then transferred to the apparatus and positioned centrally between the LCU tip *below* and the LVDT transducer probe *above* (**Figure 4.1**). Using PicoLog 6 software (PICO-ADC 20 Data logger, Pico Technology Ltd, UK), the baseline signal was recorded then irradiation commenced after 20 s, for a duration depending on the irradiation protocol (**Table 4.2**). The deflection (shrinkage) in the axial plane was measured continuously by the LVDT probe for 60 min. The resultant

(mV) signal was then converted (via a calibration factor) to µm then plotted *versus* time (s).

This real time data was then used to calculate the shrinkage strain (%) based on the equation:

$$\varepsilon = {}^{\Delta L}/_{Lo} \quad (1)$$

Where, ΔL is the change in thickness and L_o is the original disk thickness (1 mm). Shrinkage-*rate* (%/s) was also calculated for the first 15 s via numerical differentiation.

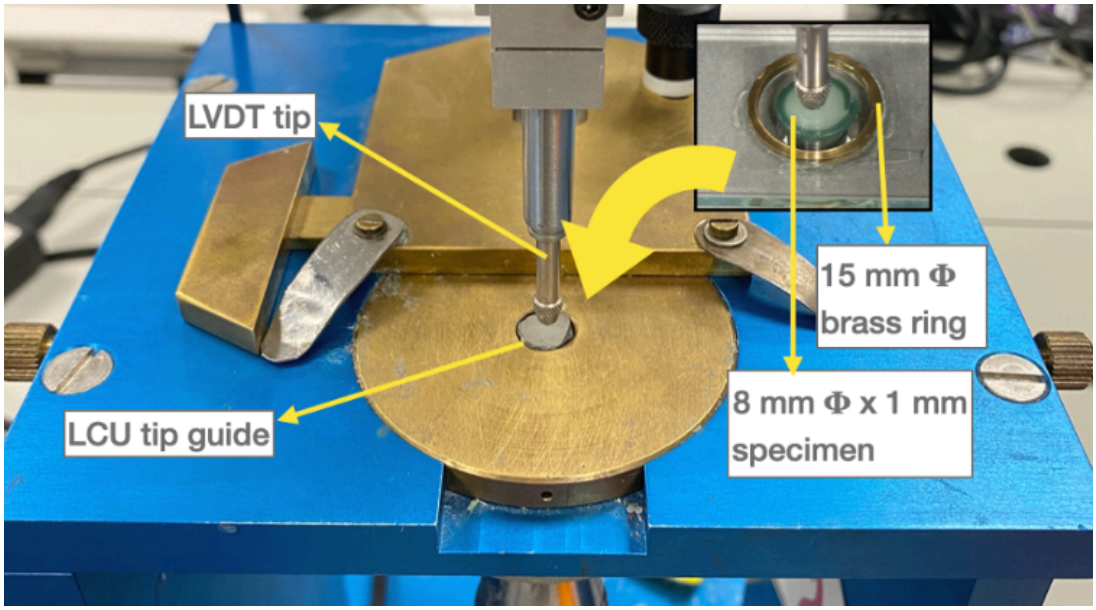

Figure 4.1: Bonded disk apparatus before assembly with plate, ring and specimen disk.

Shrinkage stress (MPa)

Shrinkage stress was measured using the *Bioman II* shrinkage stress instrument [112, 154, 165].

All instrument components were bolted to a 2 cm thick stainless-steel baseplate, including a 500 kg capacity stiff cantilever load-cell. The cantilever arm carried a bolted-on flat-ended steel rod of 10 mm diameter. Separated by a 0.8 mm specimen

gap (set via a feeler gage), a 3 mm glass plate was rigidly held with a re-designed clamp during the measurements creating a fixed specimen thickness (**Figure 4.2**). A 10 mm diameter specimen with 0.8 mm thickness was standardized to obtain a 6.25 C-factor. The designated LCU optic tips were mounted facing up, directly below the glass plate and aligned with the specimen. The re-designed clamp permitted access of all LCU types, immediately below the glass plate. Both the flat-ended metal rod and the glass plate were micro-abraded to enhance bonding.

The *Bioman II* shrinkage stress instrument was calibrated via a precise linear relationship between mV signal and directly applied loads (N). Real time data-recording started after specimen placement. After exactly 20 s (to allow for some relaxation after packing), the specimen was irradiated according to the selected protocol (**Table 4.2**) and data acquisition continued for 60 min.

The stresses produced during polymerization result in displacement of the metal rod and cantilever arm. The mV stress signal was amplified by a strain-gauge conditioning unit (E 308, RDP Electronics Ltd, Wolverhampton UK) and sent continuously to a computer via an analogue-to-digital converter (PICO-ADC 20 Data logger, Pico Technology Ltd, UK).

The measured load (N) was then divided by the specimen area (A = 78.6 mm^2) to calculate the polymerization stress (MPa) using the equation:

$$\sigma = {}^{F}/_{A} \qquad \textbf{(2)}$$

The polymerization shrinkage stress-*rate* (MPa/s) was calculated via numerical differentiation *vs* time for the first 15 s.

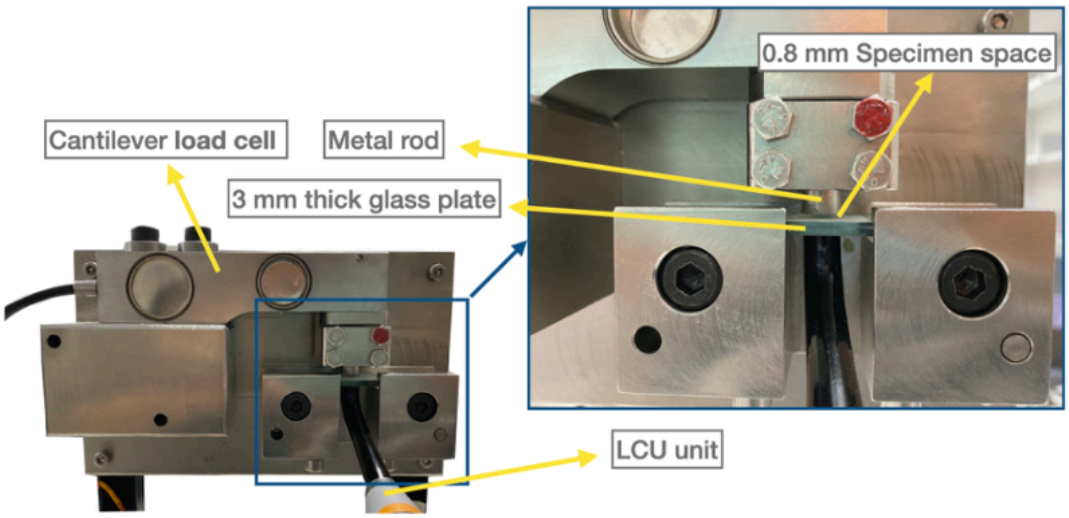

Figure 4.2: Bioman II instrument components

Statistical analysis

Data normality and homogeneity of variance were confirmed using *Shapiro-Wilk* and *Levene's* tests, respectively (α=0.05). The effect of materials and light irradiation protocols were analyzed using multiple *One-way* ANOVA followed by the *Tukey post-hoc tests* at 5% level of significance, generating homogenous sub-sets.

4.4 Results

Polymerization shrinkage strain and shrinkage stress data are presented in Figures 4.3-4.5 and Table 4.3. The maximum polymerization shrinkage strains at 1 h exhibited by the RBCs ranged between 1.63 and 3.22 % (**Table 4.3**;**Figure 4.3**). PFill had the lowest shrinkage and was significantly lower than the comparator, ECeram, regardless of its irradiance protocol ($p<0.05$) (**Figure 4.5**;**Table 4.3**). However, the shrinkage strains of PFlow, irradiated via three different protocols, were not significantly different and were comparable to EFlow and ECeram ($p>0.05$).

Polymerization shrinkage stress ranged between 1.84 and 3.60 MPa (**Figure 4.4**;**Table 4.3**). PFill produced comparable stress results regardless of the curing protocol ($p>0.05$). However, the lowest shrinkage stress when polymerized via a 10s protocol, was significantly lower than ECeram ($p<0.05$). In general, somewhat higher stress results were seen with 3s protocols. PFlow had similar maximum shrinkage stress at 1 h with 10s and 3s PowerCure protocols ($p>0.05$). PFlow materials only exhibited significantly higher shrinkage stress when polymerized with the 3sVALO protocol ($p<0.05$).

The maximum shrinkage strain-rate was significantly lower in PFill-10s and PFill-3s (PowerCure) compared to ECeram (**Figure 4.6**; **Table 4.3**). However, no differences were seen in maximum strain-*rates* between PFlow and EFlow ($p>0.05$). The maximum shrinkage stress-*rate* of PFill was comparable between different irradiation protocols, as well as with ECeram ($p>0.05$) (**Figure 4.7**; **Table 4.3**). Similarly, PFlow showed similar maximum stress-*rates,* regardless of the irradiation protocol, comparable to EFlow ($p>0.05$). There was a slight increase in maximum shrinkage stress-*rate* with high-irradiance protocols, specially when polymerized with 3sVALO (**Figure 4.6**;**Figure 4.7**).

A strong positive correlation was identified, for both 3s and 10s protocols, between 1 h shrinkage stress *versus* strain (r^2=0.97, 0.94 for 10s and 3s, respectively; **Figure 4.8**a), and also between maximum stress *rate* vs strain *rate* (r^2=0.98, 0.94 for 10s and 3s, respectively; **Figure 4.8**b).

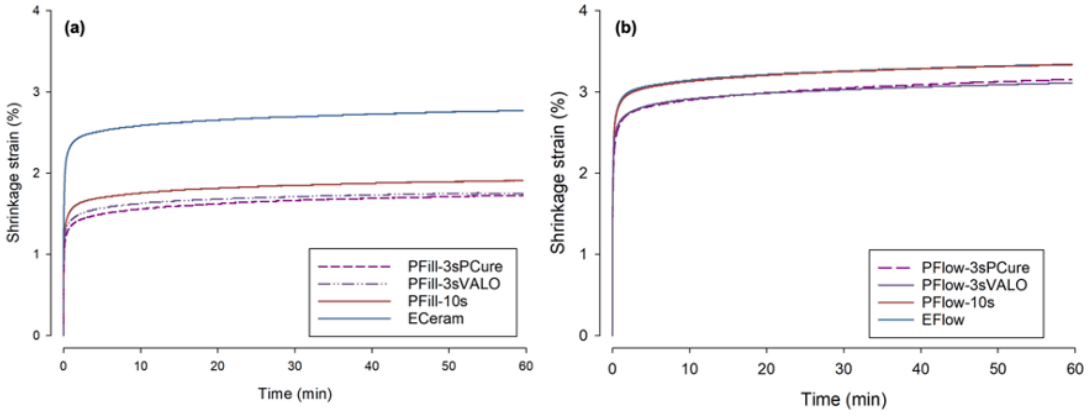

Figure 4.3: Real time shrinkage strain (%) up to 60 min: (a): for PFill & ECeram and (b): PFlow & EFlow.

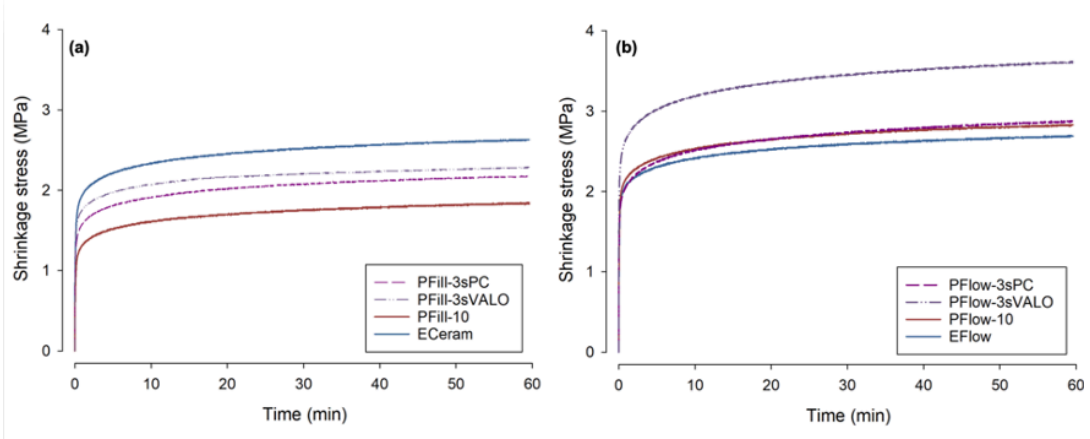

Figure 4.4: Real time shrinkage stress (MPa) up to 60 min for (a): PFill & ECeram and (b): PFlow & EFlow.

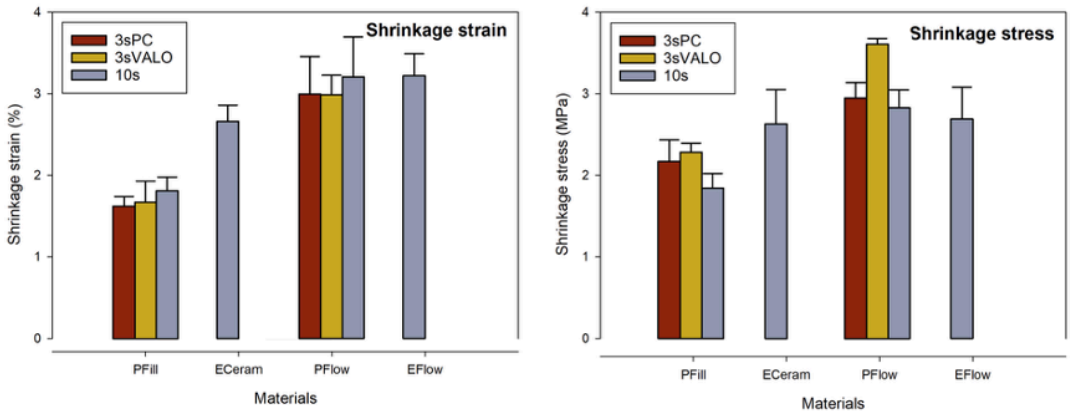

Figure 4.5: Mean shrinkage strain (%) and stress (MPa) at 60 min for PFill, PFlow, ECeram, and EFlow with different irradiation protocols.

Table 4.3: Mean (SD) of polymerization shrinkage strain (%) and shrinkage stress (MPa) after 60 min for the RBCs and their maximum rates. The letters (a-d) represent homogenous subsets within each column for each of the four parameters.

Materials and irradiation protocols	Shrinkage strain (%)	Max rate (%/s)	Shrinkage stress (MPa)	Max rate (MPa/s)
PFill-10s	**1.82** (0.17) a	**0.46**(0.13) a	**1.84** (0.18) a	**0.28** (0.08) a
PFill- 3sPC	**1.63** (0.12) a	**0.43** (0.08) a	**2.17** (0.26) ab	**0.36**(0.10) ab*
PFill- 3sVALO	**1.68** (0.26) a	**0.47** (0.19) ab	**2.28** (0.11) ab	**0.43** (0.06) ab*
ECeram-10s	**2.66** (0.20) b	**0.75** (0.09) bc	**2.63** (0.42) bc	**0.37** (0.10) ab*
PFlow-10s	**3.21** (0.49) b	**0.79** (0.23) bc	**2.83** (0.22) c	**0.44** (0.05) abc*
PFlow- 3sPC	**3.00** (0.46) b	**0.81**(0.20) c	**2.95** (0.19) c	**0.52** (0.13) bc*
PFlow- 3sVALO	**2.99** (0.24) b	**0.90** (0.16) c	**3.60** (0.07) d	**0.61** (0.04) c*
EFlow-10s	**3.22** (0.27) b	**0.81** (0.13) c	**2.69** (0.39) bc	**0.42** (0.07) ab*

* Max stress-rate was delayed by 1 s

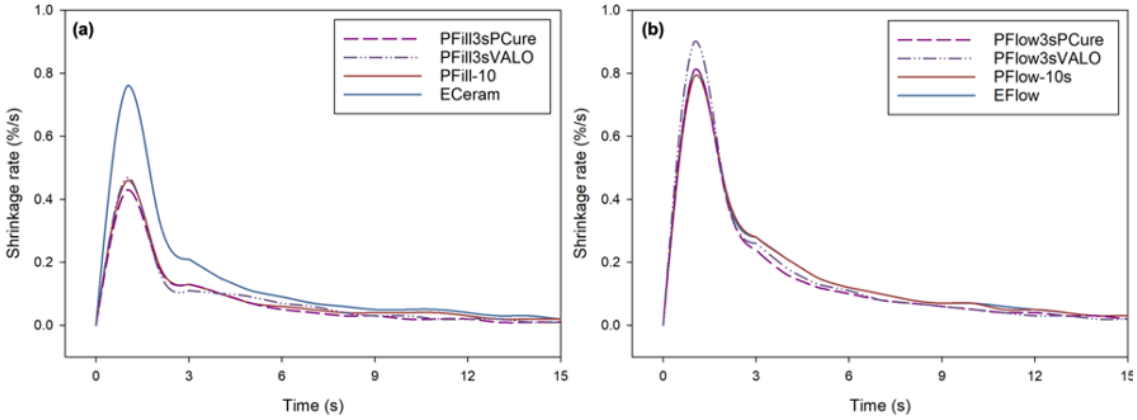

Figure 4.6: Rate of shrinkage strain (%/s) *versus* time up to 15 s for (a): PFill & ECeram and (b): PFlow & EFlow.

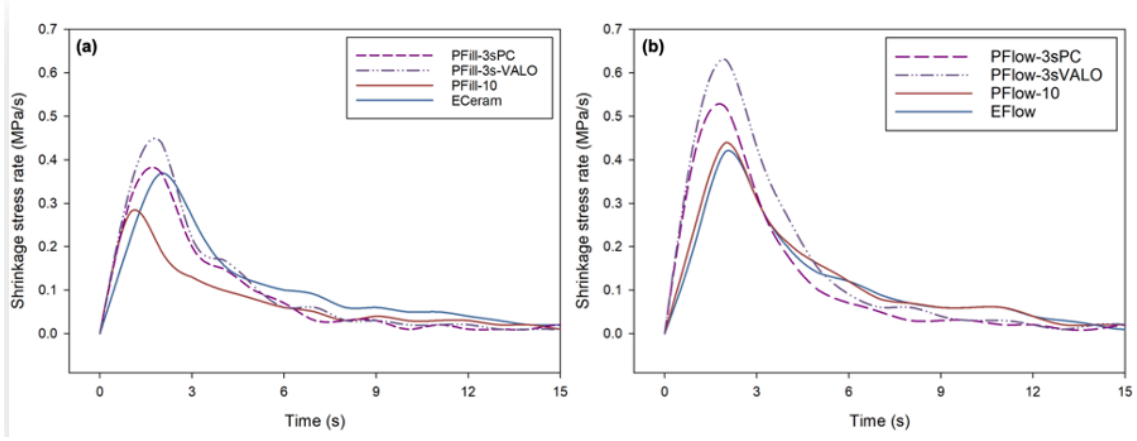

Figure 4.7: Rate of shrinkage stress (MPa/s) *versus* time up to 15 s for (a): PFill & ECeram and (b): PFlow & EFlow.

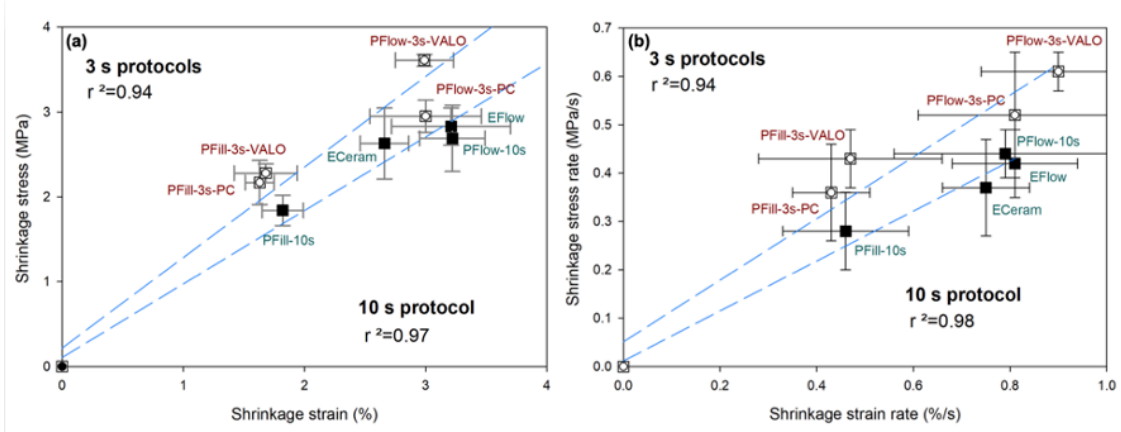

Figure 4.8: Strong positive linear correlations between (a): 60 min values for PS and SS; and (b): maximum (peak values) in PS and SS rates ($p<0.05$) for the set of four materials.

4.5 Discussion

Ultra-rapid photo-polymerized bulk fill (URPBF) materials were designed to cure with high-irradiance light over a very short time period. Previously, the efficacy of this system was investigated in regards to DC and initial viscoelastic properties. The results showed the ability of this system to respond effectively to such high irradiance over ultra-short periods with good conversion and viscoelastic properties [91, 211, 212]. This investigation aimed to measure the shrinkage behavior and kinetics of this system by comparing a standard irradiance protocol with two high irradiance 3s protocols using two different LCUs, as well as to well-established control materials. Real-time shrinkage-strain was measured with a bonded disk instrument, a widely used method with good reproducibility [112, 184, 215]. The *Bioman II* instrument was used to measure shrinkage stress. The instrument has a fixed compliance, due to the fixed cantilever beam length, with controlled specimen thickness and diameter [42, 112, 216]. Relative to the very similar earlier version (*Bioman I*) the present design permits access and deployment with any type of LCU optic [112].

The lower viscosity materials, PFlow/EFlow, contain lower filler percentages compared to PFill/ECeram and higher percentages of monomers. Hence there is a greater volume of resin matrix undergoing shrinkage. Moreover, during photo-polymerization, the reduced viscosity of these materials permits further intermolecular mobility of both free radicals and reactive species, thus prolonging the gelation and vitrification stages of the reaction and consequently delays in the termination reactions [132, 217]. As a result, flowable materials show generally higher degrees of conversion (DC) [211, 218]. Quite generally, shrinkage is strongly correlated with DC [136, 162, 218]. The higher shrinkage of PFlow/EFlow is thus entirely consistent with their higher DC%, as compared with PFill and ECeram [211]. Furthermore, the generally higher final (1 h) stresses developed in these flowable materials are consistent with the strong correlation between shrinkage stress/strain after 1 h, post irradiation, seen in **Figure 4.8** (a).

Within the PFill groups, shrinkage strains were comparable regardless of the irradiation protocol, with lowest shrinkage strain arising from a 3s PowerCure protocol. Comparable outcomes were recently published by Par *et.al* [219]. The

PowerCure irradiances reported by Par [219] are somewhat higher than those we measured with the MARC™-LC device and also outside the limits specified by the manufacturer. If the MARC™ instrument they used was the MARC™-RC this only measures the 4 mm diameter c*entral region* of the 8 mm light optic and thus generates higher mean irradiances whenever there is a less than a 100%-perfect beam profile.

PFill groups also outperformed ECeram by reduced shrinkage strain. Since PFill and ECeram are structurally similar with only few modifications to the compositions, further investigation is needed to help explain these superior results, which may be a consequence of incorporated chain-transfer agents, such as β-allyl sulphone. This reagent has been shown to enhance the overall properties of dimethacrylate polymer networks by improving the homogeneity, glass transition temperature and mechanical properties [90, 97]. PFlow and EFlow were broadly comparable in shrinkage, although PFlow with the 3s protocol, compared to the 10 s protocol, showed slightly lower shrinkage, but this was not statistically significant.

In standard photopolymerization, the vitrification stage occurs close to the time of maximum polymerization rate. Moderate shrinkage stresses begin to develop prior to this vitrification point. But they are of lower magnitude due to the flexibility of the developing network at this stage enabling slight stress relaxation [217]. Most of the modulus development and shrinkage stress is produced during and after vitrification, which restricts both molecular and macroscopic relaxation [217, 220]. This explains why all materials, except PFill polymerized in 10 s, reached the maximum shrinkage stress rate only 1 s after the maximum shrinkage strain rates. This is part of a complex and multifactorial phenomenon wherein the onset of vitrification at the glass-transition temperature is itself rate-dependent. Under high irradiance, rapidly generated radicals result in faster reaction and produce vitrification in a shorter time. This could explain the slightly lower shrinkage strain coupled with higher shrinkage stress, even though the differences did not elicit statistical difference.

Shrinkage stress development in PFill was similar for all irradiation groups. However, the lowest stress was seen in PFill polymerized with a 10 s protocol, which was significantly lower than for ECeram. These results were aligned with the outcomes of Par *et.al* comparing the shrinkage forces [219]. This might be due to a more homogenous network, facilitated by an AFCT enhanced formulation. The

modification of the polymerization by chain transfer could have reduced crosslink density, further delaying gelation and vitrification, leading to lower initial stress generation [90, 221]. Also, the AFCT agent incorporated in the resin phase can induce reshuffling of covalent bonds, enabling stress relief during network formation [97]. However, PFlow materials were comparable to EFlow, except for PFlow polymerized with 3sVALO which presented the significantly highest shrinkage stress. The resin-phase composition of PFlow and EFlow may be similar or even identical as PFlow lacks the new AFCT agent, which is consistent with the similar shrinkage behavior. The highest shrinkage stress, seen with the 3s protocol using a VALO LCU, can be attributed to: (a) the higher irradiance delivered to the specimens and (b) the wider irradiance area presented in the shrinkage stress measurement arising from the wider active tip diameter of the VALO LCU.

The maximum shrinkage strain-*rate* was comparable among material categories, except for ECeram that had a significantly higher maximum *rate* compared to PFill. The maximum shrinkage stress *rate* was similar in all non-flowable groups. For the flowable materials, PFlow polymerized with 3sVALO had a high maximum stress-*rate* compared to EFlow, which is consistent with its highest shrinkage stress magnitude.

A strong positive correlation was identified, for both 3s and 10s irradiation protocols between the 60 min values for shrinkage stress *versus* strain ($r^2 > 0.94$; Figure 8(a)). Similar correlations were previously reported [219, 221]. In general, the stress (**σ**) developing with time (**t**) may be written as:

$$\sigma(t) = E(t) \times \varepsilon(t) \quad \textbf{(3)}$$

where **E(t)** is the elastic modulus of the composite, also developing rapidly with time from an initial value virtually zero; **ε**(t) is the developing shrinkage-strain. If **E** had a fixed value, *which it does not*, then the equation would reduce to:

$$\sigma(t) = E \times \varepsilon(t) \quad \textbf{(4)}$$

Nevertheless, the linear plots of Figure 8(a) are concerned with 1 h (60 min) values for both stress and strain, derived from the set of materials, so the comparable equation would be:

$$\sigma_{1h} = E_{1h} \times \varepsilon_{1h} \quad \textbf{(5)}$$

Thus, at least with these materials and these rapid irradiation protocols, the slope in Figure 8(a) suggests a constant order of magnitude for $\mathbf{E_{1h}}$ which is effectively a generalized modulus parameter for these four composite materials after 1 h. Given the very rapid vitrification, this proportional trend, between 1 h stress and strain, is not so surprising.

The high correlations between maximum stress vs strain *rates* ($r^2 > 0.94$), seen in Figure 8(b), are also interesting observations. But it is probably inadvisable to over-interpret these data.

With higher irradiance protocols, PFill and PFlow developed similar or slightly less polymerization shrinkage strain. However, they produced similar but slightly higher shrinkage stress, with only one significantly higher shrinkage stresses seen when PFlow was polymerized with the 3sVALO protocol. A future investigation is still needed to understand this behavior in a more clinically simulated environment, and the heat generation from the high-irradiance LCUs.

4.6 Conclusions

PFill composite showed reduced shrinkage strain and comparable shrinkage stress to their comparator, ECeram, with no differences across different light irradiation protocols. PFlow performed similarly. However, it showed significantly higher shrinkage stress with the 3s protocol using a VALO LCU. High irradiation protocols over ultra-short periods may have led to reduced network mobility, leading to slightly lower shrinkage strain but slightly higher stress. The AFCT agent incorporated in PFill composite seemed to reduce the development of shrinkage stress, even with high irradiance protocols.

Discussion of Points raised by the External Examiner

1. Why change the irradiation time (10 s) compared to the DC study (20 s)?

   In our experimental design, the light curing protocols varied between studies based on the specific hypotheses. When evaluating degree of conversion, our aim was to compare the experimental groups (PowerCure system) to a challenging control group (almost double the radiant exposure), to evaluate whether 3 s polymerization can be sufficient compared to the 20 s protocol. The same hypothesis applies to the early surface viscoelastic integrity measurements. However, the shrinkage phenomenon and thermography evaluation required the standard curing protocol (10 s). The energy from the e*xtended* curing time of > 10 s can only increase (ΔT) but will probably not significantly affect the shrinkage stress [95]. VALO LCU in Xtra power mode (3s) was used in this study to evaluate the effect of different high irradiance multi-wave LCUs on shrinkage behavior.

2. Why not include a composite that sets ultrafast, but *without* the AFCT agent, as control?

   There is currently no other available resin composite designed to set ultrafast.

3. Modulus is known to be a key factor regarding shrinkage-stress. Have you checked whether this is the factor responsible for differences between PFill and ECeram?

   A great point raised. We have not directly measured the moduli for both materials. However, an 'apparent' modulus estimation, drawn from equation 5, suggest very similar moduli (at 1 h) for PFill-10s *versus* ECeram-10s.

4. Why not include a very highly filled RBC as control (eg. GrandioSO or Clearfil Maj Post)?

An interesting idea. Will definitely consider it in the near future.

5. What is the glass-transition temperature (T_g) and how do we measure it?

   Tg is the temperature where the polymer system experiences transition from a rigid (glassy) state to a more flexible state, associated with the onset of extensive main-chain segmental movements. Differential Scanning Calorimetry (DSC), Dynamic Mechanical Analysis (DMA), Dielectric thermal analysis (DETA) and Thermomechanical Analysis (TMA) are methods that can be used to measure the Tg. However, T_g is not a fixed value but depends upon the rate (or frequency) of measurement, although it is normally quoted for measurement frequencies in the range of 1 Hz.

6. What might be the effect of AFCT agents on T_g?

   Addition of AFCT to dimethacrylate network can result in more *homogeneous* networks leading a *narrower* glass transition temperature range. The modulus below the T_g does not change significantly [90].

7. Is rapid vitrification related to AFCT agents or are all ultra-fast systems expected to behave similarly?

   Ultra-rapid polymerization achieved in PFill system occurred by the use of Norrish type I as well as the AFCT agent. The rapid vitrification is results from the potent and reactive photoinitiators used. However, the AFCT agent - when added to dimethacrylate monomers - develops polymerization-induced phase separation due to the step growth photo-polymerization. This generally results in a reduced reaction rate and delayed vitrification, thus achieving reduced stress [97].

CHAPTER FIVE

Spatio-temporal temperature fields generated coronally with bulk-fill resin composites: a thermography study

Jiawei Yang[a], ***Hamad Algamaiah***[a,b,**], David C. Watts[a,c,*]

[a] Dentistry, School of Medical Sciences, University of Manchester, Manchester, UK

[b] Department of Restorative Dental Science, College of Dentistry, King Saud University, Riyadh, Saudi Arabia

[c] Photon Science Institute, University of Manchester, Manchester, UK

Published *in Dental Materials 37 (2021) 1237–1247 (Appendix C)*

5.1 Abstract

Objectives: This study aimed to investigate the effects of (i) a high-irradiance (3 s) light-curing protocol *versus* (ii) two standard-irradiance (10 s) protocols on 2D temperature maps during intra-dental photo-irradiation within a molar cavity restored with either *Ultra-Rapid Photo-Polymerized BulkFill* (URPBF) composites or a pre-heated thermo-viscous bulk-fill composite, compared to a standard bulk-fill *resin-based-composite* (RBC). The specific objectives included visual assessment of the temperature maps and quantitative assessment of several temperature/time plots at four different locations.

Methods. A caries-free lower first molar cavity served as a natural tooth mold. Resin composites were placed without intermediary adhesive. Two URPBF composites (PFill; PFlow) and one pre-heated thermo-viscous bulk-fill composite (*Viscalor*: VC) were compared to a contemporary bulk-fill composite (One Bulk Fill: OBF). Two LED-LCU devices were used: Bluephase *PowerCure* (PC) and Elipar S10 (S10), with three light-irradiation protocols (PC-3s, PC-10s and S10-10s). 2D temperature maps over the entire coronal area were recorded for 120 s during and after irradiation using a thermal imaging camera. Changes at four different levels were selected from the data sets: (0, 2 and 4 mm from the cavity top and at 1 mm below the dentin cavity floor). The maximum temperature attained (T_{max}), the mean temperature rise (ΔT), the time (s) to reach maximum temperature and the integrated areas (°C·s) under the temperature/time (T/t) plots were identified. Data were analysed via three-way ANOVA, One-way ANOVA, independent t-tests and Tukey *post-hoc* tests ($p<0.05$).

Results. All RBCs showed qualitatively similar temperature-time profiles. PFlow reached T_{max} in the shortest time. PC-3s (3000 mW/cm^2) generated comparable ΔT to S10-10s, except with PFill, where ΔT was greater. Despite the same irradiance (1200 mW/cm^2), Elipar S10 led to higher T_{max} and ΔT compared to PC-10s. The highest T_{max} and ΔT were observed at the 2 mm level, and the lowest were at 1 mm depth into the underlying dentin.

Significance. Coronal 2D temperature maps showed rises largely confined within the bulk-fill RBC materials, with maxima at 2 mm rather than 4 mm depth indicating some extent of thermal insulation for the underlying dentin and pulp. RBCs polymerized via

different irradiation protocols showed similar temperature changes. With the PC-3s protocol - and also with pre-heated VC - minimal temperature rises at 1 mm within dentin suggest their clinical safety when sufficient remaining dentin thickness is present.

Keywords*:* Thermal imaging; thermographic analysis; bulk-fill resin composite; high-irradiance; URPBF composites; pre-heating; thermo-viscous composite.

5.2 Introduction

Resin-based composites (RBCs) have become the foremost direct dental restorative materials due to their aesthetics, acceptable placement time and generally good properties [61]. Advances in formulation have enabled sufficient degrees of conversion (DC) that are the first requirement for good material properties [222, 223]. To achieve good longevity, careful placement is essential, via simplified techniques where possible. However, any technique-sensitive steps require extra attention as even minor deviations may reduce clinical performance.

Bulk-fill RBCs provide good DC and depth of cure [224, 225]. As these materials are manipulated in deep cavities, heat generated in the restoration and transferred within the cavity remains a concern for pulpal health, especially with greater radiant exitance from light-curing units (LCUs). The total heat flux arises from both the received light energy and the exothermic polymerization [226, 227]. Thus, any significant intra-pulpal temperature elevation may lead to pulpal damage and necrosis [228-230].

Multi-step free-radical addition polymerization, in which double carbon bonds (C=C) convert into single carbon bonds (C-C), is invariably an exothermic process [226, 229-231]. The exothermic heat is proportional to the number of reacted C=C bonds [231, 232]. Flowable RBCs, formulated with a greater proportion of resin monomers than non-flowable RBCs, generate more heat during polymerization [226, 231, 233].

When heat is generated (**ΔQ**) within a material substance, via incident radiant energy and/or exothermic processes, two "extreme" situations may be distinguished - as regards any temperature change (**ΔT**). These are, firstly, an *isothermal* process, where the temperature of the system remains constant, so **ΔT = 0**. For this to occur, the heat transfer must be slow enough for heat (**ΔQ**) to be transferred completely to the surroundings. This might arise in dentistry through application of a cold-water jet. The opposite extreme is an *adiabatic* process, where *the system exchanges no heat* with the surroundings and therefore the system *temperature will increase* as a function of time, during the finite period of heat generation: **ΔT(t) ≠ 0.** During dental photopolymerization of RBCs, the isothermal situation should not arise. If water-cooling were attempted this would be detrimental to effective polymerization as

moderate **ΔT** increase is desirable to promote auto-acceleration and attainment of solid vitrification.

By contrast, a partial or *quasi-adiabatic* situation is likely - and all the more so - with *rapid or ultra-rapid irradiation* from high irradiance LCUs. Here we must be careful to define exactly what we mean by the 'system'. We can distinguish between the 'RBC system' and the surrounding coronal hard tissues. Or we can define the entire 'coronal system' as encompassing both RBC and the residual coronal tissues.

Even within the 'RBC system', heat generation and associated temperature rise is not anticipated to be uniform. There may be a major 'hot spot' from which heat will diffuse throughout the restoration and beyond into the coronal tissues and towards the pulp. When the heat flow and transient temperature gradients are *entirely within the specimen*, they are controlled by a bulk material property - the *thermal diffusivity* (A). Thermal diffusivities have been measured for many RBCs and are typically *ca.* 0.220 mm^2s^{-1}. Many compare favorably with hard dental tissues [234, 235].

Transient temperature changes (**ΔT**) as a function of time (**t**) at any location in the RBC and coronal tissues may be represented by equations of the form [235]:

$$\Delta T = C.[1 - e^{-A.Y.t}] \quad \textbf{(1)}$$

Where **C** is the magnitude of the internal temperature stimulus and **Y** is a geometrical parameter. For the specimen sizes involved, it could take typically 60 s for thermal diffusion to reach equilibrium. That is, thermal diffusion takes a finite time to complete which is likely to greatly exceed irradiation periods ≤ 10 s.

Temperature changes also produce dimensional changes, depending upon the *thermal expansion coefficient* (α) [236-238]. Differences in expansion coefficient between RBC and tooth tissues could eventually produce interfacial gaps [239].

The composition, concentration and efficiency of the photo-initiator system affect the final DC of the composite and the resultant exothermic heat [240]. Temperature rise also depends on the LCU irradiance, wavelength and exposure duration [226, 241]. Although the "reciprocity law" does not hold precisely, short exposures can be partially compensated for by increased radiant exitance. Ultra-fast (3 s) photo-polymerization LCUs have been introduced with high irradiance levels (up to 3000-

3500 mW/cm^2) to reduce handling time [91, 242]. Soft-start curing protocols were proposed to relieve internal stress and to reduce polymerization shrinkage magnitudes, but reported results were inconsistent [162, 210, 229, 243, 244]. *Ultra-rapid photopolymerized bulk fill* (URPBF) resin composites have been introduced, designed to be function with high irradiance LCUs [91, 245, 246]. An addition-fragmentation chain transfer (AFCT) agent (β-allyl sulfone) within the monomer system was incorporated to improve homogeneity of the cross-linked network [90, 91, 245]. Subsequent investigations have demonstrated the utility of ultra-fast polymerization of bulk-fill RBCs and their acceptable properties in terms of DC, viscoelastic stability, polymerization shrinkage and shrinkage stress [91, 246, 247].

A thermo-viscous bulk-fill material, *Viscalor*, can be pre-heated to improve both handling properties and cavity adaptation [248]. The effect of pre-heating on intra-pulpal temperature rise has been previously investigated [234, 249-251]. Heating the materials to 60 °C can temporarily increase the flowability without affecting material integrity. The actual material temperature after removal from the heating device may be less than the pre-set temperature [250]. The effective temperature during cavity placement thus depends upon the operator, with any delays incurring material cooling towards ambient [236, 249]. Once within the cavity, dynamic temperature regulation by soft tissue/blood flow reduces temperature changes, which may lead to a reduced setting temperature rise within the tooth structure [252, 253].

Localized temperatures can be measured by placing thermocouples into the composite or cavity floor [227, 254, 255], although there are limits to characterization by thermocouples of an overall temperature field in real-time. However, infrared (IR) thermography is a non-destructive method that can measure spatio-temporal temperature profiles [226, 229, 256]. Such real-time visualization of 2D temperature maps can cover extensive areas.

This study aimed to investigate the effects of (i) a high-irradiance (3 s) light-curing protocol *versus* (ii) two standard-irradiance (10 s) protocols on 2D temperature maps during intra-dental photo-irradiation within a molar cavity restored with either *Ultra-Rapid Photo-Polymerized BulkFill* (URPBF) composites or a pre-heated thermo-viscous bulk-fill composite, compared to a standard bulk-fill *resin-based-composite*. The specific objectives included visual assessment of the temperature maps and quantitative assessment of several temperature/time plots at four different locations.

The hypothesis tested was that the high-irradiance (3 s) protocol was broadly similar in its effects to the two standard-irradiance (10 s) protocols.

5.3 Materials and methods

Four different RBCs, including two consistencies, were used in this study (**Table 5.1**). *Viscalor* was pre-heated using a Caps Warmer (VOCO, Germany) in T3 mode (up to 68 °C) for 3 min (T3-3min). Three irradiation protocols (PC-3s, PC-10s and S10-10s; **Table 5.2**) were utilized: one high irradiance (3 s of 3000 mW/cm^2 using Bluephase *PowerCure*) and two standard protocols: (10 s of 1200 mW/cm^2 using Bluephase *PowerCure* (PC) and Elipar S10, respectively). As the LCU optic tips were essentially in contact (< 1 mm from the cavity top), so the radiant exitances, verified by a MARC-LC™ device, were taken as numerically equivalent to irradiance.

Table 5.1 RBC Manufacturer information

Code	Materials	Resin matrix	Filler load % (wt)/(vol)	Manufacturer
OBF	OneBulkfill	DDDMA, UDMA, AUDMA, AFM	76.5/ 58.4 %	3M ESPE, MN, USA
PFill	Tetric PowerFill	Bis-GMA, Bis-EMA, UDMA, Aromatic Dimethacrylate, DCP	79 %/NA	Ivoclar Vivadent AG, Liechtenstein
PFlow	Tetric PowerFlow	Bis-GMA, Bis-EMA, UDMA, Aromatic Dimethacrylate, DCP	71 %/NA	Ivoclar Vivadent AG, Liechtenstein
VC	Viscalor	Bis-GMA, aliphatic dimethacrylate	83 %/NA	VOCO, Cuxhaven Germany

Table 5.2 Light-curing units and irradiation protocols.

Irradiation protocols	Light-curing unit	Emission spectra	Mode	Time	Irradiance mW/cm^2	Radiant exposure J/cm^2	Manufacturer
PC-3s	Bluephase *PowerCure*	Polywave	3 s	3 s	3000	9	Ivoclar Vivadent AG, Liechtenstein
PC-10s			Standard	10 s	1200	12	
S10-10s	Elipar S10	Monowave	Standard	10 s	1200	12	3M ESPE, MN, USA

To ensure standardization, one caries-free lower first molar was utilized as a natural tooth mold. Once the tooth roots were mounted in mixed epoxy resin and epoxy hardener (EpoThin™2, Buehler, USA) at 23±1 °C, the occlusal surface was flattened to ensure good proximity (< 1 mm) with each LCU tip. Standard occlusal preparation was then performed to create a 4 mm bucco-lingual width and 4 mm depth, with 2 mm remaining dentin thickness. The mesial wall of the cavity was then sectioned apically to 3 mm below CEJ, exposing the mesial side of the pulp chamber and ensuring 4 mm mesiodistal cavity dimension (**Figure 5.1**). The preparation was polished internally to eliminate any undercuts. The RBCs were placed as single bulk increments without their associated adhesives to facilitate subsequent removal and re-use of the cavity.

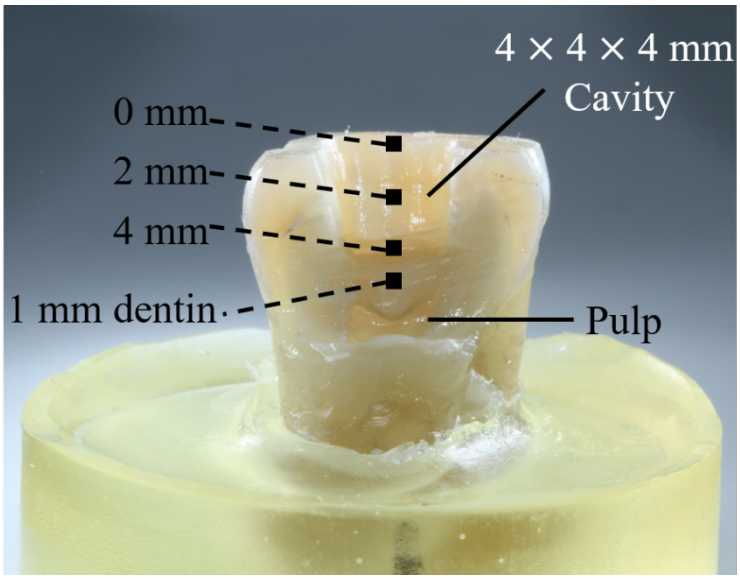

Figure 5.1 Prepared tooth cavity with four different measurement locations: (0 mm, 2 mm, 4 mm from the cavity top and 1 mm into dentin).

Real-time thermographic measurements were recorded for 120 s using an infrared thermal imaging camera (thermoIMAGER TIM 640, Micro-Epsilon Messtechnik GmbH & Co. KG) at ambient temperature. The microscope lens of the thermal camera provided a high optical resolution (640 × 480 pixels at 32 Hz, pixel size 0.1mm) with a spectral range of 7.5-13 µm, an emissivity of 1.0 and a resolution of 75 mK at 33 °C. At the same optical level, the tooth cavity was fixed 6 cm away from the camera lens (**Figure 5.2**).

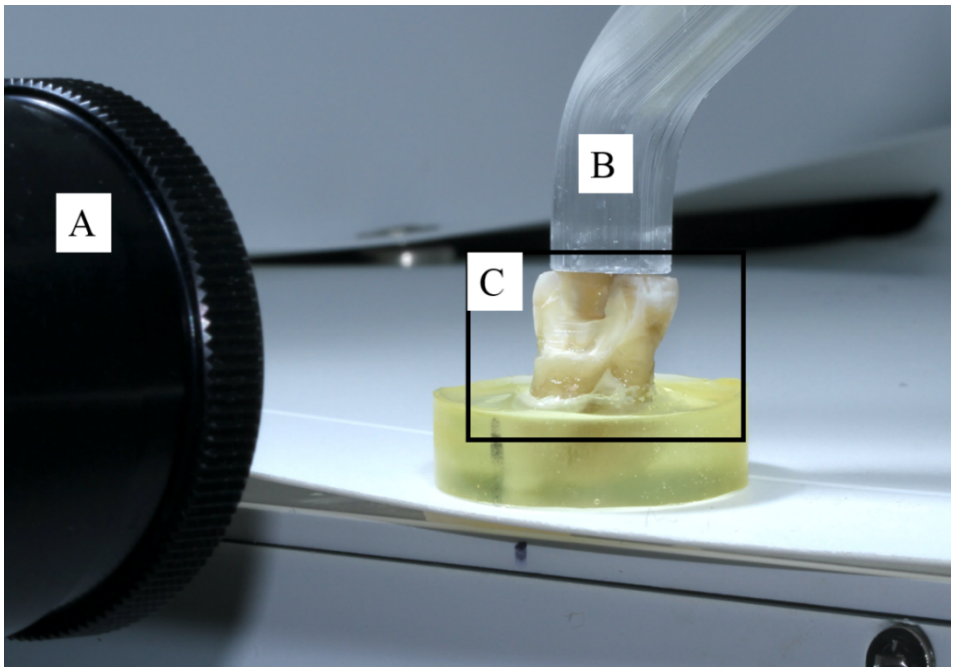

Figure 5.2 Experimental setup for thermal analysis with (A) thermal imaging camera, (B) light-curing unit and (C) prepared tooth cavity.

The empty cavity and different composites were irradiated via three protocols (**Table 5.2**): PC-3s, PC-10s and S10-10s, respectively (n=5). The real-time thermographic measurements over 120 s started immediately before irradiation at a rate of 10 Hz.

The raw videos were analysed using the *Thermal Imager Camera* TIM Software (Micro-Epsilon Messtechnik GmbH & Co. KG) over a temperature range of 20-55 °C. Temperature change at four different positions: 0, 2 and 4 mm from the top of the cavity (0, 2 and 4 mm) and 1 mm below the cavity floor (1 mm dentin) (**Figure 5.1**) were extracted from the total data for further analysis. The maximum temperature attained (T_{max}), the mean temperature rise (ΔT) and the time (s) to reach maximum temperature for the empty cavity and with each RBC were collected for each light-curing protocol at the four positions. The integrated area under each temperature-time (T/t) curve was also calculated (°C·s).

Data were entered into statistical software (SPSS, SPSS Inc., Illinois, USA) to analyze the maximum temperature attained (T_{max}), mean temperature rise (ΔT), time (s) to reach maximum temperature and integrated T/t area. Based on different materials, light-curing protocols and positions, three-way ANOVA followed by multiple One-way ANOVA, independent t-tests and Tukey *post-hoc* tests were used (α=0.05).

5.4 Results

Representative real-time thermal images of the empty cavity and RBCs cured using different protocols are shown in Figures 5.3-5.5. The temperature scale bar was set from 20 to 55 °C, in which zones of high temperature were (false color) red. Before irradiation, only slight temperature elevation (*ca.* 4.5 °C) was evident coronally pre-irradiation with VC (T3-3min) (Figures 3-5 P). During irradiation, PFlow showed the highest localized temperature rise regardless of irradiation protocol (Figures 3-5 K). Maximal temperatures generated upon polymerization were observed at the 2 mm level at the center of the material bulk. At 60 s post-irradiation, the elevated temperature spread to the outer regions and the overall temperature stabilized at *ca*. 30 °C.

Representative real-time temperature plots *for single specimens* of each RBC are collected in Figure 6, for two out of the four analyzed locations. The 2 mm (central) position was the site of maximal peak temperatures, whereas the 1 mm dentin position was the site of lowest peak temperatures. With the obvious exception of the empty cavity, the set of RBCs showed broadly similar temperature development at a given location. A general pattern of similarity was also apparent for each of the three irradiation protocols. However, at the 2 mm position, PFlow exhibited the highest temperature compared to the other RBCs.

Integrated T/t areas were calculated using a baseline of the initial temperature. The maximum temperature attained (T_{max}), mean temperature rises (ΔT), time (s) to reach maximum temperature and integrated T/t areas of the RBCs measured using different light-curing protocols are summarized in (Tables 5.3-5.6 and **Figure 5.7**). These parameters ranged over 28.8 - 54.5 °C, 3.3 - 27.1 °C, 2.9 - 13 s and 66.9 -538.3 °C·s, respectively. Three-way ANOVA demonstrated significant effects for all main factors ($p<0.001$).

Regardless of light-curing protocols, PFlow showed the highest T_{max}, ΔT and integrated T/t areas ($p<0.05$). PFill, OBF and VC (no heat and T3-3min) were next in sequence and the empty cavity showed the lowest values ($p<0.05$). PFlow and PFill took the shortest time (s) to reach the maximum temperature ($p<0.05$), showing their rapid temperature increase. Pre-heated **VC** had T_{max}, ΔT and integrated T/t areas

comparable to the other RBCs, with no difference from the non-heated VC group regardless of the irradiation protocol ($p>0.05$).

The ultra-rapid PC-3s protocol produced the highest T_{max} and ΔT across all materials, significantly higher than with the PC-10s protocol ($p<0.05$). However, S10-10s developed similar T_{max} and ΔT to PC-3s (except the ΔT of PFill) ($p>0.05$). With the same mean irradiance of 1200 mW/cm^2, using S10-10s took a longer time to reach the higher T_{max} and ΔT and the integrated T/t area were less than with PC-10s. Although the highest temperature rise was seen with the PC-3s protocol across the material bulk, at 1 mm within dentin it produced generally no difference in temperature rise than with the other protocols. Compared to the other location, 2 mm presented the highest T_{max}, ΔT and integrated T/t area results. The lowest results were found 1 mm into dentin ($p<0.05$).

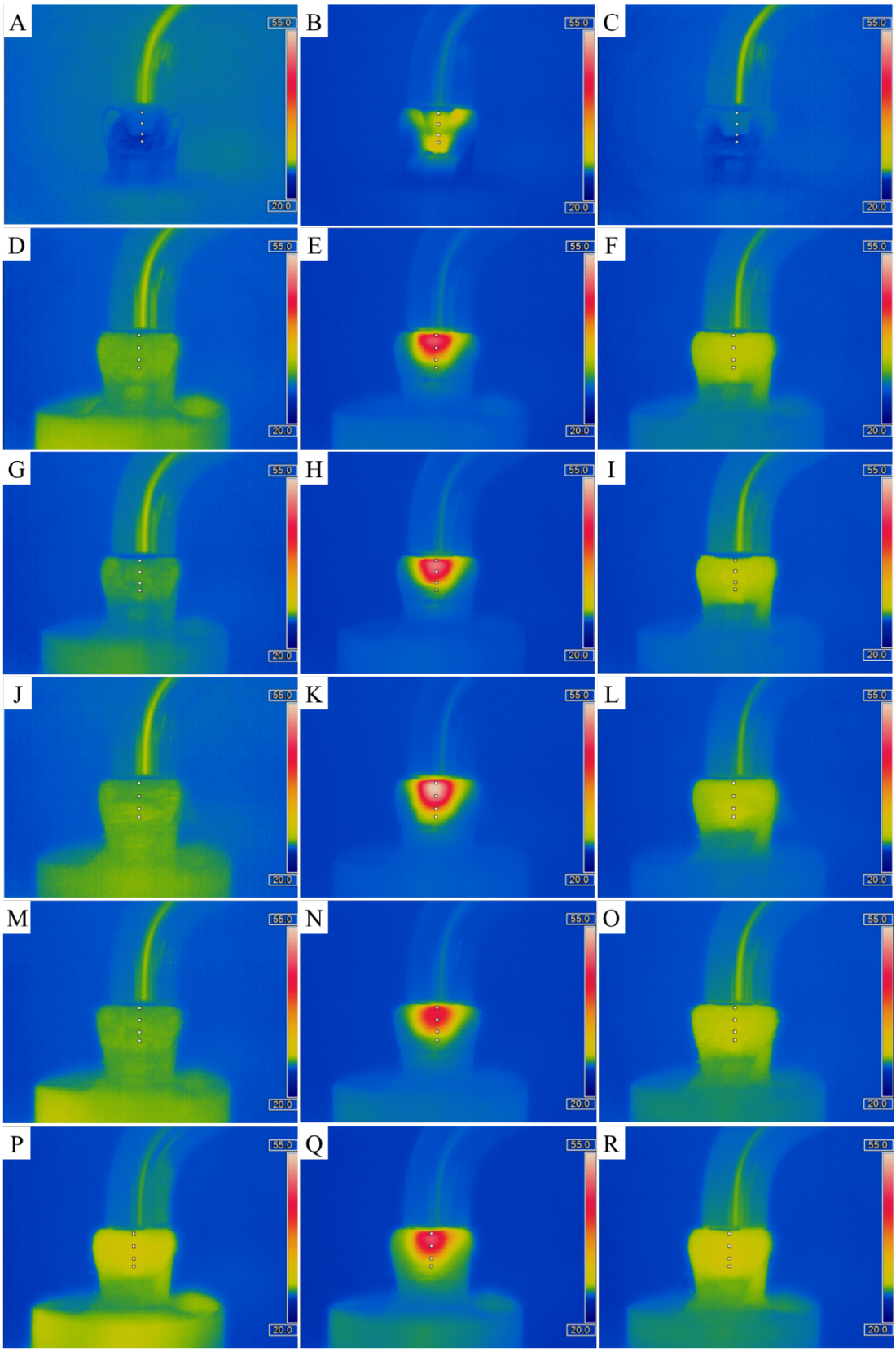

Figure 5.3 Thermal images of the empty cavity and then filled with different composites irradiated using the protocol: PC-3s. (A-C: Empty cavity; D-F: OBF; G-I: PFill; J-L: PFlow; M-O: VC (no heat); P-R: VC (T3-3min)). Left to Right columns: before irradiation, maximum temperature, 60 s post-irradiation.

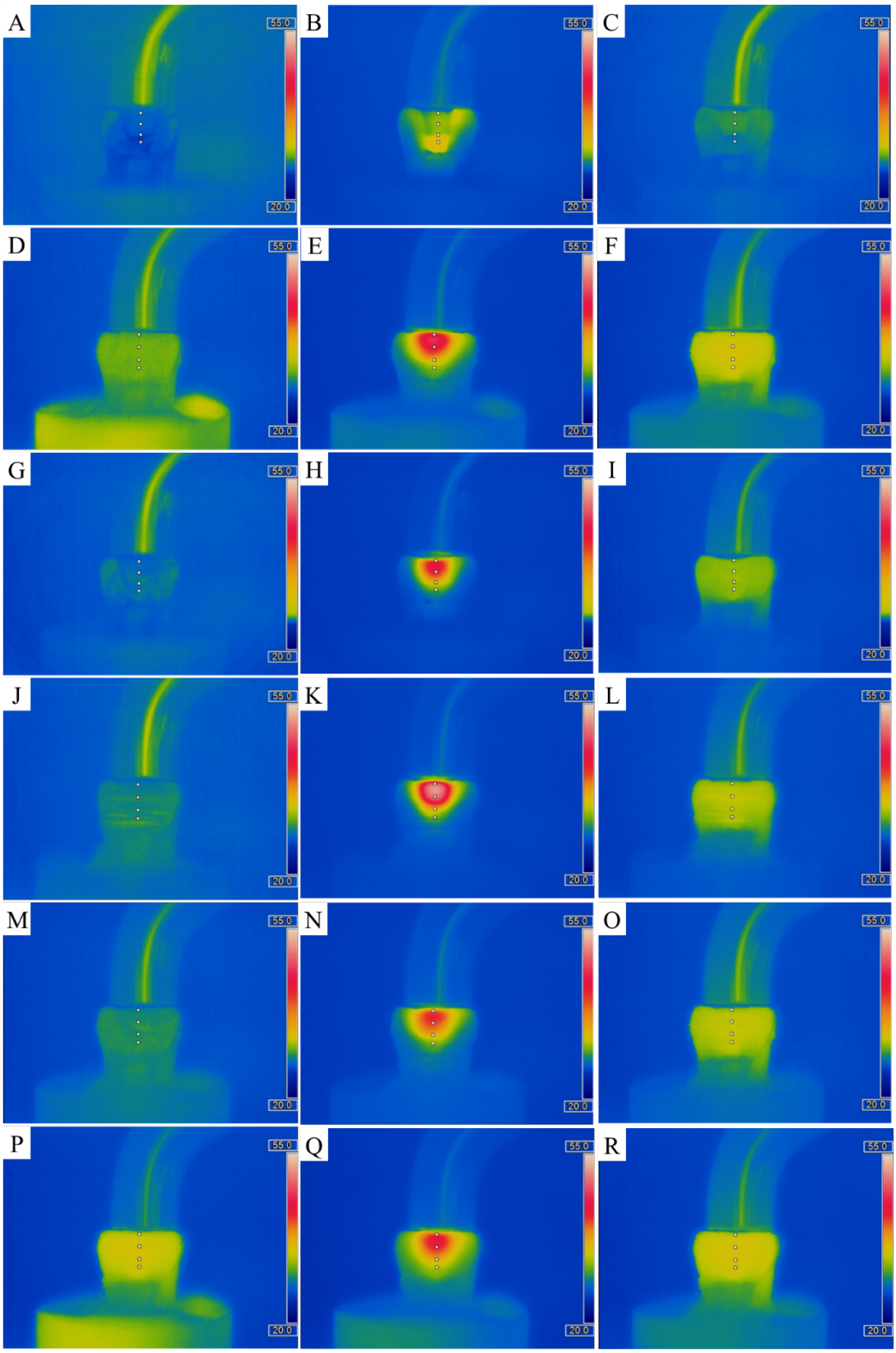

Figure 5.4 Thermal images of the empty cavity and then filled with different composites irradiated using the protocol: PC-10s. (A-C: Empty cavity; D-F: OBF; G-I: PFill; J-L: PFlow; M-O: VC (no heat); P-R: VC (T3-3min)). Left to Right columns: before irradiation, maximum temperature, 60 s post-irradiation.

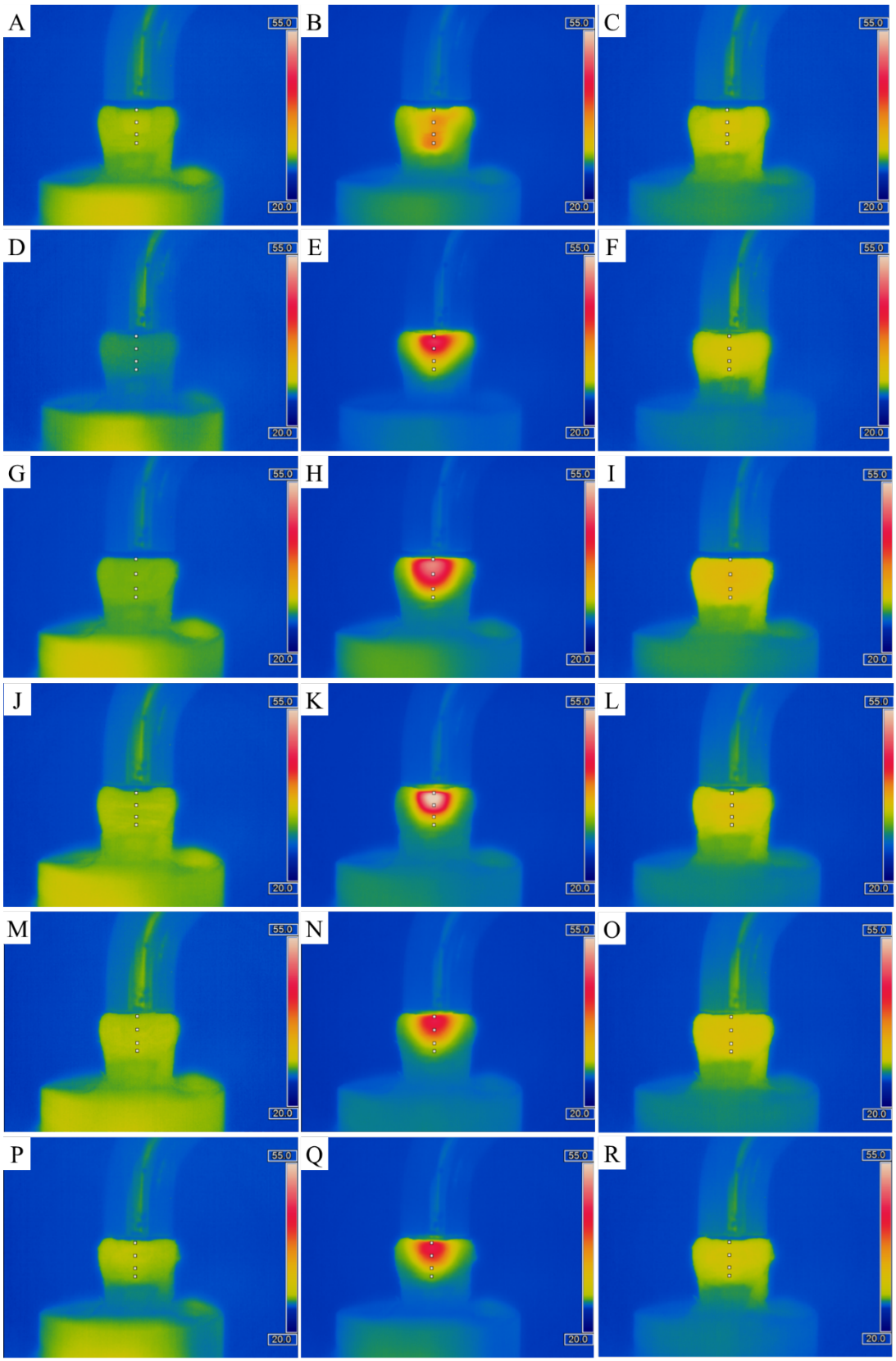

Figure 5.5 Thermal images of the empty cavity and then filled with different composites irradiated using the protocol: S10-10s. (A-C: Empty cavity; D-F: OBF; G-I: PFill; J-L: PFlow; M-O: VC (no heat); P-R: VC (T3-3min)). Left to Right columns: before irradiation, maximum temperature, 60 s post-irradiation.

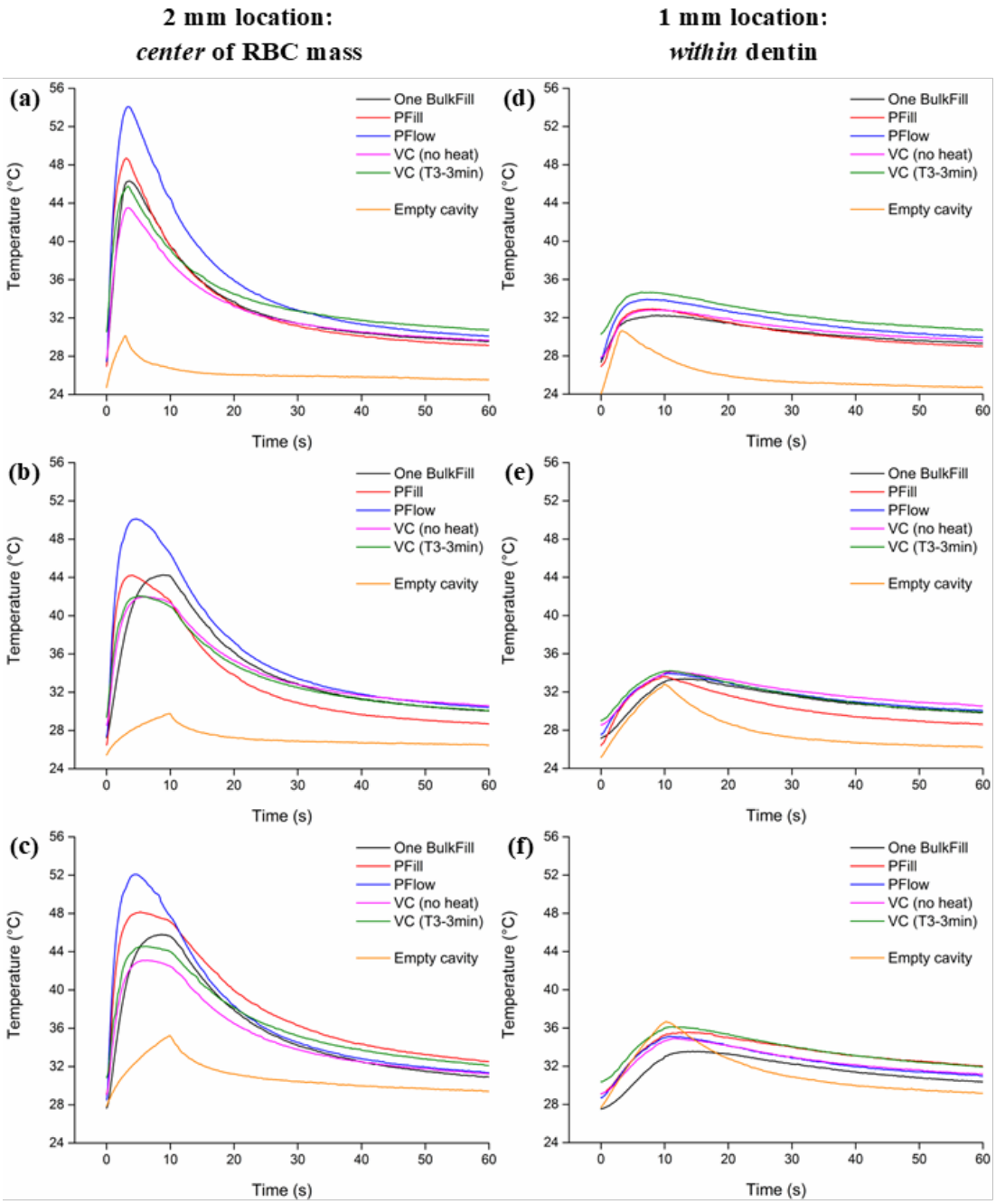

Figure 5.6 Representative real-time temperature curves for *single specimens* of RBCs cured using PC-3s (a & d), PC-10s (b & e) and S10-10s (c & f) – measured either at *the center of the RBC mass* (a-c) or at *1 mm within dentin* (d-f), (cf Figure 1). (NB Table 3 presents the mean peak temperatures for all specimens (n = 5) in each group).

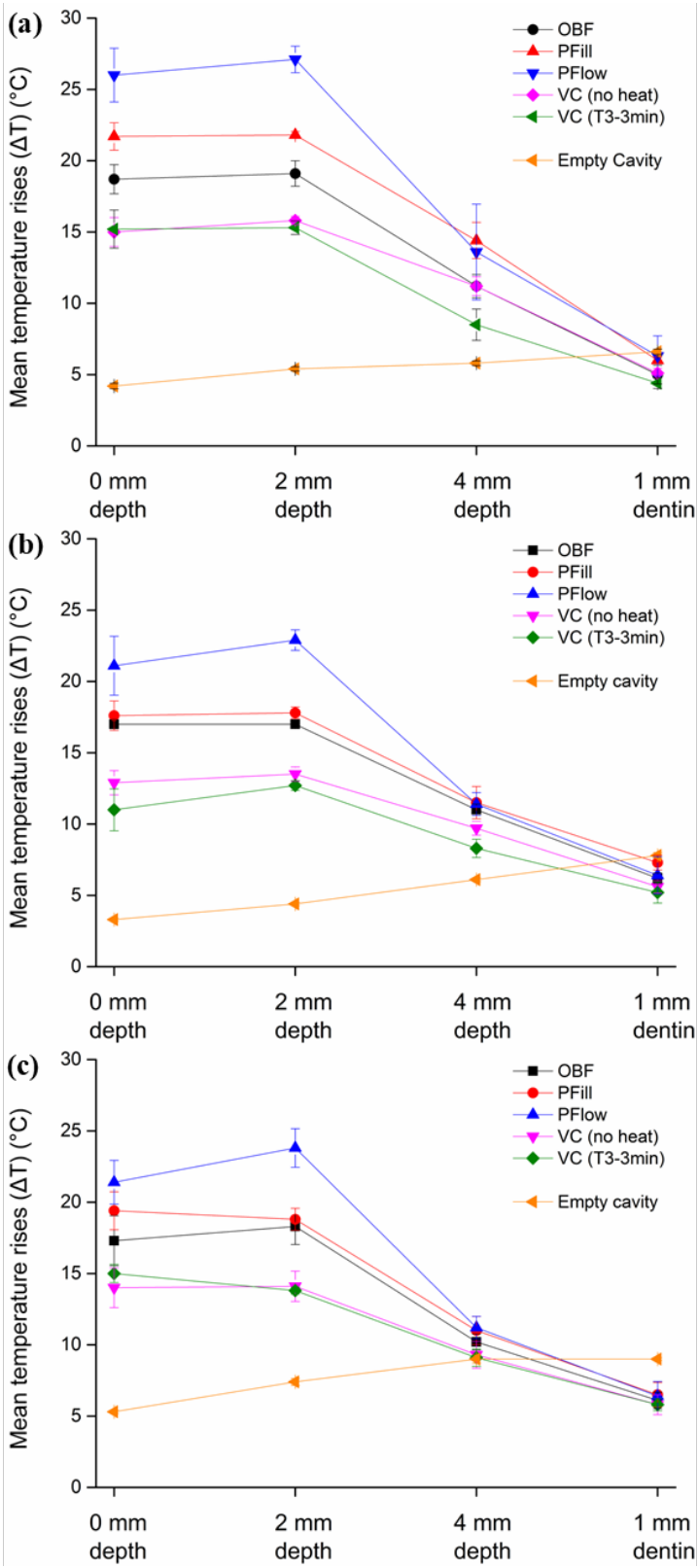

Figure 5.7 Mean temperature rise (ΔT) of RBCs measured at different positions using different irradiation protocols: (a) PC-3s, (b) PC-10s and (c) S10-10s.

Table 5.3 Maximum temperatures (T_{max}, °C) using different irradiation protocols, measured at different positions.

Materials	Protocols and Positions											
	Bluephase *PowerCure* 3 s				Bluephase *PowerCure* 10 s				Elipar S10 10 s			
	0 mm	2 mm	4 mm	1 mm dentin	0 mm	2 mm	4 mm	1 mm dentin	0 mm	2 mm	4 mm	1 mm dentin
Empty cavity	$29.2^{a\ AB}$ (0.26)	$30.2^{a\ BCD}$ (0.30)	$30.2^{a\ BCD}$ (0.43)	$30.6^{a\ CD}$ (0.54)	$28.8^{a\ A}$ (0.11)	$29.8^{a\ ABC}$ (0.08)	$31.3^{a\ DE}$ (0.31)	$32.9^{a\ F}$ (0.37)	$32.4^{a\ EF}$ (0.87)	$35.3^{a\ G}$ (1.05)	$36.7^{a\ H}$ (0.92)	$36.7^{b\ H}$ (0.98)
OBF	$45.8^{c\ C}$ (1.22)	$46.6^{c\ C}$ (1.07)	$38.5^{b\ B}$ (0.87)	$32.3^{b\ A}$ (0.70)	$44.0^{d\ C}$ (1.10)	$44.3^{c\ C}$ (0.85)	$38.2^{b\ B}$ (0.61)	$33.4^{a\ A}$ (0.96)	$44.5^{b\ C}$ (2.19)	$45.9^{bc\ C}$ (2.33)	$37.7^{ab\ B}$ (1.66)	$33.6^{a\ A}$ (1.18)
PFill	$48.5^{d\ F}$ (0.87)	$48.8^{d\ F}$ (0.40)	$41.2^{b\ D}$ (1.30)	$32.9^{bc\ A}$ (0.33)	$44.0^{cd\ E}$ (1.13)	$44.3^{c\ E}$ (0.72)	$38.0^{b\ C}$ (1.43)	$33.7^{a\ AB}$ (0.36)	$47.9^{cd\ F}$ (1.36)	$47.9^{c\ F}$ (0.97)	$40.1^{c\ CD}$ (1.25)	$35.6^{ab\ B}$ (1.15)
PFlow	$53.1^{f\ FG}$ (1.94)	$54.5^{f\ G}$ (1.04)	$41.2^{b\ C}$ (3.49)	$34.0^{cd\ A}$ (1.51)	$48.1^{e\ D}$ (2.23)	$50.3^{d\ DEF}$ (0.81)	$38.8^{b\ BC}$ (0.64)	$34.0^{a\ A}$ (0.53)	$49.3^{d\ DE}$ (1.99)	$52.3^{d\ EFG}$ (1.88)	$39.7^{bc\ C}$ (1.26)	$35.2^{ab\ AB}$ (1.54)
VC (no heat)	$42.5^{b\ EF}$ (0.86)	$43.6^{b\ F}$ (0.81)	$39.1^{b\ CD}$ (1.08)	$32.9^{bc\ A}$ (0.56)	$41.0^{bc\ DE}$ (0.91)	$42.0^{b\ EF}$ (0.72)	$38.2^{b\ C}$ (0.68)	$34.2^{a\ AB}$ (0.89)	$42.4^{b\ EF}$ (1.49)	$43.2^{b\ F}$ (0.96)	$38.5^{abc\ C}$ (1.03)	$34.9^{ab\ B}$ (0.64)
VC (T3-3min)	$44.8^{c\ FG}$ (1.42)	$45.8^{c\ G}$ (0.35)	$39.1^{b\ CD}$ (0.99)	$34.7^{d\ AB}$ (0.29)	$39.3^{b\ DE}$ (2.48)	$42.1^{b\ EF}$ (1.36)	$37.5^{b\ BCD}$ (1.71)	$34.2^{a\ A}$ (1.97)	$45.1^{bc\ G}$ (1.02)	$44.6^{b\ FG}$ (0.81)	$39.8^{bc\ DE}$ (1.11)	$36.2^{b\ ABC}$ (0.99)

For each position, the same lower case superscript letters indicate homogeneous subsets among the materials.

For each material, the same CAPITAL superscript letters indicate homogeneous subsets among different conditions.

Table 5.4 Mean temperature rises (ΔT, °C) using different irradiation protocols, measured at different positions.

Materials	Protocols and Positions											
	Bluephase *PowerCure* 3 s				Bluephase *PowerCure* 10 s				Elipar S10 10 s			
	0 mm	2 mm	4 mm	1 mm dentin	0 mm	2 mm	4 mm	1 mm dentin	0 mm	2 mm	4 mm	1 mm dentin
Empty cavity	$4.2^{a\ B}$ (0.19)	$5.4^{a\ CD}$ (0.15)	$5.8^{a\ DE}$ (0.16)	$6.6^{d\ F}$ (0.19)	$3.3^{a\ A}$ (0.11)	$4.4^{a\ B}$ (0.11)	$6.1^{a\ E}$ (0.13)	$7.8^{c\ G}$ (0.21)	$5.3^{a\ C}$ (0.11)	$7.4^{a\ G}$ (0.25)	$9.0^{a\ H}$ (0.29)	$9.0^{b\ H}$ (0.10)
OBF	$18.7^{c\ CD}$ (1.02)	$19.1^{c\ D}$ (0.89)	$11.2^{bc\ B}$ (0.81)	$5.0^{ab\ A}$ (0.65)	$17.0^{c\ C}$ (0.32)	$17.0^{c\ C}$ (0.30)	$11.0^{cd\ B}$ (0.40)	$6.2^{ab\ A}$ (0.38)	$17.3^{cd\ CD}$ (1.75)	$18.3^{c\ CD}$ (1.27)	$10.2^{ab\ B}$ (0.56)	$6.1^{a\ A}$ (0.58)
PFill	$21.7^{d\ E}$ (0.96)	$21.8^{d\ E}$ (0.25)	$14.4^{d\ C}$ (1.27)	$6.0^{bcd\ A}$ (0.23)	$17.6^{c\ D}$ (1.03)	$17.8^{c\ D}$ (0.41)	$11.5^{d\ B}$ (1.13)	$7.3^{bc\ A}$ (0.52)	$19.4^{de\ D}$ (1.33)	$18.8^{c\ D}$ (0.77)	$11.0^{b\ B}$ (0.98)	$6.5^{a\ A}$ (0.86)
PFlow	$26.0^{f\ DE}$ (1.88)	$27.1^{f\ E}$ (0.93)	$13.6^{cd\ B}$ (3.35)	$6.3^{cd\ A}$ (1.42)	$21.1^{d\ C}$ (2.07)	$22.9^{d\ CD}$ (0.72)	$11.4^{d\ B}$ (0.80)	$6.4^{abc\ A}$ (1.31)	$21.4^{e\ C}$ (1.53)	$23.8^{d\ CDE}$ (1.35)	$11.2^{b\ B}$ (0.79)	$6.4^{a\ A}$ (1.03)
VC (no heat)	$15.0^{b\ FG}$ (1.01)	$15.8^{b\ G}$ (0.29)	$11.2^{bc\ CD}$ (0.66)	$5.1^{abc\ A}$ (0.34)	$12.9^{b\ DE}$ (0.85)	$13.5^{b\ EF}$ (0.50)	$9.7^{c\ BC}$ (0.48)	$5.6^{a\ A}$ (0.43)	$14.0^{b\ EF}$ (1.39)	$14.1^{b\ EFG}$ (1.06)	$9.3^{a\ B}$ (0.94)	$5.8^{a\ A}$ (0.70)
VC (T3-3min)	$15.2^{b\ E}$ (1.34)	$15.3^{b\ E}$ (0.47)	$8.5^{ab\ B}$ (1.10)	$4.4^{a\ A}$ (0.37)	$11.0^{b\ C}$ (1.47)	$12.7^{b\ D}$ (0.35)	$8.3^{b\ B}$ (0.64)	$5.2^{a\ A}$ (0.74)	$15.0^{bc\ E}$ (0.64)	$13.8^{b\ DE}$ (0.24)	$9.1^{a\ B}$ (0.61)	$5.8^{a\ A}$ (0.43)

For each position, the same lower case superscript letters indicate homogeneous subsets among the materials.

For each material, the same CAPITAL superscript letters indicate homogeneous subsets among different conditions.

Table 5.5 Time (s) to reach maximum temperatures using different irradiation protocols at different positions.

Materials	Protocols and Positions											
	Bluephase *PowerCure* 3 s				Bluephase *PowerCure* 10 s				Elipar S10 10 s			
	0 mm	2 mm	4 mm	1 mm dentin	0 mm	2 mm	4 mm	1 mm dentin	0 mm	2 mm	4 mm	1 mm dentin
Empty cavity	$2.9^{a\ A}$ (0.07)	$2.9^{a\ A}$ (0.05)	$2.9^{a\ A}$ (0.05)	$3.2^{a\ A}$ (0.16)	$9.8^{d\ B}$ (0.16)	$9.9^{e\ B}$ (0.17)	$9.8^{c\ B}$ (0.19)	$9.9^{a\ B}$ (0.10)	$9.8^{d\ B}$ (0.24)	$9.7^{c\ B}$ (0.30)	$9.8^{ab\ B}$ (0.26)	$10.0^{a\ B}$ (0.29)
OBF	$3.0^{ab\ A}$ (0.00)	$3.2^{b\ A}$ (0.13)	$3.7^{a\ A}$ (0.73)	$8.2^{b\ BC}$ (1.91)	$7.9^{c\ B}$ (0.66)	$8.8^{d\ BC}$ (0.21)	$9.9^{c\ BC}$ (0.24)	$12.0^{c\ DE}$ (0.85)	$8.4^{c\ BC}$ (0.61)	$8.5^{c\ BC}$ (0.94)	$10.1^{b\ CD}$ (0.27)	$13.0^{c\ E}$ (2.09)
PFill	$3.0^{a\ A}$ (0.05)	$3.0^{a\ A}$ (0.05)	$2.9^{a\ A}$ (0.05)	$6.8^{b\ D}$ (0.64)	$4.2^{a\ AB}$ (0.54)	$3.6^{a\ A}$ (0.36)	$4.0^{a\ A}$ (0.21)	$9.8^{a\ E}$ (0.20)	$5.6^{b\ CD}$ (0.80)	$5.3^{ab\ BC}$ (1.08)	$9.6^{ab\ E}$ (0.30)	$12.3^{bc\ F}$ (1.09)
PFlow	$3.1^{ab\ A}$ (0.13)	$3.1^{ab\ A}$ (0.12)	$4.2^{a\ A}$ (2.23)	$7.3^{b\ BC}$ (2.80)	$4.3^{a\ A}$ (0.34)	$4.3^{b\ A}$ (0.23)	$5.4^{a\ AB}$ (0.90)	$10.2^{ab\ D}$ (0.50)	$4.0^{a\ A}$ (0.37)	$4.0^{a\ A}$ (0.32)	$8.8^{a\ CD}$ (1.28)	$10.5^{ab\ D}$ (0.43)
VC (no heat)	$3.3^{b\ A}$ (0.27)	$3.2^{b\ A}$ (0.10)	$3.2^{a\ A}$ (0.19)	$8.5^{b\ C}$ (2.02)	$6.0^{b\ B}$ (0.69)	$5.7^{c\ B}$ (0.33)	$8.5^{bc\ C}$ (1.35)	$11.2^{bc\ D}$ (0.65)	$5.2^{b\ B}$ (0.34)	$5.6^{b\ B}$ (0.47)	$9.8^{ab\ CD}$ (0.52)	$10.7^{ab\ D}$ (0.50)
VC (T3-3min)	$3.1^{ab\ A}$ (0.16)	$3.1^{ab\ A}$ (0.14)	$3.3^{a\ AB}$ (0.39)	$6.3^{ab\ DE}$ (0.72)	$4.6^{a\ BC}$ (0.40)	$4.6^{b\ C}$ (0.16)	$7.2^{b\ E}$ (1.33)	$10.2^{ab\ F}$ (0.67)	$5.2^{b\ CD}$ (0.43)	$5.6^{b\ CD}$ (0.88)	$9.9^{ab\ F}$ (0.34)	$11.1^{abc\ F}$ (0.53)

For each position, the same lower case superscript letters indicate homogeneous subsets among the materials.

For each material, the same CAPITAL superscript letters indicate homogeneous subsets among different conditions.

Table 5.6 Integrated areas (°C·s) for plots shown in Figure 6 using different light-curing protocols at different positions.

Materials	Protocols and Positions											
	Bluephase *PowerCure* 3 s				Bluephase *PowerCure* 10 s				Elipar S10 10 s			
	0 mm	2 mm	4 mm	1 mm dentin	0 mm	2 mm	4 mm	1 mm dentin	0 mm	2 mm	4 mm	1 mm dentin
Empty cavity	$66.9^{a\ A}$ (4.72)	$89.0^{a\ B}$ (10.25)	$100.3^{a\ BC}$ (7.41)	$115.94^{a\ CD}$ (11.52)	$84.5^{a\ AB}$ (3.48)	$105.8^{a\ BC}$ (7.16)	$136.4^{a\ D}$ (6.42)	$166.7^{ab\ E}$ (7.07)	$130.0^{a\ D}$ (11.72)	$180.1^{a\ E}$ (15.86)	$219.1^{a\ F}$ (14.36)	$223.0^{ab\ F}$ (10.74)
OBF	$322.8^{b\ CD}$ (36.89)	$363.1^{d\ DE}$ (23.01)	$283.2^{cd\ BC}$ (16.48)	$194.88^{b\ A}$ (11.70)	$415.4^{cd\ EF}$ (11.97)	$435.2^{d\ FG}$ (18.14)	$332.9^{cd\ CD}$ (20.08)	$241.2^{c\ AB}$ (18.13)	$430.2^{c\ F}$ (46.11)	$492.6^{c\ G}$ (44.93)	$343.6^{cd\ D}$ (23.04)	$245.9^{ab\ AB}$ (17.29)
PFill	$374.1^{c\ CDE}$ (22.08)	$394.8^{d\ E}$ (12.12)	$324.8^{de\ BC}$ (19.54)	$219.81^{bc\ A}$ (6.29)	$387.3^{c\ CDE}$ (37.42)	$403.6^{d\ E}$ (30.90)	$329.4^{cd\ CD}$ (29.71)	$239.7^{c\ A}$ (20.68)	$387.3^{bc\ CDE}$ (37.42)	$538.3^{c\ F}$ (40.95)	$390.2^{d\ DE}$ (39.84)	$264.7^{b\ AB}$ (33.48)
PFlow	$453.7^{d\ C}$ (30.74)	$500.4^{e\ C}$ (23.88)	$343.3^{e\ B}$ (43.14)	$237.49^{c\ A}$ (36.52)	$461.6^{d\ C}$ (47.88)	$527.6^{e\ C}$ (28.17)	$360.9^{d\ B}$ (34.09)	$244.4^{c\ A}$ (43.55)	$455.2^{c\ C}$ (48.78)	$533.4^{c\ C}$ (43.43)	$356.1^{d\ B}$ (30.81)	$236.8^{ab\ A}$ (37.58)
VC (no heat)	$287.4^{b\ BC}$ (24.76)	$313.7^{c\ BCD}$ (19.32)	$266.4^{c\ B}$ (22.45)	$186.51^{b\ A}$ (16.65)	$325.0^{b\ CDE}$ (21.86)	$345.8^{c\ DE}$ (16.18)	$294.1^{c\ BC}$ (18.64)	$206.0^{bc\ A}$ (12.68)	$347.9^{b\ DE}$ (35.07)	$372.5^{b\ E}$ (26.78)	$294.9^{bc\ BC}$ (24.14)	$212.0^{a\ A}$ (20.79)
VC (T3-3min)	$282.2^{b\ D}$ (25.24)	$229.8^{b\ C}$ (8.12)	$173.5^{b\ B}$ (20.27)	$127.14^{a\ A}$ (10.67)	$272.3^{b\ D}$ (34.72)	$278.8^{b\ D}$ (12.27)	$222.6^{b\ C}$ (12.27)	$158.6^{a\ AB}$ (18.72)	$344.4^{b\ E}$ (25.39)	$346.0^{b\ E}$ (10.33)	$275.2^{b\ D}$ (17.99)	$200.2^{a\ BC}$ (16.46)

For each position, the same lower case superscript letters indicate homogeneous subsets among the materials.

For each material, the same CAPITAL superscript letters indicate homogeneous subsets among different conditions.

5.5 Discussion

In restorative dentistry it is vital to ensure pulpal health by controlling all biological and clinical variables, as any substantial temperature rise may lead to irreversible pupal damage [228]. The long-term performance of RBCs is strongly dependent upon their network integrity as expressed partly via their DC [222]. During exothermic polymerization, C=C bonds convert into C-C bonds [257, 258]. Radiant energy from LCUs also contributes to the transient temperature increase [257], depending upon the LCU type, irradiance, wavelength distribution and exposure duration [226, 232, 243, 250]. Longer exposure periods may cause over-heating without significantly changing the polymerization kinetics [246, 259].

Infrared (IR) thermography is a non-destructive method that can capture temperature maps of objects. Infrared imaging has been widely used in multiple medical applications [260]. In this study, a thermal imaging camera was used to obtain real-time intra-cavity temperature maps of bulk-fill RBCs at different locations, using various irradiation protocols.

Our results showed significant ($p<0.05$) differences in T_{max}, ΔT and integrated T/t areas of the investigated RBCs. PFlow showed the highest T_{max}, ΔT and integrated T/t area. This agrees with previous studies in which, with high monomer content, more lightly filled flowable RBCs produced higher temperature rises [226, 229, 231, 233, 254]. The lower viscosity of PFlow may also contribute by enhancing free radical mobility and the rate of polymerization. However, according to a previous study, T_{max} for a pair of non-flowable and flowable composites were not significantly different [261]. But both materials were irradiated for 60 s, which is now beyond normal clinical practice. This extended radiant heating would tend to outweigh any differences in exothermic heating to produce a similar outcome.

Resin monomer composition influences temperature rise during polymerization [231]. Low-viscous and highly-reactive monomers can improve the polymerization rate and the final DC [262]. This early-stage rapid polymerization can increase the system temperature [231]. The comparable temperature rise of pre-heated **VC** to non-pre-heated composites is probably due to their similar polymerization rate and DC [259].

However, the high-molecular-mass fragmentation monomers within **OBF**, such as AUDMA and DDDMA, increase matrix viscosity and reduce polymerization rate [263-265]. Hence, **OBF** took a relatively long time to reach maximum temperature, especially with 10 s irradiation. In **PFill**, the addition-fragmentation chain reaction agent (AFCT) is incorporated as part of the ultra-rapid photo-cure formulation. This results in a sufficient DC, good initial viscoelastic properties under immediate load and controlled polymerization shrinkage stress [245, 247]. Network reconfiguration during the modified polymerization may be a factor in the slightly higher temperature rise compared to other non-flowable bulk-fills [90, 91, 265].

VC, compared to the other non-flowable RBCs, has a high filler content of 83 wt.% and thus proportionally reduced monomer content. This could explain the relatively lower T_{max}, ΔT and integrated T/t areas. In other formulations with a high portion of filler particles, absorption and scattering of light by may limit depth of cure [266, 267]. T_{max} for **VC** (T3-3min) was higher than **VC** (no heat) but significantly lower than 60.6 °C, measured in a previous study via thermocouple [253]. Pre-irradiation, only mild temperature elevation (*ca.* 4.5 °C) was evident coronally with **VC** (T3-3min) (Figures 3-5 P). After removal from a heating device and during handling, composite temperatures decrease [268, 269]. The moderate temperature of **VC** (T3-3min) before irradiation and 5.4- 5.8 °C temperature rise during irradiation suggests clinical safety despite the 3 min pre-heating period.

Apart from the exothermic reaction, ΔT also increases from LCU irradiation [233, 250, 252, 270]. Long exposure durations and higher irradiance are the two most important factors affecting pulpal temperature [233, 243, 254]. Of the three light-curing protocols (PC-3s, PC-10s and S10-10s), PC-3s, with the highest mean irradiance of 3000 mW/cm^2, led to higher T_{max} and ΔT than PC-10s (1200 mW/cm^2). However, the ΔT results of S10-10s were comparable to PC-3s, except with PFill. After 3 s irradiation, the time (s) to reach the maximum temperature was also *ca.* 3 s. However, the integrated T/t area was lower than for PC-10s (12 J/cm^2), which could be attributed to lower radiant energy delivered (9 J/cm^2).

Remaining dentin thickness is an essential thermal insulator for pulpal tissues [231, 271]. The tooth cavity and surrounding soft tissues can also dissipate heat. During irradiation, 10 s irradiation resulted in a higher ΔT within the empty cavity. Moreover, in the absence of any composite, the highest ΔT occurred at 1 mm within the dentin.

Excluding heat received by the empty cavity during irradiation, the exothermic temperature rises of the RBCs can be compared. Regardless of light-curing protocols, at the 2 mm position, the rank order of ΔT was: PFlow > PFill > OBF > VC (no heat) > VC (T3-3min). This agrees with previous studies that flowable RBCs with more C=C bonds generate more heat during polymerization [258, 271].

At different depths within the bulk-fill materials, 2 mm depth exhibited the highest T_{max}, ΔT and integrated T/t area. Thus, the central part of the material showed the highest temperature rise [226, 229, 271]. However, some studies using thermocouples found that restoration surfaces reach higher temperatures than internal or base locations [271, 272]. This may be related to different experimental setups and materials, which merits further investigation.

Adverse effects of elevated temperatures to the dentin and pulpal structures are highly important. According to an early study, as temperature increased (above normal oral temperature) *from* 5.5 *to* 11 °C, at 1mm into dentin, the possibility of pulp necrosis increased *from* 15 % *to* 60 % [228]. However, this all depends upon the duration and exact nature of the thermal challenge. A follow-up study indicated that an 11.2 °C increase would still be considered safe and not damage pulpal tissues [273]. In the present study, restoration with **VC** and the usage of the ultra-rapid PC-3s protocol showed ΔT results closer to 5.5 °C. This suggests their clinical safety. The higher temperature data observed with PC-10s and S10-10s must be due to their high radiant exposure over a longer - but still relatively short time (10 s). Remaining dentin thickness is vital for preventing thermal damage of the pulp [231, 271, 274, 275]. The present study used a 2 mm dentin thickness, which - with different irradiation protocols - led to a mild temperature-propagation period of 8.5-13 s. A thinner layer of remaining dentin may be insufficient to prevent acute temperature rise and pulp damage [271, 274]. The dentin heat-storage capacity and thermal diffusivity determine the rate of heat dissipation. Some *in vivo* and *in vitro* measurements have also demonstrated slower temperature changes within the pulp due to dynamic temperature regulation by the surrounding soft tissue and constant blood flow [226, 230, 243, 251]. The temperatures developed at 1 mm dentin in the present study could have been less in a more clinically simulative environment [275].

Generally, the magnitudes of clinical temperature changes depend upon material thermal properties and operator skills [236, 249]. Clinicians are responsible for

material selection and LCU/curing mode, the usage of incremental/bulk-fill techniques and the distance/angle between the LCU tip and the restoration surface that may affect temperature profiles within both restoration and pulp chamber [230, 270].

High irradiance protocols and pre-heating showed moderate temperature increases within the RBC materials. Flowable materials showed slightly higher temperature elevation, attributed to their higher monomer content and lower filler load (wt.%). However, a remaining dentin thickness of 2 mm can prevent thermal insult and irreversible damage to pulpal tissues. Additionally, based on the present results, it is recommended to have a 3 s interval before any additional irradiation to allow for thermal recuperation.

5.6 Conclusions

Within the limitations of this study, the following conclusions can be summarized:

1) Material composition and different light-curing protocols can influence temperature rise (ΔT) at different depths during intra-dental photo-curing, with maximal ΔT generally occurring at a 2 mm depth into bulk-fill RBCs.

2) The 3 s high-irradiance light-curing protocol with Bluphase *PowerCure* was generally comparable to the standard 10 s Elipar S10, with temperature increase *ca.* to 6 °C at 1 mm within dentin. This is considered safe for light-curing in deep cavities when sufficient remaining dentin thickness is present.

3) Pre-heating did not significantly influence VC temperature profiles, regardless of light-curing protocols and different depths. The mild temperature elevation at 1 mm within dentin (*ca.* 5.5 °C) during irradiation of VC (T3-3min) suggests that pre-heating VC, prior to placement and irradiation, is thermally safe for the dental pulp.

Discussion of Points raised by the External Examiner

1. Why was the conventional RBC: Tetric Evoceram not included as a control?

   Evoceram (irradiated for 10 s) was not required as a further control RBC to determine the thermal effects of URPBF photo curing for 3 s at high irradiance.

2. Why was the LCU changed between studies (S10, Valo, …), when we only see the effect of short irradiation?

   10 s irradiation protocols were the appropriate comparators for the control materials versus URPBF at 3 s. See further: Chapter 4, Q1.

3. The tooth was stored dry. Why did you not work with a water-saturated tooth - since water has an important influence on heat transmission?

   The tooth was stored in water prior to sectioning and was also irrigated during cavity preparation so that - during measurement (within 2 days) – the dentine structure was sufficiently hydrated.

4. What contributes most to pulpal temperature rise (PTR) – the LCU irradiation or the RBC exotherm?

   The RBC exotherm.

5. Is PTR the same in both a conventional and an ultrafast system? Cf. Randolph *et al*. *Dent Mater* 2014 (Discussion p. 125).

   Randolph *et al*. *Dent Mater* 2014,[95] evaluated bisGMA/TEGDMA monomer chemistry with different PI systems (CQ vs. TPO), cured with different irradiances and times. The TPO formulations were considered to be 'ultrafast'. When the same radiant exposure was received between CQ-based and TPO-based (20 J/cm^2), TPO produced a higher exotherm. This however was not significant at 40 J/cm^2.

The ultra-fast system in our study incorporates a different monomer composition (not only the PI system). PTRs (i.e. ΔTs at 1 mm in dentine), seen in resin composites with AFCT agents (PFill and OBF cured in PC-3s curing protocol), produced comparable effects: ΔT *ca.* 5-6 ^{o}C.

6. What exactly is 'more mobile' in flowable composites: radicals or something else (p. 125)?

Both radicals and potentially reactive monomers are more mobile than in systems of higher viscosity. As polymerization continues beyond the gel point, the reaction becomes diffusion controlled, which means that as the viscosity of the reacting medium increases with conversion. Propagation of chain radicals relies on mobility of free monomer molecules to encounter the radical chain-ends. Monomer compositions with low initial viscosities tend to enter this diffusion-controlled kinetic era at an later stage of conversion [15].

7. How does this connect with the glass transition and attainment of a 'steady state'?

If the degree of conversion in a more flowable composite – containing dimethacrylate monomers - is *higher*, then it will be more cross-linked and the T_g is likely to be *higher*.

If by 'steady state' we refer to *attainment of the final DC* at a given system temperature, the time required for this to be achieved depends on multiple variables.

However, the term 'steady state' is also used in the context of photopolymerization to refer to 'balance(s)' that may be obtained in the varied sequential steps of free-radical addition, including the initial population of free-radicals produced by irradiation of the PI system. In the case of URPBF systems, such intermediate 'steady states' may not be obtained as the system may not be in equilibrium.

8. Are you satisfied with studies determining which temperature can be considered safe for the pulp? Do they need to be further verified?

   Many previous in-*vitro* and in-*vivo* studies have established the effectiveness of dentin structure as an insulator. Most current literature refers to Zack & Cohen (1965), regarding pulpal safety. A follow up study that used the same method (Baldissara *et al*., 1997), concluded that the damage to dentin in (cavity preparation) is another main cause of pulpal damage, along with heat generated from resin composite restoration. Therefore, it is important to consider both the temperature rise as well as the duration of such increased temperature. However, a significant modifications to resin composite chemistry and LCU technology is now available which could benefit from further in-*vivo* assessment.

CHAPTER SIX

Characterizing surface viscoelastic integrity of ultra-fast photo-polymerized composites: methods development

David C. Watts[a,c,*] ***Hamad Algamaiah***[a,b,**],

[a] Dentistry, School of Medical Sciences, University of Manchester, Manchester, UK

[b] Department of Restorative Dental Science, College of Dentistry, King Saud University, Riyadh, Saudi Arabia

[c] Photon Science Institute, University of Manchester, Manchester, UK

Published *in Dental Materials 36 (2020)1255–1265 (Appendix D)*

6.1 Abstract

Objective: Resin-Composites are now available designed for polymerization using 3 s of intense light irradiation. The aim was to develop an experimental method to probe their surface viscoelastic integrity immediately following such rapid photo-cure via macroscopic surface indentation under constant stress as a function of time.

Methods: Two bulk-fill composites (Ivoclar AG) were studied: Tetric PowerFill (PFill) and PowerFlow (PFlow). Split molds were used to fabricate cylindrical (4 mm (dia) x 4 mm) paste specimens, irradiated at 23 ^{o}C at 0 mm from the top surface with a Bluephase *PowerCure* LED-LCU, with 3 s or 5 s modes, emitting 3 and 2 W/cm^2, respectively. Post-irradiation specimens were immediately transferred to an apparatus equipped with a flat-ended indentor of 1.5 mm diameter. 14 MPa compressive stress at the indentor tip was applied centrally in < 2 min and maintained constant for 2 h. Indentation (I) magnitudes were recorded in real-time (t), with I(t) data re-expressed as % indentation relative to the 4 mm specimen height. After 2 h, the indentor was unloaded and indentation recovery was monitored for a further 2 h. Parallel sets of measurements were made where indentation was delayed for 24 h. Further measurements were made with more conventional composites: EvoCeram Bulk Fill (ECeram) and Tetric EvoFlow Bulk Fill (EFlow). These were irradiated for 20 s at 1.2 W/cm^2. Kinetic data were curve-fitted to exponential growth functions and key parameters analyzed by ANOVA and *post-hoc* tests (α=0.05).

Results: I(t) plots looked initially similar to bulk creep/recovery: rapid deformation plus viscoelastic response; then, upon unloading: rapid (elastic) recovery followed by partial viscoelastic recovery. However, unlike multiply irradiated and stored bulk-creep specimens, the present specimens were exposed to only 3 or 5 s "occlusal" irradiation; generating "hard" surfaces. Subsequently, during the 2 h indentation, the polymer matrix network continued to harden and consolidate. Upon initial loading, I(t) reached 2 – 3 % indentation, depending upon the formulation. Upon unloading at 2 h, elastic recovery was only *ca.* 1 %. Delayed loading for 24 h, generated I(t) plots of significantly reduced magnitude. Most importantly, however, the I(t) plots for ECeram and EFlow, after 20 s irradiation, showed I(t) magnitudes quite comparable to the PFill and PFlow rapid-cure composites.

Significance: Macroscopic indentation creep has been shown to be a workable procedure that can be applied to rapid-cure materials to assess their immediate surface integrity and developing viscoelastic characteristics. The applied stress of 14 MPa was relatively severe and the indentation/recovery profiles of PowerFill materials with only 3 or 5 s irradiation demonstrated comparability with their established 20 s cure siblings, evidencing the suitability of the *PowerCure* system for clinical application.

Keywords: photopolymerization; dimethacrylate; AFCT; RAFT; resin-composite; indentation-creep; stretched-exponential; viscoelasticity; post-cure.

6.2 Introduction

There are several current trends in the incremental development of dental resin-composites by academic researchers and particularly by the R&D departments of dental manufacturing companies [276]. Many developments are driven by (a) competition between manufacturers and (b) requested innovations by clinical dentists. One of the items on the 'wish list' of many restorative dentists is *more rapid* photo curing (photo polymerization) that maintains the *reliability* of the cure process, assuming that the clinician follows the manufacturers' instructions precisely.

Visible Light Curing (VLC) by means of *Light Curing Units* (LCUs) has changed in many respects since the 1970s when it was first introduced [83, 277]. The major changes were: (i) the early transition from UV to *visible* blue light curing (wavelengths ca. 470 nm) and (ii) the change from filtered multi-wavelength *Quartz Tungsten halogen* (QTH) LCUs to *Light Emitting Diode* (LED-LCUs), with either a single LED chip (output at 470 nm) or two types of chip (blue: 470 nm and violet: 410 nm) [82]. The latter are effectively wide-spectrum LCUs.

Photo curing requires the active material to incorporate a photo-initiator (PI) with an *absorption* spectrum that corresponds to the *output* spectrum of the LCU. Sufficient light **irradiance** ($\mathbf{I_\lambda}$) is also necessary (corresponding to the LED emission rate: photons/s). Each photon carries a certain energy given by $\mathbf{h\nu}$ where **h** = Planck's constant and **ν** is the frequency of the light. The further major variable is the **time period** of irradiation (**t**).

The first photo-cured dental resin-composites were considered to require irradiation for **t** = 60 s. Subsequent developments have enabled irradiation times to be reduced from 60 > 40 > 20 > 10 s.

Commercial composites exist for which the required time is claimed to be as low as 5 s. And there is now a product – or product system - available for which **t** = 3 s (Ivoclar-Vivadent AG)[91].

These developments have been facilitated by (i) refinements of the photo-initiator system and (ii) boosting the irradiance (or Radiant Emittance; mW/cm^2) of the LCUs. The Ivoclar *PowerCure* system comprises an advanced Bluephase *PowerCure* LED-

LCU able to deliver 3 W/cm^2 for 3 s irradiation and two specially formulated composites: *PowerFill* and *PowerFlow*.

Photo-polymerization of resin-composites rapidly transforms fluid or 'plastic' paste formulations into hard solids *within* the irradiation period. However, further post-curing is known to occur that increases both surface and bulk mechanical properties over timescales ranging up to a month post-irradiation [15, 83]. The 3 s *PowerCure* irradiation mode should therefore be capable of producing sufficient material properties *within 3 seconds* that are *demonstrably comparable* to properties attained by generally equivalent composites after the more conventional 20 s irradiation.

The experimental challenge is to devise a method to probe mechanical material properties *immediately following* 3 s *PowerCure* irradiation. This requirement rules out time-consuming specimen preparation to fabricate flexural bar specimens, for example. It also rules out bulk compressive creep measurements that typically require 6 x 4 mm solid cylindrical specimen *that have been well irradiated from multiple directions* [170, 172, 278-280]. Nano-indentation might at first sight appear to be a possibility [281-283]. However, this requires polished specimen surfaces and only probes a shallow surface layer and a very small indentation area. Hence, with composite materials, anomalies are possible by nano-indentation of particle phases, rather than the organic matrix [284].

In this investigation, we propose a method that is novel in the context of photo-polymerized resin-composites. This involves immediate time-dependent indentation-creep measurements, with a *rigid loaded axisymmetric cylindrical flat-ended* punch, into a plane photo-polymerized composite surface. Indentation-recovery measurements are also to be made subsequently on the unloaded specimens.

The null hypotheses to be tested are that:

No significant differences exist between indentation /time profiles, during the loading and recovery periods, for 3 & 5 s *PowerCure* composites and conventionally photo-cured comparator composites.

1. Theoretical Background

Two distinct levels of theoretical analysis are relevant to this topic: (i) continuum mechanics of indentation into materials exhibiting plastic, elastic and/or viscoelastic behavior; (ii) molecular theory of photo-polymerization.

Continuum mechanics of surface indentation.

The problem of a rod or pillar loading a "foundation" material is an ancient one, dating back to the temples built in classical Greece, especially when the supporting material was non-rigid soil, with important implications for the safety of foundations. Within the terms of the classical theory of elasticity, the distribution of stress in a solid when deformed by a rigid punch was first considered in 1885 by Boussinesq [285]. Subsequently several alternative solutions were derived, as summarized by Galin [286], particularly by Harding and Sneddon [287] and Sneddon [288, 289].

A central distinction in contact mechanics is between stresses acting perpendicular to the contacting bodies' surfaces (the normal direction) and frictional stresses acting tangentially between the surfaces.

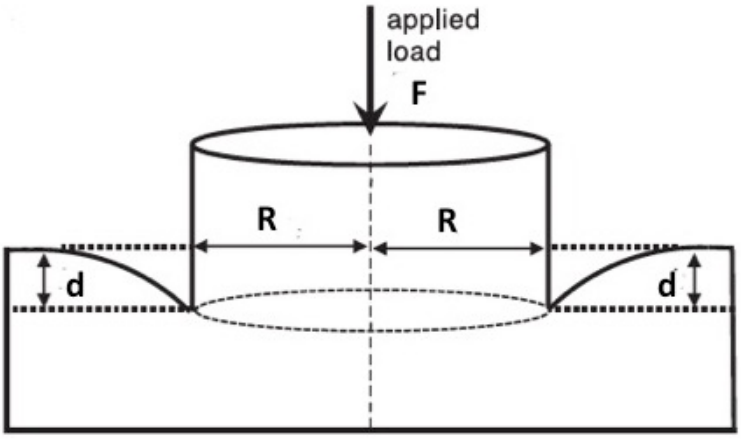

Figure 6.1 Indentation of a plane surface by a flat-ended cylindrical punch of diameter **2R** to a depth **d** under an applied axial load, **F**.

For a cylindrical flat-ended punch indentation the contact geometry is relatively simple because there is no pile-up at the contact edge. The radius of the contact remains fixed and equal to the radius, **R**, of the punch (**Figure 6.1**). When it is pressed into the free surface of an *elastic* solid, the relationship between the indentation depth (**d**) and the normal compressive force (**F**) is given by the *linear* relationship, [290] (p.117):

$$F = 2R.E^*.d \qquad \text{Equation 1}$$

where the reduced (or combined) modulus, E* is given by

$$\frac{1}{E^*} = \frac{1-\nu_1^2}{E_1} + \frac{1-\nu_2^2}{E_2} \qquad \text{Equation 2}$$

E_1 and E_2 are the elastic moduli of the test material and rod, and ν_1 and ν_2 are their Poisson's ratios.

If these 4 parameters remain constant, together with force **F**, then indentation depth (**d**) will also be constant and time invariant. However, if the modulus ($\mathbf{E_1}$) of an *elastic* test material were to *increase* (e.g) due to progressive curing, then indentations into *successive* specimens would exhibit a progressive *reduction* in elastic indentation depth, under constant load.

The present investigation is concerned with a specific strain history, wherein the *creep* (progressive deformation) is measured in response to an applied *step function* of stress, (or loading force). That is, the materials are subjected to an approximately *instantaneous* loading – and subsequent unloading. The applied stress σ at time t = 0 is:

$$\sigma_0 = F/A = F/\pi.R^2 \qquad \text{Equation 3}$$

The strain ε(t) in a *viscoelastic* material will increase with time. The creep compliance, **J**(t), is defined as the ratio:

$$J(t) = \varepsilon(t)/\sigma_0 \qquad \text{Equation 4}$$

The *relaxation magnitude,* in the compliance formulation, from "start" (0) to "finish" (∞) over the experimental time range is (J_∞ - J_0).

In *linear* viscoelastic materials, the creep compliance is independent of stress level. Under those circumstances, constitutive equations may be developed using the *Boltzmann superposition principle*, which is a statement of *linearity*: that the effect of a compound cause is the sum of the effects of individual causes. However, particularly in the case of indentation creep, the assumption of linearity may not hold making the scope for exact analysis severely circumscribed, [290, 291].

Nevertheless, a range of models have been devised to account for viscoelastic behavior. These commonly incorporate various serial or parallel combinations of elastic and viscous 'elements', rather like the spring and damper systems of a motorcar. The springs are assumed to be perfectly elastic. The dashpot element may be envisaged as a piston-cylinder assembly in which motion of the piston causes a viscous fluid to move through an aperture. However, real materials are not generally describable by models containing a small number of springs and dashpots.

The simplest pair of models, due to Voigt and Maxwell respectively, consist of a spring and dashpot - arranged *either* in parallel *or* in series. Somewhat more realistic behavior can be modeled by the *standard linear solid*, which contains three elements (**Figure 6.2**):

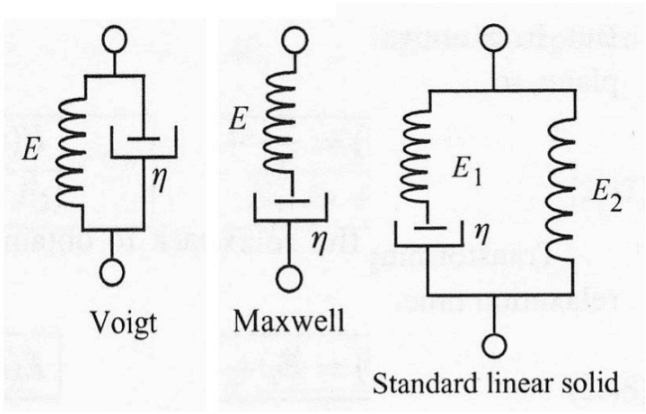

Figure 6.2: Mechanical model systems consisting of series and/or parallel combinations of elastic and viscous elements.

For the Voigt (or Kelvin) model (**Figure 6.2**), both the spring and the dashpot experience the *same deformation,* or strain, and the total stress is the sum of the stresses in each element. From this, it can be shown [291] (p. 55f) that the creep response is:

$$J(t) = \frac{1}{E}(1 - e^{-t/\tau_C}) \qquad \text{Equation 5}$$

In which $\tau_c = \eta / E$ is referred to as the retardation time.

A single exponential relaxation or retardation function undergoes most of its change over about one decade (a factor of 10) in time scale. However, real materials creep or relax over many decades of time.

There is a more general and rather ubiquitous expression for a normalized *relaxation* processes: the stretched exponential or **KWW** (after Kohlrausch, Williams, Watts) form [292, 293] with a fractional exponent: $0 < \beta \leq 1$.

$$\phi(t) = e^{-(t/\tau)^{\beta}} \qquad \text{Equation 6}$$

τ is the relaxation (or characteristic) time.

A corresponding normalized stretched-exponential *growth* process is represented by:

$$1-\phi(t)=\left\{1-e^{-(t/\tau)^{\beta}}\right\} \qquad \text{Equation 7}$$

Dynamic or frequency domain behavior, corresponding to this relaxation function, can be obtained analytically for β = 0.5 [293]. For general values of β numerical methods are available [294].

Complex materials with strongly interacting constituents often exhibit **KWW** behavior [295-298].

Crosslinked dental resin-composites incorporate strongly interacting constituents and so this functional form is likely to be applicable to the indentation creep behavior.

Indentation data can be presented either as absolute depth values (mm or μm) or as percentages of the specimen thickness. In the present work, we will use the latter option for the time-dependent growth of ***I***(t).

$$I(t)_{\%}=A.\left\{1-e^{-(t/\tau)^{\beta}}\right\} \qquad \text{Equation 8}$$

or

$$I(t)_{\%}=A.\left\{1-e^{-(t/\tau)^{\beta}}\right\}=A.\left\{1-e^{-(t^{\beta}/T)}\right\} \qquad \text{Equation 9}$$

where A corresponds to what would be the magnitude of $I(t)_{\%}$ as $\mathbf{t} \rightarrow \infty$.
Again, the parameter τ is the characteristic time. $T = \tau^{\beta}$ is an alternative representation. The fractional exponent β mathematically *stretches* the viscoelastic process over time

(**Figure 6.3**), away from a simple exponential change, known as Debye behavior, for which β = 1.

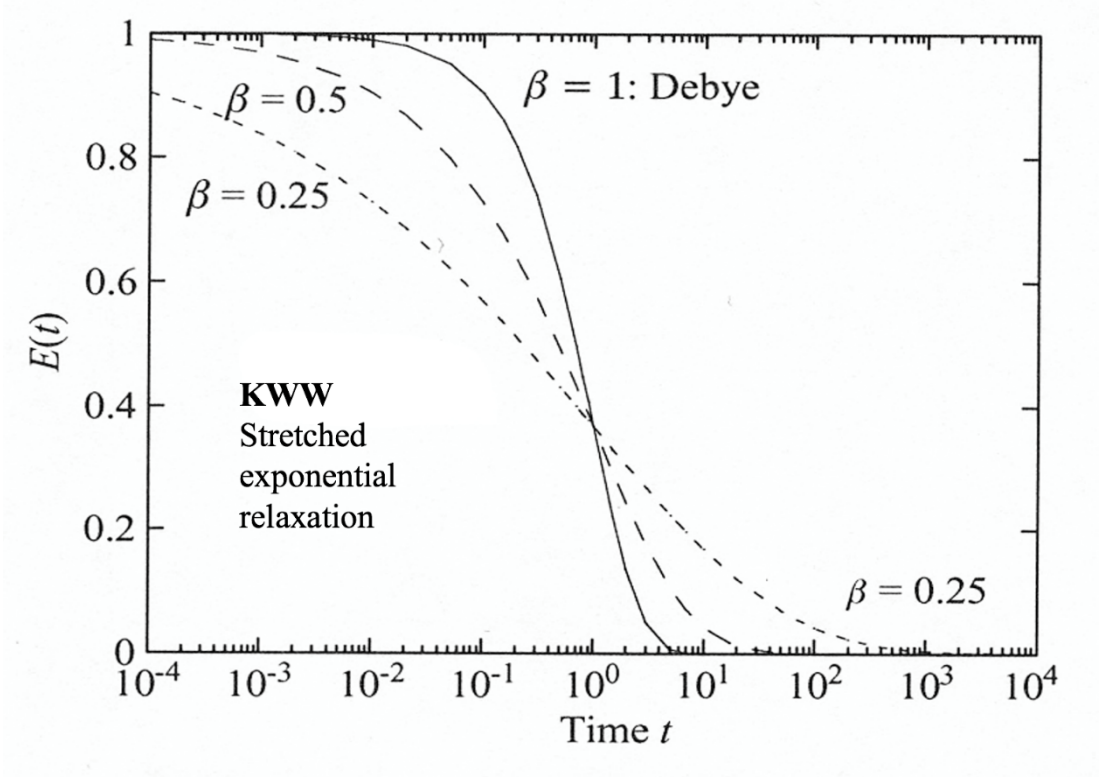

Figure 6.3 Stretched exponential relaxation functions (cf. Equation 6). Arbitrary units of (eg) modulus and (log10) time. As β reduces, the relaxation process is increasingly stretched over the time scale.

For this **KWW** approach, an expression for the *rate of indentation* (%/s) can be obtained by differentiation of equation 7:

$$\frac{dI}{dt} = (\beta/\tau).(t/\tau)^{\beta-1}.e^{-(t/\tau)^{\beta}} \qquad \text{Equation 10}$$

Molecular theory of photopolymerization

The molecular theory of free-radical photopolymerization has been widely discussed in both the polymer and dental literature, focusing especially upon the characteristics of multi-methacrylate monomers and the resulting cross-linked networks that form the matrix of resin-composites [15, 299]. Particular attention has been given to photoinitiator systems and the effects of varying light-irradiation protocols [91, 95, 191, 300]. A more recent development has been the possibility of incorporating chain-transfer agents, particularly of the reversible *addition fragmentation* (AF) type, variously denoted by the acronyms RAFT or AFCT [96]. One such agent is β-allyl sulfone (**Figure 6.4**). This becomes incorporated in the growing network and can modulate the inherently uncontrolled radical chain-reaction so that it proceeds more like a step-growth polymerization and results in a more homogenous network structure [90].

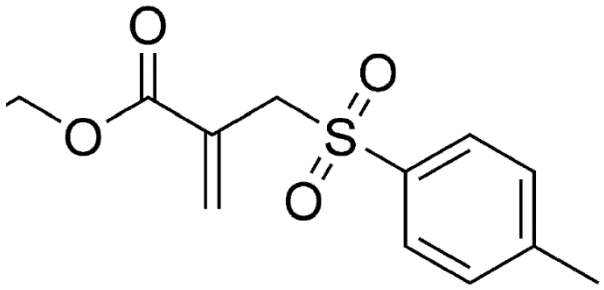

Figure 6.4 b-allyl sulfone AF chain transfer reagent.

6.3 Materials and Methods

The experimental design concerned four materials (**Table 6.1**). The independent variables were material, curing mode and post-irradiation time. The measurement times began either "immediately" or 24 h post-irradiation. A total of 48 specimens (n = 4 /group) were required.

Table 6.1: Materials Investigated: manufactured by Ivoclar-Vivadent AG, Liechtenstein

Material Codes	**Product Name**	**Lot Number**	**Resin Matrix***	**Filler Load § % (wt); (vol)**
PFill	Tetric PowerFill	W92823	Bis-GMA, Bis-EMA, UDMA, Aromatic Dimethacrylate, DCP	79; NA
PFlow	Tetric PowerFlow	WM1175		71; NA
ECeram	Tetric EvoCeram Bulk Fill	U53769	Bis-GMA, Bis-EMA and UDMA	80; 61
EFlow	Tetric EvoFlow Bulk Fill	U42390	Bis-GMA, Bis-EMA, TCDD	68.2; 46.4

**Matrix Monomers*: Bis-GMA: bisphenol-A-diglycidyl dimethacrylate; Bis-EMA: bisphenol-A-polyethylene-glycol-diether dimethacrylate; UDMA: urethane dimethacrylate,

§ *Filler percentages* as reported by the manufacturer.

Typical *contents*: Ba/Al-silicate glass, Isofiller, YbF_3, spherical mixed oxide.

Specimen Preparation:

Stainless steel (SS) split molds were used to fabricate cylindrical-shaped composite paste specimens - each 4 mm diameter and 4 mm thick. For each specimen, the resin composite material was placed in the mold, covered with Mylar strip then pressed by a glass slab to ensure a smooth surface and to eliminate any voids. The glass slab was then removed to facilitate close proximity of the light-curing tip above the composite paste surface (covered by Mylar strip).

The specimen was then irradiated directly from the top "occlusal" surface in accordance with a selected *Irradiation Protocol* (**Table 6.2**). The power density of each LCU was verified for each set of specimens using a radiometer (MARC™ Light Collector, Blue-light Analytics Inc., Halifax, NS, Canada).

Table 6.2 Irradiation Protocols with two Light-Curing Units (LCUs): P-Cure = Bluephase PowerCure (Ivoclar Vivadent AG); S10 = Elipar S10 (3M).

LCU Code	Irradiance (W/cm^2)	Irradiation Time (s)	Material Codes
P-Cure	3	3	PFill, PFlow
P-Cure	2	5	PFill, PFlow
S10	1.2	20	ECeram, EFlow

Following irradiation, each specimen was transferred within its SS mold for indentation loading either "immediately" (within 2 min) or at 24 h post-irradiation. The "24 h" specimens were stored dry at 37^{o}C in the dark.

Indentation Measurement

The indentation equipment was designed to measure the viscoelastic properties and recovery of resin composites under a static indentation stress. This was achieved by modification of an apparatus for measurement of bulk compressive creep and recovery, as described previously [170, 172, 280].

All specimens were measured within their SS molds at 23±1^{o}C. A mold containing a specimen was placed on a raised metal platform. A vertical loading rod, terminating in a 1.5 mm diameter cylindrical indentor punch (**Figure 6.5**a), was axially aligned and centralized over the specimen surface (**Figure 6.5**b). This rod also carried a platform that contacted a calibrated LVDT transducer to detect and record strain changes in the specimens (**Figure 6.5**c). A cantilever arm could be rapidly raised or lowered onto the top of the loading rod to transfer load to generate compressive stress.

The cantilever load was selected to generate, via the indentor punch, a stress of 14 MPa.

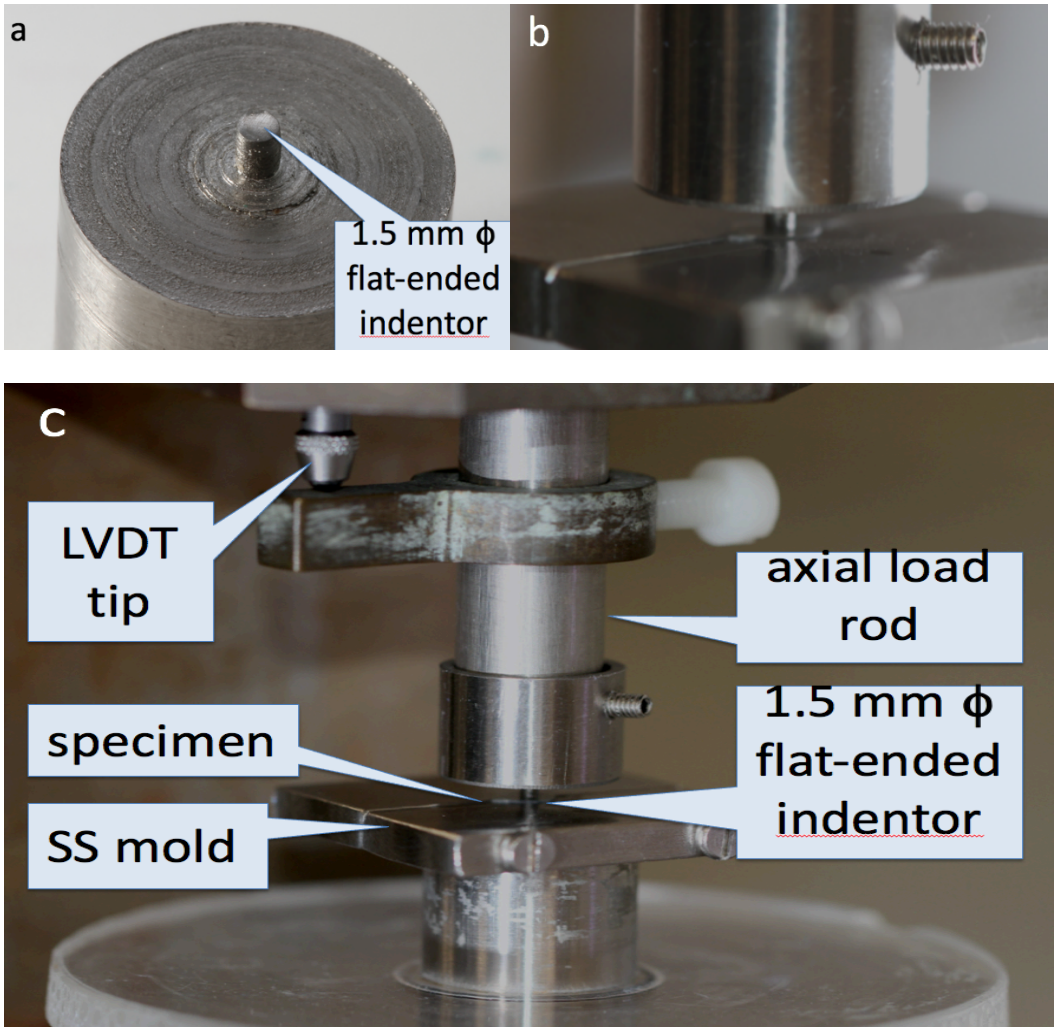

Figure 6.5 Configuration of the indentation-creep instrument: (a) the indentor punch; (b) the indentor in contact with the surface of a specimen contained within its stainless-steel split mold; (c) the assembly mounted on a fixed platform with the transducer tip registering axial movement of the load rod and indentor punch.

Once the specimen was placed in position a static force was applied, via the axial rod and the cantilever loading system (not shown), for a period of 2 h. After 2 h, the load was removed and changes in the indentation depth were monitored for a further 2 h.

The LVDT mV signals were amplified and sent to an analogue-to-digital converter and computer/software (PicoLog 6, Pico Technology, Hardwick, Cambridge, UK). These signals were converted firstly into μm displacement (Δ_t), via a calibration coefficient, and then secondly into percentage indentation depth (relative to specimen height: 4,000 μm).

$$I(t)_{\%} = [\Delta_t / L_o] \times 100 \qquad \text{Equation 11}$$

L_o is the specimen height and Δ_t is the indentation (μm).

Statistical and Graphical Analysis

Sample size calculations were made with G*power software (V. 3.1.3; Heinrich Heine University, Germany) based on a pilot study. A sample size: n = 4 was sufficient to give a power of 80%.

Each of the (n=4) datasets per material, irradiation and loading condition were averaged and plotted. Dynamic curve fitting to the indentation /time plots was achieved using SigmaPlot software (ver. 14).

SPSS 22.0 software (IBM, New York) was used for statistical analysis of key parameters. Normality of distribution was confirmed by the Shapiro-Wilk test. Two-way ANOVA was used for maximum and residual indentation (%) at both post-irradiation times showing a significant interaction ($p<0.05$). Therefore, one-way ANOVA and Tukey *post-hoc* tests were applied. Irradiation protocols were compared via independent sample t-tests ($\alpha=0.05$).

6.4 Results

The indentation *versus* time plots during the 2 h loading period were curve fitted, with the **KWW** stretched exponential function (equation 8) generating close fits for *immediate* indentation.

By contrast, a simpler exponential growth function (equation 12) was more appropriate for modeling the 24 h *delayed* loading data. The associated parameters are shown in (**Table 6.3**;**Table 6.4**) and the specific plots and equations for the critical case of PFill, after 3 s irradiation, are presented in (**Figure 6.6)**.

$$I(t)_{\%} = y_0 + a.\left\{1 - e^{-b.t}\right\}$$

Equation 12

Indentation (%) *versus* time (h) for each material, irradiation time and measurement time are plotted in **Figure 6.7** (a)-(f).

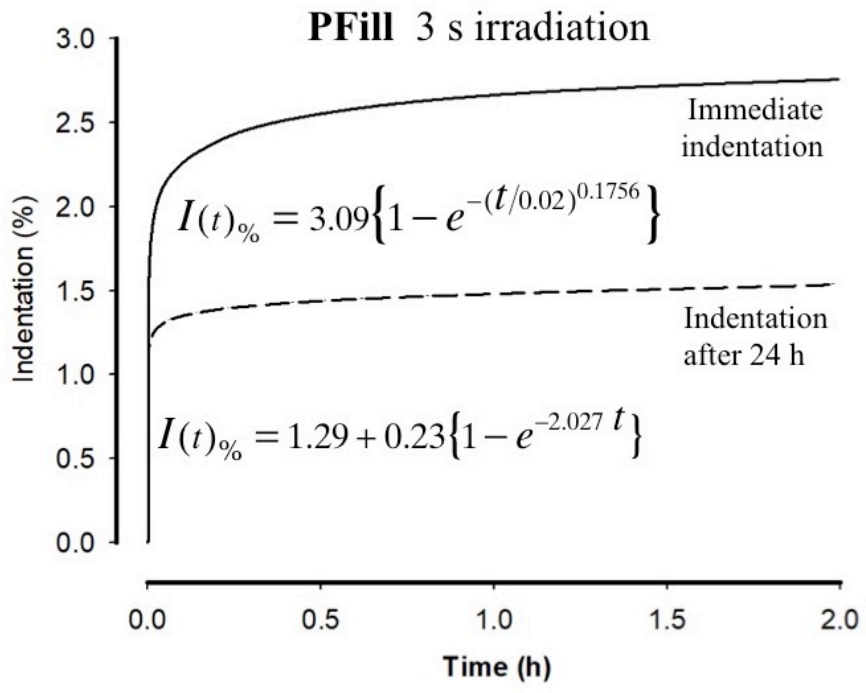

Figure 6.6: KWW *stretched* exponential analysis of *immediate* indentation creep response of PFill, irradiated for 3 s, (upper curve) and simpler exponential analysis of response after 24 h delayed indentation (lower curve).

Table 6.3: KWW *stretched*-exponential parameters for *immediate* indentation-creep response.

Material	A	Time constant: τ	Stretching exponent: β	R
PFill 3s	3.09	0.0201	0.1756	0.9981
PFill 5s	2.91	0.0122	0.2187	0.9976
PFlow 3s	3.92	0.0103	0.2303	0.9969
PFlow 5s	2.56	0.0132	0.2235	0.9987
ECeram 20s	2.70	0.0080	0.1731	0.9972
EFlow 20s	3.52	0.0081	0.1596	0.9953

Table 6.4: Exponential growth parameters for 24 h *delayed* indentation-creep response

Material	y_0	a	b	R
PFill 3s	1.29	0.23	2.0272	0.9332
PFill 5s	1.50	0.26	2.0772	0.9336
PFlow 3s	1.53	0.29	2.1434	0.9339
PFlow 5s	2.39	0.95	4.3164	0.9451
ECeram 20s	1.21	0.18	2.4531	0.9123
EFlow 20s	1.35	0.28	2.1579	0.9413

(a)

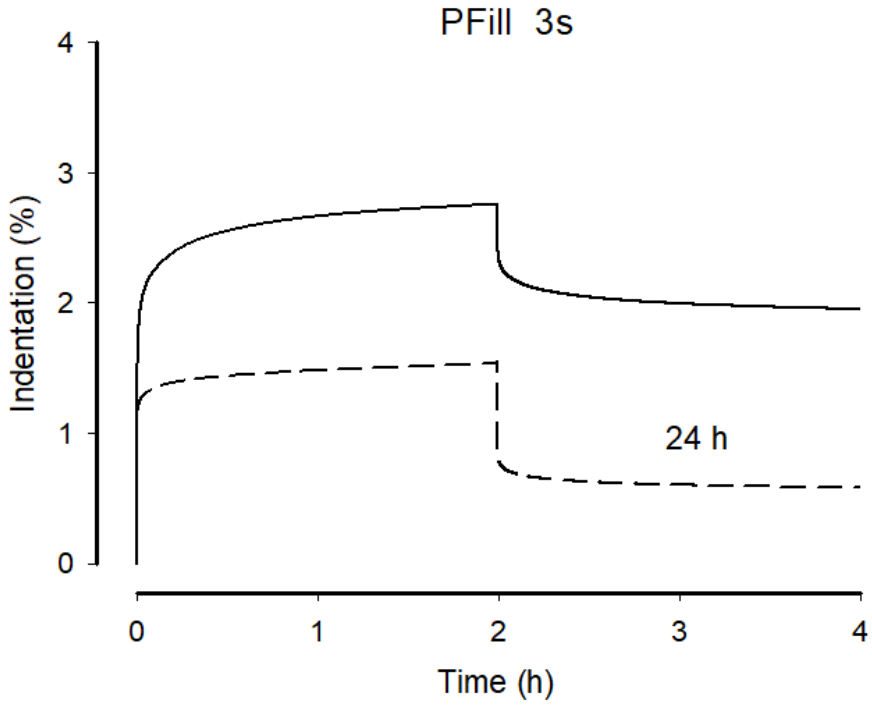
PFill 3s
Indentation (%)
0
1
2
3
4
24 h
0
1
2
3
4
Time (h)

(b)

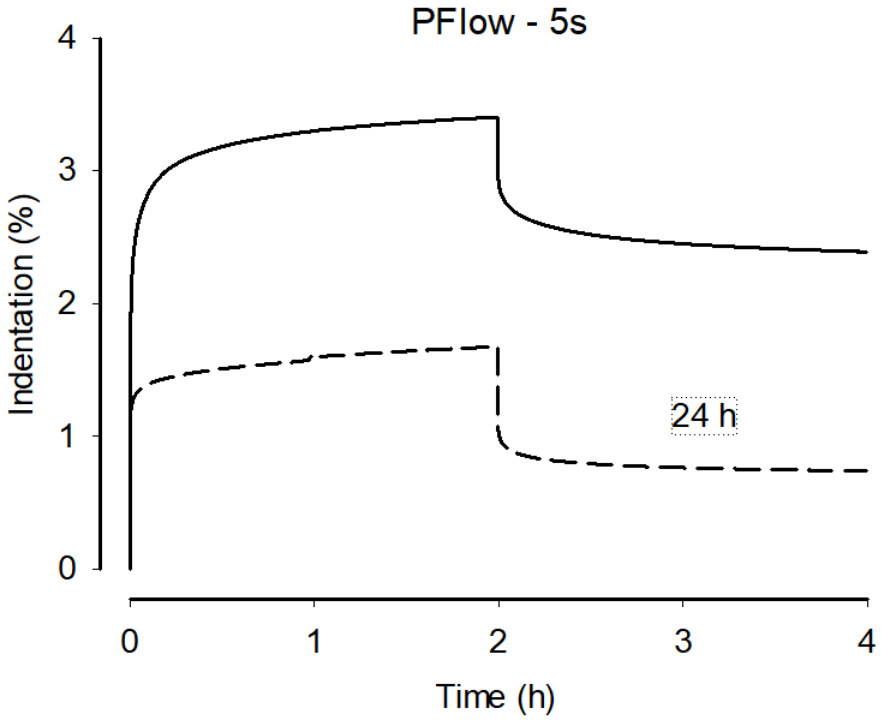
PFlow - 5s
Indentation (%)
0
1
2
3
4
24 h
0
1
2
3
4
Time (h)

(c)

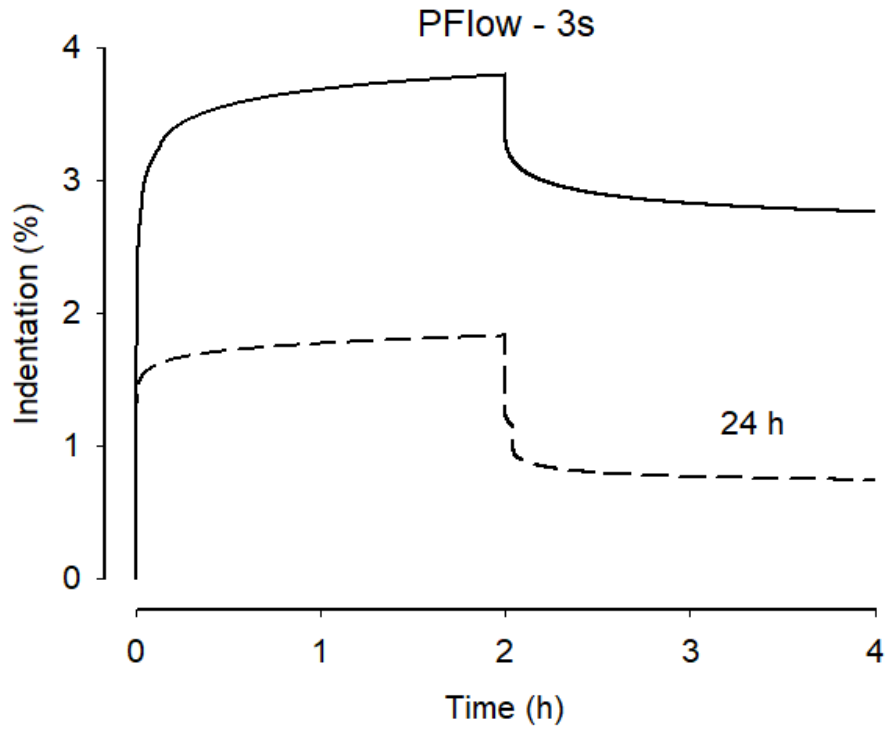
PFlow - 3s
Indentation (%)
0
1
2
3
4
24 h
0
1
2
3
4
Time (h)

(d)

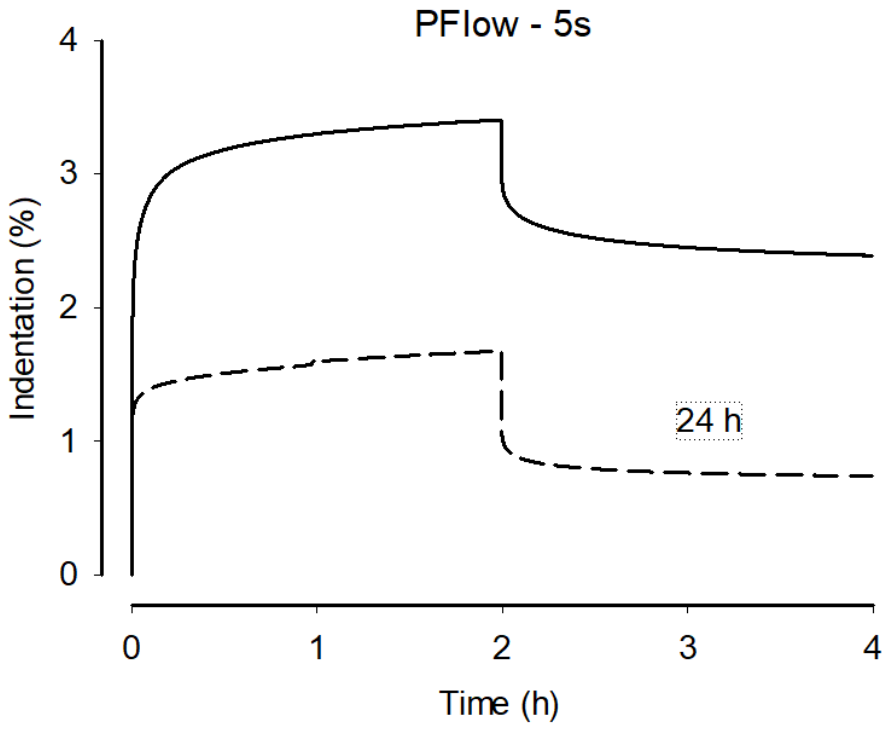
PFlow - 5s
Indentation (%)
0
1
2
3
4
24 h
0
1
2
3
4
Time (h)

(e)

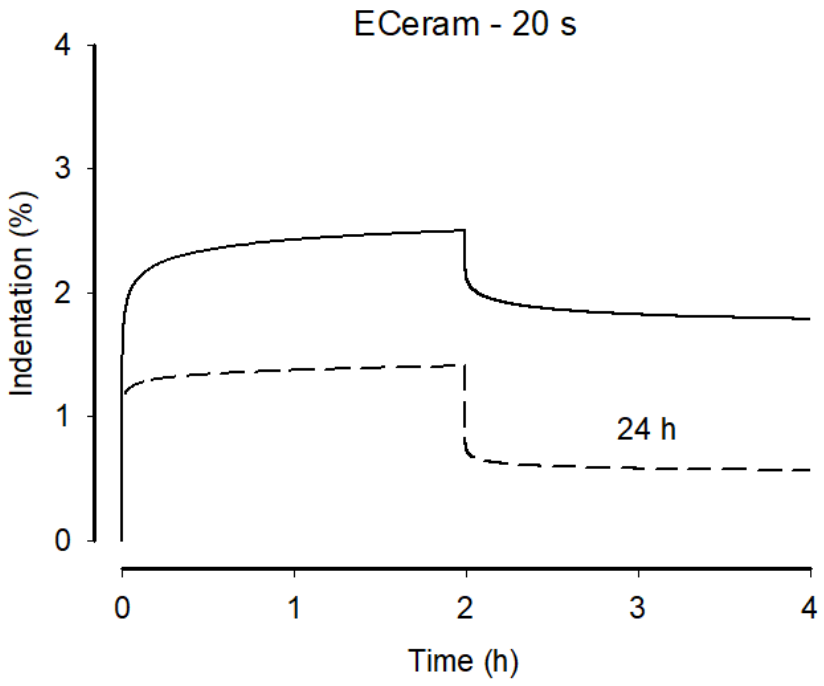

(f)

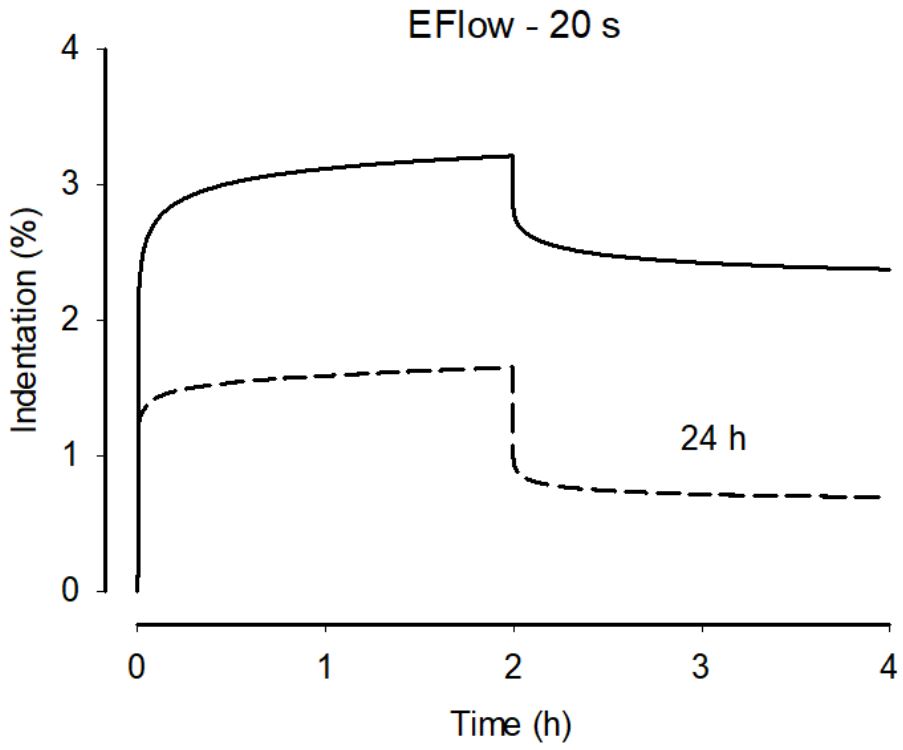

Figure 6.7: (a) – (f): Indentation as a function of time under 14 MPa stress for 2 h and unloaded recovery for 2 h for materials loaded both immediately (within 2 min – solid curves) and 24 h after irradiation (dashed curves). Each dataset plotted was the average of 4 specimens.

Figure 6.7 shows the indentation and recovery data for each group of materials for both immediate and 24 h initial loading. The maximum of the indentation (Y-scale) range was set at 4 %. This corresponds to 160 μm penetration into the surface. Immediately following light irradiation, the maximum indentations ranged between 2.5% to 3.8 %, and reduced to 1.41 % to 1.83 % following the 24 h delay. The residual indentation results seem to follow the trends for maximum indentation, ranging between 1.8 % to 2.8 % at immediate evaluation, which then reduced to 0.57 % - 0.98 % when measurements were made after 24 h. In general, all materials behaved *qualitatively* similarly but the measurement time differences (immediate *vs.* 24 h) gave statistically significant differences ($p<0.05$).

Indentation curves for the two flowable (low viscosity) formulations were greater in magnitude than for the two non-flowable (regular viscosity) composites. When loaded "immediately" the maximum indentations were notably greater than when loading was deferred for 24 h.

Furthermore, at the time of load-removal, a period of 2 h had elapsed since initiation of loading. Thus, especially with "immediately" loaded specimens, further matrix polymerization occurred during this interval so that the recovery portions of the curves were reduced in magnitude compared to the response upon initial loading. The maximum and residual indentation data are summarized for each composite group in **Figure 6.8** , **Figure 6.9** and in **Table 6.5**.

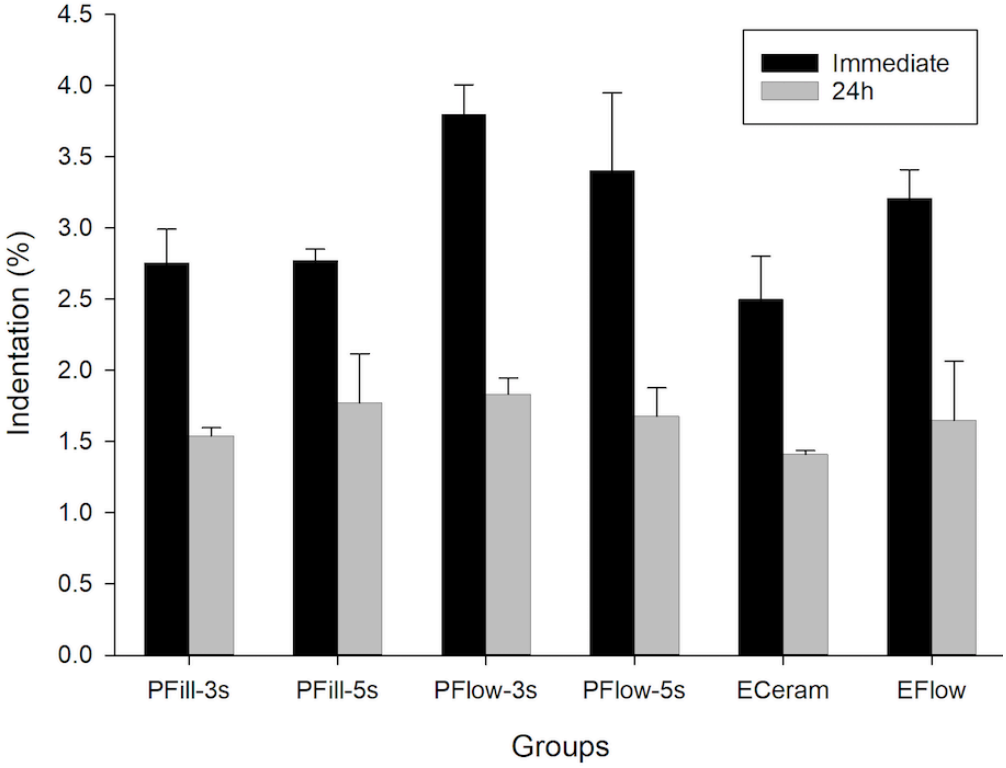

Figure 6.8 Maximum indentations (%) within 2 min (immediately) and 24 h after irradiation for each group.

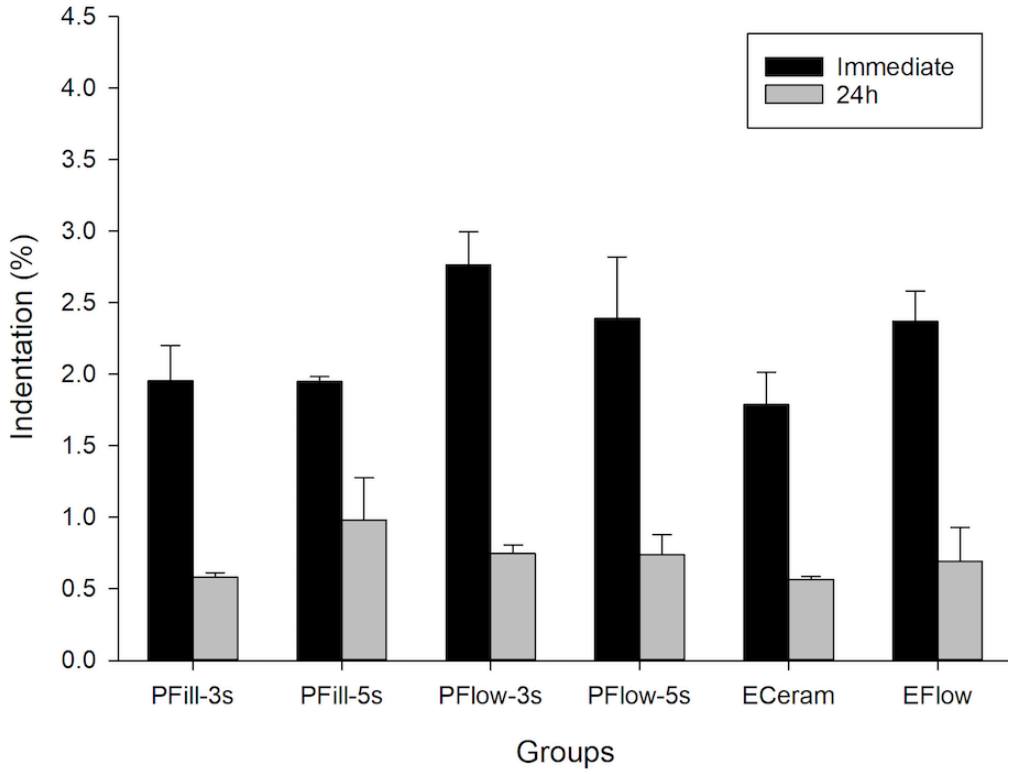

Figure 6.9: Residual indentations (%) within 2 min (immediately) and 24 h after irradiation for each group.

Table 6.5: Mean Indentation Creep parameters for 4 materials subjected to 3 irradiation (light cure) protocols (cf. Table 2) following both immediate and delayed indentation.

The parameters are (i) the maximum indentation (***I***) after 2 h loading and (ii) the residual indentation after 2 h unloading. (Standard deviations: in parentheses).

Measurement:		***Immediate*** **Indentation (< 2 min)**		***Delayed*** **Indentation (24 h)**	
Material	Irradiation	*I* max (%)	*I* residual (%)	*I* max (%)	*I* residual (%)
PFill	3 s	**2.76** (0.24)^{bcA}	**1.95** (0.25)^{abA}	**1.54** (0.06)^{aB}	**0.58** (0.03)^{bB}
	5 s	**2.77** (0.08)^{bcA}	**1.95** (0.03)^{abA}	**1.77** (0.34)^{aB}	**0.98** (0.29)^{bB}
PFlow	3 s	**3.80** (0.21)^{dA}	**2.77** (0.23)^{cA}	**1.83** (0.11)^{aB}	**0.75** (0.06)^{bB}
	5 s	**3.41** (0.54)^{cdA}	**2.39** (0.43)^{bcA}	**1.68** (0.20)^{aB}	**0.74** (0.14)^{bB}
ECeram	20 s	**2.50** (0.30)^{abA}	**1.79** (0.23)^{aA}	**1.41** (0.03)^{aB}	**0.57** (0.02)^{bB}
EFlow	20 s	**3.21** (0.20)^{cdA}	**2.37** (0.21)^{bcA}	**1.65** (0.41)^{aB}	**0.69** (0.24)^{bB}

Significant differences ($p<0.05$) are shown *between materials,* via different superscript lower-case letters and *between measurement times* via different superscript capital letters.

The experiments showed, from both maximum and residual indentations, that PFill (with either 3 s or 5 s modes) and also ECeram (20 s) had generally *reduced indentations – and thus superior outcomes* - compared to EFlow and PFlow (with either 3 s or 5 s modes). The immediate performance of PFill and PFlow composites cured for 3 s were statistically equivalent to their comparators, ECeram and EFlow cured for 20 s ($p>0.05$). However, 24 h post-irradiation showed no statistically significant differences among the materials in either maximum or residual indentations ($p>0.05$).

Further analysis utilizing independent sample t-tests confirmed a significant difference considering viscosity, with PFlow and EFlow having significantly greater maximum and residual indentations compared to non-flowable PFill and ECeram ($p<0.05$).

Furthermore, there was no significant difference in the outcome using the 3 s or the 5 s modes ($p>0.05$) of the PowerCure LCU-LED.

6.5 Discussion

The main goal of the present work was to establish a new methodology for addressing critical questions about ultra-rapid photo-polymerized composite materials. Following clinical placement, key requirements for dental restorations include sufficient mechanical integrity during functional occlusal loading. Such clinical "challenges" are normally intermittent in character. However, from a materials science and bioengineering perspective – especially with viscoelastic substances, measuring a "time domain" response to step-function loading /unloading can give representative insights that otherwise would require multiple fatigue loading (on/off) cycles [278, 279, 290].

To achieve this, we have adapted established bulk compressive creep/recovery methodologies [170, 172, 278-280] by developing an indentation-creep approach based upon a flat-ended cylindrical punch. Because the 1.5 mm diameter punch is impressed into the center of a 4 mm diameter composite surface, the specimen can be retained within its rigid stainless-steel split mold. This facilitates rapid transfer of the mold plus irradiated specimen to the loading platform in less than 2 min after 3 s irradiation. In most cases, the transfer could be completed within 30 s.

In the present work, comparator materials to the *PowerCure* composites (PFill; PFlow) were chosen from the same manufacturer (ECeram; EFlow). We have also conducted studies with the same methodology on a range of dental composites from other manufacturers. These findings, which exhibit comparable trends to the present study, will be published separately [36]. Moreover, we have made parallel investigations into the kinetics of C=C bond conversion by FTIR-ATR methods that will also be reported separately [211].

The irradiation regimes (**Table 6.2**) selected were based upon manufacturer's instructions. The delivered energy dose through the 5s and 3s modes were 10 and 9 J/cm^2, respectively. To some extent, there was an implicit assumption of the *general reciprocity hypothesis* that: "the same photo-cure outcomes will result from applying essentially constant energy densities despite reciprocal variations in the irradiance and time-period" [300]. However, with our use of the Elipar S10 LCU, the total energy delivery of 24 J/cm^2 was approximately twice that from the Bluephase *PowerCure*

LCU. This was deliberately chosen to provide a severe comparative test of the PowerFill materials. A minimum energy dose of 14 J/cm^2 was suggested [187] to cure bulk-fill resin-composites. However, the outcome depends not only on the energy dose, but on the responsiveness of the photoinitiator system, such as its quantum yield, and other factors.

Surface indentation creep has been applied previously to materials such as solid polymers where – unlike the present experiments - the surface-properties were not subject to underlying chemical change. A number of experimental and theoretical analyses have been published [187, 301-303]. Surface measurements have possible limitations, as far as evaluating bulk-fill dental composites are concerned, although it could be possible to invert the steel molds and measure indentations on the specimen surface remote from the irradiated surface. Nevertheless, the magnitudes of the surface indentations or "impressions" [301] are strongly dependent upon the state-of-cure of the underlying bulk material. This contrasts somewhat with the nature of surface microhardness indentations into resin-composites and particularly with nanoindentation [281]. Moreover, Degree of Conversion (DC) measurements of the Powerfill materials at 1 mm and 4 mm depths did not exhibit significant differences between the two depths [211].

We may critically review some of the measurement conditions of this experiment. *Firstly*, as with most conventionally photo-cured dental composites, there is a vast change in elastic modulus during the first 10 s of irradiation [304]. Therefore, with these ultra-fast materials, it was appropriate to probe the surface integrity as rapidly as possible; hence the "immediate" measurement condition. *Secondly*, a regime of load application for 2 h, followed by a further 2 h of unloaded recovery, was established by Ruyter [278] for bulk compressive creep and adopted by Watts *et al.* in many subsequent studies [170, 172, 279, 280]. *Thirdly*, the applied stress was set at 14 MPa, which is a comparatively severe condition but here applied equally to each experimental group. *Fourthly*, the measurement temperature was the constant ambient laboratory temperature of 23 ^{o}C. This contrasts with the 37 ^{o}C conditions usually implemented in our bulk compressive creep experiments. To have attempted immediate indentation-creep measurements for ultra-fast photo-cured composites held at 37 ^{o}C would have introduced complexities, logistical difficulties and potential errors. Moreover, even for bulk creep of composites, the effect of temperature over

this small interval was not a major factor [305]. Of course, the polymerization process itself releases exothermic heat, to which the heating effect of the LED-LCU is added. However, the surrounding stainless-steel mold constitutes a heat sink. Furthermore, the moderate thermal diffusivities of dental composites and ultra-short exposures of 3 or 5 s with the PowerCure LCU must reduce the overall impact of any thermal impulse.

Upon initial loading, 2 – 3 % indentation was measured, depending upon the formulation. Upon unloading at 2 h, elastic recovery was only *ca.* 1 %. The reduction in elastic recovery could be at least partly caused by an increase in elastic modulus in accordance with Equation 1. The maximum indentation-creep under 14 MPa, observed with immediate measurements after 3 s (at 3 W/cm^2) irradiation, was less than 150 μm, even for the flowable formulations. By contrast, delayed indentation by 24 h gave a maximum "impression" of only *ca.* 60 μm. These "worst- case" figures under a severe indentation stress might be compared with loss-of-surface-height during finishing and polishing and/or loss of anatomical form due to occlusal wear. However, the salient feature is that the *PowerCure* materials exhibited good viscoelastic stability, performing comparably to ECeram and EFlow, but with only half the total energy delivery. This supports their suitability for clinical application.

The post-irradiation time of 24 h was enough to elicit a significant improvement (reduced indentation) in the surface properties, which agrees with previous studies evaluating surface properties and post-curing [126, 196, 306, 307]. Higher indentation-creep was seen in the flowable bulk-fill materials compared to PFill and ECeram. However, this variation was greatly reduced after 24 h, so the null hypotheses were accepted. The higher filler content incorporated in PFill and ECeram (79, 80 %wt, respectively) possibly explains the *ca.* 25 % lower indentations compared to the flowable PFlow and PFill under *immediate* loading.

In this report, the *PowerCure* composites (PFill and PFlow) were compared to the well-established composites (ECeram and EFlow) as the monomer composition and filler content are broadly similar (**Table 6.1**). These materials incorporated a photoinitiator based on benzoyl germanium, commercially known as Ivocerin, besides CQ. Main modifications to the PFill and PFlow materials [91] including (i) the elimination of TPO photoinitiator used in ECeram and EFlow, relying on CQ as the main photoinitiator and Ivocerin as a booster (ii) addition-fragmentation chain transfer

(AFCT) reagent incorporation with the aim of inducing a more homogenous network [90, 91, 96] (iii) tricyclodocane dimethanol dimethacrylate (DCP) and propoxylated Bisphenol A dimethacrylate as added monomers.

The two mathematical functions, illustrated in **Figure 6.6** for PFill, are able to provide close fits, respectively, to either indentation-creep data for *immediate* loading (equation 8; **Table 6.3**) or for *delayed* loading (Equation 12; **Table 6.4**). **KWW** or stretched-exponential behavior is characteristic of complex materials in which hierarchical structures exist [295, 296]. The fractional exponents (β) were low and in the range 0.16 to 0.23.

Fancey [298] considered a complex and generalized Voigt model with Voigt elements connected in series (cf. **Figure 6.2**) with the aim of applicability to broad timescales. However, he noted that in these models, viscoelastic deformations are considered to vary *smoothly* i.e continuously with time. He considered an alternative approach in which viscoelastic changes are suggested to occur through discrete incremental jumps, via activated mechanical latches. On a molecular level, the phenomenon could be envisaged as segments of molecules jumping between positions of relative stability. This is certainly the concept accepted within the advanced science of polymers and networks. A link that has been proposed [308] between the **KWW** function and the potential energy barrier relationship as developed by Eyring *et al*.[309], since the latter relates the motion of matter to molecular jumps. The **KWW** function is shown to be an approximation to the potential energy barrier model [308]. Thus, during any photo-cure process, network links are formed - and some may also be broken under applied stress, particularly in a RAFT or AFCT system. Nevertheless, sufficient matrix-network connectivity is clearly established in the final polymerized materials.

6.6 Conclusions

The extent of immediate surface rigidity and developing viscoelastic characteristics of ultra-rapid photo-polymerized dental composites can be measured by a macroscopic indentation-creep method, following 3 s or 5 s exposures to irradiances, respectively, of 3 or 2 W/cm^2. The new methodology is described in detail. For rapid-irradiated *PowerCure* composites under 14 MPa *immediate* stress, the indentation-creep exhibited stretched-exponential kinetics with magnitudes after 2 h less than 150 μm. When the stress application was delayed for 24 h, the indentation magnitudes were *ca.* 60 μm. Completely comparable indentation /time profiles were exhibited by well-established composite formulations following 1.2 W/cm^2 irradiation for 20 s. As judged by the experimental indentation-creep methodology, the *PowerCure* system and materials demonstrated an acceptable level of polymerization/property performance, despite the ultra-short irradiation times, evidencing their suitability for clinical application.

Author Contributions

DCW conceived and commissioned the instrumental design, methods and theoretical analysis, guided the experiments and wrote the final manuscript to which both authors gave approval.

HA performed the experiments, collated the data, performed statistics, contributed to the interpretation of results and to manuscript writing.

Acknowledgements

The authors thank Ivoclar-Vivadent AG for provision of composite materials.

The authors declare no conflict of interest.

Highlights

- The rapidly developing surface integrity of ultra-fast (3 s) photo-cure composites can be probed "immediately" by a new macroscopic indentation-creep methodology.
- *PowerCure* system and materials demonstrated an acceptable level of polymerization/property performance, despite the ultra-short irradiation times, as judged by this experimental criterion.

CHAPTER SEVEN

Post-irradiation surface viscoelastic integrity of photo-polymerized resin-based composites

Hamad Algamaiah[a,b,*], David C. Watts[a,c,*]

[a] Dentistry, School of Medical Sciences, University of Manchester, Manchester, UK

[b] Department of Restorative Dental Science, College of Dentistry, King Saud University, Riyadh, Saudi Arabia

[c] Photon Science Institute, University of Manchester, Manchester, UK

Published *in Dental Materials 37 (2021) 1828–1833 (Appendix E)*

7.1 Abstract

Objective: A class of ultra-rapid-cure resin-based composites (RBCs) exhibit immediate post-irradiation surface viscoelastic integrity using an indentation-creep /recovery procedure. The aim of this study was to determine whether such behavior is more generally characteristic of a wider range of RBCs.

Methods: Eight representative RBCs were selected based on different clinical categories: three bulkfills (**OBF**, Filtek One Bulk Fill; **VBF**, Venus Bulkfill; **EBF**, Estelite bulkfill), three conventional non-flowables (**XTE**, Filtek Supreme XTE; **GSO**, GrandioSo; **HRZ**, Harmonize) and conventional flowables (**XTF**, Filtek Supreme XTE *Flow*; **GSF**, GrandioSo Flow). Stainless steel split molds were used to fabricate cylindrical specimens (4 mm (dia) × 4 mm). These were irradiated (1.2 W/cm^2) for 20 s on the top surface. Post-irradiation specimens (n=3), within their molds, were centrally loaded with a flat-ended 1.5 mm diameter indenter under 14 MPa stress: either *immediately* (< 2 min) or after 24 h *delayed* indentation. Stress was maintained for 2 h, then - after removal - recovery measurements continued for a further 2 h. Indentation depth (%) *versus* time was measured continuously to an accuracy of < 0.1 μm. Data were analyzed by One-way ANOVA and Tukey *post-hoc* tests (α=0.05).

Results: Time-dependent viscoelastic indentation was observed for all RBCs. For *immediate* indentation, the maximum indentation range was 1.43-4.92 %, *versus* 0.70-2.22 % for 24 h *delayed* indentation. Following 2 h recovery, the residual indentation range was 0.86-3.58% after *immediate* indentation, reducing to 0.22-1.27 % for *delayed* indentation.

The greatest *immediate* indentation was shown by VBF followed by XTF and GSF. OBF, HRZ, XTE and GSO had significantly lower indentations (greater hardness). XTE showed a significantly *reduced indentation maximum* compared to OBF ($p<0.05$).
Indentations *delayed* until 24 h post-irradiation were reduced ($p<0.05$) for most materials.

Significance: The indentation-creep methodology effectively characterized resin-based composites within several categories. Viscoelastic properties evaluated by the indentation-creep method confirmed that highly filled RBCs were more resistant to

indentation. Indentations were reduced after 24 h post-irradiation due to further matrix-network development.

Keywords: Indentation-creep; Bulk fill; polymerization; viscoelastic properties; viscoelastic integrity

7.2 Introduction

Resin-based composites (RBCs) are now the primary material of choice as a direct dental restorative material. Advantages of RBCs include an adequate working time and immediate initial strength upon photo-polymerization. After sufficient post-irradiation time to allow for post-curing, RBCs increase in both surface and bulk mechanical properties [177, 307]. The long-term clinical performance of RBCs depends on their ability to resist occlusal forces.

The behavior of resin composites under stress mainly depends on the internal composition. Filler content, shape and size are primary factors in determining their mechanical properties. Elastic modulus strongly correlated with filler load ($r=0.90$) and a similar correlation was found with surface hardness ($r>0.82$), [177]. Moreover, filler load had a greater influence on other properties than material category [44]. Monomer types, composition and degree of conversion also affect the stability and mechanical performance of RBCs [25]. Other factors being equal, more rigid organic matrices (involving Bis-GMA, Bis-EMA, UDMA, etc), exhibit greater RBC moduli that are less prone to deformation [25]. The surrounding environmental media can also affect RBC mechanical performance [35, 310].

Many incremental modifications have been made in RBC formulations to improve their mode of clinical application. One approach has been to reduce the required clinical irradiation time, most commonly to 10 s, by deploying LED light-curing units (LED-LCUs) of enhanced *radiant emittance*. This is often referred to as *irradiance*, although more strictly the latter term refers to the 'intensity' in W/m^2 of light *incident on the target* composite surface, [74]. The light energy (E) potentially 'delivered' to a composite surface (J/cm^2) is the product of irradiance and time, although effective "delivery" requires an appropriate photoinitiator (PI) system with an absorption spectrum matched by the output spectrum of the LCU source [311].

An Ultra-rapid photo-polymerized bulk fill (URPBF) composite system was introduced in 2019 (*PowerCure*: Ivoclar Vivadent AG, Liechtenstein), that can undergo ultra-fast cure within 3 s using appropriate LED-LCU equipment with 3 W/m^2 irradiance. Such rapid transformation of this system has been investigated *inter alia* as

regards degree of conversion (DC), shrinkage phenomenon, thermal output and associated kinetics [211, 312, 313].

The question arose as to the surface viscoelastic integrity of such ultra-fast *PowerCure* materials, especially *immediately* following the 3 s or 5 s irradiation times. To investigate this experimentally, a novel indention-creep methodology was devised [212]. During 2 h indentation under 14 MPa stress, the indentation-creep behavior was continuously measured and then the indentation-recovery plots were also measured for a further 2 h. There were indeed measurable and increasing surface indentations, rather than absolute surface rigidity, after both 3 s and 5 s irradiation periods. However, this behavior was also apparent in the two clinically established comparator materials.

Accordingly, the objective of this investigation was to assess the ability of this indentation-creep/recovery methodology to characterize representative resin-composites from a range of manufacturers, including RBCs with varied clinical applications, immediately and after 24 h delay.

The research hypothesis investigated was:

There is no significant difference in the pattern of indentation creep/recovery behavior between the evaluated RBCs, Either: (1) *Immediately*; or (2) after *24 h delayed indentation.*

7.3 Materials and methods

Specimen preparation

Based on a pilot study and power calculation using G*power software (V. 3.1.3; Heinrich Heine University, Germany), the experimental design consisted of 48 specimens (n=3). A stainless-steel split mold was used to fabricate cylindrical-shaped composite paste specimens, with 4 mm diameter and 4 mm depth, from eight different resin composites (**Table 7.1**). Three of these materials were in the Bulk-Fill category and five were of a 'conventional' – or non-Bulk-Fill category. Of these five, two composites were also of the flowable type.

Sixteen groups were based on the eight different materials measured at two post-irradiation times. Each composite was placed in the split mold, with an overlying Mylar strip, and pressed by a glass slab to ensure a smooth flat surface and to eliminate voids. The glass slab was then removed to facilitate perpendicular and immediate contact of the light-curing tip to the material (covered in Mylar strip). The specimens were then photo-polymerized from the top surface using a LED-LCU (Elipar S10, 3M, MN, USA) with 1.2 W/cm^2 Irradiance for 20 s. Specimens were transferred within their molds to the loading platform (**Figure 7.1**) and loaded by the indentor (stress 14 MPa) either *immediately* (within 2 min) or *after a delay* of 24 h post-irradiation. The 24 h post-irradiation specimens were kept dry in a 37 ^{o}C incubator. The radiant exitance was verified for every set of three specimens using a radiometer (MARC™-LC, Bluelight Analytics Inc., Halifax, NS, Canada).

Table 7.1: Materials investigated and category codes: (BF = Bulk-Fill; NB = non-BF; FL= flowable).

Code	Material	Category	Resin matrix	Filler % (wt)/(vol)	Manufacturer	Lot number
OBF	*Filtek* One Bulk Fill	BF	DDDMA, UDMA, AUDMA, AFM	76.5/ 58.5	3M ESPE, St. Paul, MN, US	N859232
VBF	Venus Bulkfill	BF-FL	UDMA, EBPDMA	65/ 38	Heraeus Kulzer, Hanau, DE	10102
EBF	Estelite Bulkfill	BF-FL	Bis-GMA, TEGDMA, BisMPEPP,Mequinol, Dibutyl hydroxyl toluene	70/ 56	Tokuyama, JP	076E10
HRZ	Harmonize Dentin	NB	Bis-GMA, Bis-EMA, TEGDMA	81/ 64.5	Kerr, Orange, CA, USA	6273752
GSO	GrandioSo	NB	Bis-GMA, Bis-EMA and TEGDMA	89/ 73	VOCO, Cuxhaven, DE	1929072
XTE	*Filtek* Supreme XTE	NB	Bis-GMA, Bis-EMA, UDMA, PEGDMA	78.5/ 63.3	3M ESPE, St. Paul, MN, US	N836906
XTF	*Filtek* Supreme XTE Flow	NB-FL	Bis-GMA, BisEMA,TEGDMA	65/ 46	3M ESPE, St. Paul, MN, US	N522058
GSF	GrandioSo Flow	NB-FL	Bis-GMA, Bis-EMA and TEGDMA	81/??	VOCO, Cuxhaven, DE	1939767

Indentation measurement apparatus

Details of the indentation measurement apparatus (**Figure 7.1**) and procedures were published previously [212].

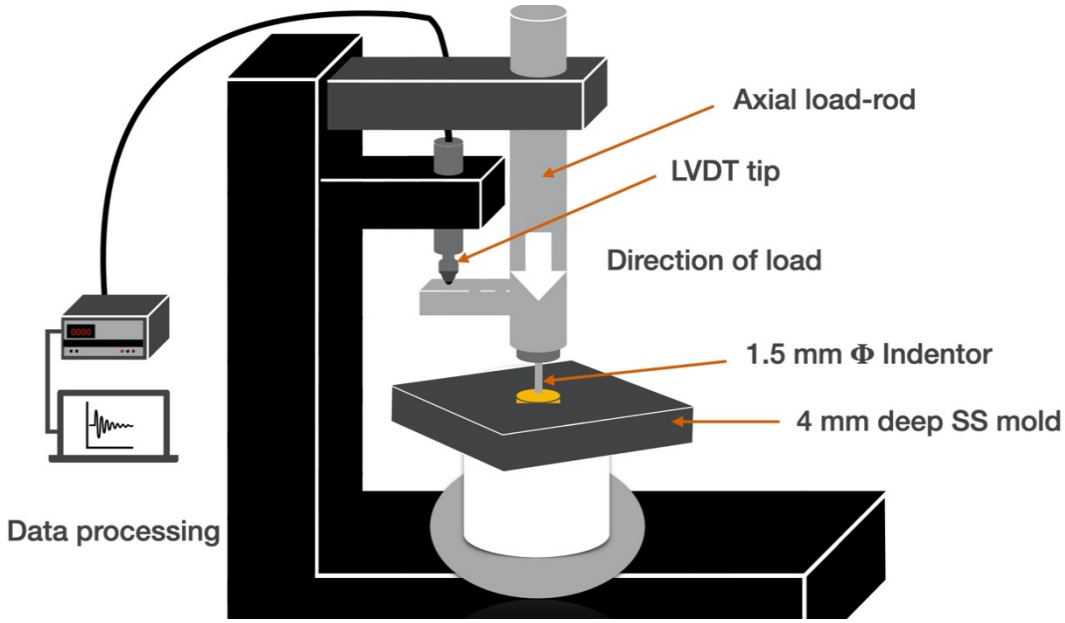

Figure 7.1: Indentation creep apparatus. The axial load-rod (terminating in an indentor punch) was held in a cantilever loading device within a frictionless linear-bearing [10].

Statistical analysis

The data from all groups were analyzed using SPSS 25.0 software (IBM SPSS Statistics, SPSS Inc., New York, USA). Once the Shapiro-Wilk test confirmed the normality of the data, Two-way ANOVA analysis of variance was applied to maximum and residual indentations of each material at different measurement times, at a significance level of 5%, revealing statistical interactions ($p<0.05$). Then One-way ANOVA was utilized followed by Tukey *post-hoc* tests ($\alpha=0.05$).

7.4 Results

The maximum and residual indentation data and the indentation *versus* time, I(t), plots are presented for each of the composite groups in **Table 7.2**, **Figure 7.2** and **Figure 7.3**.

Table 7.2: Mean Indentation Creep parameters for 8 composites subjected to the same irradiation protocol following both *immediate* (< 2 min) and (24 h) *delayed* indentation.

The parameters are (i) the maximum indentation (***I***) after 2 h loading and (ii) the residual indentation after 2 h unloading. (Standard deviations: in parentheses).

Significant differences are shown between materials, via different superscript lower-case letters and between measurement times via different superscript capital letters.

Material	**Immediate Indentation (%)**		**Delayed indentation (%)**	
Code	I_{max} (%)	$I_{residual}$ (%)	I_{max} (%)	$I_{residual}$ (%)
VBF	**4.92** (0.07)^{gA}	**3.58** (0.08)^{hA}	**1.80** (0.09)^{cdB}	**0.72** (0.08)^{abcdB}
XTF	**3.51** (0. 38)^{fA}	**2.65** (0.37)^{gA}	**2.22** (0.14)^{dB}	**1.27** (0.09)^{dB}
GSF	**3.51** (0.53)^{fA}	**2.54** (0.37)^{gA}	**1.49** (0.16)^{bcdB}	**0.53** (0.12)^{abcB}
EBF	**2.78** (0.21)^{efA}	**1.75** (0.14)^{fA}	**1.46** (0.32)^{cdB}	**0.59** (0.23)^{abcdB}
OBF	**2.19** (0.32)^{deA}	**1.52** (0.29)^{efA}	**1.26** (0.11)^{abcB}	**0.51** (0.07)^{abcB}
HRZ	**1.82** (0.18)^{cdA}	**1.10** (0.28)^{cdefA}	**1.11**(0.26)^{abcA}	**0.44** (0.25)^{abB}
GSO	**1.52** (0.41)^{bcdA}	**0.96** (0.34)^{bcdeA}	**0.70** (0.11)^{aB}	**0.22** (0.03)^{aB}
XTE	**1.43** (0.07)^{abc}	**0.86** (0.07)^{abcdA}	**0.79** (0.10)^{abA}	**0.22** (0.02)^{aA}

Time-dependent viscoelastic behavior was observed for all materials, with evidence of initial plastic deformation immediately following photo-polymerization, followed by viscoelastic creep. Measured immediately following photo- polymerization, the maximum indentations ranged between 1.43-4.92 % and reduced to 0.70-2.22 % after 24 h post-irradiation indentation-delay. Following recovery for 2 h, the residual

indentation range was between 0.86-3.58 % at immediate evaluation, which reduced to 0.22-1.27 % after 24 h indentation-delay.

(i) Under immediate loading, Venus Bulkfill (VBF) exhibited the significantly highest maximum indentation compared to all other materials ($p<0.5$). The flowable composites (XTF, GSF) were the next highest, both in maximum and residual indentations.

EBF was not significantly higher than OBF ($p>0.05$) but OBF was comparable to both HRZ and GSO. The flowable composites (XTF, GSF) were significantly higher indentations ($p<0.5$) than the three conventional non-flowable composites (HRZ, GSO, XTE) which were generally comparable. Following *immediate* indentation, trends in *residual* indentation followed the maximum indentation.

(ii) Under 24 h delayed loading, indentation depths were approximately 50 % of the immediate depths (**Figure 7.2**). ($p<0.5$). VBF was then comparable to the other bulk fill composites (EBF, OBF) and the conventional HRZ. Moreover, OBF, HRZ, GSO and XTE performed similarly after the 24 h post-irradiation delay. Following 24 h *delayed* indentation, XTF had the highest maximum and residual indentation from all other materials.

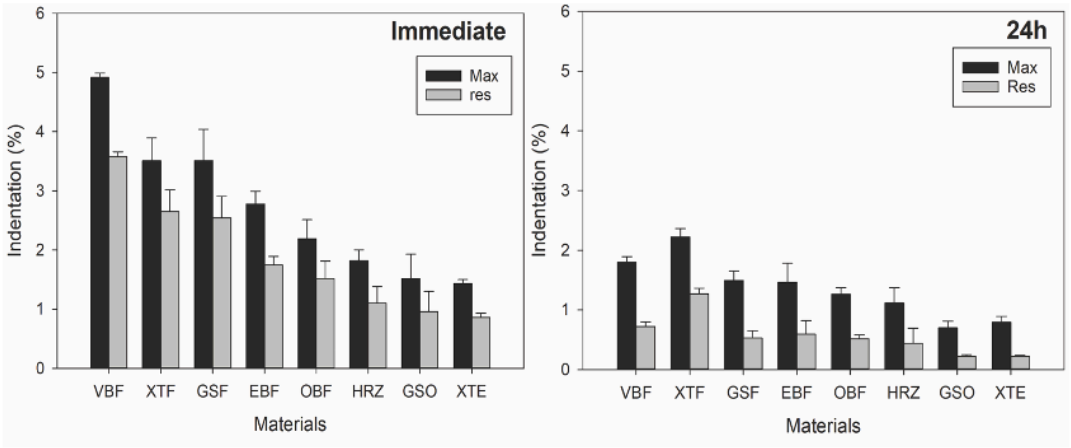

Figure 7.2: Maximum and Residual indentations (%) measured after loading either within 2 min (immediate) or after 24 h (delayed) post-irradiation, for each composite.

(a)

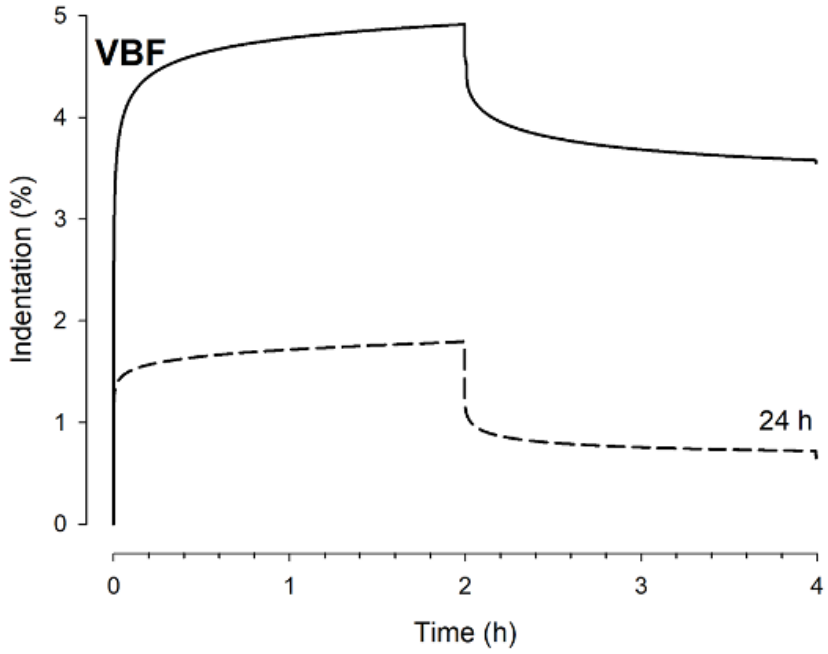
VBF
Indentation (%)
Time (h)
24 h
0
1
2
3
4
5

(b)

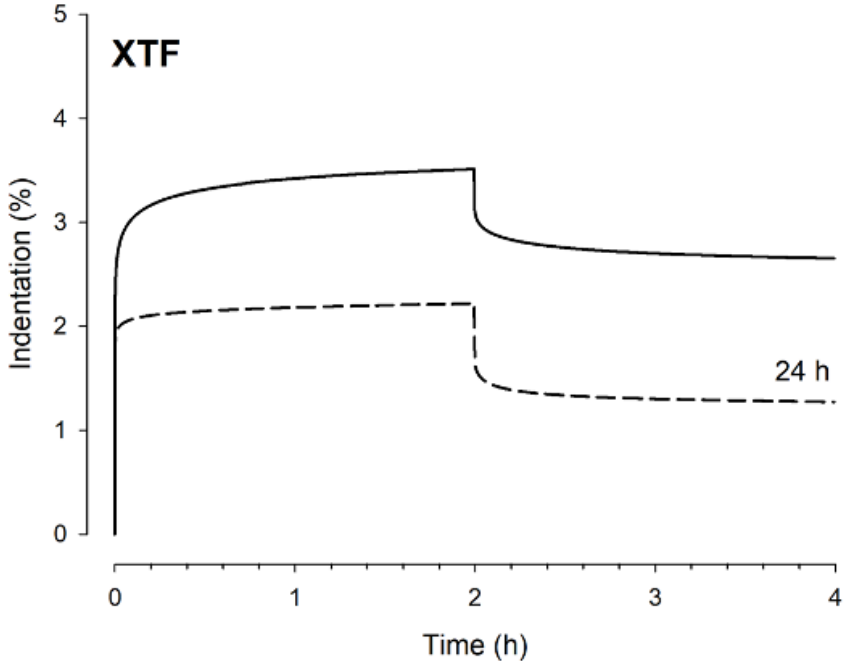
XTF
Indentation (%)
Time (h)
24 h
0
1
2
3
4
5

(c)

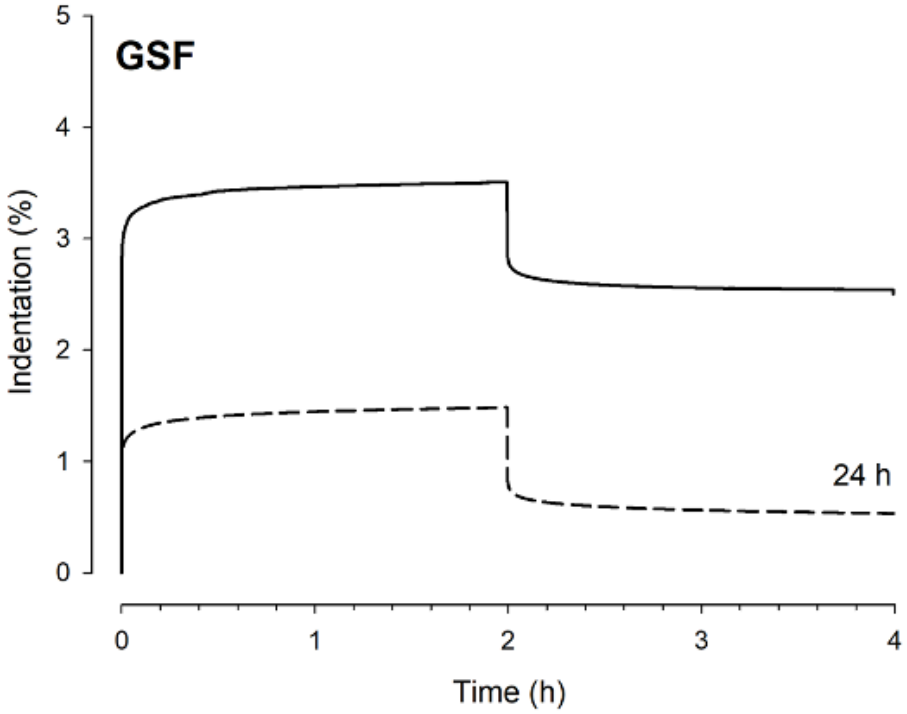
GSF
Indentation (%)
Time (h)
24 h
0
1
2
3
4
5

(d)

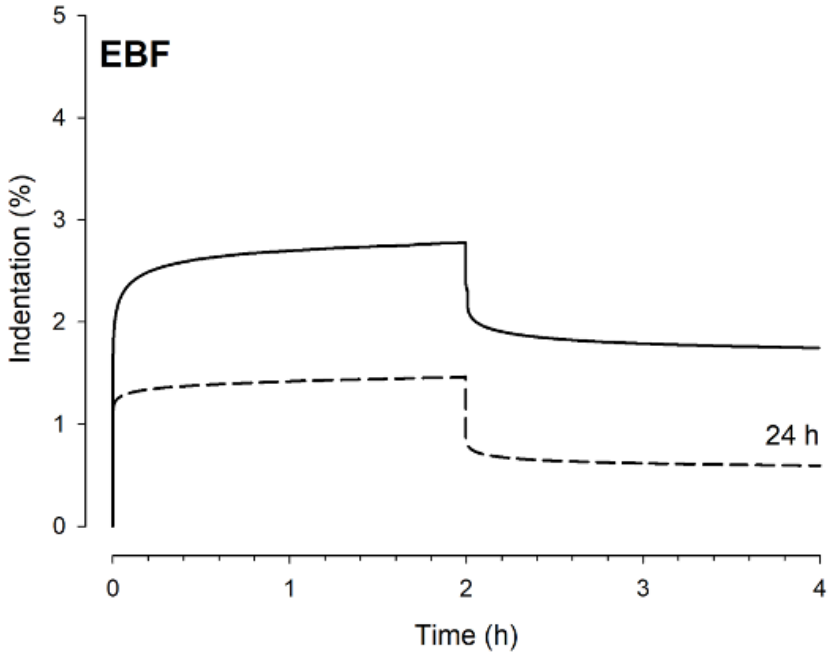
EBF
Indentation (%)
Time (h)
24 h
0
1
2
3
4
5

(e)

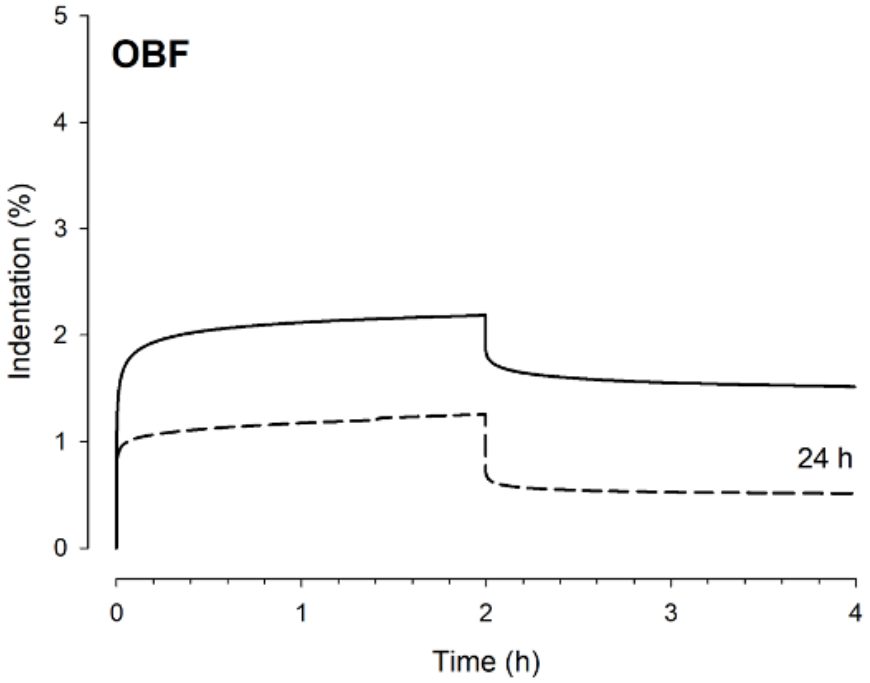
OBF
Indentation (%)
0
1
2
3
4
5
24 h
0
1
2
3
4
Time (h)

(f)

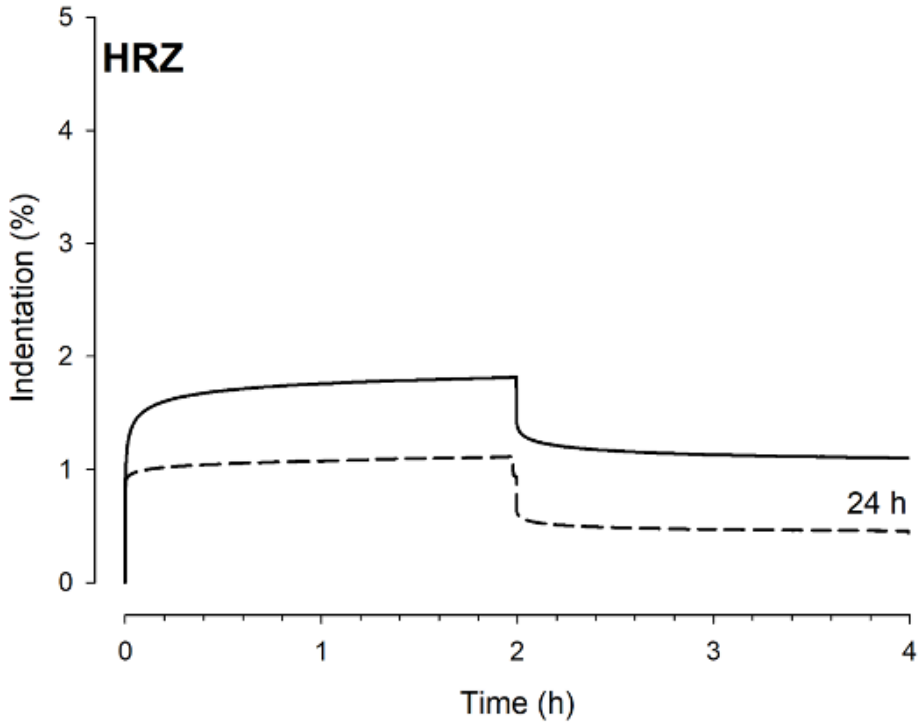
HRZ
Indentation (%)
0
1
2
3
4
5
24 h
0
1
2
3
4
Time (h)

(g)

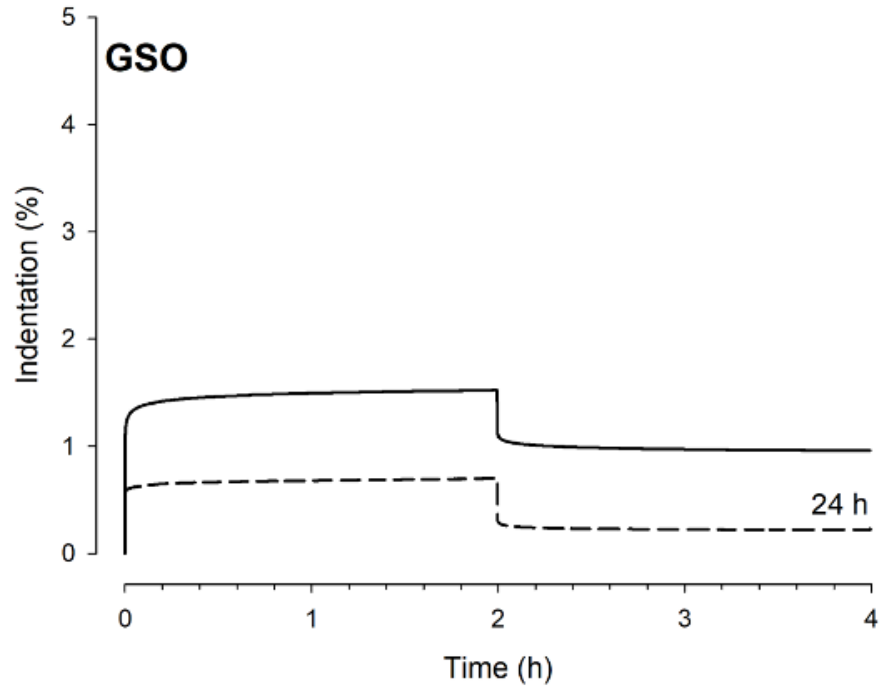

(h)

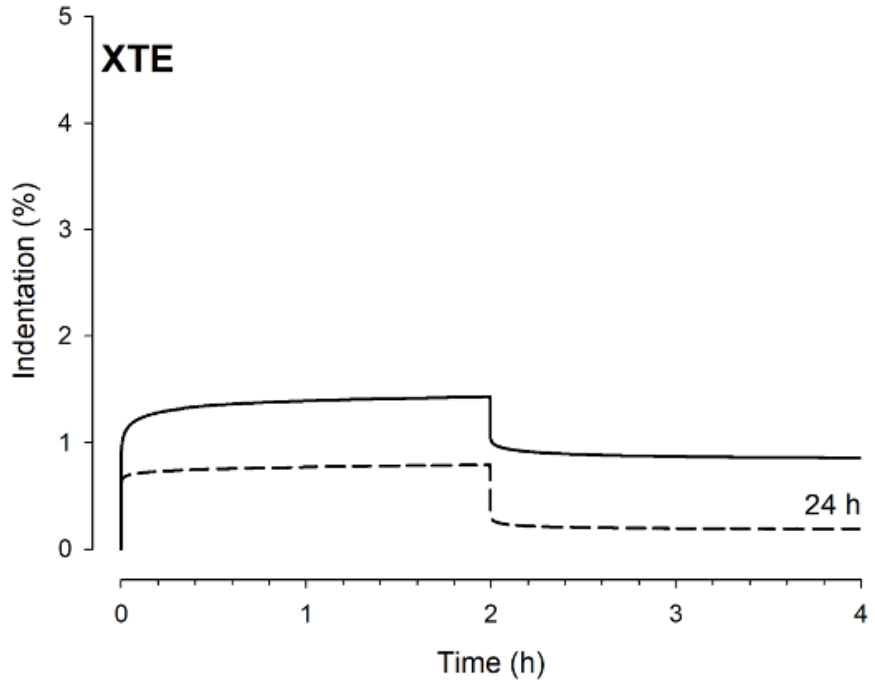

Figure 7.3: (a) – (h): Indentation as a function of time under 14 MPa stress for 2 h and unloaded recovery for 2 h for materials loaded both *immediately* (within 2 min – solid curves) and after a 24 h delay, post-irradiation (dashed curves).

7.5 Discussion

The ability of dental composites to attain an immediate surface integrity following irradiation is necessary for good clinical performance. In this study, the immediate integrity and developing viscoelastic characteristics of eight different resin composite materials, with varied composition and clinical applications, were evaluated using a novel indentation method [212]. This time-dependent method uses a flat-ended punch indenter, of diameter 1.5 mm, which transfers an instantaneous 14 MPa stress to the composite surface, over 2 h.

Despite differences in detail among the diverse RBC materials, an identical pattern of surface indentation behavior was apparent with all materials to that seen in our previous study [212]. Thus, our research (null) hypothesis was confirmed. Immediate indentation maxima ranged from *ca.* 1 to 5 percent and after 24 h, the maxima reduced to *ca.* 50 % of the immediate values. Expressed in absolute depth values, the above range is 40 – 200 μm, under 14 MPa stress, or a "compliance" range of *ca*. 3-14 μm/MPa.

The differences in indentation magnitudes were principally attributable to the range of particle reinforcement incorporated in each material. The conventional non-flowable materials (HRZ, GSO, XTE) had generally greater surface hardness (lesser indentations) than others upon immediate loading, followed by the non-flowable bulkfill and EBF materials, then finally the conventional flowable resin composites. Except with HRZ and XTE, 24 h time elicited a significant improvement in surface viscoelastic properties ($p<0.5$) [196, 306, 314].

The same irradiation protocol for photopolymerization was applied to all materials, receiving 24 J/cm^2. Immediate indentation challenges the RBC surface during the early glass stage of resin-matrix formation. The present results confirmed the greater influence of filler-mass-fraction compared to the RBC category. This is a similar result to previous studies [44, 177]. Comparing GSO and XTE, respectively, to their flowable counterparts GSF and XTF (Figure 3) confirm how filler content can strongly influence the surface integrity [111, 179, 315]. This supports the importance of a restoration-capping layer of highly-filled resin composite.

The organic matrix is also vital determinant in polymer surface integrity. Overall, 24 h post irradiation allowed for further polymer matrix-network development, [196, 306, 314]. The flexible aliphatic monomer units in TEGDMA result in a flexible polymer, thus more prone to deformation. However, the strong hydrogen bonds found between the aliphatic monomer units, in Bis-GMA, Bis-EMA and UDMA, results in more rigid polymers [25].

Flowable EBF resin composite performed similarly to the non-flowable OBF bulkfill. This could be explained by the rapid conversion rate based on RAP technology in the EBF material leading to faster network development. The RAP based materials have previously shown a rapid conversion and good surface properties compared to other conventional camphorquinone /amine-based materials, as reported by Ilie *et al*, [316].

Since the elastic modulus development of resin composite occurs within *ca.* 10 s [304], high indentation could be exhibited by materials with lower elastic modulus such as XTF, GSF and VBF. These materials have lower elastic moduli compared to their non-flowable comparators [179, 282]. The development of elastic modulus post-polymerization varies dependent on the monomer content/composition, and filler-mass-fraction [25, 44].

The viscoelastic behavior of restorative materials can be compared to dentin. Most previous studies have evaluated creep of natural dentin via nanoindentation methods. A recent study measured the viscoelasticity of human dentin by a bulk creep method. The maximum bulk creep "compliance" of dentin was 0.36 μm/MPa [317]. This is an interesting area for future comparative study.

7.6 Conclusion

The indentation-creep methodology effectively characterized resin-based composites within several categories. Viscoelastic properties evaluated by the indentation method confirmed that the previously established pattern of behavior is generic and not restricted to products manufactured by a single company. Highly filled resin composite materials were more resistant to indentation. The hardness of all materials improved after 24 h post-irradiation due to further matrix-network development.

Discussion Points raised by the External Examiner –Chapters 6& 7

1. What is the added value of creep measurements, compared to hardness?

   Macroscopic indentation (or bulk compressive loading), together with creep-recovery upon unloading, produces time-dependent deformation that can characterize the integrity of the network at – and below – the material surface. Because the indentation develops over several (eg 2) hours, the measurements probe the viscoelastic character of the network.

2. Higher filler content has a positive impact on several properties: greater indentation resistance, higher modulus - closer to dentin, lower shrinkage, etc. So why is this not more acknowledged as an essential basis for polymer classification, as compared with filler size?
   cf Randolph: Dental composite materials for direct restoration?

   I totally agree. But unfortunately, ‘many’ manufacturers tend to use terms that can sell products and their compliance with information needed by researchers (compared to clinicians) is generally low.

CHAPTER EIGHT

General discussion and future work

8.1 General discussion

Photopolymerization in Dentistry

The ongoing desire for faster and less complex steps in placement of dental restorative materials is being facilitated by advances in materials chemistry and light-curing technology.

In the 1970s, the first photopolymerization or 'light curing' units (LCUs) emitted ultra-violet (UV) and near UV light. With the development, by the late 1970s, of VIS-LCUs - emitting light of longer wavelengths from the visible part of the electromagnetic spectrum, these quickly replaced UV-LCUs. There were several reasons for this, as follows:
(i) the transmission of photons through dental composites increases with wavelength, so VIS-LCUs can irradiate to greater depth than UV-LCUs;
(ii) a photo-initiator system absorbing in the blue-VIS region was developed;
(iii) UV light can induce mutations in DNA so UV-LCUs were more hazardous to the soft tissues of both patient and operator.

Photopolymerization requires the delivery of a sufficient '***photon dose'*** – essentially equivalent to the product of *irradiance* (photons *per* second) and *irradiation time* (seconds). It follows that the same photon dose can be delivered by *increasing* irradiance (using "brighter" LCUs) and *decreasing* the irradiation time (giving a faster clinical step). If there could be an exact *inverse-proportionality* in the empirical relationship between irradiance and time, this would validate the so-called ***reciprocity hypothesis***. The available evidence suggests that such reciprocity is *limited*: *i.e.* not generally exact [300]. But this depends partly on the (Norrish) type of photoinitiator utilized: (Type I *versus* Type II) [73, 93]. In practice, this means that a safety factor (slightly longer clinical irradiation time) is advisable than that predicted assuming reciprocity.

Nevertheless, with the development of blue and violet light-emitting diodes (LEDs) of greatly increased radiant emittance, *the requisite irradiation time* using LED-LCUs has progressively reduced: from 60 s > 40 s > 20 s > an 'industry standard' of 10 s. Major dental companies have been divided as to the feasibility, desirability and

effectiveness of reducing this still further: to 5 s or 3 s or even 1 s. During this period, the class of composites known as “bulk fill” has also been developed and widely accepted by the dental profession. These have a greatly increased depth of cure.

Ultra-Rapid Photopolymerization: Does it work and is it safe?

During the past 5 years, Ivoclar AG (Liechtenstein) has developed and then marketed a high-irradiance LCU and composite system, known as the *PowerCure*™ system. This deploys a high irradiance protocol of 3 W/cm^2 over an ultra-short irradiation time of 3 s. These photo-cured materials termed: *Ultra-Rapid Photopolymerized Bulk-Fill* (URPBF) *Resin-Composites*. They include both non-flowable (*Tetric PowerFill*™) and flowable (*Tetric PowerFlow*™) formulations.

Aiming to investigate - and potentially validate - this high irradiance system we identified the following specific research questions, as follows:

(i) How efficient is this ‘short time/high irradiance’ protocol in curing 4 mm thickness of materials with different viscosities?

(ii) What are the effects of high irradiance on their polymerization shrinkage and shrinkage stress?

(iii) What are the effects of high irradiance on the polymerization exotherm and the heating effect of the LCU?

(iv) How can we investigate network development immediately following 3 s polymerization.

Therefore, ***the overall research question*** of this thesis was: Is *ultra-rapid photo-polymerization* possible, efficient and safe? A systematic study design was then structured to assess the polymerization of this URPBF resin composite system - from both the materials and photo-cure perspectives - by measuring: the achievable Degree of Conversion (DC), the shrinkage behavior, thermal analysis and early viscoelastic integrity.

In chapter 3, the aim was to determine the degrees of conversion, conversion kinetics and the effects of post-irradiation time on ultra-rapid photo-polymerized bulkfills (URPBF) under conditions equivalent to clinical depths of 1 and 4 mm. We studied,

by FTIR spectroscopy, the rapid photopolymerization materials (code-named: PFill and PFlow) and compared results to their predecessor composites (ECeram and EFlow), [112, 130]. Degrees-of-Conversion for PFill and PFlow, following the 3 s high-irradiance protocol, were generally similar to their comparators ECeram and EFlow (cured for 20 s), during the first 24 h post-irradiation, for both 1 mm and 4 mm thicknesses [211]. An AFCT (addition-fragmentation chain-transfer) agent, have previously shown to reduce polymerization rate when added to a mixture in 5 wt% concentration [97]. However, high irradiance from the *BluePhase PowerCure*™ LCU as well as the *Ivocerin*™ photo-initiator both might have compensated for possible rate-reduction, resulting in high conversion prior to vitrification [97, 211].

Polymerization shrinkage and shrinkage stress development of the URPBF composites were investigated in chapter 4. In this study, we introduced a second multi-wave high-irradiance LCU (VALO™ LCU emitting 3.2 W/cm^2) to assess the effect of wider active-curing tip, as the specimens' diameter were wider (8-10 mm). Both shrinkage strain and stress were measured in real-time for 1 h post-irradiation, as most of shrinkage phenomena occur within the first hour [207].

PFill produced the lowest polymerization *shrinkage* when polymerized with high-irradiance protocols (1.6 % and 1.7 % with PowerCure™ and VALO™ LCUs, respectively) compared to when irradiated for (a standard) 10 s (1.8 %). These results were all lower than for ECeram (2.7%) ($p<0.05$). Subsequently, PFill exhibited slightly higher *shrinkage stress* (2.2 MPa and 2.3 MPa for PowerCure™ and VALO™ LCUs respectively) compared to 10 s curing (1.8 MPa). However, regardless of the curing protocol, PFill produced lower shrinkage stress than ECeram (2.6 MPa). Similar behavior was seen in PFlow except that over 3s the VALO™ unit produced significantly higher shrinkage stress (3.6 MPa) [90, 97, 219, 312].

In this study, we used the Bonded Disk apparatus and Bioman II, respectively, for measurement of polymerization shrinkage and shrinkage stress [112]. The ability to monitor and analyze the change in dimensions in real-time enabled the calculation of shrinkage *rate* development. Real-time shrinkage and shrinkage stress plots helped in understanding the shrinkage behavior. We recall that, whereas shrinkage is a material property, shrinkage-stress is not. Thus, by using *disk* specimens with specific C-factors, both these measurement methods (along with possibly all alternate methods)

do not directly represent the clinical shapes of cavities and restorations. There are no established stress measurement methods using simulated clinical cavities because stress distributions in cavities are very complex, with differences in compliance over regions of hard tissue and natural tooth structure [145, 318]. Finite Element (FE) models are of value, but these make their own assumptions, not least by mainly assuming linear elastic – rather than viscoelastic – behavior.

Exothermic reactions and the effects of high irradiance on temperature fields in materials and a tooth cavity were investigated in chapter 5. We measured effects of a high-irradiance (3s) light-curing protocol *versus* two standard-irradiance (10s) protocols on Bulk Fill RBCs, including URPBF composites, during intra-dental photo-irradiation. We used visual and quantitative assessment, via 2D temperature maps plus several temperature/time plots. Using thermal imaging, 2D temperature maps over the entire coronal area were recorded for 120 s during and after irradiation [226].

Material composition and different light-curing protocols can influence maximum temperature (T_{max}), mean temperature rise (ΔT), and the time (s) to reach maximum temperature at different depths during intra-dental photo-curing [313]. Mean temperature rise (ΔT) within the material bulk, at 2 mm depth, was significantly higher in PFill and PFlow polymerized in PowerCure™-3s mode (21.8 and 27.1 ^{o}C), compared to PowerCure™-10s (17.8 and 22.9 ^{o}C). However, PowerCure™-3s thermal output were comparable to Elipar S10™-10s, except for PFill. Nonetheless, 1 mm of remaining dental thickness was sufficient to ensure a minimal temperature rise at 1mm within dentin, upon 4 mm bulk placement technique. This suggests freedom from significant thermal damage from rapid photopolymerization and thus the clinical safety of this treatment [313]. Furthermore, the moderate thermal diffusivities of dental composites and ultra-short exposure with the PowerCure LCU must reduce the overall impact of any thermal impulse.

Based on comparison with previous studies, the polymerization-related characteristics of the URPBF system resulted in an acceptable polymerization with acceptable shrinkage and shrinkage stress development and thermal safety (when sufficient remaining dentin thickness is present) [226, 313]. However, the effect of rapid network

development, within 3 s, had to be investigated to determine/validate the mechanical network integrity.

Three second irradiation should produce sufficient network development to withstand loading immediately following 3s irradiation. This should be equivalent to a typical material network developed immediately after 20 s curing. However, it is challenging to achieve such a measurement experimentally, as specimen preparation is time consuming for most current surface and bulk mechanical methods, often including at least minor finishing and polishing pre-test. Therefore, an experimental method for measuring early surface viscoelastic integrity was proposed in chapter 6. This deploys a flat-ended macroscopic indentor axially aligned over the specimen immediately (< 2min) post-irradiation. This transfers a 14 MPa compressive stress for a period of 2 h. Such *indentation-creep* measurements were successful in characterizing URPBF composites immediately post-irradiation. Maximum indentation (I_{max}%) ranged between 2.5% and 3.8% upon immediate loading, compared to 1.4% to 1.8% when loading after a 24 h delay. Flowable materials showed deeper indentation compared to non-flowable bulkfills. PFill and PFlow polymerized in 3 s resulted in immediate indentation values comparable to their counterparts ECeram and EFlow [212]. Furthermore, in 24 h delayed indentation, no differences were detected in maximum indentation results between the materials regardless of the materials type or curing protocol, which is attributed to further network development (see chapter 3).

This indentation-creep method was mainly developed to assess characterize URPBF composites. The opportunity to characterize several representative resin-composites from a range of manufacturers, including RBCs with varied clinical applications, was made in chapter 7. The indentation-creep/recovery method was successful in characterizing eight representative RBCs, including three bulkfills (**OBF**, **VBF**, **EBF**), three conventional non-flowables (**XTE**, **GSO**, **HRZ**) and conventional flowables (**XTF**, **GSF**). All materials showed time-dependent viscoelastic indentation. Immediate indentation revealed maximum indentation results between 1.4% and 4.9%, *versus* 0.7 to 2.2% for 24 h delayed indentation. Similar to results in chapter 6, flowable materials exhibited higher maximum indentation [319]. However, network developments up to 24 h significantly improved indentation resistance of all materials. Viscoelastic properties evaluated by the indentation-creep method confirmed that highly filled RBCs were more resistant to indentation [212, 319].

Critical reflection

In our experimental design, light curing protocols varied somewhat between studies based on the specific hypotheses under consideration. When evaluating degree of conversion, our aim was to subject the experimental groups (PowerCure system) to challenging control groups (with almost double the radiant exposure), to determine whether 3 s polymerization at high irradiance can be sufficient compared to the 20 s protocol. The same hypothesis applied to the early surface viscoelastic integrity measurements. However, the shrinkage phenomena and thermography evaluation required a standard curing protocol (10 s). The energy from the extended curing time of > 10 s can only increase (ΔT) but will probably not significantly affect the shrinkage stress [95].

There were many previous attempts to achieve ultra-fast photopolymerization. Early attempts were by increasing the Irradiance delivered to CQ-based resin composites [76, 187, 191, 320]. However, such high intensity delivery increased the autoacceleration causing the early onset of vitrification through the diffusion-controlled nature of the propagation phase. The rate of polymerization was then significantly affected by light intensity [132], since the curing rate is proportional to the square root of the applied light intensity, assuming steady-state conditions [143]. So, the fast reaction rate reduces the viscous flow time due to the increased rigidity, resulting in higher post-gel stresses [143, 206].
Further attempts to achieve ultra-fast photopolymerization were by utilizing more potent photoinitiators such as Norrish Type I [71, 73, 92, 321]. These highly reactive photoinitiators showed higher molar absorptivity compared to CQ [94], but also were associated with higher polymerization stress rate [95].
Therefore, incorporating covalent adaptable networks (CANs) into monomer network were suggested to possibly achieve a controlled polymerization with more homogenous networks [96]. For instance, reversible addition–fragmentation chain transfer (RAFT or AFCT) approach e.g. using β-allyl sulfone, or thiol-yne oligomers were incorporated in dental polymers[90, 104]. Both these agents- when added to dimethacrylate monomers- developed polymerization-induced phase separation due to

the step growth photo-polymerization. This resulted in reduced polymerization shrinkage and shrinkage stress due to mainly two contributing factors related to the addition–fragmentation chain transfer process (i) direct stress relief from the constant bond rearrangement; (ii) reduction in the reaction rate [97].

In *Tetric PowerFill* resin composite, the combination of: high filler load, Norrish type I photoinitiator (*Ivocerin*™), incorporation of β-allyl sulfone (AFCT), and using high irradiance protocol seemed to balance the rate of the reaction. This ultimately resulted in a comparable degree of conversion, reduced polymerization shrinkage and shrinkage stress, and comparable surface viscoelastic integrity to their comparators *Tetric EvoCeram Bulkfill*.

With the above information, it is important to understand that the previous results are in-*vitro* and should be interpreted carefully. Specimens were polymerized under standardized conditions and all measurements were conducted in a standardized process. In clinical application, special care must be taken when using URPBF as short irradiation protocol is very time-sensitive and small deviations in positioning during irradiation may significantly affect the polymerization-related properties, which then could affect the long-term physical and mechanical stability [91, 322].

The '*Polyvision'* feature in *BluePhase PowerCure*™ LCU can offer an assisted guide (with a response speed of 100 ms) during polymerization. Upon slight movement, an alarm – in the form of acoustic signals- are emitted, and the curing time is then automatically extended by 10% to compensate for the movement. But in excessive movement, the alarm will be triggered and the light will shut off. Therefore, this feature should not be underestimated and should always be used with the 3 s curing mode.

In summary, this thesis focused on investigation of a new concept of photopolymerization that has pushed the limit beyond what was previously thought possible. As with many advanced materials, it is essential to maintain an open mind about new claims and concepts and simultaneously to devise and apply both standard and novel experimental methods to objectively evaluate new technologies.

Future studies

As confirmed by the work reported in this thesis, the main modifications to URPBF composites were in photopolymerization technology and chemical formulations incorporating *Ivocerin*™ photoinitiations and AFCT agents. Further analysis could be done on the AFCT effect on resin composite with low viscosity to understand why no AFCT agent incorporated in *PowerFlow.*

Also, the modifications incorporated in URPBF resulted in modified polymerization reaction which work synergistically with a high-irradiance protocol. However, there are other available resin composites with similar modifications that could behave similarly. For instance, *Estelite bulkfill*™ (Tukoyama, Japan) is a flowable bulkfill material modified with RAP polymerization technology (see section 1.1.5), which could achieve sufficient polymerization via high irradiance and short irradiation time. Also, there are other materials with incorporated *Addition fragmentation monomer* (AFM) chemistry – a similar concept to AFCT- such as *One Bulk Fill*™ (3M Dental, USA), that can produce good conversion with minimal shrinkage-stress development.

Furthermore, future work is also necessary to investigate the cytotoxicity and the long-term performance of URPBF composites as there are only a few published (in-*vitro*) studies that evaluated long term physical and mechanical properties [323, 324]. At present, there is one clinical trial: a 2-year cohort study by *Lawson et al*. 2022, on 69 PowerCure™ posterior restorations. 52 of these 69 restorations were followed-up. They performed well with only one showing post-operative sensitivity [325]. Even though 2 years are still short for a material to be considered definitively successful, the results are promising. Therefore, further evidence is needed utilizing randomized controlled trials (RCTs).

8.2 Conclusions

- URPBF composites produced an overall comparable conversion at clinically relevant times: 5 min and 24 h post-irradiation, despite the ultra-short irradiation times and regardless of the specimen depth.

- Polymerization kinetics and the rate of polymerization were material dependent and mainly influenced by irradiation protocols, specimen thickness and material viscosity.

- Material composition and different light-curing protocols can influence temperature rise (ΔT) at different depths during intra-dental photo-curing, with maximal ΔT generally occurring at a 2 mm depth into bulk-fill RBCs.

- The temperature fields produced by a 3 s high-irradiance light-curing protocol with *Bluphase PowerCure*™ was generally comparable to the standard 10 s *Elipar S10*™, with temperature increases up to *ca.* 6 ºC, at 1 mm within dentin. This is considered safe for light-curing in deep cavities when sufficient remaining dentin thickness is present.

- The extent of immediate surface rigidity and developing viscoelastic characteristics of URPBF can be measured by a macroscopic indentation-creep method immediately post-irradiation, which can also effectively characterize resin-based composites within several categories.

- URPBF composites demonstrated an acceptable level of polymerization/property performance, despite the ultra-short irradiation times, evidencing their suitability for clinical application.

- Highly filled resin composite materials were more resistant to indentation. The hardness of all materials improved after 24h post-irradiation due to further matrix- network development. Especially with occlusal restorations, it is important to use a highly filled and wear-resistant composite.

- The AFCT agent incorporated in an URPBF composite modifies the polymerization reaction. This is consistent with further network reconfiguration and reshuffling of covalent bonds prior to gelation and vitrification. This can increase DC and simultaneously reduce shrinkage stress, even with high irradiance protocols. Collectively, all these factors may cause slightly higher temperature rises compared to other non-flowable bulkfills.

References

1. Widström E, Forss H. Selection of restorative materials in dental treatment of children and adults in public and private dental care in finland. Swed D J, 1994; 18: 1-7.
2. Opdam N, Bronkhorst E, Loomans B, Huysmans M-C. 12-year survival of composite vs. Amalgam restorations. Journal of dental research, 2010; 89: 1063-1067.
3. Kessler R. The minamata convention on mercury: A first step toward protecting future generations. Environ Health Perspect, 2013; 121: A304-309.
4. Petersen P, Baez R, Kwan S, Ogawa H. Future use of materials for dental restoration. World Health Organization: Geneva, Switzerland, 2009: 1-56.
5. Simonsen RJ. From prevention to therapy: Minimal intervention with sealants and resin restorative materials. J Dent, 2011; 39 Suppl 2: S27-33.
6. Murdoch-Kinch CA, McLean ME. Minimally invasive dentistry. J Am Dent Assoc, 2003; 134: 87-95.
7. Heintze SD, Ilie N, Hickel R, Reis A, Loguercio A, Rousson V. Laboratory mechanical parameters of composite resins and their relation to fractures and wear in clinical trials-a systematic review. Dent Mater, 2017; 33: e101-e114.
8. Demarco F, Corrêa M, Cenci M, Moraes R, Opdam NJ. Longevity of posterior composite restorations: Not only a matter of materials. Dent Mater, 2012; 28: 87-101.
9. Kopperud S, Rukke H, Kopperud H, Bruzell E. Light curing procedures–performance, knowledge level and safety awareness among dentists. J Dent, 2017; 58: 67-73.
10. Altaie A, Hadis M, Wilson V, German M, Nattress B, Wood D, Palin W. An evaluation of the efficacy of led light curing units in primary and secondary dental settings in the united kingdom. Operative Dentistry, 2021; 46: 271-282.
11. Brunthaler A, Konig F, Lucas T, Sperr W, Schedle A. Longevity of direct resin composite restorations in posterior teeth. Clin Oral Investig, 2003; 7: 63-70.
12. Opdam N. Clinical trials: Randomization, completeness of data and restoration longevity. Dent Mater, 2016; 32: 489-491.
13. Ferracane JL. Resin-based composite performance: Are there some things we can't predict? Dent Mater, 2013; 29: 51-58.
14. Randolph LD, Palin WM, Leprince JG. Composition of dental resin-based composites for direct restorations. In: *Dental composite materials for direct restorations*: Springer; 2018. pp. 11-24.
15. Stansbury JW. Dimethacrylate network formation and polymer property evolution as determined by the selection of monomers and curing conditions. Dent Mater, 2012; 28: 13-22.
16. Sideridou E. *Polymeric materials in dentistry*: Nova Science Publishers; 2010.
17. Rueggeberg FA, Giannini M, Arrais CAG, Price RBT. Light curing in dentistry and clinical implications: A literature review. Braz Oral Res, 2017; 31: e61.
18. Bowen RL. Properties of a silica-reinforced polymer for dental restorations. J Am Dent Assoc, 1963; 66: 57-64.
19. Moszner N, Salz U. New developments of polymeric dental composites. Progress Polym Sci, 2001; 26: 535-576.
20. Peutzfeldt A. Resin composites in dentistry: The monomer systems. Eur J Oral Sci, 1997; 105: 97-116.
21. Gonçalves F, Boaro L, Miyazaki C, Kawano Y, Braga R. Influence of polymeric matrix on the physical and chemical properties of experimental composites. Braz oral res, 2015; 29: 1-7.
22. Floyd CJ, Dickens SH. Network structure of bis-gma- and udma-based resin systems. Dent Mater, 2006; 22: 1143-1149.
23. Foster J, Walker RJ. Dental filling materials. In: Google Patents; 1975.

24. Kerby RE, Knobloch LA, Schricker S, Gregg B. Synthesis and evaluation of modified urethane dimethacrylate resins with reduced water sorption and solubility. Dent Mater, 2009; 25: 302-313.
25. Sideridou I, Tserki V, Papanastasiou G. Study of water sorption, solubility and modulus of elasticity of light-cured dimethacrylate-based dental resins. Biomaterials, 2003; 24: 655-665.
26. Sideridou I, Tserki V, Papanastasiou G. Effect of chemical structure on degree of conversion in light-cured dimethacrylate-based dental resins. Biomaterials, 2002; 23: 1819-1829.
27. Atai M, Watts DC, Atai Z. Shrinkage strain-rates of dental resin-monomer and composite systems. Biomaterials, 2005; 26: 5015-5020.
28. Cornelio RB, Wikant A, Mjosund H, Kopperud HM, Haasum J, Gedde UW, Ortengren UT. The influence of bis-ema vs bis gma on the degree of conversion and water susceptibility of experimental composite materials. Acta Odontol Scand, 2014; 72: 440-447.
29. Ferracane JL. Hygroscopic and hydrolytic effects in dental polymer networks. Dent Mater, 2006; 22: 211-222.
30. Busscher HJ, Rinastiti M, Siswomihardjo W, van der Mei HC. Biofilm formation on dental restorative and implant materials. J Dent Res, 2010; 89: 657-665.
31. Weinmann W, Thalacker C, Guggenberger R. Siloranes in dental composites. Dent Mater, 2005; 21: 68-74.
32. Bechtold J, Dos Santos PJ, Anido-Anido A, Di Hipolito V, Alonso RC, D'Alpino PH. Hardness, polymerization depth, and internal adaptation of class ii silorane composite restorations as a function of polymerization protocol. Eur J Dent, 2012; 6: 133-140.
33. Zimmerli B, Strub M, Jeger F, Stadler O, Lussi A. Composite materials: Composition, properties and clinical applications. A literature review. Schweiz Monatsschr Zahnmed, 2010; 120: 972-986.
34. Lien W, Vandewalle KS. Physical properties of a new silorane-based restorative system. Dent Mater, 2010; 26: 337-344.
35. Algamaiah H, Danso R, Banas J, Armstrong SR, Whang K, Rawls HR, Teixeira EC. The effect of aging methods on the fracture toughness and physical stability of an oxirane/acrylate, ormocer, and bis-gma-based resin composites. Clinic Oral Investig, 2019.
36. Boaro LC, Goncalves F, Guimaraes TC, Ferracane JL, Pfeifer CS, Braga RR. Sorption, solubility, shrinkage and mechanical properties of "low-shrinkage" commercial resin composites. Dent Mater, 2013; 29: 398-404.
37. Monsarrat P, Garnier S, Vergnes JN, Nasr K, Grosgogeat B, Joniot S. Survival of directly placed ormocer-based restorative materials: A systematic review and meta-analysis of clinical trials. Dent Mater, 2017; 33: e212-e220.
38. Cavalcante LM, Schneider LF, Silikas N, Watts DC. Surface integrity of solvent-challenged ormocer-matrix composite. Dent Mater, 2011; 27: 173-179.
39. Randolph LD, Palin WM, Leloup G, Leprince JG. Filler characteristics of modern dental resin composites and their influence on physico-mechanical properties. Dental Materials, 2016; 32: 1586-1599.
40. CHUNG KH, Greener E. Correlation between degree of conversion, filler concentration and mechanical properties of posterior composite resins. Journal of oral rehabilitation, 1990; 17: 487-494.
41. Satterthwaite JD, Vogel K, Watts DC. Effect of resin-composite filler particle size and shape on shrinkage–strain. Dent Mater, 2009; 25: 1612-1615.
42. Satterthwaite JD, Maisuria A, Vogel K, Watts DC. Effect of resin-composite filler particle size and shape on shrinkage-stress. Dent Mater, 2012; 28: 609-614.
43. Elbishari H, Silikas N, Satterthwaite J. Filler size of resin-composites, percentage of voids and fracture toughness: Is there a correlation? Dent Mater J, 2012; 31: 523-527.

44. Ilie N, Hickel R. Investigations on mechanical behaviour of dental composites. Clin Oral Investig, 2009; 13: 427-438.
45. Ilie N, Hickel R, Valceanu AS, Huth KC. Fracture toughness of dental restorative materials. Clin Oral Investig, 2012; 16: 489-498.
46. Htang A, Ohsawa M, Matsumoto H. Fatigue resistance of composite restorations: Effect of filler content. Dent Mater, 1995; 11: 7-13.
47. Ilie N, Hickel R. Macro-, micro- and nano-mechanical investigations on silorane and methacrylate-based composites. Dent Mater, 2009; 25: 810-819.
48. Curtis AR, Palin WM, Fleming GJ, Shortall AC, Marquis PM. The mechanical properties of nanofilled resin-based composites: The impact of dry and wet cyclic pre-loading on bi-axial flexure strength. Dental Materials, 2009; 25: 188-197.
49. Leprince J, Palin WM, Mullier T, Devaux J, Vreven J, Leloup G. Investigating filler morphology and mechanical properties of new low-shrinkage resin composite types. Journal of oral rehabilitation, 2010; 37: 364-376.
50. Chen MH. Update on dental nanocomposites. J Dent Res, 2010; 89: 549-560.
51. Klapdohr S, Moszner N. New inorganic components for dental filling composites. Monatshefte Fur Chemie, 2005; 136: 21-45.
52. Mitra SB, Wu D, Holmes BN. An application of nanotechnology in advanced dental materials. J Am Dent Assoc, 2003; 134: 1382-1390.
53. Darvell BW. *Materials science for dentistry*. 10th ed: Woodhead publishing; 2018.
54. Lung CY, Matinlinna JP. Aspects of silane coupling agents and surface conditioning in dentistry: An overview. Dent Mater, 2012; 28: 467-477.
55. Karabela MM, Sideridou ID. Effect of the structure of silane coupling agent on sorption characteristics of solvents by dental resin-nanocomposites. dental materials, 2008; 24: 1631-1639.
56. Arksornnukit M, Takahashi H, Nishiyama N. Effects of silane coupling agent amount on mechanical properties and hydrolytic durability of composite resin after hot water storage. Dental materials journal, 2004; 23: 31-36.
57. Kwon T, Bagheri R, Kim Y, Kim K, Burrow M. Cure mechanisms in materials for use in esthetic dentistry. J Investig Clin Dent, 2012; 3: 3-16.
58. Yu B, Lee YK. Influence of color parameters of resin composites on their translucency. Dent Mater, 2008; 24: 1236-1242.
59. Lutz F, Phillips RW. A classification and evaluation of composite resin systems. The Journal of prosthetic dentistry, 1983; 50: 480-488.
60. Anusavice KJ, Shen C, Rawls HR. *Phillips' science of dental materials*: Elsevier Health Sciences; 2013.
61. Ferracane JL. Resin composite--state of the art. Dent Mater, 2011; 27: 29-38.
62. Collins CJ, Bryant RW, Hodge KL. A clinical evaluation of posterior composite resin restorations: 8-year findings. J Dent, 1998; 26: 311-317.
63. Randolph LD, Palin WM, Leprince JG. Developing a more appropriate classification system for modern resin-based composite technologies. In: *Dental composite materials for direct restorations*: Springer; 2018. pp. 89-96.
64. Kloosterboer JG. Network formation by chain crosslinking photopolymerization and its applications in electronics. In: *Advances in polymer sciences*: Springer; 1988. pp. 1-61.
65. Cramer NB, Stansbury JW, Bowman CN. Recent advances and developments in composite dental restorative materials. J Dent Res, 2011; 90: 402-416.
66. Flory PJ. Fundamental principles of condensation polymerization. Chemical reviews, 1946; 39: 137-197.
67. Brauer G. Initiator-accelerator systems for acrylic resins and composites. In: *Biomedical and dental applications of polymers*: Springer; 1981. pp. 395-409.
68. Puckett AD, Fitchie JG, Kirk PC, Gamblin J. Direct composite restorative materials. Dent Clin North Am, 2007; 51: 659-675, vii.

69. Musanje L, Ferracane JL, Sakaguchi RL. Determination of the optimal photoinitiator concentration in dental composites based on essential material properties. Dent Mater, 2009; 25: 994-1000.
70. Ferracane JL. Current trends in dental composites. Critical Reviews in Oral Biology & Medicine, 1995; 6: 302-318.
71. Santini A, Gallegos IT, Felix CM. Photoinitiators in dentistry: A review. Prim Dent J, 2013; 2: 30-33.
72. Ikemura K, Endo T. A review of the development of radical photopolymerization initiators used for designing light-curing dental adhesives and resin composites. Dent Mater J, 2010; 29: 481-501.
73. Leprince J, Hadis M, Shortall A, Ferracane J, Devaux J, Leloup G, Palin W. Photoinitiator type and applicability of exposure reciprocity law in filled and unfilled photoactive resins. Dent Mater, 2011; 27: 157-164.
74. Price RB, Ferracane JL, Shortall AC. Light-curing units: A review of what we need to know. J Dent Res, 2015; 94: 1179-1186.
75. Aguiar FH, Lazzari CR, Lima DA, Ambrosano GM, Lovadino JR. Effect of light curing tip distance and resin shade on microhardness of a hybrid resin composite. Braz Oral Res, 2005; 19: 302-306.
76. Kramer N, Lohbauer U, Garcia-Godoy F, Frankenberger R. Light curing of resin-based composites in the led era. Am J Dent, 2008; 21: 135-142.
77. Mills R, Jandt K, Ashworth S. Dental composite depth of cure with halogen and blue light emitting diode technology. British dental journal, 1999; 186: 388-391.
78. Kramer N, Lohbauer U, García-Godoy F, Frankenberger R. Light curing of resin-based composites in the led era. Am J Dent, 2008; 21: 135.
79. Price RB, Labrie D, Rueggeberg FA, Felix CM. Irradiance differences in the violet (405 nm) and blue (460 nm) spectral ranges among dental light-curing units. J Esthet Restor Dent, 2010; 22: 363-377.
80. Caughman WF, Rueggeberg FA, CURTIS JR JW. Clinical guidelines for photocuring: Restorative resins. The Journal of the American Dental Association, 1995; 126: 1280-1286.
81. Stahl F, Ashworth SH, Jandt KD, Mills RW. Light-emitting diode (led) polymerisation of dental composites: Flexural properties and polymerisation potential. Biomaterials, 2000; 21: 1379-1385.
82. Jandt KD, Mills RW. A brief history of led photopolymerization. Dental Materials, 2013; 29: 605-617.
83. Rueggeberg FA. State-of-the-art: Dental photocuring—a review. Dental materials, 2011; 27: 39-52.
84. Heck K, Manhart J, Hickel R, Diegritz C. Clinical evaluation of the bulk fill composite quixfil in molar class i and ii cavities: 10-year results of a rct. Dent Mater, 2018; 34: e138-e147.
85. Bayraktar Y, Ercan E, Hamidi MM, Çolak H. One-year clinical evaluation of different types of bulk-fill composites. J Investig clin Dent, 2017; 8: e12210.
86. Chesterman J, Jowett A, Gallacher A, Nixon P. Bulk-fill resin-based composite restorative materials: A review. Br Dent J, 2017; 222: 337-344.
87. Van Ende A, De Munck J, Lise DP, Van Meerbeek B. Bulk-fill composites: A review of the current literature. J Adhes Dent, 2017; 19: 95-109.
88. Fugolin APP, Pfeifer CS. New resins for dental composites. J Dent Res, 2017; 96: 1085-1091.
89. Ibarra ET, Lien W, Casey J, Dixon SA, Vandewalle KS. Physical properties of a new sonically placed composite resin restorative material. Gen Dent, 2015; 63: 51-56.
90. Gorsche C, Griesser M, Gescheidt G, Moszner N, Liska R. B-allyl sulfones as addition–fragmentation chain transfer reagents: A tool for adjusting thermal and mechanical properties of dimethacrylate networks. Macromolecules, 2014; 47: 7327-7336.

91. Ilie N, Watts DC. Outcomes of ultra-fast (3 s) photo-cure in a raft-modified resin-composite. Dent Mater, 2020; 36: 570-579.
92. Leprince J, Hadis M, Ferracane J, Shortall A, Leloup G, Palin W. Lucirin-tpo: Photoinitiator reactivity and curing time reduction. Dent Mater, 2009; 26: e127.
93. Leprince JG, Palin WM, Hadis MA, Devaux J, Leloup G. Progress in dimethacrylate-based dental composite technology and curing efficiency. Dent Mater, 2013; 29: 139-156.
94. Randolph LD, Palin WM, Bebelman S, Devaux J, Gallez B, Leloup G, Leprince JG. Ultra-fast light-curing resin composite with increased conversion and reduced monomer elution. Dental Materials, 2014; 30: 594-604.
95. Randolph LD, Palin WM, Watts DC, Genet M, Devaux J, Leloup G, Leprince JG. The effect of ultra-fast photopolymerisation of experimental composites on shrinkage stress, network formation and pulpal temperature rise. Dent Mater, 2014; 30: 1280-1289.
96. Barner-Kowollik C. *Handbook of raft polymerization*: John Wiley & Sons; 2008.
97. Shah PK, Stansbury JW, Bowman CN. Application of an addition–fragmentation-chain transfer monomer in di (meth) acrylate network formation to reduce polymerization shrinkage stress. Polym Chem, 2017; 8: 4339-4351.
98. Gorsche C, Koch T, Moszner N, Liska R. Exploring the benefits of β-allyl sulfones for more homogeneous dimethacrylate photopolymer networks. Polymer Chemistry, 2015; 6: 2038-2047.
99. Sampaio CS, Chiu KJ, Farrokhmanesh E, Janal M, Puppin-Rontani RM, Giannini M, Bonfante EA, Coelho PG, Hirata R. Microcomputed tomography evaluation of polymerization shrinkage of class i flowable resin composite restorations. Oper Dent, 2017; 42: E16-E23.
100. Opdam N, Loomans B, Roeters F, Bronkhorst E. Five-year clinical performance of posterior resin composite restorations placed by dental students. Journal of dentistry, 2004; 32: 379-383.
101. Opdam N, Van De Sande F, Bronkhorst E, Cenci M, Bottenberg P, Pallesen U, Gaengler P, Lindberg A, Huysmans M, Van Dijken J. Longevity of posterior composite restorations: A systematic review and meta-analysis. Journal of dental research, 2014; 93: 943-949.
102. Ge Y, Wang S, Zhou X, Wang H, Xu HH, Cheng L. The use of quaternary ammonium to combat dental caries. Materials, 2015; 8: 3532-3549.
103. Cramer NB, Couch CL, Schreck KM, Carioscia JA, Boulden JE, Stansbury JW, Bowman CN. Investigation of thiol-ene and thiol-ene-methacrylate based resins as dental restorative materials. Dent Mater, 2010; 26: 21-28.
104. Bacchi A, Nelson M, Pfeifer CS. Characterization of methacrylate-based composites containing thio-urethane oligomers. Dent Mater, 2016; 32: 233-239.
105. White SR, Sottos NR, Geubelle PH, Moore JS, Kessler MR, Sriram S, Brown EN, Viswanathan S. Autonomic healing of polymer composites. Nature, 2001; 409: 794-797.
106. Althaqafi KA, Satterthwaite J, Silikas N. A review and current state of autonomic self-healing microcapsules-based dental resin composites. Dental Materials, 2020; 36: 329-342.
107. Jandt KD, Watts DC. Nanotechnology in dentistry: Present and future perspectives on dental nanomaterials. Dental Materials, 2020; 36: 1365-1378.
108. Priyadarsini S, Mukherjee S, Mishra M. Nanoparticles used in dentistry; a review. Journal of oral biology and craniofacial research, 2017.
109. Besinis A, De Peralta T, Handy RD. The antibacterial effects of silver, titanium dioxide and silica dioxide nanoparticles compared to the dental disinfectant chlorhexidine on streptococcus mutans using a suite of bioassays. Nanotoxicology, 2014; 8: 1-16.

110. Cheng L, Weir MD, Xu HH, Antonucci JM, Kraigsley AM, Lin NJ, Lin-Gibson S, Zhou X. Antibacterial amorphous calcium phosphate nanocomposites with a quaternary ammonium dimethacrylate and silver nanoparticles. Dent Mater, 2012; 28: 561-572.
111. Alshabib A, Silikas N, Watts D. Hardness and fracture toughness of resin-composite materials with and without fibers. Dent Mater, 2019; 35: 1194-1203.
112. Ferracane J, Hilton T, Stansbury J, Watts D, Silikas N, Ilie N, Heintze S, Cadenaro M, Hickel R. Academy of dental materials guidance—resin composites: Part ii—technique sensitivity (handling, polymerization, dimensional changes). Dent Mater, 2017; 33: 1171-1191.
113. Ilie N, Hilton T, Heintze S, Hickel R, Watts DC, Silikas N, Stansbury J, Cadenaro M, Ferracane J. Academy of dental materials guidance—resin composites: Part i—mechanical properties. Dent Mater, 2017; 33: 880-894.
114. Ronald L. Sakaguchi. *Craig's restorative dental materials*. thirteen's ed. Mosby, Inc., an affiliate of Elsevier Inc.; 2012.
115. dos Santos GB, Alto RV, Filho HR, da Silva EM, Fellows CE. Light transmission on dental resin composites. Dent Mater, 2008; 24: 571-576.
116. Rheims J, Koser J, Wriedt T. Refractive-index measurements in the near-ir using an abbe refractometer. Measur Sci Tech, 1997; 8: 601-605.
117. Duchowicz PR, Fioressi SE, Bacelo DE, Saavedra LM, Toropova AP, Toropov AA. Qspr studies on refractive indices of structurally heterogeneous polymers. Chemomet Intelligen Lab Sys, 2015; 140: 86-91.
118. Tyas MJ, Jones DW, Rizkalla AS. The evaluation of resin composite consistency. Dent Mater, 1998; 14: 424-428.
119. Silikas N, Watts D. Rheology of urethane dimethacrylate and diluent formulations. Dental Materials, 1999; 15: 257-261.
120. Lee J-H, Um C-M, Lee I-b. Rheological properties of resin composites according to variations in monomer and filler composition. Dental Materials, 2006; 22: 515-526.
121. Al-Ahdal K, Silikas N, Watts DC. Rheological properties of resin composites according to variations in composition and temperature. Dent Mater, 2014; 30: 517-524.
122. Leprince JG, Leveque P, Nysten B, Gallez B, Devaux J, Leloup G. New insight into the "depth of cure" of dimethacrylate-based dental composites. Dental Materials, 2012; 28: 512-520.
123. Ilie N, Bucuta S, Draenert M. Bulk-fill resin-based composites: An in vitro assessment of their mechanical performance. Operative dentistry, 2013; 38: 618-625.
124. Reis AF, Vestphal M, Amaral RCD, Rodrigues JA, Roulet JF, Roscoe MG. Efficiency of polymerization of bulk-fill composite resins: A systematic review. Braz Oral Res, 2017; 31: e59.
125. Tsai PC, Meyers IA, Walsh LJ. Depth of cure and surface microhardness of composite resin cured with blue led curing lights. Dental Materials, 2004; 20: 364-369.
126. Al-Ahdal K, Ilie N, Silikas N, Watts DC. Polymerization kinetics and impact of post polymerization on the degree of conversion of bulk-fill resin-composite at clinically relevant depth. Dent Mater, 2015; 31: 1207-1213.
127. Par M, Gamulin O, Marovic D, Klaric E, Tarle Z. Raman spectroscopic assessment of degree of conversion of bulk-fill resin composites–changes at 24 hours post cure. Operative dentistry, 2015; 40: E92-E101.
128. Par M, Lapas-Barisic M, Gamulin O, Panduric V, Spanovic N, Tarle Z. Long term degree of conversion of two bulk-fill composites. Acta Stomatol Croat, 2016; 50: 292-300.
129. Ferracane JL. Elution of leachable components from composites. J Oral Rehabil, 1994; 21: 441-452.

130. Moraes LG, Rocha RS, Menegazzo LM, de Araujo EB, Yukimito K, Moraes JC. Infrared spectroscopy: A tool for determination of the degree of conversion in dental composites. J Appl Oral Sci, 2008; 16: 145-149.
131. Fugolin APP, Bacchi A, Pfeifer CS. Curing reaction and kinetics. In: *Dental composite materials for direct restorations*: Springer; 2018. pp. 27-42.
132. Lovelh L, Newman S, Bowman C. The effects of light intensity, temperature, and comonomer composition on the polymerization behavior of dimethacrylate dental resins. J Dent Res, 1999; 78: 1469-1476.
133. Viljanen EK, Skrifvars M, Vallittu PK. Degree of conversion of a copolymer of an experimental monomer and methyl methacrylate for dental applications. Journal of applied polymer science, 2004; 93: 1908-1912.
134. Asmussen E. Restorative resins: Hardness and strength vs. Quantity of remaining double bonds. Scand J Dent Res, 1982; 90: 484-489.
135. Gonçalves JF. Effect of light curing units on degree of conversion, microhardness and mechanical properties of a bulk fill composite: Universidade Federal de Uberlândia; 2019.
136. Braga RR, Ferracane JL. Contraction stress related to degree of conversion and reaction kinetics. J Dent Res, 2002; 81: 114-118.
137. Fonseca AS, Labruna Moreira AD, de Albuquerque PP, de Menezes LR, Pfeifer CS, Schneider LF. Effect of monomer type on the cc degree of conversion, water sorption and solubility, and color stability of model dental composites. Dent Mater, 2017; 33: 394-401.
138. Ferracane JL, Condon JR. Rate of elution of leachable components from composite. Dent Mater, 1990; 6: 282-287.
139. Price RB, Whalen J, Price TB, Felix CM, Fahey J. The effect of specimen temperature on the polymerization of a resin-composite. Dental materials, 2011; 27: 983-989.
140. Baroudi K, Saleh AM, Silikas N, Watts DC. Shrinkage behaviour of flowable resin-composites related to conversion and filler-fraction. journal of dentistry, 2007; 35: 651-655.
141. Dewaele M, Truffier-Boutry D, Devaux J, Leloup G. Volume contraction in photocured dental resins: The shrinkage-conversion relationship revisited. Dent Mater, 2006; 22: 359-365.
142. Braga R, Ferracane J. Contraction stress related to degree of conversion and reaction kinetics. J Dent Res, 2002; 81: 114-118.
143. Braga RR, Ballester RY, Ferracane JL. Factors involved in the development of polymerization shrinkage stress in resin-composites: A systematic review. Dent Mater, 2005; 21: 962-970.
144. Feilzer A, Dauvillier B. Effect of tegdma/bisgma ratio on stress development and viscoelastic properties of experimental two-paste composites. J dent res, 2003; 82: 824-828.
145. Schneider LFJ, Cavalcante LM, Silikas N. Shrinkage stresses generated during resin-composite applications: A review. J dent biomech, 2010; 2010: 1-14.
146. Ferracane JL. Buonocore lecture. Placing dental composites--a stressful experience. Oper Dent, 2008; 33: 247-257.
147. Kinomoto Y, Torii M. Photoelastic analysis of polymerization contraction stresses in resin composite restorations. J Dent, 1998; 26: 165-171.
148. Ferracane JL, Hilton TJ. Polymerization stress–is it clinically meaningful? Dental materials, 2016; 32: 1-10.
149. Peutzfeldt A, Asmussen E. Determinants of in vitro gap formation of resin composites. Journal of dentistry, 2004; 32: 109-115.
150. Ferracane J. Models of caries formation around dental composite restorations. Journal of dental research, 2017; 96: 364-371.
151. Watts DC. Reaction kinetics and mechanics in photo-polymerised networks. Dental Materials, 2005; 21: 27-35.

152. Algamaiah H, Sampaio CS, Rigo LC, Janal MN, Giannini M, Bonfante EA, Coelho PG, Reis AF, Hirata R. Microcomputed tomography evaluation of volumetric shrinkage of bulk-fill composites in class ii cavities. J Esthet Restor Dent, 2017; 29: 118-127.
153. Feilzer A, De Gee A, Davidson C. Setting stress in composite resin in relation to configuration of the restoration. J dent res, 1987; 66: 1636-1639.
154. Watts DC, Satterthwaite JD. Axial shrinkage-stress depends upon both c-factor and composite mass. Dent Mater, 2008; 24: 1-8.
155. Maktabi H, Balhaddad AA, Alkhubaizi Q, Strassler H, Melo MAS. Factors influencing success of radiant exposure in light-curing posterior dental composite in the clinical setting. Am J Dent, 2018; 31: 320-328.
156. Calheiros FC, Daronch M, Rueggeberg FA, Braga RR. Degree of conversion and mechanical properties of a bisgma: Tegdma composite as a function of the applied radiant exposure. Journal of Biomedical Materials Research Part B: Applied Biomaterials: An Official Journal of The Society for Biomaterials, The Japanese Society for Biomaterials, and The Australian Society for Biomaterials and the Korean Society for Biomaterials, 2008; 84: 503-509.
157. Ilie N, Hickel R. Investigations on a methacrylate-based flowable composite based on the sdr™ technology. Dent Mater, 2011; 27: 348-355.
158. Kalra S, Singh A, Gupta M, Chadha V. Ormocer: An aesthetic direct restorative material; an in vitro study comparing the marginal sealing ability of organically modified ceramics and a hybrid composite using an ormocer-based bonding agent and a conventional fifth-generation bonding agent. Contemp Clin Dent, 2012; 3: 48-53.
159. Poggio C, Chiesa M, Scribante A, Mekler J, Colombo M. Microleakage in class ii composite restorations with margins below the cej: In vitro evaluation of different restorative techniques. Med Oral Patol Oral Cir Bucal, 2013; 18: e793-798.
160. Münchow EA, Meereis CTW, de Oliveira da Rosa WL, da Silva AF, Piva E. Polymerization shrinkage stress of resin-based dental materials: A systematic review and meta-analyses of technique protocol and photo-activation strategies. J Mech Behav Biomed Mater, 2018; 82: 77-86.
161. Calheiros FC, Kawano Y, Stansbury JW, Braga RR. Influence of radiant exposure on contraction stress, degree of conversion and mechanical properties of resin composites. Dent Mater, 2006; 22: 799-803.
162. Stansbury JW, Trujillo-Lemon M, Lu H, Ding X, Lin Y, Ge J. Conversion-dependent shrinkage stress and strain in dental resins and composites. Dent Mater, 2005; 21: 56-67.
163. Lim B-S, Ferracane J, Sakaguchi R, Condon J. Reduction of polymerization contraction stress for dental composites by two-step light-activation. Dent Mater, 2002; 18: 436-444.
164. Hirata R, Clozza E, Giannini M, Farrokhmanesh E, Janal M, Tovar N, Bonfante EA, Coelho PG. Shrinkage assessment of low shrinkage composites using micro-computed tomography. J Biomed Mater Res B Appl Biomater, 2015; 103: 798-806.
165. Watts DC, Marouf A, Al-Hindi A. Photo-polymerization shrinkage-stress kinetics in resin-composites: Methods development. Dent Mater, 2003; 19: 1-11.
166. El-Nawawy M, Koraitim L, Abouelatta O, Hegazi H. Depth of cure and microhardness of nanofilled, packable and hybrid dental composite resins. Am J Biomed Eng, 2012; 2: 241-250.
167. Wilson KS, Antonucci JM. Interphase structure–property relationships in thermoset dimethacrylate nanocomposites. Dent Mater, 2006; 22: 995-1001.
168. Fischer-Cripps AC. Contact mechanics. In: *Nanoindentation*: Springer; 2011. pp. 1-19.
169. Cock D, Watts D. Time-dependent deformation of composite restorative materials in compression. Journal of Dental Research, 1985; 64: 147-150.

170. El Hejazi A, Watts D. Creep and visco-elastic recovery of cured and secondary-cured composites and resin-modified glass-ionomers. Dental Materials, 1999; 15: 138-143.
171. Stafford GD, Huggett R. Creep and hardness testing of some denture base polymers. J Prosth Dent, 1978; 39: 682-687.
172. El-Safty S, Silikas N, Watts DC. Creep deformation of restorative resin-composites intended for bulk-fill placement. Dent Mater, 2012; 28: 928-935.
173. Baroudi K, Silikas N, Watts DC. Time-dependent visco-elastic creep and recovery of flowable composites. Eur J Oral Sci, 2007; 115: 517-521.
174. Papadogianis Y, Boyer DB, Lakes RS. Creep of conventional and microfilled dental composites. J Biomed Mater Res, 1984; 18: 15-24.
175. Stafford GD, Handley RW. Transverse bend testing of denture base polymers. J Dent, 1975; 3: 251-255.
176. Glantz P, Bates J. Creep in some acrylic dental resins. J Odontologisk revy, 1973; 24: 283.
177. Jun S, Kim D, Goo H, Lee H. Investigation of the correlation between the different mechanical properties of resin composites. Dent Mater J, 2013; 32: 48-57.
178. Ruyter IE, Øysæd H. Compressive creep of light cured resin based restorative materials. Acta Odontologica Scandinavica, 1982; 40: 319-324.
179. Papadogiannis D, Tolidis K, Gerasimou P, Lakes R, Papadogiannis Y. Viscoelastic properties, creep behavior and degree of conversion of bulk fill composite resins. Dent Mater, 2015; 31: 1533-1541.
180. Ferracane J, Greener E. The effect of resin formulation on the degree of conversion and mechanical properties of dental restorative resins. Journal of biomedical materials research, 1986; 20: 121-131.
181. Cheng L, Xia X, Yu W, Scriven L, Gerberich W. Flat-punch indentation of viscoelastic material. J Polym Sci, 2000; 38: 10-22.
182. Vandewalle KS, Ferracane JL, Hilton TJ, Erickson RL, Sakaguchi RL. Effect of energy density on properties and marginal integrity of posterior resin composite restorations. Dent Mater, 2004; 20: 96-106.
183. Watts DC. Let there be more light! Dental Materials, 2015; 31: 2.
184. Silikas N, Eliades G, Watts DC. Light intensity effects on resin-composite degree of conversion and shrinkage strain. Dent Mater, 2000; 16: 292-296.
185. Bernardo M, Luis H, Martin MD, Leroux BG, Rue T, Leitao J, DeRouen TA. Survival and reasons for failure of amalgam versus composite posterior restorations placed in a randomized clinical trial. J Am Dent Assoc, 2007; 138: 775-783.
186. Heintze SD, Rousson V. Clinical effectiveness of direct class ii restorations - a meta-analysis. J Adhes Dent, 2012; 14: 407-431.
187. Daugherty MM, Lien W, Mansell MR, Risk DL, Savett DA, Vandewalle KS. Effect of high-intensity curing lights on the polymerization of bulk-fill composites. Dent Mater, 2018; 34: 1531-1541.
188. Besegato JF, Jussiani EI, Andrello AC, Fernandes RV, Salomao FM, Vicentin BLS, Dezan-Garbelini CC, Hoeppner MG. Effect of light-curing protocols on the mechanical behavior of bulk-fill resin composites. J Mech Behav Biomed Mater, 2019; 90: 381-387.
189. Ilie N. Impact of light transmittance mode on polymerisation kinetics in bulk-fill resin-based composites. J Dent, 2017; 63: 51-59.
190. Ilie N, Durner J. Polymerization kinetic calculations in dental composites: A method comparison analysis. Clin Oral Investig, 2014; 18: 1587-1596.
191. Hadis M, Leprince JG, Shortall AC, Devaux J, Leloup G, Palin WM. High irradiance curing and anomalies of exposure reciprocity law in resin-based materials. J Dent, 2011; 39: 549-557.
192. AlShaafi MM. Effects of delivering the same radiant exposures at 730, 1450, and 2920 mw/cm2 to two resin-based composites. Eur J Dent, 2017; 11: 22.
193. Bunsen RW, Roscoe HE. *Photochemische untersuchungen*: Engelmann; 1892.

194. Palagummi SV, Hong T, Wang Z, Moon CK, Chiang MYM. Resin viscosity determines the condition for a valid exposure reciprocity law in dental composites. Dent Mater, 2020; 36: 310-319.
195. Wang R, Liu H, Wang Y. Different depth-related polymerization kinetics of dual-cure, bulk-fill composites. Dent Mater, 2019; 35: 1095-1103.
196. Watts DC, Amer OM, Combe EC. Surface hardness development in light-cured composites. Dent Mater, 1987; 3: 265-269.
197. Alshali RZ, Silikas N, Satterthwaite JD. Degree of conversion of bulk-fill compared to conventional resin-composites at two time intervals. Dent Mater, 2013; 29: e213-217.
198. Czasch P, Ilie N. In vitro comparison of mechanical properties and degree of cure of bulk fill composites. Clinical oral investigations, 2013; 17: 227-235.
199. Calheiros C, Daronch M, Rueggeberg F, Braga R. Effect of temperature on composite polymerization stress and degree of conversion. Dental Materials, 2014; 30: 613-618.
200. Burtscher P. Stability of radicals in cured composite materials. Dent Mater, 1993; 9: 218-221.
201. Abu-elenain DA, Lewis SH, Stansbury JW. Property evolution during vitrification of dimethacrylate photopolymer networks. Dental Materials, 2013; 29: 1173-1181.
202. Miletic V, Pongprueksa P, De Munck J, Brooks NR, Van Meerbeek B. Curing characteristics of flowable and sculptable bulk-fill composites. Clinical oral investigations, 2017; 21: 1201-1212.
203. Shah PK, Stansbury JW. Role of filler and functional group conversion in the evolution of properties in polymeric dental restoratives. Dent Mater, 2014; 30: 586-593.
204. Halvorson RH, Erickson RL, Davidson CL. The effect of filler and silane content on conversion of resin-based composite. Dental Materials, 2003; 19: 327-333.
205. Hirata R, Kabbach W, De Andrade OS, Bonfante EA, Giannini M, Coelho PG. Bulk fill composites: An anatomic sculpting technique. J Esth Rest Dent, 2015; 27: 335-343.
206. Kleverlaan CJ, Feilzer AJ. Polymerization shrinkage and contraction stress of dental resin composites. Dent Mater, 2005; 21: 1150-1157.
207. Ferracane JL. Placing dental composites—a stressful experience. Oper dent, 2008; 33: 247-257.
208. Soares CJ, Rodrigues MdP, Vilela ABF, Pfeifer CS, Tantbirojn D, Versluis A. Polymerization shrinkage stress of composite resins and resin cements–what do we need to know? Braz oral res, 2017; 31: 49-63.
209. Calheiros FC, Braga RR, Kawano Y, Ballester RY. Relationship between contraction stress and degree of conversion in restorative composites. Dent Mater, 2004; 20: 939-946.
210. Atria PJ, Sampaio CS, Cáceres E, Fernández J, Reis AF, Giannini M, Coelho PG, Hirata R. Micro-computed tomography evaluation of volumetric polymerization shrinkage and degree of conversion of composites cured by various light power outputs. Dent Mater J, 2018; 37: 33-39.
211. Algamaiah H, Silikas N, Watts DC. Conversion kinetics of rapid photo-polymerized resin composites. Dent Mater, 2020: 1266-1274.
212. Watts DC, Algamaiah H. Characterizing surface viscoelastic integrity of ultra-fast photo-polymerized composites: Methods development. Dent Mater, 2020: 1255-1265.
213. Watts DC, Cash A. Kinetic measurements of photo-polymerization contraction in resins and composites. Measurement Sci Tech, 1991; 2: 788-794.
214. Al Sunbul H, Silikas N, Watts DC. Polymerization shrinkage kinetics and shrinkage-stress in dental resin-composites. Dent Mater, 2016; 32: 998-1006.
215. Watts DC, Marouf A. Optimal specimen geometry in bonded-disk shrinkage-strain measurements on light-cured biomaterials. Dent Mater, 2000; 16: 447-451.

216. Davidson C, De Gee AJ. Relaxation of polymerization contraction stresses by flow in dental composites. J Dent Res, 1984; 63: 146-148.
217. Lu H, Stansbury JW, Bowman CN. Towards the elucidation of shrinkage stress development and relaxation in dental composites. Dent Mater, 2004; 20: 979-986.
218. Habib E, Wang R, Zhu X. Correlation of resin viscosity and monomer conversion to filler particle size in dental composites. Dent Mater, 2018; 34: 1501-1508.
219. Par M, Marovic D, Attin T, Tarle Z, Tauböck TT. Effect of rapid high-intensity light-curing on polymerization shrinkage properties of conventional and bulk-fill composites. J Dent, 2020; 101: 103448.
220. Charton C, Colon P, Pla F. Shrinkage stress in light-cured composite resins: Influence of material and photoactivation mode. Dent Mater, 2007; 23: 911-920.
221. Min S, Ferracane J, Lee I. Effect of shrinkage strain, modulus, and instrument compliance on polymerization shrinkage stress of light-cured composites during the initial curing stage. Dent Mater, 2010; 26: 1024-1033.
222. Al-Ahdal K, Ilie N, Silikas N, Watts DC. Polymerization kinetics and impact of post polymerization on the degree of conversion of bulk-fill resin-composite at clinically relevant depth. Dent Mater, 2015; 31: 1207-1213.
223. Ferracane JL. Resin-based composite performance: Are there some things we can't predict? Dent Mater, 2013; 29: 51-58.
224. Palin WM, Leprince JG, Hadis MA. Shining a light on high volume photocurable materials. Dent Mater, 2018; 34: 695-710.
225. Zorzin J, Maier E, Harre S, Fey T, Belli R, Lohbauer U, Petschelt A, Taschner M. Bulk-fill resin composites: Polymerization properties and extended light curing. Dent Mater, 2015; 31: 293-301.
226. Kim M-J, Kim RJ-Y, Ferracane J, Lee I-B. Thermographic analysis of the effect of composite type, layering method, and curing light on the temperature rise of photo-cured composites in tooth cavities. Dent Mater, 2017; 33: e373-e383.
227. Lempel E, Őri Z, Kincses D, Lovász BV, Kunsági-Máté S, Szalma J. Degree of conversion and in vitro temperature rise of pulp chamber during polymerization of flowable and sculptable conventional, bulk-fill and short-fibre reinforced resin composites. Dent Mater, 2021.
228. Zach L, Cohen G. Pulp response to externally applied heat. Oral Surgery, Oral Medicine, Oral Pathology, 1965; 19: 515-530.
229. Chang H-S, Cho K-J, Park S-J, Lee B-N, Hwang Y-C, Oh W-M, Hwang I-N. Thermal analysis of bulk filled composite resin polymerization using various light curing modes according to the curing depth and approximation to the cavity wall. J Appl Oral Sci, 2013; 21: 293-299.
230. Zarpellon DC, Runnacles P, Maucoski C, Gross DJ, Coelho U, Rueggeberg FA, Arrais CAG. Influence of class v preparation on in vivo temperature rise in anesthetized human pulp during exposure to a polywave® led light curing unit. Dental materials, 2018; 34: 901-909.
231. Al-Qudah AA, Mitchell CA, Biagioni PA, Hussey DL. Thermographic investigation of contemporary resin-containing dental materials. J Dent, 2005; 33: 593-602.
232. Al-Qudah AA, Mitchell CA, Biagioni PA, Hussey DL. Effect of composite shade, increment thickness and curing light on temperature rise during photocuring. J Dent, 2006; 35: 238-245.
233. Baroudi K, Silikas N, Watts DC. In vitro pulp chamber temperature rise from irradiation and exotherm of flowable composites. Int J Paediatr Dent, 2009; 19: 48-54.
234. Karacan AO, Ozyurt P. Effect of preheated bulk-fill composite temperature on intrapulpal temperature increase in vitro. J Esthet Restor Dent, 2019; 31: 583-588.
235. Watts D, Cahn RW, Haasen P, Kramer EJ, Williams DF. *Dental restorative materials. In: Materials science and technology: A comprehensive treatment. Vol.14: Dental and*

medical materials. D. F. Williams, ed.. Weinheim, FRG: VCH Verlagsgesellschaft mbH. (Chapter 6) 209-258 (p.231); 1992.
236. Watts DC, McAndrew R, Lloyd CH. Thermal diffusivity of composite restorative materials. J Dent Res, 1987; 66: 1576-1578.
237. Versluis A, Douglas WH, Sakaguchi RL. Thermal expansion coefficient of dental composites measured with strain gauges. Dent Mater, 1996; 12: 290-294.
238. Alnazzawi A, Watts DC. Simultaneous determination of polymerization shrinkage, exotherm and thermal expansion coefficient for dental resin-composites. Dent Mater, 2012; 28: 1240-1249.
239. Sideridou I, Achilias DS, Kyrikou E. Thermal expansion characteristics of light-cured dental resins and resin composites. Biomaterials, 2004; 25: 3087-3097.
240. Cidreira Boaro LC, Pereira Lopes D, de Souza ASC, Lie Nakano E, Ayala Perez MD, Pfeifer CS, Gonçalves F. Clinical performance and chemical-physical properties of bulk fill composites resin —a systematic review and meta-analysis. Dent Mater, 2019; 35: e249-e264.
241. Shortall AC, Harrington E. Temperature rise during polymerization of light-activated resin composites. J Oral Rehab, 1998; 25: 908-913.
242. Kutuk ZB, Gurgan S, Hickel R, Ilie N. Influence of extremely high irradiances on the micromechanical properties of a nano hybrid resin based composite. Am J Dent, 2017; 30: 9-15.
243. Rueggeberg FA, Giannini M, Arrais CAG, Price RBT. Light curing in dentistry and clinical implications: A literature review. Braz Oral Res, 2017; 31.
244. Lim BS, Ferracane JL, Sakaguchi RL, Condon JR. Reduction of polymerization contraction stress for dental composites by two-step light-activation. Dent Mater, 2002; 18: 436-444.
245. Algamaiah H, Silikas N, Watts DC. Polymerization shrinkage and shrinkage stress development in ultra-rapid photo-polymerized bulk fill resin composites. Dent Mater, 2021.
246. Algamaiah H, Silikas N, Watts DC. Conversion kinetics of rapid photo-polymerized resin composites. Dent Mater, 2020; 36: 1266-1274.
247. Watts DC, Algamaiah H. Characterizing surface viscoelastic integrity of ultra-fast photo-polymerized composites: Methods development. Dent Mater, 2020; 36: 1255-1265.
248. Metalwala Z, Khoshroo K, Rasoulianboroujeni M, Tahriri M, Johnson A, Baeten J, Fahimipour F, Ibrahim M, Tayebi L. Rheological properties of contemporary nanohybrid dental resin composites: The influence of preheating. Polym Test, 2018; 72: 157-163.
249. Rueggeberg FA, Daronch M, Browning WD, De Goes MF. In vivo temperature measurement: Tooth preparation and restoration with preheated resin composite. J Esthet Restor Dent, 2010; 22: 314-322.
250. Daronch M, Rueggeberg FA, Hall G, De Goes MF. Effect of composite temperature on in vitro intrapulpal temperature rise. Dent Mater, 2007; 23: 1283-1288.
251. Runnacles P, Arrais CAG, Pochapski MT, dos Santos FA, Coelho U, Gomes JC, De Goes MF, Gomes OMM, Rueggeberg FA. In vivo temperature rise in anesthetized human pulp during exposure to a polywave led light curing unit. Dent Mater, 2015; 31: 505-513.
252. Lohbauer U, Zinelis S, Rahiotis C, Petschelt A, Eliades G. The effect of resin composite pre-heating on monomer conversion and polymerization shrinkage. Dent Mater, 2009; 25: 514-519.
253. Yang J, Silikas N, Watts DC. Pre-heating effects on extrusion force, stickiness and packability of resin-based composite. Dent Mater, 2019; 35: 1594-1602.
254. Akarsu S, Aktuğ Karademir S. Influence of bulk-fill composites, polimerization modes, and remaining dentin thickness on intrapulpal temperature rise. BioMed Res Int, 2019; 2019: 4250284.

255. Runnacles P, Arrais CAG, Maucoski C, Coelho U, De Goes MF, Rueggeberg FA. Comparison of in vivo and in vitro models to evaluate pulp temperature rise during exposure to a polywave® led light curing unit. J Appl Oral Sci, 2019; 27.
256. Jo S-A, Lee C-H, Kim M-J, Ferracane J, Lee I-B. Effect of pulse-width-modulated led light on the temperature change of composite in tooth cavities. Dent Mater, 2019; 35: 554-563.
257. Randolph LD, Palin WM, Watts DC, Genet M, Devaux J, Leloup G, Leprince JG. The effect of ultra-fast photopolymerisation of experimental composites on shrinkage stress, network formation and pulpal temperature rise. Dent Mater, 2014; 30: 1280-1289.
258. Atai M, Ahmadi M, Babanzadeh S, Watts DC. Synthesis, characterization, shrinkage and curing kinetics of a new low-shrinkage urethane dimethacrylate monomer for dental applications. Dent Mater, 2007; 23: 1030-1041.
259. Yang J, Silikas N, Watts DC. Pre-heating time and exposure duration: Effects on post-irradiation properties of a thermo-viscous resin-composite. Dent Mater, 2020; 36: 787-793.
260. Vollmer M, Möllmann K-P. *Infrared thermal imaging: Fundamentals, research and applications*. Second edition. ed. Weinheim: Wiley-VCH; 2018.
261. Choi SH, Roulet JF, Heintze SD, Park SH. Influence of cavity preparation, light-curing units, and composite filling on intrapulpal temperature increase in an in vitro tooth model. Oper Dent, 2014; 39: E195-E205.
262. Atai M, Watts DC. A new kinetic model for the photopolymerization shrinkage-strain of dental composites and resin-monomers. Dent Mater, 2006; 22: 785-791.
263. Ilie N. Sufficiency of curing in high-viscosity bulk-fill resin composites with enhanced opacity. Clin Oral Invest, 2019; 23: 747-755.
264. Wang R, Wang Y. Depth-dependence of degree of conversion and microhardness for dual-cure and light-cure composites. Oper Dent, 2019.
265. Shah PK, Stansbury JW, Bowman CN. Application of an addition-fragmentation-chain transfer monomer in di(meth)acrylate network formation to reduce polymerization shrinkage stress. Polym Chem, 2017; 8: 4339-4351.
266. Emami N, Sjödahl M, Söderholm K-JM. How filler properties, filler fraction, sample thickness and light source affect light attenuation in particulate filled resin composites. Dent Mater, 2005; 21: 721.
267. Marovic D, Par M, Crnadak A, Sekelja A, Negovetic Mandic V, Gamulin O, Rakić M, Tarle Z. Rapid 3 s curing: What happens in deep layers of new bulk-fill composites? Materials, 2021; 14: 515.
268. Daronch M, Rueggeberg FA, Moss L, De Goes MF. Clinically relevant issues related to preheating composites. J Esthet Rest Dent, 2006; 18: 340-350.
269. Lempel E, Őri Z, Szalma J, Lovász BV, Kiss A, Tóth Á, Kunsági-Máté S. Effect of exposure time and pre-heating on the conversion degree of conventional, bulk-fill, fiber reinforced and polyacid-modified resin composites. Dent Mater, 2019; 35: 217-228.
270. Mouhat M, Mercer J, Stangvaltaite L, Örtengren U. Light-curing units used in dentistry: Factors associated with heat development-potential risk for patients. Clin Oral Investig, 2017; 21: 1687-1696.
271. Kim RJ-Y, Lee I-B, Yoo J-Y, Park S-J, Kim S-Y, Yi Y-A, Hwang J-Y, Seo D-G. Real-time analysis of temperature changes in composite increments and pulp chamber during photopolymerization. BioMed Res Int, 2015; 2015: 923808-923806.
272. Kim RJ-Y, Son S-A, Hwang J-Y, Lee I-B, Seo D-G. Comparison of photopolymerization temperature increases in internal and external positions of composite and tooth cavities in real time: Incremental fillings of microhybrid composite vs. Bulk filling of bulk fill composite. J Dent, 2015; 43: 1093-1098.

273. Baldissara P, Catapano S, Scotti R. Clinical and histological evaluation of thermal injury thresholds in human teeth: A preliminary study. J Oral Rehabil, 1997; 24: 791-801.
274. Lin M, Xu F, Lu TJ, Bai BF. A review of heat transfer in human tooth—experimental characterization and mathematical modeling. Dent Mater, 2010; 26: 501-513.
275. Kodonas K, Gogos C, Tziafas D. Effect of simulated pulpal microcirculation on intrapulpal temperature changes following application of heat on tooth surfaces. Int Endod J, 2009; 42: 247-252.
276. Maas MS, Alania Y, Natale LC, Rodrigues MC, Watts DC, Braga RR. Trends in restorative composites research: What is in the future? Brazilian oral research, 2017; 31.
277. Watts D, Amer O, Combe E. Characteristics of visible-light-activated composite systems. British Dental Journal, 1984; 156: 209-215.
278. Oden A, Ruyter I, Øys H. Creep and recovery of composites for use in posterior teeth during static and dynamic compression. Dental Materials, 1988; 4: 147-150.
279. Kaleem M, Masouras K, Satterthwaite JD, Silikas N, Watts DC. Viscoelastic stability of resin-composites under static and dynamic loading. Dental Materials, 2012; 28: e15-e18.
280. Al-Ahdal K, Silikas N, Watts DC. Development of viscoelastic stability of resin-composites incorporating novel matrices. Dental Materials, 2015; 31: 1561-1566.
281. Yang S, Zhang Y, Zeng K. Analysis of nanoindentation creep for polymeric materials. J of appl phys, 2004; 95: 3655-3666.
282. El-Safty S, Akhtar R, Silikas N, Watts D. Nanomechanical properties of dental resin-composites. Dent Mater, 2012; 28: 1292-1300.
283. El-Safty S, Silikas N, Akhtar R, Watts D. Nanoindentation creep versus bulk compressive creep of dental resin-composites. Dental Materials, 2012; 28: 1171-1182.
284. Ilie N, Hickel R, Watts DC. Spatial and cure-time distribution of dynamic-mechanical properties of a dimethacrylate nano-composite. Dental Materials, 2009; 25: 411-418.
285. Boussinesq J. *Application des potentiels à l'étude de l'équilibre et du mouvement des solides élastiques: Principalement au calcul des déformations et des pressions que produisent, dans ces solides, des efforts quelconques exercés sur une petite partie de leur surface ou de leur intérieur: Mémoire suivi de notes étendues sur divers points de physique, mathematique et d'analyse*: Gauthier-Villars; 1885.
286. Galin LA. *Kontakn'e zadachi teorii uprugosti*: Gos. Izdat. Tech.-Teor. Liter; 1953.
287. Harding J, Sneddon I. The elastic stresses produced by the indentation of the plane surface of a semi-infinite elastic solid by a rigid punch. In: *Mathematical Proceedings of the Cambridge Philosophical Society*: Cambridge University Press; 1945. pp. 16-26.
288. Sneddon IN. Boussinesq's problem for a flat-ended cylinder. In: *Mathematical Proceedings of the Cambridge Philosophical Society*: Cambridge University Press; 1946. pp. 29-39.
289. Sneddon IN. The relation between load and penetration in the axisymmetric boussinesq problem for a punch of arbitrary profile. International journal of engineering science, 1965; 3: 47-57.
290. Lakes R, Lakes RS. *Viscoelastic materials*: Cambridge university press; 2009.
291. Findley W, Lai J, Onaran K. Linear viscoelastic constitutive equations, creep and relaxation in nonlinear viscoelastic materials. In: New York: Dover; 1989.
292. Kohlrausch R. Theorie des elektrischen rückstandes in der leidener flasche. Annalen der Physik, 1854; 167: 179-214.
293. Williams G, Watts DC. Non-symmetrical dielectric relaxation behaviour arising from a simple empirical decay function. Transactions of the Faraday society, 1970; 66: 80-85.

294. Williams G, Watts DC, Dev S, North A. Further considerations of non symmetrical dielectric relaxation behaviour arising from a simple empirical decay function. Transactions of the faraday Society, 1971; 67: 1323-1335.
295. Palmer RG, Stein DL, Abrahams E, Anderson PW. Models of hierarchically constrained dynamics for glassy relaxation. Physical Review Letters, 1984; 53: 958.
296. Berry GC, Plazek DJ. On the use of stretched-exponential functions for both linear viscoelastic creep and stress relaxation. Rheologica Acta, 1997; 36: 320-329.
297. Cardona M, Chamberlin RV, Marx W. Comment on the history of the stretched exponential function. arXiv preprint arXiv:0710.4446, 2007.
298. Fancey KS. A mechanical model for creep, recovery and stress relaxation in polymeric materials. Journal of materials science, 2005; 40: 4827-4831.
299. Wydra JW, Cramer NB, Stansbury JW, Bowman CN. The reciprocity law concerning light dose relationships applied to bisgma/tegdma photopolymers: Theoretical analysis and experimental characterization. Dent Mater, 2014; 30: 605-612.
300. Sadeghyar A, Watts DC, Schedle A. Limited reciprocity in curing efficiency of bulk-fill resin-composites. Dental Materials, 2020; 36: 997-1008.
301. Chu S, Li J. Impression creep; a new creep test. Journal of Materials Science, 1977; 12: 2200-2208.
302. Hill R. Similarity analysis of creep indentation tests. Proceedings of the Royal Society of London. Series A: Mathematical and Physical Sciences, 1992; 436: 617-630.
303. Berthoud P, G'sell C, Hiver J. Elastic-plastic indentation creep of glassy poly (methyl methacrylate) and polystyrene: Characterization using uniaxial compression and indentation tests. Journal of Physics D: Applied Physics, 1999; 32: 2923.
304. Kim MH, Min SH, Ferracane J, Lee IB. Initial dynamic viscoelasticity change of composites during light curing. Dent Mater, 2010; 26: 463-470.
305. El-Safty S, Silikas N, Watts D. Temperature-dependence of creep behaviour of dental resin-composites. Journal of dentistry, 2013; 41: 287-296.
306. Par M, Gamulin O, Marovic D, Klaric E, Tarle Z. Effect of temperature on post-cure polymerization of bulk-fill composites. J Dent, 2014; 42: 1255-1260.
307. Kaiser C, Price R. Effect of time on the post-irradiation curing of six resin-based composites. Dent Mater, 2020; 36: 1019-1027.
308. Dobreva A, Gutzow I, Schmelzer J. Stress and time dependence of relaxation and the kohlrausch stretched exponent formula. Journal of non-crystalline solids, 1997; 209: 257-263.
309. Glasstone S, Laidler KJ, Eyring H. The theory of rate processes; the kinetics of chemical reactions, viscosity, diffusion and electrochemical phenomena. In: McGraw-Hill Book Company; 1941.
310. Al Sunbul H, Silikas N, Watts D. Surface and bulk properties of dental resin-composites after solvent storage. Dent Mater, 2016; 32: 987-997.
311. Watts DC, Kaiser C, O'Neill C, Price RB. Reporting of light irradiation conditions in 300 laboratory studies of resin-composites. Dent Mater, 2019; 35: 414-421.
312. Algamaiah H, Silikas N, Watts DC. Polymerization shrinkage and shrinkage stress development in ultra-rapid photo-polymerized bulk fill resin composites. Dental Materials, 2021; 37: 559-567.
313. Yang J, Algamaiah H, Watts DC. Spatio-temporal temperature fields generated coronally with bulk-fill resin composites: A thermography study. Dental Materials, 2021.
314. Tjandrawinata R, Irie M, Suzuki K. Flexural properties of eight flowable light-cured restorative materials, in immediate vs 24-hour water storage. Oper Dent, 2005; 30: 239-249.
315. Leprince J, Palin W, Vanacker J, Sabbagh J, Devaux J, Leloup G. Physico-mechanical characteristics of commercially available bulk-fill composites. J Dent, 2014; 42: 993-1000.

316. Ilie N, Kreppel I, Durner J. Effect of radical amplified photopolymerization (rap) in resin-based composites. Clinic oral investig, 2014; 18: 1081-1088.
317. Wang X, Zhou J, Kang D, Swain MV, Menčík J, Jian Y, Zhao K. The bulk compressive creep and recovery behavior of human dentine and resin-based dental materials. Dental Materials, 2020.
318. Witzel MF, Ballester RY, Meira JB, Lima RG, Braga RR. Composite shrinkage stress as a function of specimen dimensions and compliance of the testing system. Dental Materials, 2007; 23: 204-210.
319. Algamaiah H, Watts DC. Post-irradiation surface viscoelastic integrity of photo-polymerized resin-based composites. Dental Materials, 2021; 37: 1828-1833.
320. Unterbrink GL, Muessner R. Influence of light intensity on two restorative systems. J Dent, 1995; 23: 183-189.
321. Haas M, Radebner J, Eibel A, Gescheidt G, Stueger H. Recent advances in germanium-based photoinitiator chemistry. Chem–Eur J, 2018.
322. Ilie N, Bauer H, Draenert M, Hickel R. Resin-based composite light-cured properties assessed by laboratory standards and simulated clinical conditions. Oper Dent, 2013; 38: 159-167.
323. Par M, Spanovic N, Marovic D, Attin T, Tarle Z, Tauböck TT. Rapid high-intensity light-curing of bulk-fill composites: A quantitative analysis of marginal integrity. Journal of Dentistry, 2021; 111: 103708.
324. Marovic D, Par M, Macan M, Klarić N, Plazonić I, Tarle Z. Aging-dependent changes in mechanical properties of the new generation of bulk-fill composites. Materials, 2022; 15: 902.
325. Lawson N. 24-month clinical performance of an ultra-rapid polymerization time bulk-fill composite. In: *AADOCR*. Atlanta, GA: J Dent Res 2022.

Appendices

Appendix A

DENTAL MATERIALS 36 (2020) 1266–1274

Available online at www.sciencedirect.com

ScienceDirect

journal homepage: www.intl.elsevierhealth.com/journals/dema

Conversion kinetics of rapid photo-polymerized resin composites

Hamad Algamaiah[a,c,*], *Nikolaos Silikas*[a], *David C Watts*[a,b,**]

[a] *Biomaterials Science, Division of Dentistry, School of Medical Sciences, University of Manchester, UK*
[b] *Photon Science Institute, University of Manchester, UK*
[c] *Department of Restorative Dental Science, College of Dentistry, King Saud University, Saudi Arabia*

ARTICLE INFO

Article history:
Accepted 21 July 2020

Keywords:
Resin composite
Photopolymerization
FTIR
Degree of conversion
AFCT
Polymerization kinetics

ABSTRACT

Objective. To measure the degrees of conversion (DC), conversion kinetics, and the effect of post-irradiation time on rapid photo-polymerized bulk-fill resin composites under conditions equivalent to clinical depths of 1 and 4 mm.

Methods. 36 specimens (n = 3), based on two resin composites incorporating PowerCure rapid-polymerization technology in two consistencies (PFill; PFlow) and two comparators with matching consistencies (Eceram; EFlow), were investigated from the same manufacturer (Ivoclar AG, Liechtenstein). Specimens were prepared within 4 mm diameter cylindrical molds, of either 1 mm or 4 mm depths respectively, to simulate near-surface and deep locations in a bulk-fill restoration. The independent variables in this study were: materials, thickness and time. Two high irradiance polymerization protocols were utilized for PowerCure materials: 2000 and 3050 mW/cm^2 for 5 and 3 s, respectively. A standard (1200 mW/cm^2) polymerization protocol was used with control materials. FTIR was utilized to measure DC in real-time for 24 h post-irradiation. The data were analyzed using *Welch's*-ANOVA, *Games-Howell post-hoc test*, kinetic dual-exponential sum function and independent sample t-tests (p = 0.05).

Results. The DC of the materials ranged between 44.7–59.0 % after 5 min, which increased after 24 h reaching 55.7–71.0 % ($p < 0.05$). Specimen thickness did not influence the overall DC. At 5 min, the highest DC was shown in EFlow. But PFlow, irradiated for 3 s and 5 s exhibited comparable results ($p > 0.05$). PFill composite irradiated with the 3 s and 5 s protocols did not differ from ECeram ($p > 0.05$). Specimen thickness and material viscosity affected polymerization kinetics and rate of polymerization (RP_{max}). Faster polymerization occurred in 1 mm specimens (except PFill-5 s and ECeram). PFill and PFlow exhibited faster conversion than the controls. RP_{max} varied across the specimen groups between 4.3–8.8 %/s with corresponding DC $_{RPmax}$ between 22.2–45.3 %.

Significance. Polymerization kinetics and RP_{max} were influenced by specimen thickness and material viscosity. PFill and PFlow materials produced an overall comparable conversion at 5 min and 24 h post-irradiation, despite the ultra-short irradiation times, throughout the 4 mm specimen thickness.

* Corresponding authors at: Department of Restorative Dental Science, College of Dentistry, King Saud University, Riyadh, Saudi Arabia..
** Corresponding authors at: University of Manchester, School of Medical Sciences and Photon Science Institute, Coupland 3 Building, Oxford Road, Manchester M13 9PL, UK.
E-mail addresses: hamad.algamaiah@postgrad.manchester.ac.uk (H. Algamaiah), david.watts@manchester.ac.uk (D.C. Watts).
https://doi.org/10.1016/j.dental.2020.07.008
0109-5641/

Appendix B

DENTAL MATERIALS 37 (2021) 559–567

Available online at www.sciencedirect.com

ScienceDirect

journal homepage: www.intl.elsevierhealth.com/journals/dema

Polymerization shrinkage and shrinkage stress development in ultra-rapid photo-polymerized bulk fill resin composites

Hamad Algamaiah[a,b,*], *Nikolaos Silikas*[a,c], *David C. Watts*[a,c,**]

[a] *Biomaterials Science, Division of Dentistry, School of Medical Sciences, University of Manchester, UK*
[b] *Department of Restorative Dental Sciences, College of Dentistry, King Saud University, Saudi Arabia*
[c] *Photon Science Institute, University of Manchester, UK*

ARTICLE INFO

Article history:
Received 1 February 2021
Received in revised form
23 February 2021
Accepted 23 February 2021

Keywords:
Polymerization
Photopolymerization
Resin composite
Bulk fill
URPBF
Shrinkage
Stress
AFCT
Bioman II

ABSTRACT

Objective. To determine the polymerization shrinkage (%) and shrinkage stress (MPa) characteristics of ultra-rapid photo-polymerized bulk fill resin composites.

Methods. Two ultra-rapid photo-polymerized bulk fill (URPBF) materials: PFill and PFlow were studied, along with their comparators ECeram and EFlow. PFill contains an *addition fragmentation chain transfer* (AFCT) agent. The URPBR materials were irradiated using two different 3 s high irradiance protocols (3000 and 3200 mW/cm^2 based on Bluephase *PowerCure* and VALO LCUs, respectively) and one 10 s standard protocol (1200 mW/cm^2 based on a Bluephase *PowerCure* LCU). Bonded disk and Bioman II instruments were used to measure Polymerization shrinkage % and shrinkage stress MPa, respectively, for 60 min at 23 ± 1 °C (n = 5). Maximum shrinkage-*rate* and maximum shrinkage stress-*rate* were also calculated for 15 s via numerical differentiation. The data were analyzed via multiple One-way ANOVA and Tukey post-*hoc* tests ($\alpha = 0.05$).

Results. PFill groups, regardless of their irradiance protocol, showed significantly lower PS than the comparator, ECeram ($p < 0.05$). However, PFlow irradiated via different protocols, was comparable to EFlow and ECeram ($p > 0.05$). PFill consistently produced stress results which were significantly lower than ECeram ($p < 0.05$) and were comparable for both high irradiance protocols ($p > 0.05$). PFlow only exhibited significantly higher shrinkage stress when polymerized with the 3 sVALO protocol ($p < 0.05$).

The maximum shrinkage strain-*rate* (%/s) was significantly lower in PFill-10s and PFill-3s groups (using *PowerCure* LCU) compared to ECeram. However, no differences were seen between PFlow and EFlow ($p > 0.05$). The maximum shrinkage stress-*rate* of PFill and PFlow was comparable between different irradiation protocols, as well as to their comparator ECeram ($p > 0.05$).

Significance. High irradiation protocols over ultra-short periods led to slightly lower shrinkage strain but slightly higher stress, possibly due to reduced network mobility. The AFCT agent incorporated in PFill composite seemed to reduce shrinkage stress development, even with high irradiance protocols.

* *Corresponding author at*: Department of Restorative Dental Science, College of Dentistry, King Saud University, Riyadh, Saudi Arabia.
** *Corresponding author at*: University of Manchester, School of Medical Sciences and Photon Science Institute, Coupland 3 Building, Oxford Road, Manchester M13 9PL, UK.
E-mail addresses: dr.algamaiah@gmail.com (H. Algamaiah), David.watts@manchester.ac.uk (D.C. Watts).
https://doi.org/10.1016/j.dental.2021.02.012
0109-5641/

Appendix C

DENTAL MATERIALS 37 (2021) 1237–1247

Available online at www.sciencedirect.com

ScienceDirect

journal homepage: www.intl.elsevierhealth.com/journals/dema

Spatio-temporal temperature fields generated coronally with bulk-fill resin composites: A thermography study

Jiawei Yang[a], *Hamad Algamaiah*[a,b,**], *David C. Watts*[a,c,*]

[a] *Dentistry, School of Medical Sciences, University of Manchester, Manchester, UK*
[b] *Department of Restorative Dental Science, College of Dentistry, King Saud University, Riyadh, Saudi Arabia*
[c] *Photon Science Institute, University of Manchester, Manchester, UK*

ARTICLE INFO

Article history:
Received 25 May 2021
Received in revised form 1 June 2021
Accepted 1 June 2021

Keywords:
Thermal imaging
Thermographic analysis
Bulk-fill resin composite
High-irradiance
URPBF composites
Pre-heating
Thermo-viscous composite

ABSTRACT

Objective. This study aimed to investigate the effects of (i) a high-irradiance (3s) light-curing protocol *versus* (ii) two standard-irradiance (10s) protocols on 2D temperature maps during intra-dental photo-irradiation within a molar cavity restored with either *Ultra-Rapid Photo-Polymerized Bulk Fill* (URPBF) composites or a pre-heated thermo-viscous bulk-fill composite, compared to a standard bulk-fill *resin-based-composite* (RBC). The specific objectives included visual assessment of the temperature maps and quantitative assessment of several temperature/time plots at four different locations.

Methods. A caries-free lower first molar cavity served as a natural tooth mold. Resin composites were placed without intermediary adhesive. Two URPBF composites (PFill; PFlow) and one pre-heated thermo-viscous bulk-fill composite (*Viscalor*: VC) were compared to a contemporary bulk-fill composite (One Bulk Fill: OBF). Two LED-LCU devices were used: Bluephase *PowerCure* (PC) and Elipar S10 (S10), with three light-irradiation protocols (PC-3s, PC-10s and S10-10s). 2D temperature maps over the entire coronal area were recorded for 120 s during and after irradiation using a thermal imaging camera. Changes at four different levels were selected from the data sets: (0, 2 and 4 mm from the cavity top and at 1 mm below the dentin cavity floor). The maximum temperature attained (T_{max}), the mean temperature rise (ΔT), the time (s) to reach maximum temperature and the integrated areas (°C s) under the temperature/time (T/t) plots were identified. Data were analysed via three-way ANOVA, One-way ANOVA, independent t-tests and Tukey *post-hoc* tests ($p < 0.05$).

Results. All RBCs showed qualitatively similar temperature-time profiles. PFlow reached T_{max} in the shortest time. PC-3s (3000 mW/cm^2) generated comparable ΔT to S10-10s, except with PFill, where ΔT was greater. Despite the same irradiance (1200 mW/cm^2), Elipar S10 led to higher T_{max} and ΔT compared to PC-10s. The highest T_{max} and ΔT were observed at the 2 mm level, and the lowest were at 1 mm depth into the underlying dentin.

* *Corresponding author at*: University of Manchester, School of Medical Sciences, Coupland 3 Building, Oxford Road, Manchester M13 9PL, UK.
** *Corresponding author at*: Department of Restorative Dental Science, College of Dentistry, King Saud University, Riyadh, Saudi Arabia.
E-mail addresses: dr.algamaiah@gmail.com (H. Algamaiah), david.watts@manchester.ac.uk (D.C. Watts).
https://doi.org/10.1016/j.dental.2021.06.008

Appendix D

DENTAL MATERIALS 36 (2020) 1255–1265

Available online at www.sciencedirect.com

ScienceDirect

journal homepage: www.intl.elsevierhealth.com/journals/dema

Characterizing surface viscoelastic integrity of ultra-fast photo-polymerized composites: Methods development

David C. Watts[a,b,*], *Hamad Algamaiah*[a,c,**]

[a] *Biomaterials Science, Division of Dentistry, School of Medical Sciences, University of Manchester, UK*
[b] *Photon Science Institute, University of Manchester, UK*
[c] *Department of Restorative Dental Science, College of Dentistry, King Saud University, Saudi Arabia*

ARTICLE INFO

Article history:
Received 13 July 2020
Received in revised form
28 July 2020
Accepted 28 July 2020

Keywords:
Photopolymerization
Dimethacrylate
AFCT
RAFT
Resin-composite
Indentation-creep
Stretched-exponential
Viscoelasticity
Post-cure

ABSTRACT

Objective. Resin-Composites are now available designed for polymerization using 3 s of intense light irradiation. The aim was to develop an experimental method to probe their surface viscoelastic integrity immediately following such rapid photo-cure via macroscopic surface indentation under constant stress as a function of time.

Methods. Two bulk-fill composites (Ivoclar AG) were studied: Tetric PowerFill (PFill) and PowerFlow (PFlow). Split molds were used to fabricate cylindrical {4 mm (dia) × 4 mm} paste specimens, irradiated at 23 °C at 0 mm from the top surface with a Bluephase*PowerCure* LED-LCU, with 3 s or 5 s modes, emitting 3 and 2 W/cm^2, respectively. Post-irradiation specimens were immediately transferred to an apparatus equipped with a flat-ended indentor of 1.5 mm diameter. 14 MPa compressive stress at the indentor tip was applied centrally in < 2 min and maintained constant for 2 h. Indentation (I) magnitudes were recorded in real-time (t), with I(t) data re-expressed as % indentation relative to the 4 mm specimen height. After 2 h, the indentor was unloaded and indentation recovery was monitored for a further 2 h. Parallel sets of measurements were made where indentation was delayed for 24 h. Further measurements were made with more conventional composites: EvoCeram Bulk Fill (ECeram) and Tetric EvoFlow Bulk Fill (EFlow). These were irradiated for 20 s at 1.2 W/cm^2. Kinetic data were curve-fitted to exponential growth functions and key parameters analyzed by ANOVA and *post-hoc* tests ($\alpha = 0.05$).

Results. I(t) plots looked initially similar to bulk creep/recovery: rapid deformation plus viscoelastic response; then, upon unloading: rapid (elastic) recovery followed by partial viscoelastic recovery. However, unlike multiply irradiated and stored bulk-creep specimens, the present specimens were exposed to only 3 or 5 s "occlusal" irradiation; generating "hard" surfaces. Subsequently, during the 2 h indentation, the polymer matrix network continued to harden and consolidate. Upon initial loading, I(t) reached 2–3% indentation, depending upon the formulation. Upon unloading at 2 h, elastic recovery was only *ca.* 1 %. Delayed loading for 24 h, generated I(t) plots of significantly reduced magnitude. Most importantly, however, the I(t) plots for ECeram and EFlow, after 20 s irradiation, showed I(t) magnitudes quite comparable to the PFill and PFlow rapid-cure composites.

* *Corresponding author at*: University of Manchester, School of Medical Sciences and Photon Science Institute Coupland 3 Building, Oxford Road, Manchester M13 9PL, UK.
** *Corresponding author at*: Department of Restorative Dental Science, College of Dentistry, King Saud University, Riyadh, Saudi Arabia.
E-mail addresses: david.watts@manchester.ac.uk (D.C. Watts), dr.algamaiah@gmail.com (H. Algamaiah).
https://doi.org/10.1016/j.dental.2020.07.009

Appendix E

DENTAL MATERIALS 37 (2021) 1828–1833

Available online at www.sciencedirect.com

ScienceDirect

journal homepage: www.intl.elsevierhealth.com/journals/dema

Post-irradiation surface viscoelastic integrity of photo-polymerized resin-based composites

Hamad Algamaiah[a,b,**], *David C. Watts*[a,c,*]

[a] *Dentistry, School of Medical Sciences, University of Manchester, Manchester, UK*
[b] *Department of Restorative Dental Science, College of Dentistry, King Saud University, Riyadh, Saudi Arabia*
[c] *Photon Science Institute, University of Manchester, Manchester, UK*

ARTICLE INFO

Article history:
Received 11 September 2021
Received in revised form
13 September 2021
Accepted 13 September 2021

Keywords:
Indentation-creep
Bulk fill
Resin-based composites
Photo-polymerization
Creep
Viscoelastic properties

ABSTRACT

Objective. A class of *ultra-rapid-cure* resin-based composites (RBCs) exhibited immediate post-irradiation surface viscoelastic integrity using an indentation-creep/recovery procedure. The aim of this study was to determine whether such behavior is more generally characteristic of a wider range of RBCs.

Methods. Eight representative RBCs were selected based on different clinical categories: three bulkfills (**OBF**, Filtek One Bulk Fill; **VBF**, Venus Bulkfill; **EBF**, Estelite Bulkfill), three conventional non-flowables (**XTE**, Filtek Supreme XTE; **GSO**, GrandioSo; **HRZ**, Harmonize) and conventional flowables (**XTF**, Filtek Supreme XTE *Flow*; **GSF**, GrandioSo Flow). Stainless steel split molds were used to fabricate cylindrical specimens (4 mm (dia) × 4 mm). These were irradiated (1.2 W/cm^2) for 20 s on the top surface. Post-irradiation specimens (n = 3), within their molds, were centrally loaded with a flat-ended 1.5 mm diameter indenter under 14 MPa stress: either *immediately* (<2 min) or after 24 h *delayed* indentation. Stress was maintained for 2 h, then – after removal – recovery measurements continued for a further 2 h. Indentation depth (%) *versus* time was measured continuously to an accuracy of <0.1 μm. Data were analyzed by One-way ANOVA and Tukey *post-hoc* tests ($\alpha = 0.05$).

Results. Time-dependent viscoelastic indentation was observed for all RBCs. For *immediate* indentation, the maximum indentation range was 1.43–4.92%, *versus* 0.70–2.22% for 24 h *delayed* indentation. Following 2 h recovery, the residual indentation range was 0.86–3.58% after *immediate* indentation, reducing to 0.22–1.27% for *delayed* indentation. The greatest *immediate* indentation was shown by VBF followed by XTF and GSF. OBF, HRZ, XTE and GSO had significantly lower indentations (greater hardness). XTE showed a significantly *reduced indentation maximum* compared to OBF ($p < 0.05$). Indentations *delayed* until 24 h post-irradiation were reduced ($p < 0.05$) for most materials.

Significance. The indentation-creep methodology effectively characterized resin-based composites within several categories. Viscoelastic properties evaluated by the indentation-creep method confirmed that highly filled RBCs were more resistant to indentation. Indentations were reduced after 24 h post-irradiation due to further matrix-network development.

* *Corresponding author at*: University of Manchester, School of Medical Sciences, Coupland 3 Building, Oxford Road, Manchester M13 9PL, UK.
** *Corresponding author at*: Department of Restorative Dental Science, College of Dentistry, King Saud University, Riyadh, Saudi Arabia.
E-mail addresses: dr.algamaiah@gmail.com (H. Algamaiah), david.watts@manchester.ac.uk (D.C. Watts).

https://doi.org/10.1016/j.dental.2021.09.012
0109-5641/

Appendix F

An example of sample size calculation, G*power software version 3.1.3 (Franz Faul, Heinrich Heine Universität, Germany) was used based on a pilot study in **chapter 6**. Once the data of the pilot were entered, a sample size of (n=4) was sufficient to satisfy a power of 80%.

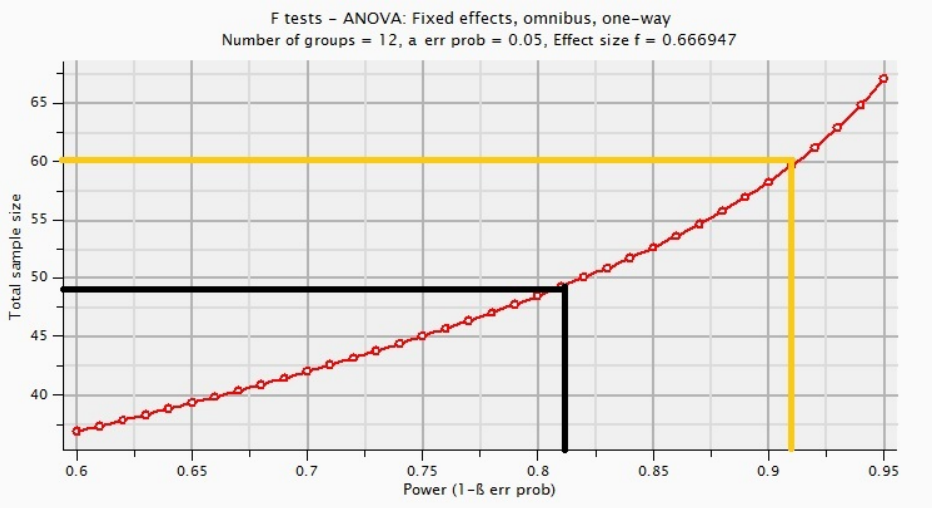

Sample size calculation using G*power software.